

Inkless Soft Lithography: Utilizing Immobilized Enzymes and Small Molecules
to Pattern Self-Assembled Monolayers via Catalytic Microcontact Printing

by

Briana N. Vogen

Department of Chemistry
Duke University

Date: _____

Approved:

Eric J. Toone, Supervisor

Robert L. Clark

Stephen L. Craig

Jie Liu

Dissertation submitted in partial fulfillment of
the requirements for the degree of Doctor
of Philosophy in the Department of
Chemistry in the Graduate School
of Duke University

2010

ABSTRACT

Inkless Soft Lithography: Utilizing Immobilized Enzymes and Small Molecules
to Pattern Self-Assembled Monolayers via Catalytic Microcontact Printing

by

Briana N. Vogen

Department of Chemistry
Duke University

Date: _____

Approved:

Eric J. Toone, Supervisor

Robert L. Clark

Stephen L. Craig

Jie Liu

An abstract of a dissertation submitted in partial
fulfillment of the requirements for the degree
of Doctor of Philosophy in the Department of
Chemistry in the Graduate School
of Duke University

2010

Copyright by
Briana N. Vogen
2010

Abstract

During the past two decades, soft lithographic techniques that circumvent the limitations of photolithography have emerged as important tools for the transfer of patterns with sub-micron dimensions. Among these techniques, microcontact printing (μ CP) has shown special promise. In μ CP, an elastomeric stamp is first inked with surface-reactive molecules and placed in contact with an ink-reactive surface, resulting in pattern transfer in the form of self-assembled monolayers in regions of conformal contact. The resolution in μ CP is ultimately limited to the diffusion of ink and the elastomechanical properties of the bulk stamping material.

One way to improve resolution is to eliminate diffusion by using inkless methods for pattern transfer. Inkless catalytic- μ CP uses a chemical reaction between a stamp-immobilized catalyst and surface bearing cognate substrate to transfer pattern in the areas of conformal contact. By using pre-assembled cognate surfaces, the approach extends the range of surfaces readily amenable to patterning while obviating diffusive resolution limits imposed by traditional μ CP.

In this thesis, we report two methods using inkless catalytic μ CP: biocatalytic- μ CP utilizes an immobilized enzyme as a catalyst whereas catalytic-

μ CP utilizes an immobilized small molecule as a catalyst, such as an acid or base. Both catalytic techniques demonstrate pattern transfer at the microscale while using unconventional, acrylate-based stamp materials. Previous results produced with catalytic- μ CP have shown pattern transfer with sub-50 nm edge resolution. In this demonstration of catalytic- μ CP, we use the technique to demonstrate a bi-layered patterning technique for H-terminated silicon, the foremost material in semi-conductor fabrication. This technique simultaneously protects the underlying silicon surface from degradation while a highly-reactive organic overlayer remains patternable by acidic-functionalized PU stamps. Line widths as small as 150 nm were reproduced on the reactive SAM overlayer, which would not be possible without circumvention of diffusion. Before and after patterning, no oxidation of the underlying silicon was observed, preserving desired electronic properties throughout the whole process. This bi-patterning technique could be extended to other technologically-relevant surfaces for further application in organic-based electronic devices and other related technologies.

Dedication

To my parents and to my beloved G.G.

Table of Contents

Abstract.....	iv
List of Tables	xiii
List of Figures	xiv
List of Abbreviations	xix
Acknowledgements	xxiv
1. Introduction	1
1.1 Overview	1
1.2 Principles of microcontact printing	10
1.2.1 Master and mask fabrication.....	11
1.2.2 Stamp fabrication using PDMS as a stamp material	17
1.2.3 Pattern transfer and SAM formation	19
1.3 Limitations of microcontact printing.....	22
1.3.1 Molecular ink diffusion	22
1.3.2 Stamp deformation.....	25
1.3.3 Availability and technological applicability of ink-substrate systems..	29
1.4 Resolution improvement of patterning SAMs by manipulation of ink diffusion.....	30
1.4.1 Printing SAMs using various molecular inks.....	31
1.4.1.1 Use of inking pads for use in traditional μ CP methods.....	31
1.4.1.2 High-speed μ CP	32
1.4.1.3 Microdisplacement μ CP.....	32
1.4.1.4 Submerged μ CP	34
1.4.1.5 Use of low-diffusion inks in μ CP	34
1.4.2 Patterning pre-formed SAMs using μ CP	36
1.4.2.1 Nanotransfer printing	36
1.4.2.2 Catalytic- μ CP.....	37

2. Biocatalytic microcontact printing.....	49
2.1 Overview	49
2.2 Demonstration of biocatalytic- μ CP with model system ExoI-ssDNA	50
2.2.1 Acrylamide-based elastomeric stamps.....	50
2.2.1.1 Bulk material of elastomeric stamp.....	50
2.2.1.2 Synthesis of bifunctional linker for stamp	51
2.2.1.3 Stamp fabrication protocols.....	53
2.2.2 Model enzyme-substrate system parameters using ExoI-ssDNA.....	54
2.2.2.1 Model Enzyme: Exonuclease I (ExoI).....	54
2.2.2.2 Model substrate: ssDNA on gold and glass surfaces	56
2.2.3 ExoI activity assays.....	60
2.2.3.1 MALDI-TOF mass spectrometry for ExoI-ssDNA solution-based assay ¹³⁷	60
2.2.3.2 Fluorescence microscopy of glass-immobilized 3'-TAMRA ssDNA after incubation with ExoI in solution	61
2.2.3.3 AFM of ssDNA SAMs on gold.....	62
2.2.4 Stamp activation and stamping protocols	63
2.2.5 AFM imaging of biocatalytic- μ CP on ssDNA-functionalized gold substrates	66
2.2.6 Confocal fluorescent microscopy of biocatalytic- μ CP on ssDNA-functionalized ITC-glass substrates.....	70
2.2.7 Using confocal fluorescent microscopy of to determine extent of ablation caused by biocatalytic- μ CP.....	72
2.2.8 Using MALDI-TOF spectroscopy to determine the extent of ablation caused by biocatalytic- μ CP.....	77
2.2.9 Conclusions from biocatalytic- μ CP using ExoI-ssDNA as a model system.....	80
2.3 Resolution of biocatalytic- μ CP dependence on tether length.....	82
3. Expansion of biocatalytic- μ CP to other enzyme-substrate systems.....	86

3.1 Overview	86
3.2 Carboxyesterases and lipases for use in biocatalytic- μ CP	89
3.2.1 Acetyl esterase (AES)	90
3.2.2 BioH esterase (BioH)	92
3.2.3 <i>R.oryzae</i> lipase (ROL).....	94
3.3 Selection of functional ester protecting group for carboxyesterase-benzoic ester model system.....	96
3.4 Synthesis of para-fluorinated alkanethiol and disulfide benzyl esters and subsequent surface characterization.....	98
3.5 Activity assays in solution with synthetic benzyl ester disulfide substrate	102
3.6 Activity assays of immobilized synthetic benzyl ester disulfide substrates 12 and 16 on gold.....	106
3.7 Formation of mixed SAMs using benzyl ester thiols 14 or 18 with butanethiol.....	109
3.8 Activity assays in solutions with synthetic benzyl ester thiols 14 and 18..	111
3.9 Activity assays on surfaces with synthetic benzyl ester thiols 14 and 18 ..	115
4. Catalytic microcontact printing	118
4.1 Overview	118
4.2 Universal bi-layered patterning technique.....	123
4.2.1 Substrate properties and components	124
4.2.2 Stamping materials.....	128
4.2.2.1 Masters for catalytic-PU stamps	128
4.2.2.2 Catalytic- μ CP stamp fabrication.....	129
4.2.3 Patterning NHS-functionalized SAMs using catalytic- μ CP at the microscale	136
4.2.4 Patterning NHS-functionalized SAMs using catalytic- μ CP sub-microscale	141
4.2.5 Conclusions from universal bi-layered patterning technique using catalytic- μ CP	143

4.3 The relationship between the hydrolyzing efficiency and pKa of the catalytic PU stamps	143
5. Experimental section	154
5.1 Biocatalytic- μ CP on SAMs of ssDNA.....	154
5.1.1 General procedures for biocatalytic- μ CP.....	154
5.1.2 Synthesis of NTA-acrylate 3 for use in acrylamide-based stamps for biocatalytic- μ CP.....	155
5.1.3 ExoI expression and purification. ¹⁵⁶	160
5.1.4 ssDNA immobilization on surfaces.	161
5.1.4.1 ssDNA SAMs on gold surfaces. ⁹¹	161
5.1.4.2 ssDNA immobilization on glass surfaces.....	162
5.1.5 MALDI-TOF mass spectrometry activity assay for ssDNA-ExoI in solution.....	162
5.1.6 Stamp fabrication, activation, and biocatalytic- μ CP stamping protocols. ¹³⁷	163
5.1.7 AFM tips and MHA-modified AFM tips.	164
5.1.8 Preparation of glass-immobilized ssDNA for MALDI-TOF spectroscopy.....	165
5.2 Synthesis of acrylamide-TEG-NTA-lys 9.....	165
5.3 Expansion of enzyme-substrate system for biocatalytic- μ CP: Carboxyesterase/lipase and aromatic ester-functionalized SAMs.....	173
5.3.1 Carboxyesterase and lipase DNA isolation and transformation, and protein transformation, expression, and purification.	173
5.3.1.1 PCR amplification of the BioH gene from genomic DNA.	173
Genomic DNA isolation.....	173
PCR amplification of BioH from genomic DNA.	175
BamH1 and HindIII restriction enzymatic digests of BioH and pET22b vector DNAs.	176
Ligation of BioH DNA into pET22b vector.	177

5.3.1.2 DNA transformation methods for all vectors containing carboxyesterase or lipase into XL-10, BL-21, and/or Origami(DE3) cells.....	179
5.3.1.3 AES protein overexpression and purification.	181
5.3.1.4 BioH protein overexpression and purification.....	183
5.3.1.5 ROL protein overexpression and purification.	184
5.3.2 Synthesis of fluorinated benzylic esters for use with esterases and lipases for biocatalytic- μ CP.	186
Synthesis of 11-(10-Carboxy-decyldisulfanyl)-undecanoic acid (11) from 11-mercaptoundecanoic acid (10). ²²³	186
Synthesis of 11-[10-(4-Fluoro-benzyloxycarbonyl)-decyldisulfanyl]-undecanoic acid 4-fluoromethyl-benzyl ester (12) from 11-(10-Carboxy-decyldisulfanyl)-undecanoic acid (11). ²²⁴	186
Synthesis of 11-[10-(4-Trifluoromethyl-benzyloxycarbonyl)-decyldisulfanyl]-undecanoic acid 4-trifluoromethyl-benzyl ester (13) from 11-(10-Carboxy-decyldisulfanyl)-undecanoic acid (11). ²²⁴	187
Synthesis of 4-(trifluoromethyl)benzyl 11-mercaptoundecanoate (14) from 11-[10-(4-trifluoromethyl-benzyloxycarbonyl)-decyldisulfanyl]-undecanoic acid 4-trifluoromethyl-benzyl ester (13).	188
Synthesis of bis(4-fluorobenzyl) 4,4'-disulfanediyldipropoanoate (16) from 4,4'-dithiobutyric acid (15). ²²⁴	188
Synthesis of bis(4-trifluoromethylbenzyl) 4,4'-disulfanediyldipropoanoate (17) from 4,4'-dithiobutyric acid (15). ²²⁴	189
Synthesis of 4-(trifluoromethyl)benzyl 4-mercaptobutanoate (18) from 11-[10-(4-trifluoromethyl-benzyloxycarbonyl)-decyldisulfanyl]-undecanoic acid 4-trifluoromethyl-benzyl ester (13).	189
Synthesis of 11,11'-Disulfanediylbis(undecan-1-ol) from 11-mercapto-1-undecanol 19. ²²⁵	190
Synthesis of disulfanediylbis(undecane-11,1-diyl) bis(2-(4-(trifluoromethyl)phenyl)acetate) 21 from 11,11'-disulfanediylbis(undecan-1-ol) 20.	191

Synthesis of 11-mercaptoundecyl 2-(4-(trifluoromethyl)phenyl)acetate 22 from disulfanediybis(undecane-11,1-diyl) bis(2-(4- (trifluoromethyl)phenyl)acetate) 21.	191
5.3.3 Activity assays of fluorinated benzylic esters in solution and as gold SAMs with esterases and lipases.....	192
5.4 Catalytic microcontact printing.....	194
5.4.1. General methods for catalytic- μ CP.....	194
5.4.2. Silicon-PMMA master fabrication for small features ≤ 500 nm.	195
5.4.2 Materials for polyurethane acrylate (PU) stamps.....	196
5.4.2.1 Synthesis of PU pre-polymer. ²²⁶	196
5.4.2.2 Fabrication for acid-immobilized stamps from PU pre-polymer. .	197
5.4.3 Formation of NHS-functionalized SAMs on silicon <111> surfaces. ...	198
5.4.4 Stamping protocol.	200
References	201
Biographical sketch.....	227

List of Tables

Table 1. Intensity values of cleaved fluorophore-functionalized ssDNA on ITC surfaces before and after exposure to detergent (SDS).....	74
Table 2. (Flat) Stamp-immobilized ExoI activity assay on glass substrate.	75
Table 3. XPS signal ratios of F1s and C1s relative to gold and corresponding contact angles for SAMs formed from 12 and 16.	102
Table 4. XPS signal ratios and corresponding contact angles for SAMs formed from 12 and 16 before and after incubation with BioH or ROL enzymes.	107
Table 5. XPS data for Mixed SAMs of 14 and BT Before and After Incubation with enzymes BioH and ROL.....	115
Table 6. XPS data for 1:1 Mixed SAMs of 18 and BT Before and After Incubation with Enzymes BioH and ROL.	116
Table 7. Acids co-polymerized with PU pre-polymeric mixture for catalytic- μ CP.	146

List of Figures

Figure 1. Diagram showing relief, intaglio, and planographic printing techniques on paper. In each, a master (dark gray) is inked (black) and placed in contact with paper, resulting in the printed image on the right.....	4
Figure 2. Lithography stone (left) and mirror-print (right) on paper. ¹⁰	6
Figure 3. Integrated circuit of Atmel Diopsis 740 System on Chip. ¹¹	7
Figure 4. Overview of fabrication of stamp for μ CP using a silicon master and subsequent stamping of alkanethiolate SAMs.....	11
Figure 5. SEM images of Si/PMMA master for soft lithography (left). Elastomeric stamp made from master (right).....	14
Figure 6. Master fabrication for soft lithography via EBL or photolithography (PL).....	15
Figure 7. General mask fabrication for photolithography using EBL and a positive resist.	16
Figure 8. Stamp fabrication from master for use in μ CP.....	17
Figure 9. Side-view diagram showing the orientation of bound alkanethiolate species to a crystalline gold surface.	20
Figure 10. Traditional μ CP using a PDMS stamp to print alkanethiols on gold..	21
Figure 11. Pathways for ink diffusion in traditional μ CP.....	23
Figure 12. Topography and feature descriptors of a PDMS stamp.	26
Figure 13. Schematic illustration of possible deformations and distortions of microstructures on PDMS stamps.	27
Figure 14. Contact inking of stamps for use in traditional μ CP.....	32
Figure 15. Microdisplacement printing using adamantane-terminated SAMs and <i>n</i> -alkanethiols.	33
Figure 16. Nanotransfer printing of gold films with Au-functionalized PDMS stamp and mercapto-terminated silicon substrate.....	37
Figure 17. Inkless catalytic- μ CP with an acidic ox-PDMS stamp on acid-labile, silyl ether-terminated SAMs.....	39

Figure 18. Heterogeneous catalysis through μ CP: Cu^{I} -catalyzed azide-alkyne coupling in areas of conformal contact.	40
Figure 19. Nanoscale-confined peptide synthesis using elastomeric stamps.	41
Figure 20. Catalytic- μ CP on H-terminated silicon surfaces using chemically-patterned flat stamps containing Pd or Pt catalyst NPs with alkene- or alkyne-terminated molecular ink.....	42
Figure 21. Electrochemical nanoimprinting with solid-state superionic stamps to pattern metallic nanostructures.	43
Figure 22. Preparation of polyurethane acrylate stamps.	45
Figure 23. Chemical catalytic- μ CP using piperidine-functionalized stamps on Fmoc-terminated SAMs.	46
Figure 24. Biocatalytic-microcontact printing.....	49
Figure 25. Synthesis of N^{ϵ} -acrylamido, N^{α} -bis(carboxymethyl)-lysine 3.....	52
Figure 26. a) Stamp fabrication platform. b) Optical micrograph of a polymerized NTA-acrylate stamp in contact with glass at 63X (10 μm scalebar).	54
Figure 27. ExoI enzyme (PDB: 1FXX). ¹⁵⁶ The active site residues are colored pink and the C-terminal His ₆ -tag is colored red.....	56
Figure 28. Schematic of ssDNA-alkanethiols adsorbed to gold before and after treatment with MCH.	58
Figure 29. Reaction between 3'-TAMRA-ssDNA-NH ₂ -5' ssDNA with ITC-functionalized glass slides.	59
Figure 30. Fluorescent microscopy of isothiocyanate-functionalized glass surface ($\lambda_{\text{excited}} = 530\text{-}560\text{ nm}$ and $\lambda_{\text{emm}} = 580\text{-}640\text{ nm}$).	62
Figure 31. Three juxtaposed AFM lateral force images taken of a surface that had been incubated with a drop of ExoI enzyme solution. ExoI enzyme in reaction buffer was deposited on the ssDNA-functionalized surface, creating a meniscus line of enzymatic digestion.....	63
Figure 32. Protocol for the activation of NTA-acrylamide stamp and biocatalytic- μ CP stamping on substrate-immobilized ssDNA.....	65
Figure 33. Biocatalytic- μ CP "writing." a) AFM height image of ssDNA-gold surface exposed to ExoI-immobilized stamps for 12 hours at 4 °C. b) AFM height	

image of feature edge and c) corresponding 1D height profile of edge at white line.....	68
Figure 34. AFM lateral force image and trace of a 15- μ m feature replicated from an acylamide hydrogel stamp via biocatalytic- μ CP.....	69
Figure 35. a) and b) Confocal fluorescence microscopy images of biocatalytic- μ CP on immobilized 3'-cyTAMRA-ssDNA. c) Optical micrograph of the stamp used for a and b in contact with glass.	71
Figure 36. Confocal fluorescence microscopy shows a linear trend between percent immobilized 3'-cyTAMRA-ssDNA and fluorescence intensity. Experimental results correspond to ~70% removal of the 3'-cyTAMRA fluorophore. ¹³⁷	73
Figure 37. MALDI-TOF spectroscopy of 3'-TAMRA-ssDNA-hexylamine-5' immobilized on glass slides before (left) and after (right) exposure to biocatalytic- μ CP with flat stamps (with ATT matrix).....	79
Figure 38. Synthesis of acrylamido-TEG-NTA lysine 11.....	84
Figure 39. The three regions of bifunctional SAMs on gold.	88
Figure 40. Reaction of a hydrolase with protected alkanethiols.	90
Figure 41. Methods to monitor activity of esterases with pNPEs.....	91
Figure 42. Testing AES and BioH activities with pNPA monitored via a change in pH over time.....	92
Figure 43. Testing ROL activity with pNPB monitored via a change in pH over time.....	95
Figure 44. Testing AES and BioH activity with pFPA monitored via a change in pH over time.....	98
Figure 45. Synthesis of long p-fluorinated benzyl esters 12, 13, and 14 from 11-mercaptoundecanoic acid 10.	99
Figure 46. Synthesis of short p-fluorinated benzyl esters 16, 17, and 18 from 4,4'-dithiobutyric acid 15.....	100
Figure 47. High-resolution XPS spectra of F1s, Au4p, and C1s peaks for SAMs formed on gold using para-fluorinated benzyl esters 12 and 16.	101
Figure 48. Testing AES activity with ester 16 monitored via a change in pH over time.....	103

Figure 49. Testing BioH activity with ester 16 monitored via a change in pH over time.....	104
Figure 50. Testing ROL activity with ester 16 monitored via a change in pH over time.....	105
Figure 51. Desired reaction between esterase and fluorinated benzyl ester-terminated SAMs on gold.....	106
Figure 52. High-resolution XPS spectra of F1s, Au4p, and C1s peaks for SAMs formed on gold using trifluorinated benzyl esters 13 and 17.....	111
Figure 53. Testing BioH and ROL activity with ester 14 monitored via a change in pH over time.....	112
Figure 54. Testing BioH and ROL activity with ester 18 monitored via a change in pH over time.....	114
Figure 55. Preparation of polyurethane acrylate stamps co-polymerized with 2-mercaptoethanesulfonic acid.....	120
Figure 56. Structure and characteristics of the bi-layered system for SAMs.....	123
Figure 57. Functionalization of bi-layered SAMs on silicon surfaces.....	126
Figure 58. Preparation of PU monomer 14 from isophorone diisocyanate 10 and polyethylene glycol 11 (avg mw: 400 g/mol). ¹⁰⁹	129
Figure 59. PU prepolymer mixture and fabrication of PU stamps. ^{109, 120}	131
Figure 60. SEM images of Si/SiO ₂ masters bearing 8 μm squares and corresponding patterned sulfonic acid-functionalized stamp. ¹⁴²	133
Figure 61. SEM images of Si/SiO ₂ masters bearing lines of varying widths (150 – 500 nm) and corresponding patterned sulfonic acid-functionalized stamp.....	134
Figure 62. Master and catalytic stamp defects due to removal of PMMA from master.....	135
Figure 63. XPS analysis of the NHS-hydrolysis efficiency with featureless catalytic stamps.....	138
Figure 64. SEM images of the patterned NHS-functionalized SAMs after reacting with catalytic stamp bearing 8 μm squares.....	140
Figure 65. SEM images of the patterned NHS-modified SAMs on silicon after reacting with patterned catalytic stamp bearing lines with 150, 320, and 500 nm widths.....	142

Figure 66. SEM images of surfaces patterned with different acidic stamps.....	148
Figure 67. Dependence of pKa on the decrease in C1s/Si2p ratio vs. stamping time for catalytic hydrolysis of the NHS ester on surfaces.....	149
Figure 68. Dependence on pKa on the decrease in %C on NHS-functionalized surface over time during stamping with acidic stamps.....	150
Figure 69. Linear fit of second-order kinetics for surface-immobilized acidic hydrolysis of NHS-ester terminated SAMs.....	151

List of Abbreviations

ACN – acetonitrile

AES – acetyl esterase

AFM – atomic force spectroscopy

APS – ammonium persulfate

ASF – atomic sensitivity factor

ATT – 6-aza-2-thiothymine

Boc – *tert*-butyl carbamate

BT - butanethiol

CAD – computer-aided design

CDCl₃ – deuterated chloroform

CHCl₃ - chloroform

CH₂Cl₂ – dichloromethane

CuAAC – Cu azide-alkyne cycloaddition

D₂O – deuterium oxide

DCM – dichloromethane

DMAP – 4-dimethylaminopyridine

DMF – dimethylformamide

DNA – deoxyribonucleic acid

dsDNA – double-stranded deoxyribonucleic acid

DTT – dithiothreitol

EBL – electron beam lithography

ECT – eicosanethiol

EDC – 1-ethyl-3-[3-dimethylaminopropyl]carbodiimide

ESI-MS – electrospray ionization mass spectrometry

EtOAc – ethyl acetate

ExoI – Exonuclease I

Fmoc – 9H-fluoren-9-ylmethoxycarbonyl

Hex – hexane

His₆-tag – hexahistidine-tag

IC – integrated circuit

IPA – isopropyl alcohol

IPTG – isopropyl thiogalactopyranoside

ITC – isothiocyanate

LFM – lateral force spectroscopy

MALDI-TOF – matrix-assisted laser desorption ionization – time-of-flight

MCH – mercaptohexanol

MeOH – methanol

MIBK – methyl isobutyl ketone

m.p. – melting point

MPTMS – mercapto-propyl-trimethoxysilane

NHS – *N*-hydroxy-succinimide

NMR – nuclear magnetic resonance

NTA – nitrilotriacetic acid

NP – nanoparticle

ox-PDMS – oxidized polydimethylsiloxane

PBS – phosphate buffer solution

PDMS – polydimethylsiloxane

PEG – polyethylene glycol

pFPA – para-fluorophenyl acetate

PL – photolithography

PLE – pig liver esterase

PMA – phosphomolybdic acid

PMMA – poly(methyl methacrylate)

pNPA – para-nitrophenyl acetate

pNPB – para-nitrophenyl butyrate

pNPE – para-nitrophenyl ester

PTFE – polytetrafluoroethylene

PU – polyurethane acrylate

R_a – arithmetic average roughness

R_{rms} – root mean square roughness

ROL – *Rhizopus oryzae* lipase

SAM – self-assembled monolayer

SDS – sodium dodecyl sulfate

SEM – scanning electron microscopy

ssDNA – single-stranded deoxyribonucleic acid

TAMRA – tetramethyl-6-carboxyrhodamine

TBDMS – *tert*-butyl dimethyl silyl

TEG – tetraethylene glycol

TEMED – N,N,N',N'-tetramethylethylenediamine

TFA – trifluoroacetic acid

THF – tetrahydrofuran

TIC – total ion count

TMS – trimethylsilyl

UV – ultra-violet

μCP – microcontact printing

XPS – X-ray photoelectron spectroscopy

Acknowledgements

This Ph.D. degree is the culmination of my formal education and therefore, I would like to thank every instructor, coach, and mentor who has helped guide my educational growth and experience. Foremost, I would like to extend my deepest gratitude to my graduate advisor, Prof. Eric J. Toone, for his exceptional guidance and unending patience for the last six years – to him, I will always be indebted and eternally grateful. I would also like to thank Profs. Robert L. Clark and Stephen L. Craig as well as Drs. Daniel G. Cole and Kurt D. Wulff, whom first inspired me as an undergraduate summer scientist. Truly, I would have never pursued a graduate degree without the aforementioned people. I would also like to thank my preliminary/dissertation exam committee for their ongoing advisement throughout my tenure at Duke. Last, but certainly not least, to the professors in the Division of Molecular and Life Sciences at Loras College, particularly Profs. David C. Speckhard, Kenneth W. McLaughlin, and Suzanne Seleem, thank you for your wisdom, honesty, and encouragement.

I must also thank so many of my peers at Duke. To the past and present members of the Toone lab, thank you all for providing such a collaborative and unique laboratory environment in which to work. Foremost, I must thank Dr. Alexander A. Shestopalov for his exceptional knowledge and advice, continued

effort on our joint research endeavors, comedic commentary, and delightful cooking. To Dr. Matthew J. Walters, thank you for being an outstanding graduate student mentor and friend. To Carleen Morris, thank you for your diligent help in our joint research projects as well as to Dr. Andrea Luteran-Yackenovitch, Dr. James Parise, Dr. David Gooden, David Carlson, Allison Schmitt, Yves Wang, and Jason King, thank you for research advice and your friendship. Many thanks to Dr. Matthew S. Johannes from the Clark lab for continued willingness to collaborate with us, Amanda J. Hoertz from the McCafferty lab for her research help and advice, and Romin Bonakdar for his help in the laboratory. To my incredible friends across the disciplines at Duke, especially TMK, KAR, HG, and LOC, and those involved in the GPSC Men's Campout Committee, PLU, and Girls' Lunch, thank you for making graduate life exciting and totally unforgettable – I will cherish our memories together forever.

Finally, I would like to thank my parents, Noel and Judy, for their unwavering love, encouragement, visits, and plane tickets home. To my friends from the Midwest, thank you for your emails, phone calls, visits, and presents especially Dr. Jenny Arens-Gubbels and Sarah Wiechert. I must also thank Michael Hart, my best friend and love of my life, for all his support and encouragement during the most difficult years of my life so far.

1. Introduction

1.1 Overview

The first efforts to manipulate surfaces in order to store and convey information were developed by Cro-Magnon man (*Homo sapiens*) over 34,000 years ago. These paintings of animals and stenciled hand prints on cave walls not only represented a new art form,¹ but also commenced the record of human history by revolutionizing communication beyond time and space. For many thousands of years, writing on stone, cloth, and paper was used for the decoration of garments, the production of documents, and the creation of art.² However, when more than one copy of a text or design was required, copies had to be created serially by hand. Thus, for example, from the 5th to the mid-15th century, Catholic monks devoted entire lifetimes copying the Bible to spread Christianity to people throughout the world.³ The need for copies inspired many cultures to seek alternatives to time-consuming serial processes when more than one copy of an object was needed.

To increase copy count more easily, parallel methodologies for writing characters, or “printing,” were developed in which more than one complete character or figure could be produced simultaneously. Relief printing methods date back to 3,000 B.C. in Mesopotamia, in which an impress was rolled onto clay

tablets to form complex works of art. Circa 200 A.D., a wood block with relief features was first used in China to print three different colors on a silk cloth; soon after this “block printing” technique was used to print solid text. Similar methodologies were used in Egypt, Europe, and India a few centuries later until the development of movable type around 1040 A.D. The first movable type system, credited to the Chinese Bi Sheng, consisted of movable characters made of porcelain. These characters were placed together on a composing stick, inked, and used to print ordered characters in a parallel fashion multiple times. Johannes Gutenberg adapted this method in the mid-15th century and invented the well-known and revolutionary movable type printing press. The “Gutenberg press” not only provided the world with a massive quantity of inexpensive Bibles, but also increased the literacy of the world’s population beyond higher social classes. Gutenberg’s invention is considered a giant step toward the democratization of knowledge by transforming the world’s printing techniques and communication forever.⁴

This great feat in printing still had many serial and time-consuming aspects. Single characters had to be molded out of metals and placed in separate lines. Only after thousands of these characters were constructed could they be placed into rows, inked, and pressed onto paper. Finally after placing thousands

of characters, the resulting image could be stamped as many times as desired, but the lines had to be disassembled before a new page could be put together. This process was convenient for low-copy number needs, but was not practical for very high-throughput demands. In addition, illustrations could not be placed in books using movable type processes. The alleviation of the latter problem was developed only a few years after the invention of the Gutenberg printing press, and evolved into a new popular method for the mass production of images for books and posters. Instead of molding raised characters, templates for intaglio printing were constructed by etching or engraving patterns into a metal surface. To make prints from this master, the entire surface was inked, the excess ink wiped off, and paper was applied at high pressures. The paper was forced into the recesses of the intaglio both inking it in areas of contact and producing slightly-raised images on the paper.⁵⁻⁶

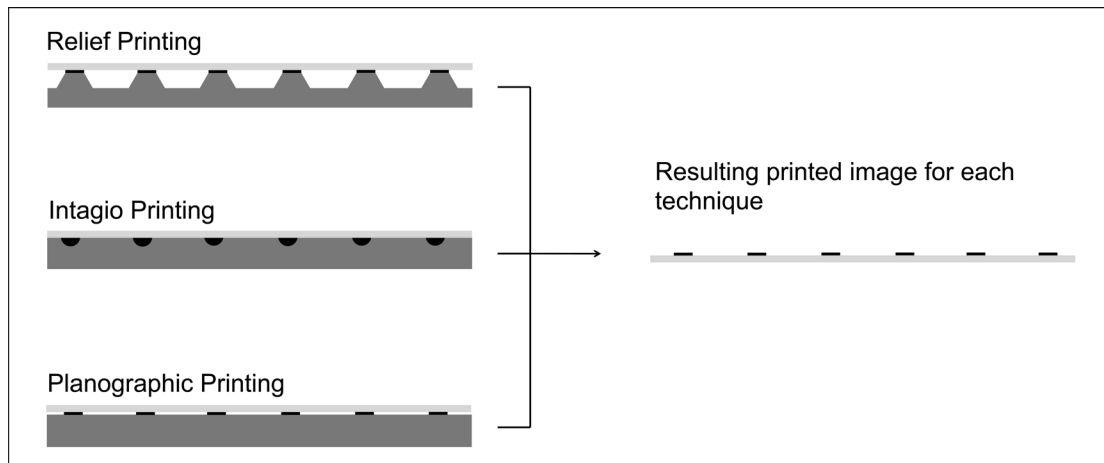


Figure 1. Diagram showing relief, intaglio, and planographic printing techniques on paper. In each, a master (dark gray) is inked (black) and placed in contact with paper, resulting in the printed image on the right.

Despite the success of the Gutenberg and intaglio processes, new methods to improve the laborious printing process and to decrease printing costs were needed to keep pace with the growing literacy of the population. At the turn of the 19th century, the German playwright Alois Senefelder invented the first chemical method of printing – a planographic technique he called “lithography,” from the Greek words for “stone” (“lithos”) and “to write” (“graphein”). Originally intending to copy his own plays, Senefelder realized the importance of his invention not only as an expedient method for the reproduction of his own work, but for music and drawings as well.⁷⁻⁸ Chemical lithography exploited the chemical concepts of hydrophobicity and hydrophilicity using by using a water-repulsing pencil made of wax, soap, and lampblack to draw images on

hydrophilic slabs of limestone. After the image was completed, the entire surface of the limestone was covered with gum arabic containing a small amount of nitric acid – etching the entire surface except for those areas protected by the waxy substance. The mixture was removed after etching and oily ink was rolled onto the wetted surface, resulting in the etched (hydrophilic) areas rejecting the ink, thus perfectly inking only the hydrophobic image on the stone. A press was generally used to transfer the inked pattern onto paper, resulting in an accurate mirror image of the original drawing.⁶ This technique was ideal for high-throughput copying incorporating both characters and images in one plane, expediting the printing process far beyond the Gutenberg press. Over the centuries, Senefelder and his successors have vastly improved the materials and methodology of lithography. As a result of these advances, offset lithography remains the most widely-used method for the high-throughput reproduction of books, posters, and maps.⁶⁻⁸ Photolithography, the process of chemically altering a surface material using light, was discovered in 1822 by Nicéphore Niépce in France. Using an etched print of Pope Pius VII, Niépce reproduced the image through a glass plate by exposure to sunlight for several hours on the first known negative resist – bitumen. These areas exposed to sunlight became hard

and soluble to a mixture of turpentine and lavender oil. Eventually, Niépce streamlined his process into the invention of photography.⁹



Figure 2. Lithography stone (left) and mirror-print (right) on paper.¹⁰

Remarkably, the concepts of photolithographic printing inspired an entirely new system of printing on surfaces that resulted in a different form of information storage over a hundred years later – the microfabrication of materials for integrated circuits (ICs). Modern-day photolithography is a top-down fabrication technique that utilizes the exposure of a photosensitive polymer deposited on a flat metal surface to light, changing the dissolution properties of the cured polymer. Other metals (or molecules) can be deposited on the surface, polymer again applied and exposed, and the process repeated until the desired circuitry had been formed.

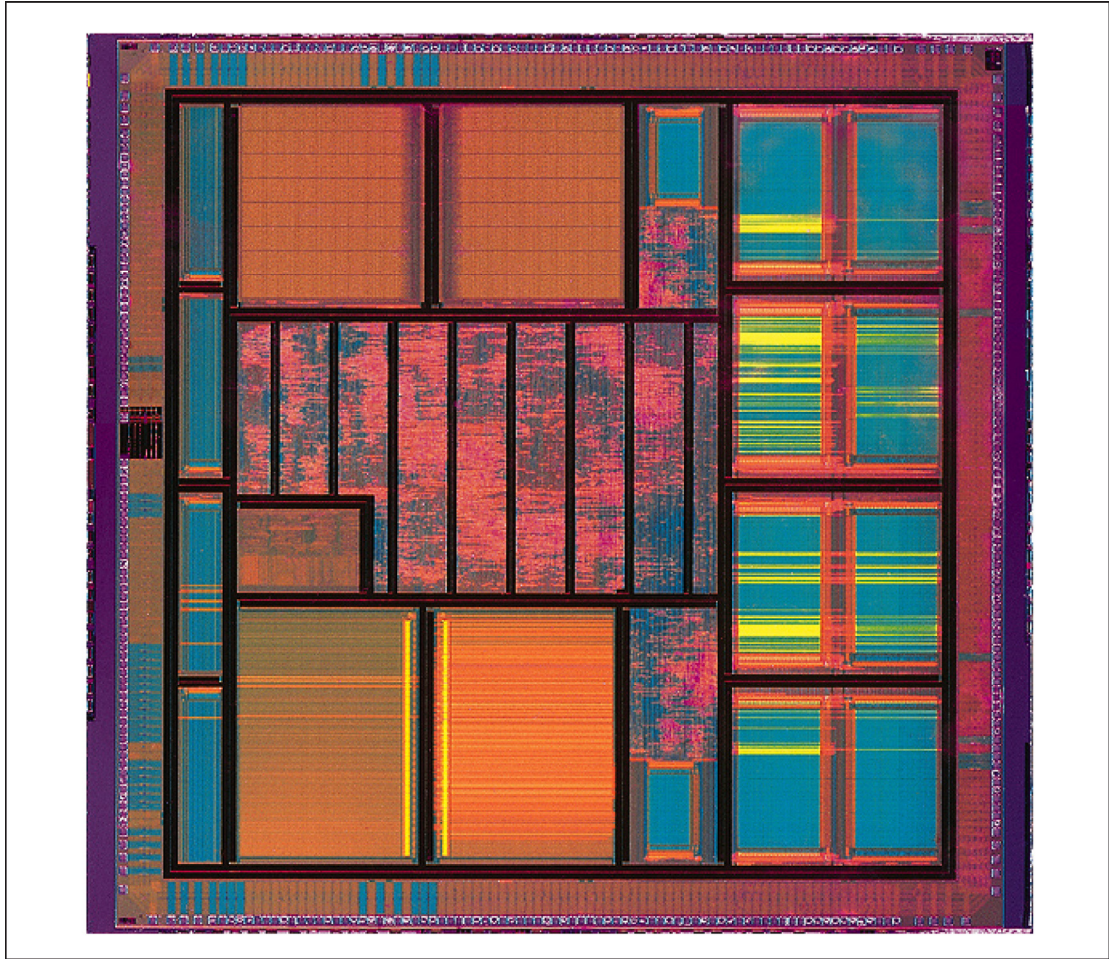


Figure 3. Integrated circuit of Atmel Diopsis 740 System on Chip.¹¹

The integrated circuit (IC) was invented independently in the late 1950's by both Jack Kilby (Texas Instruments) and Bob Noyce (Fairchild Semiconductor) vastly decreasing the size of computers built in the 1940's containing circuits constructed only of discrete components and tubes to smaller, more efficient, and more economical computers consisting of integrated components. Since the invention of the IC, the number of transistors that can be inexpensively placed on an IC doubles every two years on average. Gordon E. Moore, the co-founder of

Intel, first made this observation in 1965 and “Moore’s Law” has held true until present day.¹²⁻¹³ Today, photolithography is the foremost parallel technique used to generate patterned surfaces for ICs as well as the most widely-used method for the parallel fabrication of 2D patterned surfaces for biological and chemical assays and the production of patterned templates for the molding of polymers for soft lithographic methods on the micro- and nanoscales.^{9, 14} Recent advances in photolithography permit resolution below 30.0 nm¹³ and fabrication of 45-nm full transistors.¹⁵

Although still the foremost high-throughput parallel patterning technique for high resolution features below 100 nm, photolithography remains of only limited utility due to requirements for expensive, complex instrumentation, long set-up times, and a limited set of reliable photoresists.¹⁶⁻¹⁷ The resolution of photolithography is determined by the behavior of light and high-frequency radiation, limiting its utility for patterning non-planar and large surfaces. Finally, photolithography and related serial patterning methods require the dust-free environment of a clean room, further increasing cost and limiting the widespread use of the technique.¹⁶⁻²³ As such, photolithography is of only limited utility in fields such as (bio)organic sensing and organic thin-film

semiconductors, which require the use of ordered molecular systems on conventional, inorganic semiconductor materials.

The development of soft lithography in 1993 by Kumar and Whitesides²⁴ circumvented many of the limitations of photolithography. Soft lithography uses a flexible elastomeric stamp as the key element for pattern transfer to substrate and organic molecules as dyes, as opposed to the inorganic materials commonly used in pattern transfer in lithographic methods.²⁵ Microcontact printing (μ CP), the most common embodiment of soft lithography, uses an elastomeric stamp to print surface features in relief through the self-assembly of molecular inks on a surface in areas of conformal contact. Originally, μ CP of alkanethiols on gold was used as an etch resist for potential applications in electronics as a fast, convenient, and inexpensive alternative to photolithographic methods.^{24, 26} Methyl-terminated, long-chain ($>C_{16}$) alkanethiols provided the best etch resists on gold against cyanide-based etchants (1 M KOH, 0.1 mM KCN, sat. O₂, room temperature).²¹ In addition to using microstructures of gold as masks for the subsequent etching of silicon, electroless deposition of nickel, optical diffraction gratings, patterned crystallization, and patterning of proteins using μ CP were demonstrated within a year of its invention.²¹ Because μ CP did not directly use light to pattern surfaces, μ CP and related soft lithographic methods were

originally intended to replace photolithography in the electronics industry.¹⁷ However, due to various advances in photolithography, μ CP has never exceeded resolution of photolithography.

μ CP has now gained universal recognition as a versatile, simple, and inexpensive technique for patterning large surface areas with micro- and nanoscale features, obviating both the high costs and expensive equipment of photolithography.^{16, 23, 27} Due to the accessibility of the technique, μ CP has become the method of choice for patterning a variety of both planar and non-planar substrates with biological, organic, and inorganic materials^{17, 25, 28-30} for a range of purposes, including the fabrication of DNA, proteins, and glycopolymer microarrays;^{14, 31-45} biosensors;⁴⁶⁻⁴⁷ cell patterning and tissue engineering;⁴⁸⁻⁵⁴ the preparation of organic thin-film transistors and photovoltaic devices;⁵⁵⁻⁵⁹ and microelectronics.^{21, 60-68} Here we review traditional μ CP, its potential limitations, and discuss unconventional μ CP approaches that aim to circumvent the diffusive resolution limitations of traditional μ CP.

1.2 Principles of microcontact printing

The goal of soft lithography is to replicate the features of a master mold for a high-throughput, low-cost pattern transfer. To fabricate a stamp capable of pattern transfer via μ CP, a master mold is first made by conventional

lithographic techniques. Pre-polymer is added to this mold, cured, and peeled off, providing a negatively-patterned stamp in relief. The stamp is inked with a surface-reactive molecule and placed on a cognate substrate, forming SAMs in the areas of conformal contact (Figure 4).

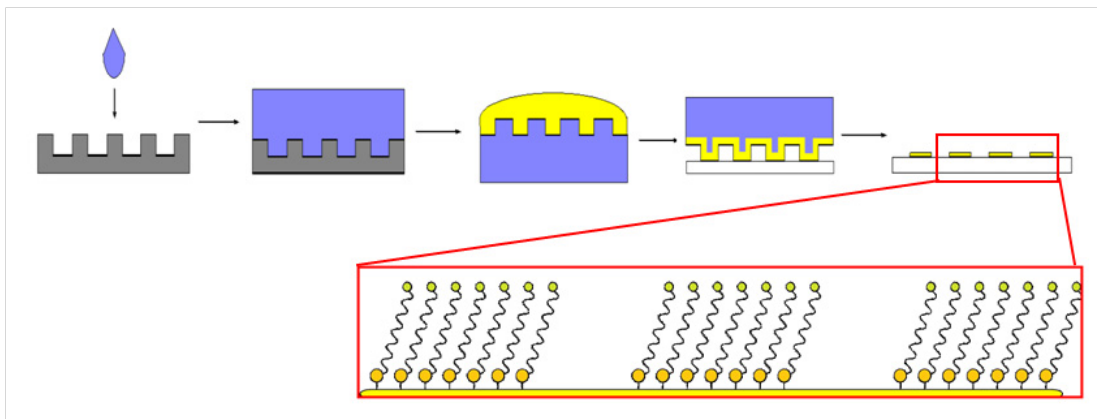


Figure 4. Overview of fabrication of stamp for μ CP using a silicon master and subsequent stamping of alkanethiolate SAMs.

1.2.1 Master and mask fabrication

Most elastomeric stamps for traditional μ CP are molded against masters made by photolithography or e-beam lithography (EBL).^{9, 17, 25} The majority of all present-day lithographic techniques have three main aspects to their design: i) a material (normally a resist) capable of being manipulated on the micro- and nanoscales in order to ii) fabricate a master or a mask as a pattern template, and, iii) a medium or set of conditions capable of transferring the patterns from the master/mask to other surfaces.¹⁸

Conventional methods for pattern fabrication using lithographic methods are generally serial and slow, involving some type of writing tool to either etch part of the surface, deposit a material on a surface, or chemically modify the surface to create a pattern.¹⁸ The most popular methods for generating masters and masks for both photolithography and soft lithography involve the use of a top-down serial writing technique.⁹ The resolution of this technique depends on the “sharpness” or the radius of the writing tool, which can range from features visible by the naked eye down to single nanometers.

EBL is the method of choice for the fabrication of both masters and masks for patterning small, high-resolution features 5 nm and larger.^{16, 18, 29} EBL uses tightly focused, high-energy electrons to expose electron-sensitive resists, resulting in feature sizes from micrometers to single nanometers.^{16, 69} Computer aided design (CAD) is incorporated to direct the electron gun, making specific patterns ranging from actual text and pictures to dots, lines, and shapes.⁹ After the resist is exposed to the electron beam, it is developed in an appropriate solvent mixture to obtain the patterned surface. Metals and other materials can be deposited on the original pattern to add complexity to the original pattern, such as in the generation of ICs. Alternatively, pre-polymer can be added to

form a stamp containing the mirror image of the master pattern and used in mold fabrication.^{16, 18}

Masks for photolithography and masters for soft lithography displaying micron and sub-micron features are fabricated using EBL in very similar ways, but using different substrates. The substrate for a photomask is typically optically flat glass or quartz covered with a thin layer of an adsorber pattern metal such as chromium. Masters for soft lithographic techniques generally do not need to be transparent for subsequent pattern transfer and are typically made of silicon.^{9, 69-70} Robust photomasks and masters can often be reused multiple times without damage, adding to the parallel fabrication intrinsic to both techniques.²¹ Many facilities provide photomasks bearing various features, such as a matrix of squares or lines of varying widths, for general use so they need not be created manually by the user for pattern generation by photolithography.

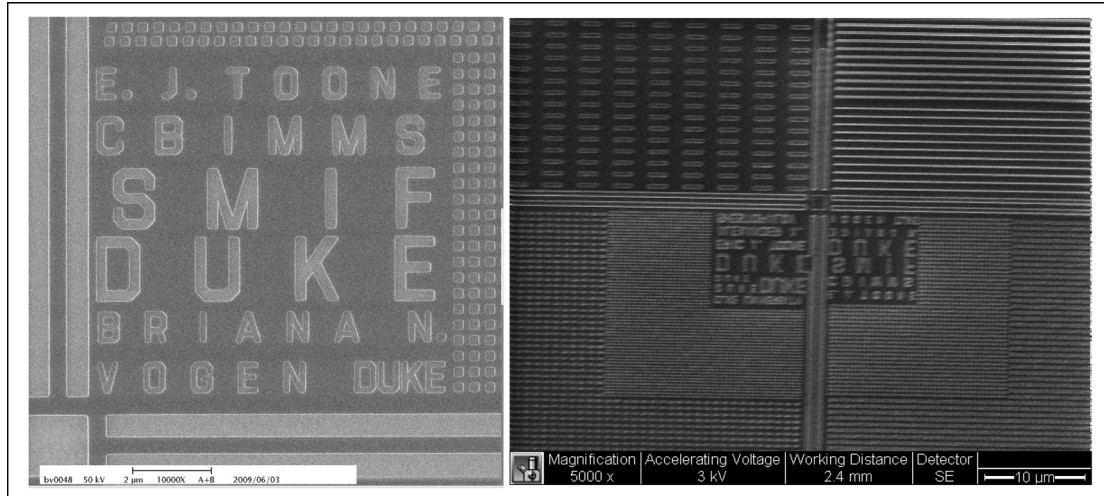


**Figure 5. SEM images of Si/PMMA master for soft lithography (left).
Elastomeric stamp made from master (right).**

Once a resist has been spin-coated on the substrate, baked, and exposed to an electron beam, the polymer chains of a resist can undergo one of two chemical processes: i) cross-linking resulting in an increase in molecular weight and reduction of solubility in a developer, or ii) chemical bond cleavage resulting in a decrease in molecular weight and increase of solubility in a developer.^{16, 18, 22, 69} The former process describes a negative resist such as SU-8 while the latter describes a positive resist such as polymethylmethacrylate (PMMA). In both cases, substrates are developed in a corresponding solvent/developer solution resulting in relief pattern formation such as a 1:3 methyl isobutyl ketone: isopropyl alcohol solution for PMMA. As shown in Figure 5, this resulting

pattern can be used directly in subsequent stamp fabrication for soft lithography.^{17, 25, 28}

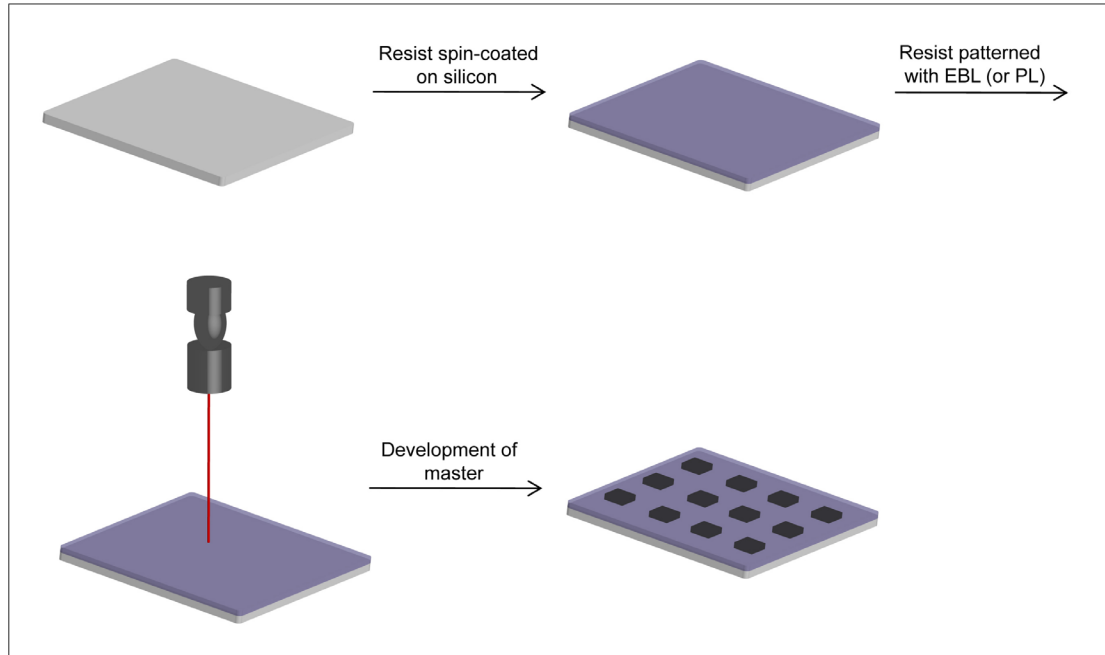


Figure 6. Master fabrication for soft lithography via EBL or photolithography (PL).

Finally, wet chemical etching through the exposed chromium absorbing layer and removal of the remainder of the photoresist produces a photomask ready for pattern replication via photolithography and/or soft lithography.^{16, 18, 22,}

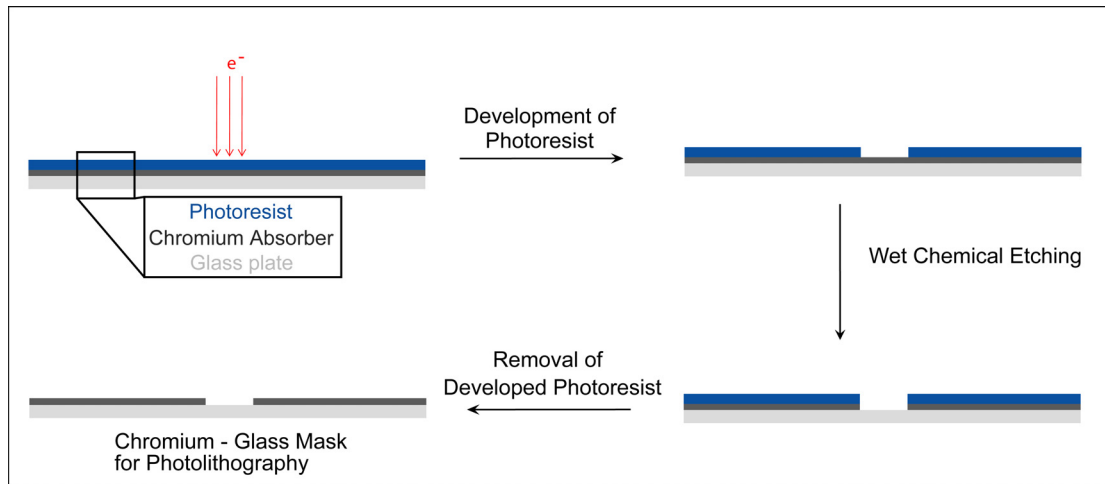


Figure 7. General mask fabrication for photolithography using EBL and a positive resist.

In summary, masters for use in soft lithography are patterned either directly by EBL for sub-micron features or by photolithography for large features in general-use cleanrooms. EBL is also used to pattern high-resolution transparencies for use in photolithography as photomasks.

1.2.2 Stamp fabrication using PDMS as a stamp material

The most commonly-used stamp material for μ CP is polydimethylsiloxane (PDMS), commercially-available from Dow Corning as Sylgard 184. A PDMS pre-polymer is first mixed with curing agent (Sylgard Curing Agent 184) in a 10:1 (v:v) mixture, and added to the fabricated master. The PDMS is then cured by heating from 100-150 °C for 10-45 minutes or left at room temperature overnight. Finally, the PDMS is removed from the master and cut to size.^{25, 71}

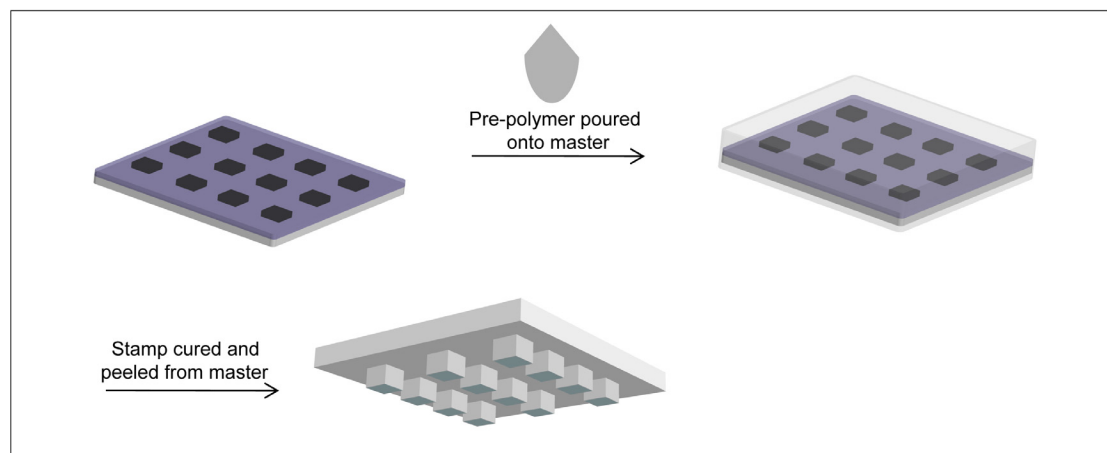


Figure 8. Stamp fabrication from master for use in μ CP.

In addition to commercial availability, PDMS has several attractive properties for use in μ CP. First, PDMS is an isotropic elastomer capable of conformal contact with surfaces over large surface areas (~ 30 cm x 40 cm)^{17, 24-25} as well as deformable enough to transfer pattern to nonplanar surfaces.^{17, 25, 72-73} The

Young's modulus of PDMS is ~750 kPa, which allows PDMS to both conform to surfaces and effect stamp release from molds.⁷¹ Second, cured PDMS provides a chemically inert surface with a low interfacial free energy ($\sim 2 \times 10^{-3} \text{ J/m}^2$),^{71, 74} allowing a PDMS replica to be easily released from masters without damaging the master or itself.^{25, 71} Third, PDMS cures as an isotropic, homogenous mixture that is optically transparent down to 240 nm.^{25, 71} Optical transparency ensures good conformal contact with a surface. Fourth, PDMS is a robust stamping material, and has been able to stamp over 100 times over a period of months without degradation of the polymer or transferred patterns.^{17, 25, 64} Elastomeric PDMS stamps are capable of printing features down to ~300 nm over large surface areas.²⁸ Fifth, the mechanical properties of cured PDMS are minimally affected by ethanol (2.5% swelling), a solvent in which alkanethiols are soluble.^{17, 25, 71, 75} Ethanol is volatile and rapidly evaporates from the surface of the stamp, concentrating the thiol ink.⁷⁵ Sixth, the surface chemistry of PDMS can be readily manipulated to facilitate stamping of various chemical and biological molecules/cells.⁷⁶⁻⁸⁰ One of the most popular surface passivation techniques for PDMS is oxygen plasma treatment, which creates a hydrophilic surface for stamping polar inks and biological molecules.^{28, 76, 81}

1.2.3 Pattern transfer and SAM formation

Historically the most common ink-substrate system for μ CP is alkanethiolates and gold.^{21, 24, 26} Gold is a popular substrate for SAMs and μ CP for several reasons. 1) Gold is readily available commercially and easily coated by vapor deposition. 2) Gold does not oxidize readily, making it inert outside a clean room and at atmospheric pressure in a laboratory setting. 3) Protocols to pattern gold using photolithographic methods, chemical etchants, micromachining, etc. are well-known and easy to use.⁸² 4) Monolayers on gold are easily analyzed using existing and varied analytical techniques such as quartz crystal microbalances, ellipsometry, and X-ray photoelectron spectroscopy. 5) Gold binds thiolates with high affinity⁸³ and the resulting monolayers of simple, long-chain alkanethiols such as dodecanethiol are well-ordered and crystalline.⁸⁴ In fact, the affinity between thiols and gold is so high that thiols will displace other materials from the surface, including chemisorbed disulfides.⁸⁵ Although formed at room temperature, these monolayers can withstand relatively harsh environments and elevated temperatures.⁸² 5) Gold is biocompatible – cells, DNA, proteins, and other biological materials have been patterned on gold and retained biological viability.^{19, 23, 28, 35-36, 41-43, 86-87}

When forming highly-ordered SAMs on gold, the sulfur atoms of alkanethiols form a $(\sqrt{3} \times \sqrt{3})R30^\circ$ overlayer on Au(111) where the sulfur atoms (yellow) are positioned in the 3-fold hollows of the gold lattice (brown). To maximize van der Waals interactions between neighboring chains, the alkanethiols orient themselves $\sim 30^\circ$ from the surface normal and twist relative to one another by $\sim 90^\circ$ (Figure 9).^{21, 49, 82}

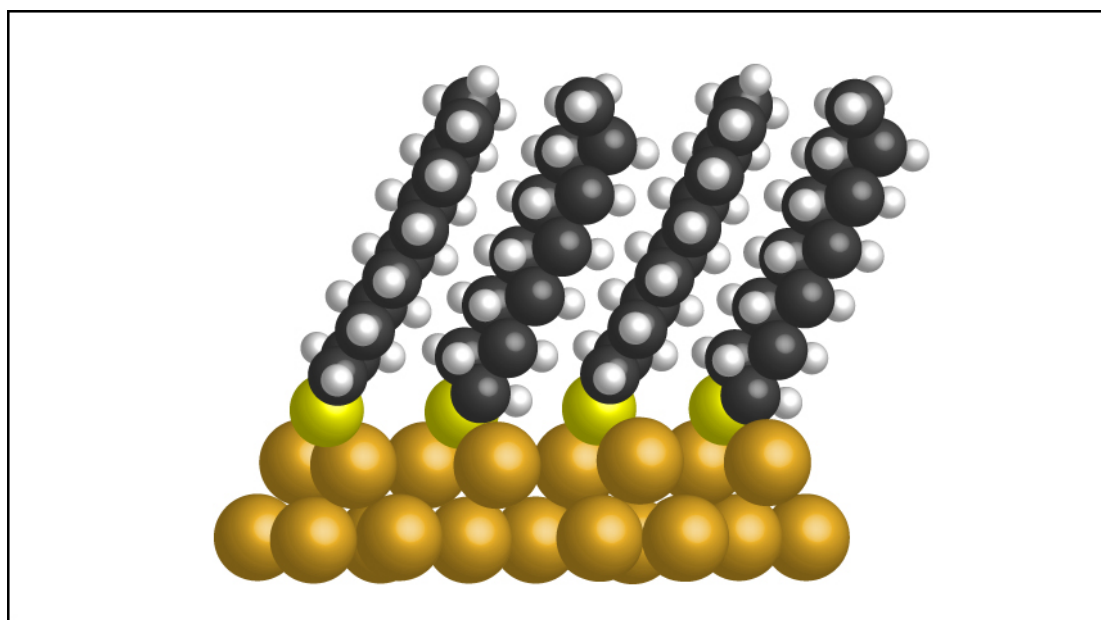


Figure 9. Side-view diagram showing the orientation of bound alkanethiolate species to a crystalline gold surface.

To form patterns of monolayers on gold, a PDMS stamp is typically inked with an ethanolic solution of alkanethiols or alkanedisulfides (0.1-10 mM) for a few seconds to a few minutes. The stamp is placed on a clean, gold substrate for a few seconds to a few minutes to transfer the surface-reactive alkanethiols or

alkanedisulfides to the gold substrate (Figure 10). The voids on the stamp serve as transport barriers and prevent SAM formation in areas not contacted by the stamp. Post-stamping, the stamp can be washed to remove any remaining ink and either the same or a different ink applied to the stamp for patterning other surfaces.^{75, 82} Once the alkanethiols are printed, they act as protective resists to cyanide etchants. Unprotected gold is completely dissolved by etching.²¹

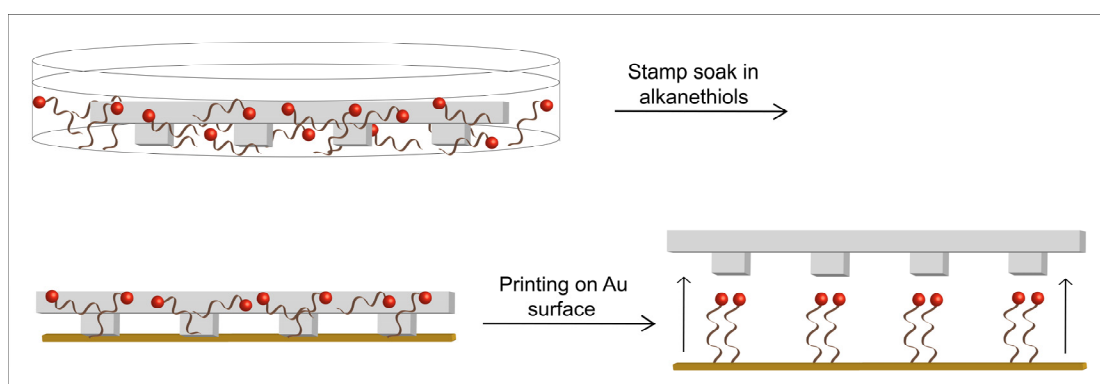


Figure 10. Traditional μ CP using a PDMS stamp to print alkanethiols on gold.

In summary, μ CP is an inexpensive, parallel process for patterning large surfaces with self-assembled monolayers. This methodology is easily accessible to non-specialist scientists due to minimal environmental constraints and commercial availability of required materials.

In spite of its many advantages, traditional μ CP of alkanethiols and disulfides on gold using a PDMS stamp has a multitude of restrictions that limit

its use in patterning features around or below 300 nm.^{28, 75} Below we consider the nature and origin of these limitations.

1.3 Limitations of microcontact printing

The invention and potential application of μ CP for patterning surfaces was immediately realized in the growing field of microfabrication. Within five years of its invention, μ CP had been expanded to other substrates such as silicon copper, and palladium.^{17, 21, 25, 47, 88} Terminal functional groups on alkanethiols were explored as a means to control the surface properties to facilitate coupling reactions at the surface. Finally, various biological and chemical molecules were patterned directly onto surfaces, forming patterns of proteins, monolayers of DNA, non-fouling polyethylene glycol monolayers, and so forth.^{14, 17, 19, 21, 25, 28, 36, 41-42, 47, 49, 76, 80, 86-96} In spite of these novel demonstrations of the power of μ CP, three intrinsic properties of traditional μ CP limit the applicability of the technique for patterning features below 300 nm: ink diffusion,^{22, 62, 75, 97-99} stamp deformation,¹⁰⁰⁻¹⁰⁶ and restricted availability of patternable substrates eligible for use in technological applications.^{28, 49, 107}

1.3.1 Molecular ink diffusion

Traditional μ CP utilizes molecular ink diffusion from a stamp to a substrate for pattern transfer in the areas of conformal contact.^{84, 108} Despite the

clear and demonstrated utility of this μ CP approach to pattern surfaces, the diffusive nature of pattern transfer limits the feature resolution possible with μ CP. Unwanted diffusion occurs during printing, depositing molecular ink beyond areas of conformal contact.

When an elastomeric stamp is brought into conformal contact with a substrate, a variety of diffusive processes deposit ink on and beyond the limits of the stamp feature, diminishing pattern resolution.⁷⁵ As shown in Figure 11, the ink not only diffuses through the stamp (paths 1-2) and deposits onto the substrate in the areas of conformal contact, but also travels on the surface through lateral spreading (paths 3-5) and through the ambient in the gas phase (path 6).^{22, 75, 99} The extent of lateral diffusion depends on stamping time as well as the nature and quantity of ink on the stamp.

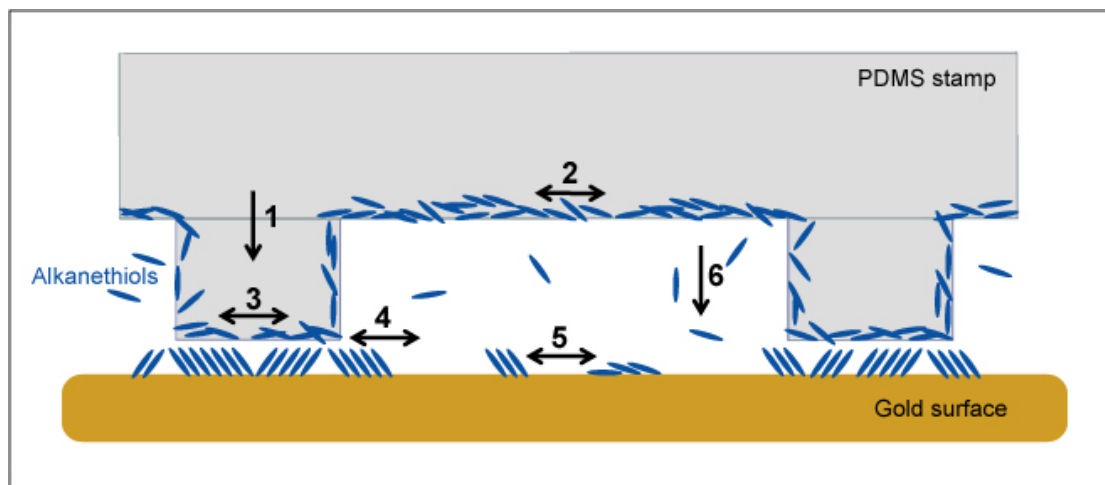


Figure 11. Pathways for ink diffusion in traditional μ CP.

Most stamps are dried with a stream of inert air before printing, limiting the lateral spreading of inks on the surface of the stamp (paths 2 and 3). However, due to the bulk properties of PDMS, a large volume of molecular ink is retained within the stamp, constantly resupplying the surface with fresh ink. Lateral diffusion of the ink on the surface has been shown to cause at least 50 nm of feature enlargement at the edges, independent of time and ink concentration.^{75, 109} To decrease spreading, short stamping times with low ink concentration result in reduced diffusion, but also in poorly ordered, weakly protective SAMs.⁷⁵ Lateral spreading from initial attachment points (path 5) can also occur in μ CP, although the strength of the Au-S bond minimizes this effect for patterning gold.^{75, 110}

Diffusion through the gas phase is even more difficult to control. The extent of gas diffusion during stamping is directly proportional to vapor pressure, and consequently molecular weight.^{75, 100} Even high molecular weight inks such as hexadecanethiol (258.51 g/mol; m.p. 18-20 °C) and eicosanethiol (314.62 g/mol; m.p. 37 °C) diffuse through the gas phase during μ CP.¹⁰⁰

The most accurate pattern transfer using traditional μ CP of alkanethiols on gold utilized a high-molecular weight ink which is a solid at room temperature, eicosanethiol (ECT), with a PDMS stamp bearing sub-micron

features. Accurate pattern transfer of features ~ 300 nm was achieved with 150 nm broadening of features using a 0.2 mM ethanolic solution of ink and 3 seconds stamping time.⁷⁵

Clearly, ink diffusion in traditional μ CP is a double-edged sword – without sufficient stamping time (~ 3 seconds for small features of eicosanethiol (ECT)), printed alkanethiols cannot fully protect an area in conformal contact with a cognate surface by forming ordered monolayers. However, increasing the stamping time will result in increased blurring of edge features and thus decreased resolution of pattern transfer.

1.3.2 Stamp deformation

Ink diffusion is not the only effect limiting the resolution of traditional μ CP. Stamp deformation of PDMS due its elastomechanical properties limits feature size on a single stamp. The low Young's modulus of PDMS (~ 750 kPa) allows bending around nonplanar surfaces to achieve conformal contact; however, the same effect also limits the mechanical stability of relief features on a stamp. The structural features of height h , distance between features d , and feature width l are limited relative to one another in producing pattern without deformation of features (Figure 12). Beyond certain aspect ratios, stamp

deformations occur during stamping, resulting in defects during pattern transfer.^{75, 101, 103}

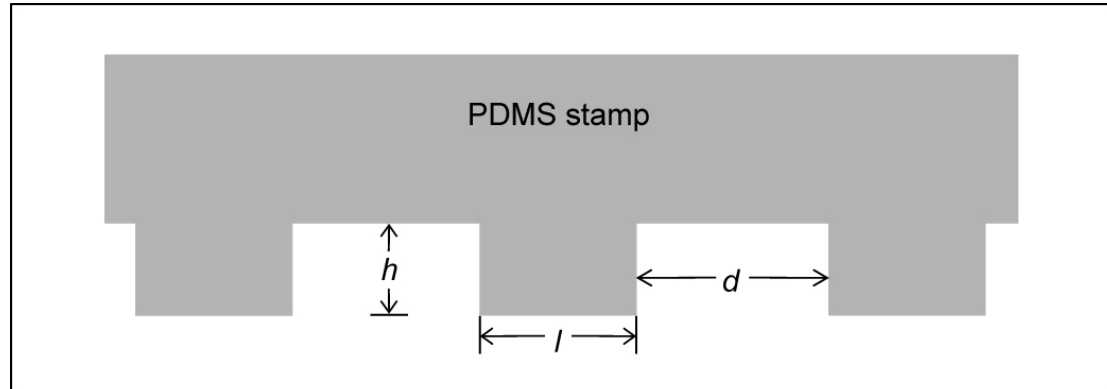


Figure 12. Topography and feature descriptors of a PDMS stamp.

The effects of gravity, capillary forces, and adhesion play significant roles in the deformation of features in elastomeric stamps during printing.^{75, 103} As shown in Figure 12, buckling of the stamp features under their own weight or upon loading can occur if an aspect ratio (h/l) of 0.2 – 2 is not maintained.^{62, 75, 103} Aspect ratios above 2 produce a particular type of lateral collapse of features during the stamping process. Due to the adhesive nature of capillary forces, liquid remaining on the surface and/or between stamp features can result in an adhesive pairing of features instead of complete buckling (Figure 13).^{101, 103, 111} When the aspect ratio is below 0.2, “roof collapse” or stamp sagging occurs between features due to gravity.¹⁰³

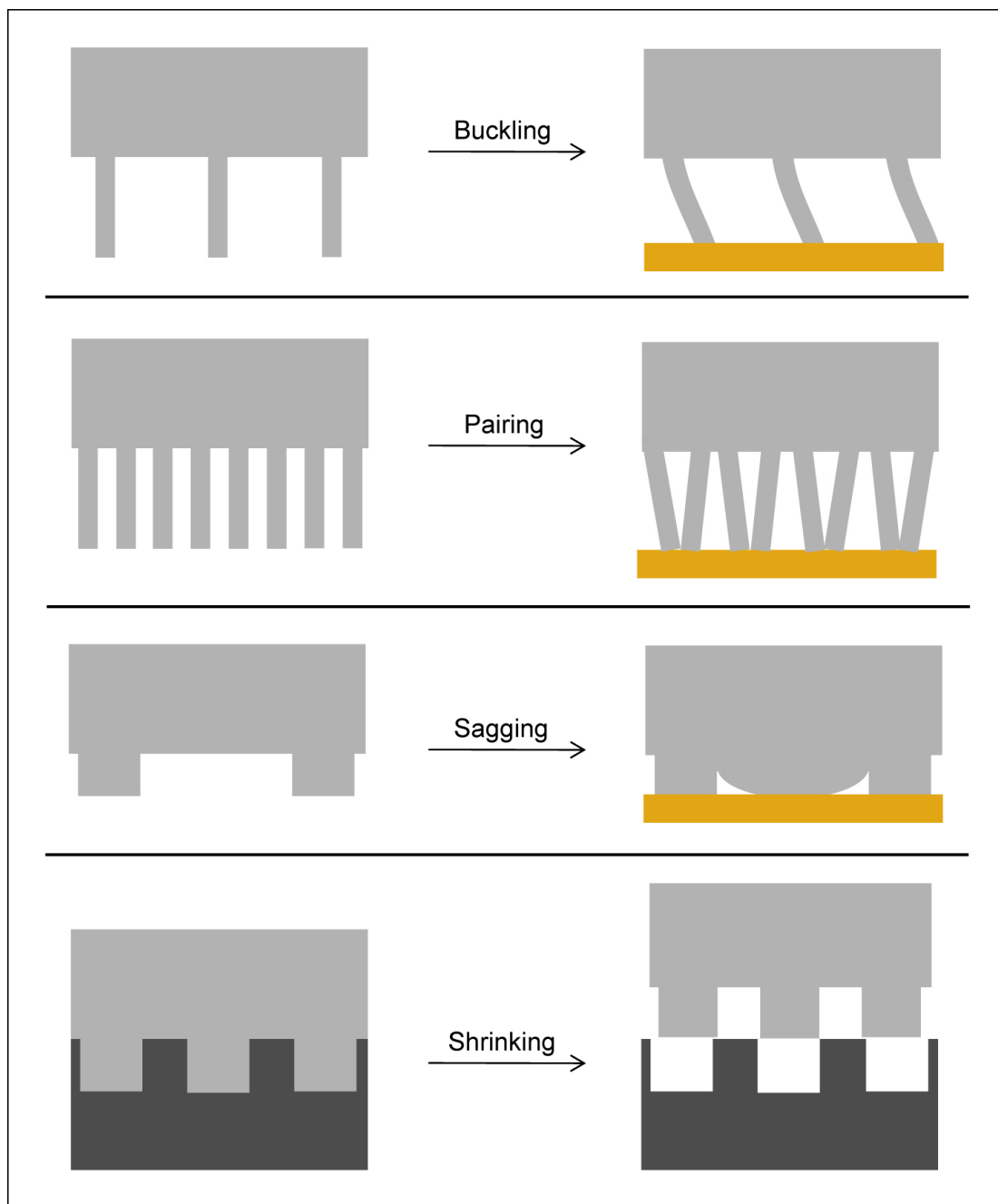


Figure 13. Schematic illustration of possible deformations and distortions of microstructures on PDMS stamps.

In addition to feature deformation due to aspect ratios beyond 0.2 – 2, PDMS can also be deformed due to the surrounding environment. During curing, the volume of a PDMS stamp decreases by roughly 1%.²⁵ PDMS stamps also swell when exposed to various nonpolar solvents such as toluene and hexane and swell minimally when exposed to ethanol (2.5%), causing stamp features to bulge upon inking and during pattern transfer.^{74, 112} An inability to use a variety of solvents limits the use of PDMS to only non-polar molecules, restricting its application in patterning organic and biological molecules.²⁸

Other studies using PDMS as a stamping material demonstrated that uncured, low molecular weight PDMS was transferred from the stamp to the surface, contaminating the substrate.¹¹³⁻¹¹⁴ In addition, oxidized PDMS (ox-PDMS) stamps can also contaminate the substrate with low-molecular weight PDMS deposition. Treatment of the surface with oxygen plasma or ozone/UV etching results in a hydrophilic surface capable of stamping hydrophilic molecules and polar inks.^{41, 76, 79} Ox-PDMS has elastomechanical properties very different from PDMS, resulting in the formation of cracks on the stamp surface following oxidation.¹¹⁵ This behavior not only disrupts the topography of the stamping area, but also allows migration of low-molecular weight PDMS

fragments to the stamp surface, leading to the recovery of the hydrophobic character of PDMS and preventing reuse of the stamp.^{28, 81, 115}

1.3.3 Availability and technological applicability of ink-substrate systems

The majority of research using traditional μ CP is dedicated to surfaces such as gold and silicon oxide due to the simplicity of the reaction of alkanethiols/sulfides with gold and of silanes with silicon oxide.^{25, 28, 30} Using these two surfaces and cognate attachment chemistry, inorganic materials, organic molecules and polymers, cells, DNA, proteins, and other biological materials have been patterned on gold and retained biological viability.^{19, 23, 28, 35-36, 41-43, 86-87} However, neither of these surfaces are technologically relevant. In addition, gold has a fairly large grain size (30-50 nm),¹¹⁶ which limits the resolution of μ CP-based methods.

The ability to pattern H-terminated silicon with μ CP, the current starting point for all semiconductors, would be useful for organic-based electronics.^{28, 117-118} Also, the ability to pattern potentially useful semiconductors with high thermal conductivity such as germanium and diamond is not possible with traditional μ CP. Printing on atomically flat surfaces such as silicon and mica would also obviate the limitation of grain size.¹¹⁹⁻¹²¹

In summary, the use of PDMS stamps in traditional μ CP has resulted in patterning surfaces with ~ 300 nm with ~ 150 nm edge resolution. However, these stamping parameters were very specific in order to maximize resolution and minimize feature size and cannot be universally applied to other ink-substrate systems, including more technologically-relevant materials.

1.4 Resolution improvement of patterning SAMs by manipulation of ink diffusion

Many groups have attempted to increase the resolution of μ CP by modifying or eliminating the molecular ink in the stamping process for printing SAMs or printing on pre-formed SAMs. The use of inking pads⁹⁷ and high-molecular weight inks^{75, 94, 97, 122-125} as well as the manipulation of stamping time,^{75, 126} stamping environment,^{112, 127-129} and ink concentration^{75, 126} have been shown to decrease the effect of diffusion on resolution and feature size attainable by μ CP. In addition, manipulation of pre-formed SAMs by deposition of metal on SAMs by μ CP¹³⁰⁻¹³¹ and stamp-immobilized chemical manipulation^{81, 88, 120-121, 132-139} offers the possibility of the complete elimination of diffusion.

1.4.1 Printing SAMs using various molecular inks

1.4.1.1 Use of inking pads for use in traditional μ CP methods

One of the principal hypotheses offered by Delamarche and co-workers in their study of the role of ink diffusion in traditional μ CP is that the bulk properties of PDMS result in sequestration of a large volume of molecular ink within the stamp, constantly resupplying the surface with more ink.⁷⁵ Libioulle and co-workers investigated the use of an inking pad in lieu of wet inking, in which a flat block of PDMS was incubated with a solution of thiols (Figure 14).⁹⁷ A PDMS stamp with relief features was placed in conformal contact with this “inking pad” and subsequently used to print gold surfaces. The authors noted increased pattern contrast with both HDT and ECT indicative of decreased diffusion through the gas phase. However, minimum feature size was unaffected by contact inking as opposed to wet inking, independent of stamping time and concentration. The concentration of ink on the stamping pad and stamping time both still significantly affected the resolution of pattern transfer, indicating lateral diffusion of ink remains problematic in this variation of μ CP.

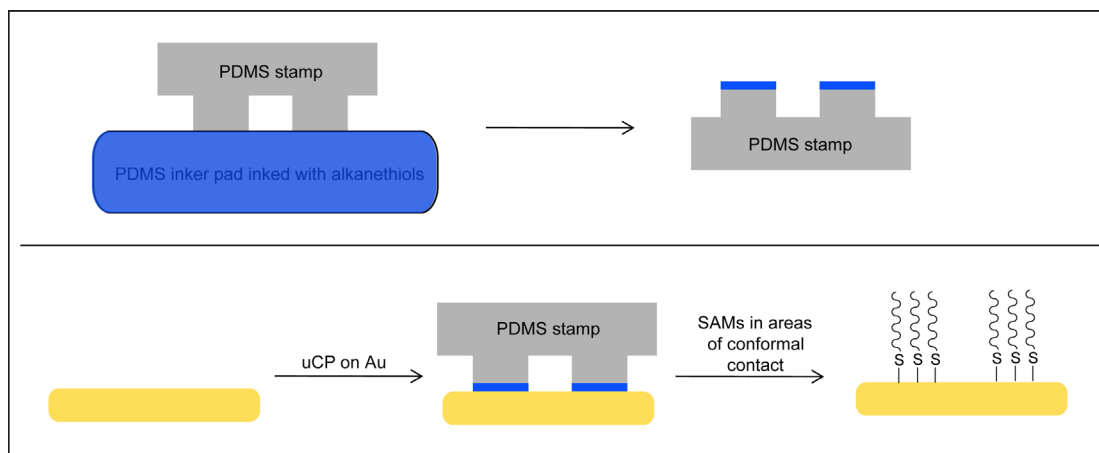


Figure 14. Contact inking of stamps for use in traditional μ CP.

1.4.1.2 High-speed μ CP

Another of the principle conclusions from ink diffusion studies by Delamarche and co-workers was the dependence of diffusion on time and ink concentration.⁷⁵ This conclusion was confirmed through high-speed μ CP, where HDT SAMs printed with a stamp ink concentration of 15-39 mM using a piezoelectric stage over a range of milliseconds, demonstrated that the most ordered SAMs and optimal feature resolution was obtained between 2 and 9 ms. At these high printing speeds and low ink concentrations, lateral and gas phase diffusion were suppressed and adequate protection of Au was obtained for etching.¹²⁶

1.4.1.3 Microdisplacement μ CP

Suppression of the lateral diffusion of thiol ink molecules across a surface using the displacement of a bulky thiol has been demonstrated by Weiss and co-

workers (Figure 15).¹²⁷⁻¹²⁸ First, a SAM of a bulky adamantane thiol is formed on a gold surface and subsequently patterned with a PDMS stamp inked with either 1-decanethiol or 11-mercaptopundecanoic acid. Upon conformal contact with the substrate, the alkanethiol displaces adamantane SAMs from the surface. Spreading does not occur due to the surrounding adamantane molecules on the surface. However, the extent of adamantane displacement is dependent on stamping time and ink concentration, which are two main problems displayed by traditional μ CP. Therefore, microdisplacement μ CP solves only resolution issues associated with lateral diffusion when compared to traditional μ CP methods.

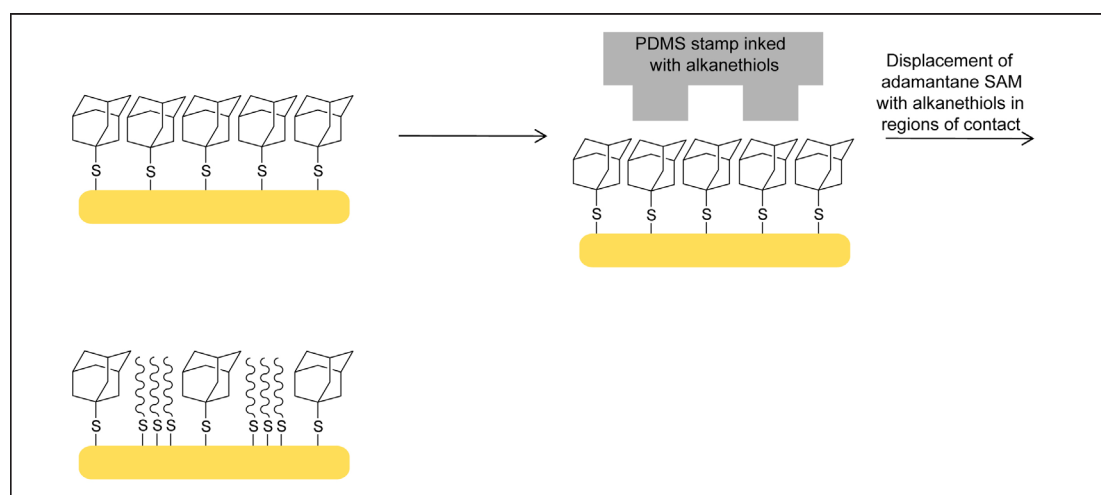


Figure 15. Microdisplacement printing using adamantane-terminated SAMs and *n*-alkanethiols.

1.4.1.4 Submerged μ CP

Due to the immiscibility of hydrophobic ink molecules in water, submerged μ CP using hydrophobic inks has been shown to inhibit gas and lateral diffusion of ink, permitting printing with hydrophobic long-chain thiols at feature sizes near 500 nm.¹¹² In addition, high-aspect ratio PDMS stamps demonstrated pattern transfer of microscale features using submerged μ CP under water with alkanethiols.¹²⁹ Differences in the mechanical stability of high aspect ratio structures of PDMS stamp features in water, ethanol, and air were also studied, showing that ethanol as a solvent for PDMS stamps minimizes feature collapse.¹⁴⁰ However, since alkanethiolates are typically patterned on gold using ethanol as a solvent, the applicability of submerged μ CP in ethanol is obviously limited.

1.4.1.5 Use of low-diffusion inks in μ CP

A phenomenon also observed by Delamarche and co-workers was the increased etch-resistance of high molecular weight alkanethiols on gold such as ECT.⁷⁵ Use of inks of even higher molecular weight than ECT or inks with multiple attachment points may reduce or eliminate lateral and gas diffusion.^{75, 94, 122} However, the use of increasingly bulky materials results in loosely-packed monolayer, which fails to protect the underlying gold substrate from etching or

oxidation.^{28, 75} Liebau and co-workers demonstrated the use of high-molecular weight thioethers as inks for μ CP but these molecules form disordered monolayers, resulting in little to no etch resistance.¹²²

The more recent use of these molecules in conjunction with positive- μ CP resulted in ~ 100 nm features – the smallest features printed using dendrimeric ink and positive- μ CP under ambient conditions to-date on gold.⁹² Positive- μ CP utilizes two different inks: a surface is first patterned with an ink forming poorly ordered monolayers, which is then dipped in an etch-resistant adsorbate solution.¹²³ The adsorbate monolayer adheres only to the surface in places lacking high-molecular weight thioethers. Subsequent etching results in a positive replica of the original master (the negative of what would be obtained with traditional μ CP).^{92, 123}

In addition, Li and co-workers performed nano-contact printing with a modified PDMS stamp using a dendrimeric ink, resulting in features bearing widths as small as 50 nm silicon substrates and thus the successful obviation of ink diffusion.¹²⁴⁻¹²⁵

1.4.2 Patterning pre-formed SAMs using μ CP

1.4.2.1 Nanotransfer printing

Nanotransfer printing is an additive technique in which a metal-functionalized stamp is reacted with a substrate, resulting in metal deposition onto the SAMs in regions of stamp-substrate contact (Figure 16). The first demonstration of this technique did not utilize SAMs, but patterned an oxidized silicon surface with a Au/Ti functionalized PDMS stamp, resulting in $-\text{Ti-O-Si}$ bonds and a Au-terminated surface in the areas of pattern transfer.¹⁴¹ In a second demonstration of this technique, SAMs were used as a covalent “glue” to transfer material from a stamp to a substrate in areas of contact.¹³⁰ To pattern a silicon substrate, the silicon surface is chemically oxidized creating surface hydroxyl groups on the native oxide layer. This surface was subsequently functionalized with mercapto-propyl-trimethoxysilane (MPTMS) resulting in SAMs bearing a terminal mercapto group. Gold does not adhere to PDMS; thus, evaporation of a thin layer of gold on top of a PDMS stamp with relief features and subsequent stamping on mercapto-terminated monolayers on silicon resulted in high-fidelity pattern transfer of gold features less than 100 nm wide on silicon substrates with \sim 5-15 nm edge resolution.¹³⁰ This technique was also demonstrated on gallium arsenide (GaAs) surfaces using alkanedithiol monolayers for the deposition of

gold in areas of stamp contact.¹³¹ Pattern uniformity was again observed, but with 50 nm edge resolution.

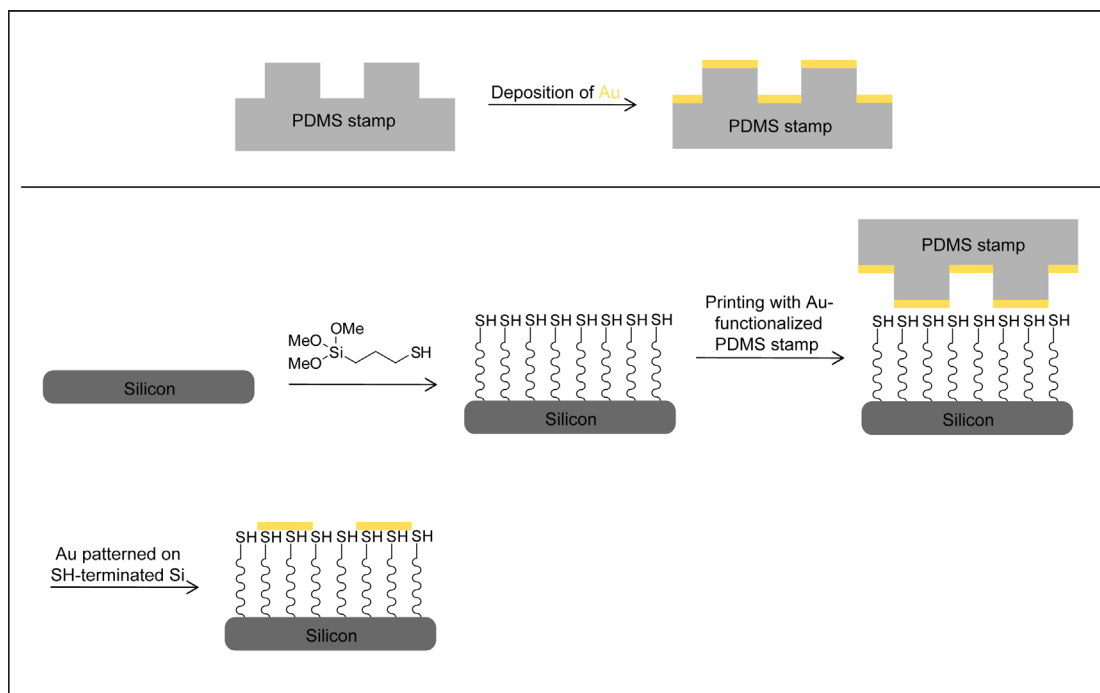


Figure 16. Nanotransfer printing of gold films with Au-functionalized PDMS stamp and mercapto-terminated silicon substrate.

1.4.2.2 Catalytic- μ CP

An alternative approach to resolution enhancement involves eliminating diffusive ink completely and instead achieving pattern transfer through a specific chemical reaction between substrate and stamp, eliminating diffusion-related blurring issues. In this approach, a stamp is made catalytically active toward a functionalized substrate and components of the stamp-substrate system are either covalently or specifically immobilized, preventing pattern blurring

through lateral and gas phase diffusion. Therefore, resolution of pattern transfer is limited only by the stamping material and the properties of the stamping surface itself.

The first application of inkless catalytic μ CP was reported in 2003 by Reinhoudt and co-workers, using deprotection of silyl ether-functionalized SAMs immobilized on gold by a stamp bearing acid catalyst (Figure 17). A surface-oxidized PDMS stamp was brought into contact with SAMs functionalized in acid-labile trimethylsilyloxy (TMS) or *tert*-butyldimethylsilyloxy (TBDMS) groups. Due to the acidity of the oxidized stamp, the terminal silyloxy groups were hydrolyzed to alcohols in areas of conformal contact. Although pattern transfer was observed and sub-micron features with 60-nm edge resolution were obtained, XPS data showed only 30% deprotection of terminal TMS groups.⁸¹ In addition, ox-PDMS has very different elastomechanical properties than does PDMS – cracks form on the surface of the stamp following oxidation. This behavior not only disrupts the topography of the stamping area, but also allows migration of low-molecular weight PDMS fragments to the stamp surface, thus leading to the recovery of the hydrophobic character of PDMS and preventing reuse of the stamp.²⁸

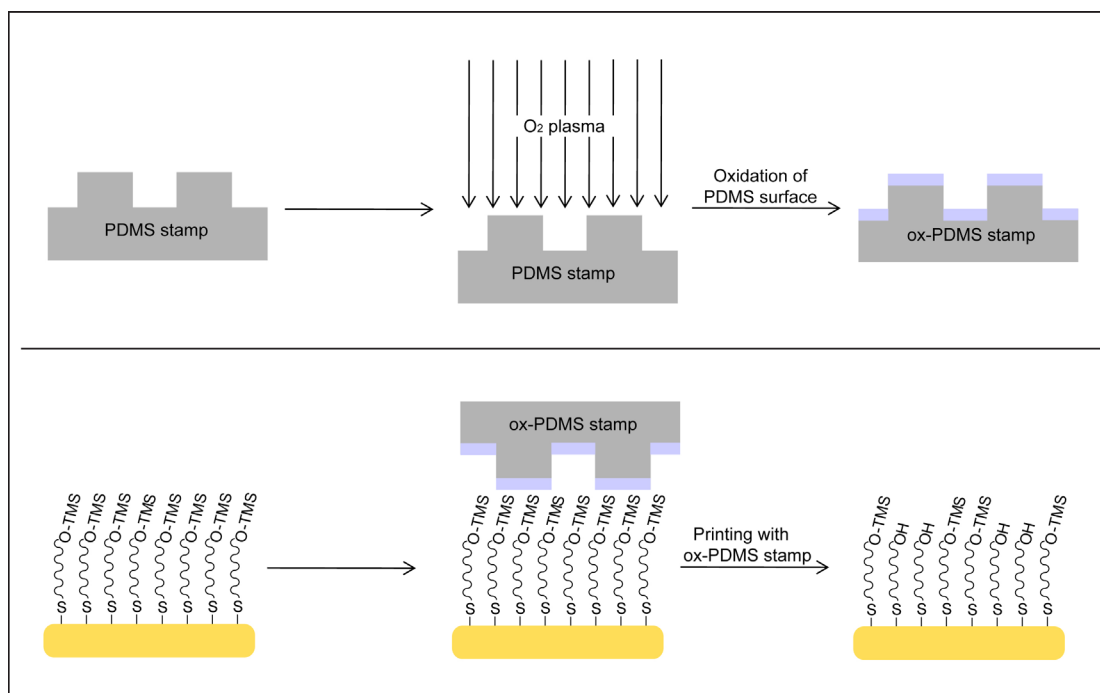


Figure 17. Inkless catalytic- μ CP with an acidic ox-PDMS stamp on acid-labile, silyl ether-terminated SAMs.

More recently, the same group demonstrated heterogeneous catalysis with μ CP by using a copper-functionalized stamp to catalyze an azide-alkyne cycloaddition (CuAAC) reaction (Figure 18).¹³² A surface-bound azide was exposed to dissolved alkyne, and upon stamping with the Cu-functionalized stamp, the CuAAC reaction between surface-immobilized azide and alkyne was catalyzed only in areas of stamp contact. After patterning, surfaces were reacted with an alkyne-terminated fluorophore or fluorinated molecule and pattern transfer was subsequently confirmed by fluorescence microscopy. Using flat stamps, XPS confirmed chemical functionalization of the underlying SAM.

However, only 5- μm wide features were prepared, and this technique has not yet been applied at the nanoscale.

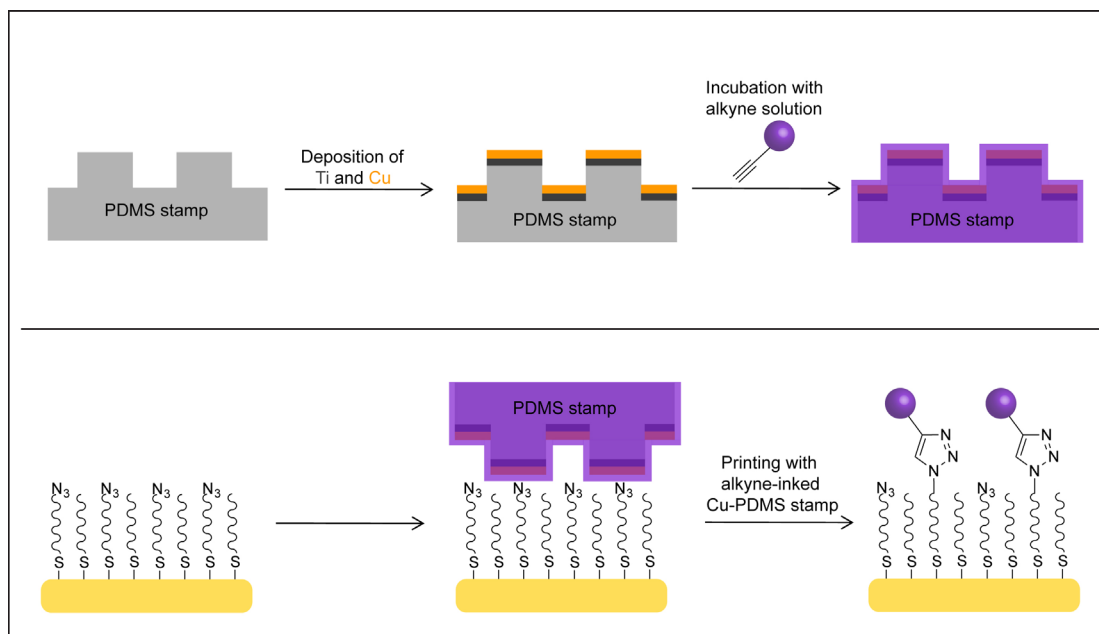


Figure 18. Heterogeneous catalysis through μCP : Cu^{I} -catalyzed azide-alkyne coupling in areas of conformal contact.

In an embodiment of nanoscale-confined surface functionalization using a flat elastomeric stamp, covalent amidation was demonstrated using ox-PDMS stamps inked with *N*-protected amino acids on amine-terminated gold surfaces (Figure 19).¹³³ The coupling was performed without a catalyst present, confirming that nanoscale confinement of *N*-protected amino acids on NH_2 -terminated SAMs at a stamp-substrate interface facilitates covalent amidation. Stepwise coupling and Fmoc-deprotection steps resulted in the successful production of short peptides with 90% efficiency for each step.¹³³ This technique

demonstrated the feasibility of stamp-facilitated chemical modification of surfaces by peptide coupling on inorganic substrates; however, no pattern transfer using ox-PDMS stamps displaying relief features was attempted.

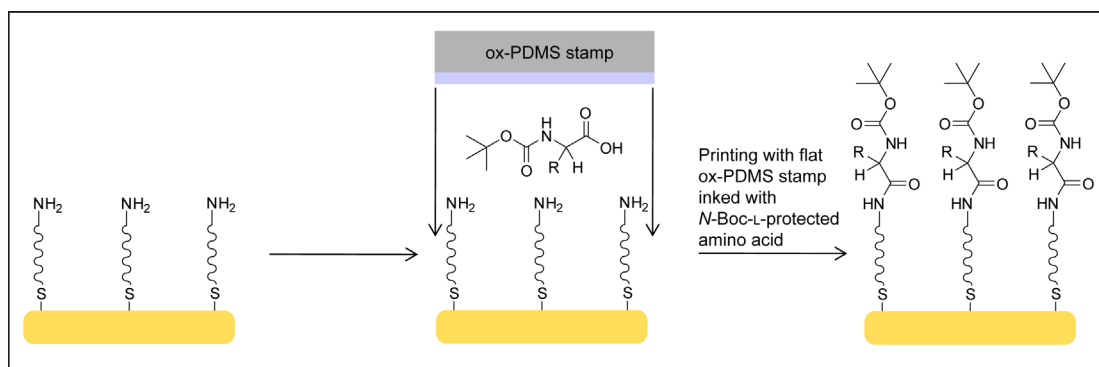


Figure 19. Nanoscale-confined peptide synthesis using elastomeric stamps.

Catalytic- μ CP methods with <100 nm resolution have been demonstrated by Mizuno and Buriak utilizing a hydrosilylation reaction catalyzed by a h-PDMS/PDMS stamp containing 20 nm Pd or Pt nanoparticles (NPs) and inked with alkenes/alkynes to pattern H-terminated silicon surfaces (Figure 20).¹³⁴⁻¹³⁵ Although replication of the NP features was achieved, the applicability of the approach is clearly limited. Stamp features are produced by self-assembly of block co-polymers that bind Pd or Pt NPs. After self-assembly on silicon, the surface is covered in PDMS pre-polymer and cured. Once removed from the surface, the NPs are taken up with the stamp, fabricating a stamp functionalized with NPs on the surface. Due to the nature of the self-assembly process and replication of patterns from random NP arrays, features such as squares, lines,

circles, and text cannot be patterned simultaneously. In these studies, only circles and lines have been patterned. Furthermore, the reaction between the ink and the surface can occur in the absence of a metal catalyst, promoted by both heat and UV light. Most importantly, areas not functionalized by hydrosilylation are susceptible to oxidation, resulting in degradation of the electronic properties of silicon in those areas.

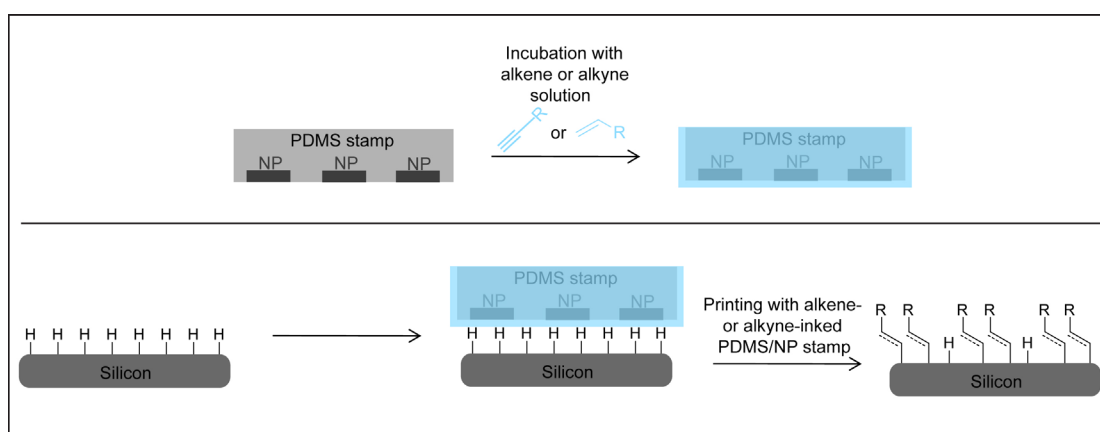


Figure 20. Catalytic- μ CP on H-terminated silicon surfaces using chemically-patterned flat stamps containing Pd or Pt catalyst NPs with alkene- or alkyne-terminated molecular ink.

A non-soft lithographic embodiment of catalytic- μ CP was demonstrated by Hsu and co-workers to directly pattern metallic nanostructures on silver films.¹³⁶ A pre-patterned solid electrolyte or superionic conductor (Ag_2S) was used as a stamp to etch a metallic film of silver in conformal contact upon application of an electrical bias (Figure 21). Pattern transfer occurs when metal at the stamp-substrate interface is processively dissolved, resulting in a pattern on

the metal substrate complementary to that on the stamp. Using this technique, 3D high-fidelity pattern transfer was achieved down to 100 ± 10 nm. However, this technique is limited to metallic films, use of specialized equipment, and results in no chemical difference between the inside and outside of patterned features.

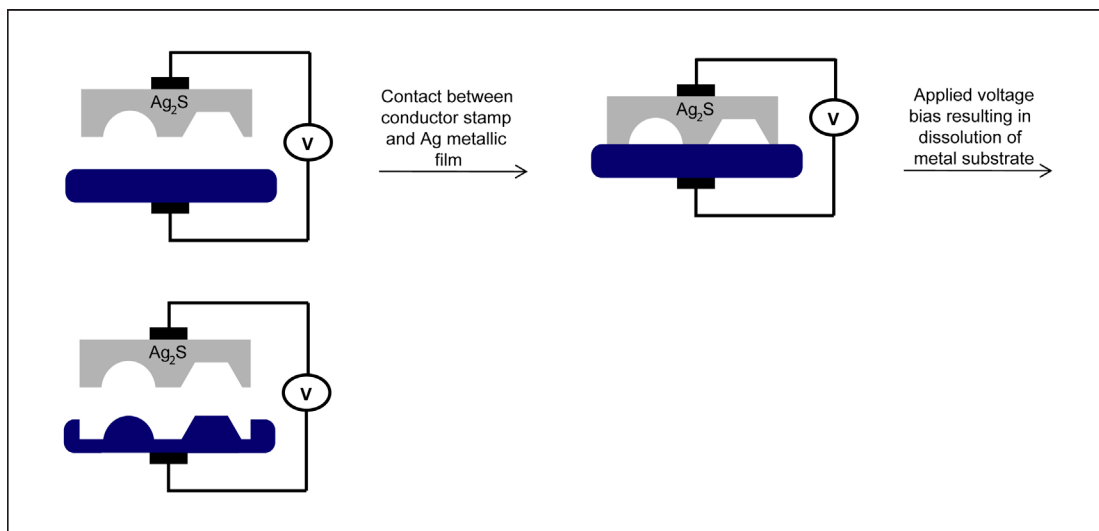


Figure 21. Electrochemical nanoimprinting with solid-state superionic stamps to pattern metallic nanostructures.

In our own laboratory, both biocatalytic and chemical catalytic inkless μCP methods have been developed for use in patterning gold and H-terminated silicon surfaces. The development of inkless biocatalytic- μCP ,¹³⁷ which uses a stamp-immobilized enzyme to pattern surface-immobilized cognate substrate, is described in detail in Chapters 2 and 3. Inkless chemical catalytic- μCP has been

demonstrated with chemically-modified basic and acidic stamps to pattern cognate substrate on both gold and silicon surfaces.

The first embodiment of inkless chemical catalytic- μ CP was demonstrated in our laboratory by Shestopalov and co-workers. Piperidine-modified polyurethane (PU) stamps were used to pattern SAMs terminated in 9-fluorenylmethoxycarbonyl (Fmoc) protection groups.¹³⁹ Fmoc-protected primary amines are selectively cleaved under mildly basic, nonhydrolytic conditions using aliphatic amines, such as piperidine. In order to immobilize such a chemical catalyst, the PU prepolymeric mixture was co-polymerized with piperidine-4-ylmethanamine, which reacted with acrylate via a Michael addition (Figure 22).

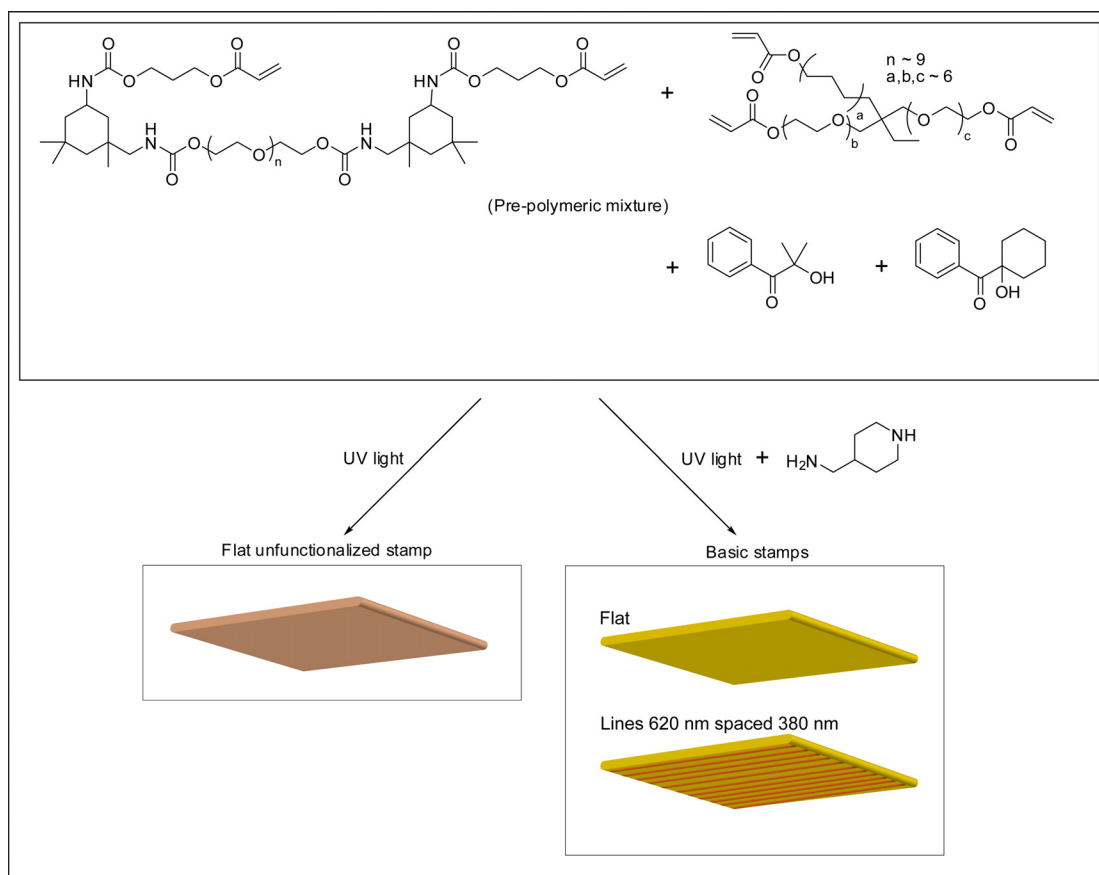


Figure 22. Preparation of polyurethane acrylate stamps.

Both flat and patterned piperidine-immobilized PU stamps were used in catalytic- μ CP on SAMs of Fmoc-protected amines. Printing with patterned stamps bearing 620 nm lines separated by 380 nm with an aspect ratio of 0.15 resulted in high-fidelity pattern transfer with demonstrated edge resolution of less than 50 nm, as observed via SEM and AFM imaging techniques.¹³⁹ Thus, the resolution of the technique is limited only by the mechanical properties of the stamp material and/or by the granular size of the gold substrate, indicating a diffusion-free process.

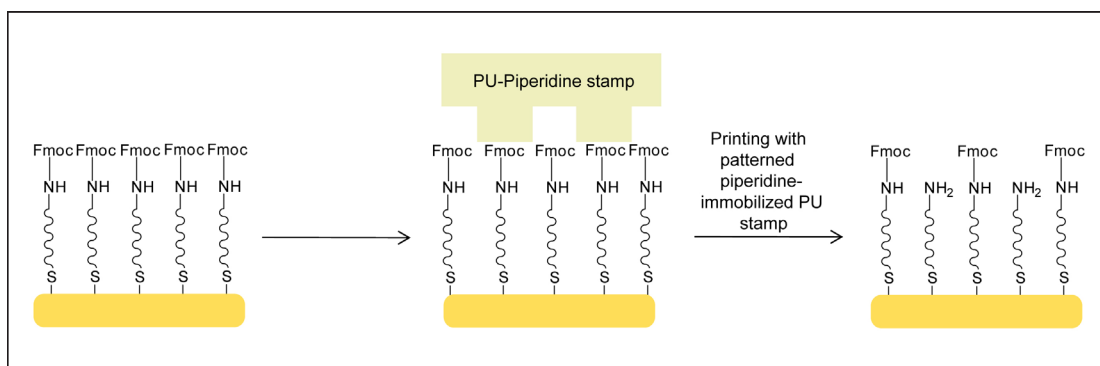


Figure 23. Chemical catalytic- μ CP using piperidine-functionalized stamps on Fmoc-terminated SAMs.

A gold substrate incubated with a flat catalytic stamp was analyzed with XPS and showed near 100% cleavage of the Fmoc group after 3 hours at 50 °C. The second use of the piperidine-immobilized PU stamp on fresh Fmoc-protected substrate also resulted in near 100% cleavage using the same stamping conditions, demonstrating not only the completion of the reaction, but also the truly catalytic nature of the technique. Printing with flat PU stamps containing no catalyst resulted in no significant change in elemental composition observable via XPS analysis.¹³⁹

In spite of its demonstrated advantages over traditional μ CP methods such as obviating stamp deformation and diffusion, near 100% deprotection was achieved only after prolonged reaction times and at elevated temperatures. To overcome these limitations, Shestopalov and co-workers investigated acid-immobilized catalytic stamp-substrate systems.^{88, 120-121, 138, 142} PU pre-polymeric

mixture was co-polymerized with 2-mercaptoethanesulfonic acid (via Michael addition) in fabrication of acidic patterned and flat stamps. SAMs displaying either terminal *tert*-butyl carbamate- (Boc) and *tert*-butyldimethylsilyl- (TBDMS) protection groups were immobilized on gold surfaces and subsequently incubated with sulfonic acid-immobilized stamps.

Printing with patterned stamps with feature widths as small as 240 nm with aspect ratio as low as 0.042 resulted in high-fidelity pattern transfer with edge resolution of less than 50 nm.¹²⁰ Again, the resolution of the technique is limited only by the mechanical properties of the stamp material and/or by the granular size of the gold substrate, indicating a diffusion-free process. After stamping Boc- and TBS-functionalized SAMs with an acidic-functionalized flat stamp, XPS analysis showed complete deprotection of both monolayers to the corresponding amine or alcohol, respectively, after only one minute of stamping time at room temperature.¹²⁰ This methodology is thus a significant improvement over the base-catalyzed μ CP method both in terms of stamping time and reaction conditions.

To increase the applicability of this method, Boc-protected SAMs oxide-free silicon substrates were fabricated from H-terminated silicon and incubated with both patterned and flat sulfonic acid-modified PU stamps.¹²¹ Pattern

transfer was achieved at the microscale (6.5 μm features), demonstrating the feasibility of the technique, while XPS analysis showed complete deprotection of the Boc group, resulting in the corresponding amine, after 5 minutes at room temperature.¹²¹ This system demonstrates the first example of a soft lithographic method that chemically patterns SAMs on oxide-free silicon to display two different distinct chemical functional groups. Further exploration of catalytic- μCP using sulfonic acid-functionalized PU stamps to pattern SAMs on oxide-free silicon surfaces in our laboratory is discussed in Chapter 4.

2. Biocatalytic microcontact printing

2.1 Overview

Here we describe the development of catalytic soft lithographic techniques that employ an enzyme catalyst immobilized to a polymeric stamp for the replication of patterns on functionalized SAMs. The use of immobilized enzymes to chemically modify functionalized SAMs has previously been used in serial AFM-based writing techniques, but not in stamping applications.¹⁴³⁻¹⁴⁴ Using a model system of reversibly immobilized Exonuclease I (ExoI) and immobilized single-stranded DNA (ssDNA), we sought to demonstrate both the feasibility of biocatalytic- μ CP and its advantages over conventional and unconventional μ CP techniques. Several other enzyme-substrate systems were also tested for potential application in biocatalytic- μ CP.

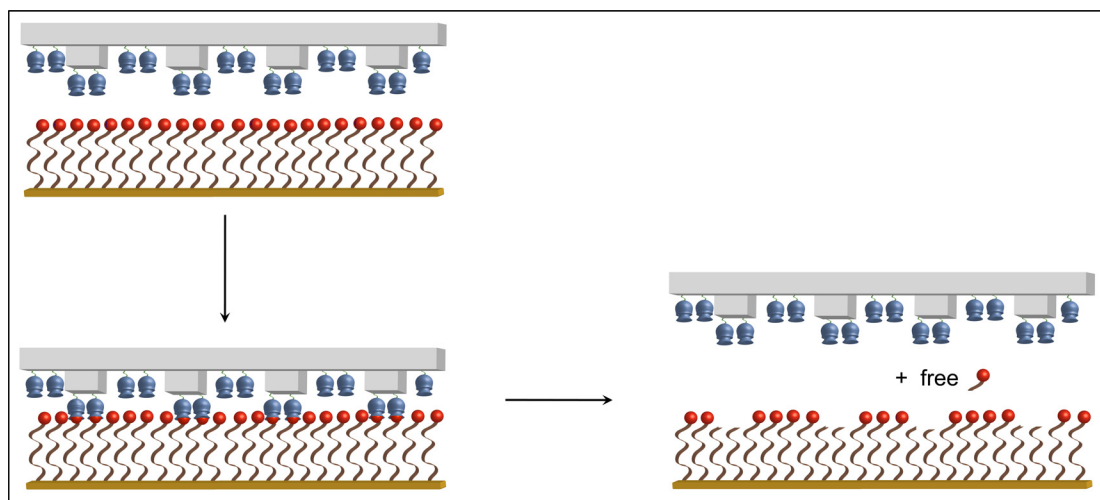


Figure 24. Biocatalytic-microcontact printing.

2.2 Demonstration of biocatalytic- μ CP with model system ExoI-ssDNA

2.2.1 Acrylamide-based elastomeric stamps

2.2.1.1 Bulk material of elastomeric stamp

Our process required a stamp support capable of immobilizing enzymes while performing μ CP. Although historically the elastomeric stamping material of choice in μ CP for patterning alkanethiols on gold,²⁴ native PDMS is not suitable for stamping hydrophilic materials such as polar inks or biological molecules. Although oxidation or chemical modification improve performance in these applications, both result in stamp defects.^{23, 81} We therefore considered alternative elastomeric stamping materials that are both compatible with biological materials and readily amenable to synthetic manipulation.

Agarose and acrylamide have been used to form reusable hydrogel stamps for patterning surfaces with both aqueous solutions of hydrophilic materials and living cells. Grzybowski and co-workers reported the use of agarose and acrylamide micropatterned stamps to print features as small as 50 μ m on a PDMS surface using an oxidative ink (KCr_2O_7).¹⁴⁵ Whitesides and co-workers reported the use of micropatterned agarose stamps to print live bacteria on agar plates in the 100- μ m to millimeter range.⁹⁰ Both agarose and acrylamide are used extensively in molecular biology and biochemistry for the

electrophoretic separation of nucleic acids and proteins,¹⁴⁶ are non-fouling,¹⁴⁷⁻¹⁴⁹ and broadly biocompatible.

Several advantages of acrylamide over agarose suggested its use as a bifunctional support material for biocatalytic- μ CP. First, enzymatic reactions have previously been demonstrated in acrylamide gels.¹⁴⁷⁻¹⁴⁸ Second, monoacrylates provide a specific handle for polymerization. Finally, acrylic acid is easily coupled to a variety of alcohols and amines, providing the additional functionality required for enzyme immobilization.¹⁵⁰⁻¹⁵¹

2.2.1.2 Synthesis of bifunctional linker for stamp

After selecting a stamp support, we turned our attention to chemical moieties capable of reversible enzyme immobilization. Specific reversible immobilization ensures ordered, oriented enzyme at the surface while facilitating replacement of inactive or degraded enzyme with new catalyst. Nitrilotriacetic acid (NTA) groups act as chelators for transition metal ions such as Ni^{+2} and immobilize proteins containing terminal histidine residues (His₆-tag).¹⁵²⁻¹⁵⁴ Many proteins are expressed with an N- or C-terminal His₆-tag to facilitate purification through standard IMAC protocols, an approach that offers a universal system for the reversible immobilization of His₆-tagged proteins on stamps. The catalyst

can be stripped from the stamp through competitive binding of EDTA or imidazole, and new catalyst can be loaded upon fresh chelation of Ni²⁺.

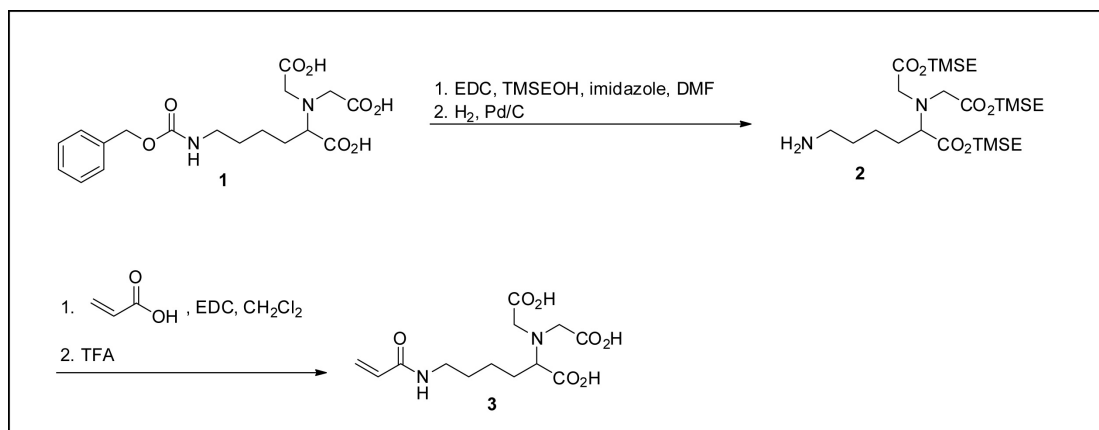


Figure 25. Synthesis of N^ε-acrylamido, N^α-bis(carboxymethyl)-lysine 3.

Acrylate 3 was prepared from commercially-available N^α,N^α-bis(carboxymethyl),N^ε-Z-lysine 1 in four steps in according to the protocols of Ho and co-workers and Hochuli and co-workers^{152, 154} (Figure 25). CBz-protected NTA-lysine 1 was esterified with 2-(trimethylsilyl)ethanol using 1-ethyl-3-[3-dimethylaminopropyl]carbodiimide (EDC), resulting in the protection of all three carboxylates of the NTA moiety as the corresponding 2-(trimethylsilyl)ethyl esters. Hydrogenolysis, which removed the CBz protecting group from the side-chain amino group, was followed by EDC-promoted amidation with acrylic acid. Finally, deprotection of the TMSE esters with trifluoroacetic acid (TFA) produced the desired acrylamido-NTA derivative 3.

2.2.1.3 Stamp fabrication protocols

With polymerizable bulk material and bifunctional NTA-acrylate in hand, stamp preparation protocols were investigated. Although both Grzybowski and Whitesides fabricated hydrophilic stamps against PDMS masters,^{90, 145} we found silicon-poly(methyl methacrylate) (Si/PMMA) masters fabricated by electron-beam lithography (EBL) to be superior to PDMS both with regard to mechanical stability and relief feature fidelity in polymerized acrylate stamps.

To obtain an NTA-functionalized stamp, an aqueous solution of NTA-acrylate **3** in commercially available (40:1 w/v) acrylamide/bisacrylamide was allowed to polymerize in the presence of ammonium persulfate (APS) and N,N,N',N'-tetramethylethylenediamine (TEMED) under a suspended Si/PMMA master. After ten minutes, the master was removed and the stamp was easily peeled away from the fabrication platform (Figure 26). The stamp was cut to approximately 1 cm² before activation with Ni⁺² and exposure to His₆-tagged enzyme.

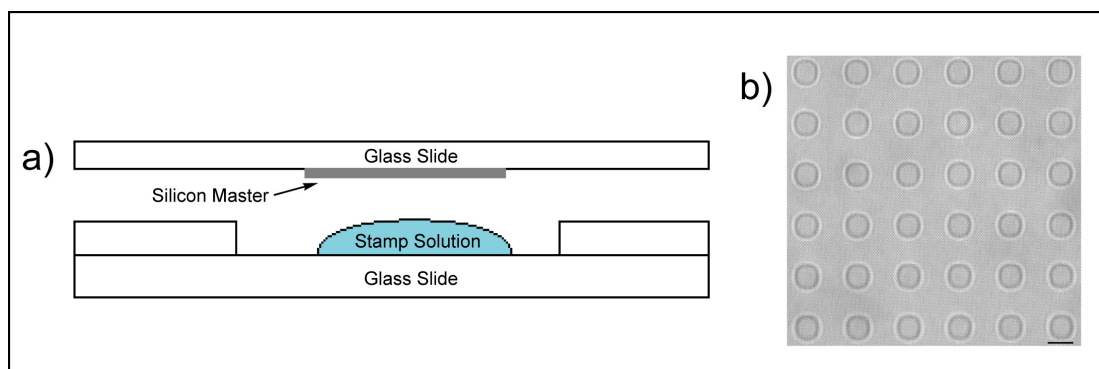


Figure 26. a) Stamp fabrication platform. b) Optical micrograph of a polymerized NTA-acrylate stamp in contact with glass at 63X (10 μm scalebar).

2.2.2 Model enzyme-substrate system parameters using ExoI-ssDNA

To increase the likelihood of success in demonstrating our biocatalytic- μCP technique, we chose as our initial enzyme-substrate system one that is well-known in biology, well-studied in conjunction with Au-immobilized SAMs, and that has previously demonstrated activity in immobilized biochemical catalysis. Chilkoti and co-workers used the enzyme DNaseI, a nonspecific ssDNA and dsDNA endonuclease, as a chemical “ink” in DPN.¹⁴³ In these experiments, an AFM tip was inked with DNase I and used to “write” patterns via enzymatic ablation of thiol-functionalized ssDNA SAMs on a gold surface.

2.2.2.1 Model Enzyme: Exonuclease I (ExoI)

Exonuclease I (ExoI) offers several advantages relative to DNaseI for biocatalytic- μCP . First, although both enzymes are monomeric, DNaseI is an bovine endonuclease that cleaves ssDNA and dsDNA nonspecifically to release

multi-base oligonucleotide products¹⁵⁵ while ExoI, an exonuclease from *E. coli*, catalyzes processive hydrolysis of its ssDNA substrate from the 3' to 5' termini.¹⁵⁶ If the physical parameters of our system allow only a single base to be hydrolyzed, DNaseI will fail to produce hydrolysis while ExoI should remain effective. Second, ExoI requires no cofactor other than Mg²⁺ while DNaseI requires both Ca²⁺ and Mg²⁺ for activity.^{137, 155-156} Third, although both enzymes have been cloned into a pET vector and expressed with a terminal His₆-tag, His₆-tagged DNaseI shows poor solubility at neutral pH, presumably due to the lack of glycosylation of the recombinant protein.¹⁵⁶⁻¹⁵⁷

ExoI plays roles in DNA recombination and repair.^{156, 158} The "C"-shaped protein (Figure 27) consists of three well-defined regions: an N-terminal (exonuclease) domain (1-201 residues), an SH3-like domain (202-354 residues), and an C-terminal region (359-475 residues). Residues 355-358 make up a disordered linker connecting the SH3 domain to the C-terminus domain, actually closing the "C" into an "O." (Residues 355-358 are not visible in electron density maps due to disorder.)¹⁵⁶

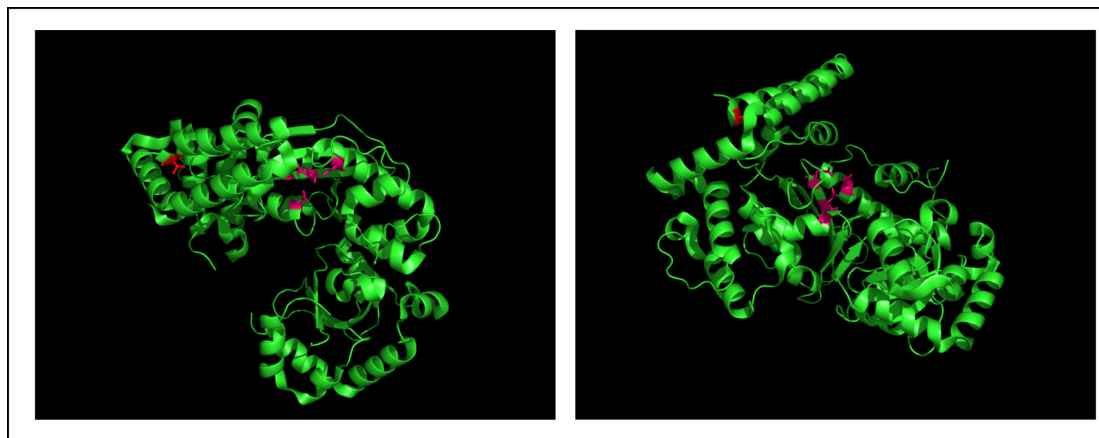


Figure 27. ExoI enzyme (PDB: 1FXX).¹⁵⁶ The active site residues are colored pink and the C-terminal His₆-tag is colored red.

2.2.2.2 Model substrate: ssDNA on gold and glass surfaces

Synthetic oligonucleotides are commercially available both in native form and chemically modified with various tags for immobilization and/or imaging. Additionally, methods for the immobilization of ssDNA on surfaces have been well-studied.^{14, 41, 87, 91, 159-163} Of particular interest are ssDNA-alkanethiol SAMs studied by Tarlov and co-workers⁹¹ and Satija and co-workers,¹⁶¹ in which the bonding behavior of ssDNA-alkanethiols to gold was studied using various surface characterization techniques. This work showed ssDNA-alkanethiols not only react with the gold through the terminal thiol group (chemisorption), but also nonspecifically adsorb to the surface through nitrogen-bearing nucleotides (physisorption). ssDNA-SAMs thus form a mixture of orthogonal DNA showing

typical cant angles and DNA laying flat on the surface, producing disordered monolayers with low DNA surface coverage.^{91, 161}

Physisorption through nitrogenous bases is reversible. To create ordered monolayers, both groups attempted to minimize physisorbed ssDNA by treating gold surfaces with a mercaptohexanol (MCH) spacer, as shown in Figure 28. MCH was chosen as an ideal “spacer” molecule because of its solubility in water and inability to bind DNA. Treatment of gold-ssDNA surfaces with 1 mM MCH solution produced specifically-bound ssDNA-alkanethiols near-orthogonal to the surface and bound only through the terminal sulfur atom. Moderately-spaced ssDNA nearly orthogonal to the surface is an ideal surface for biocatalytic- μ CP, providing both adequate spacing and appropriate substrate orientation for enzyme binding.

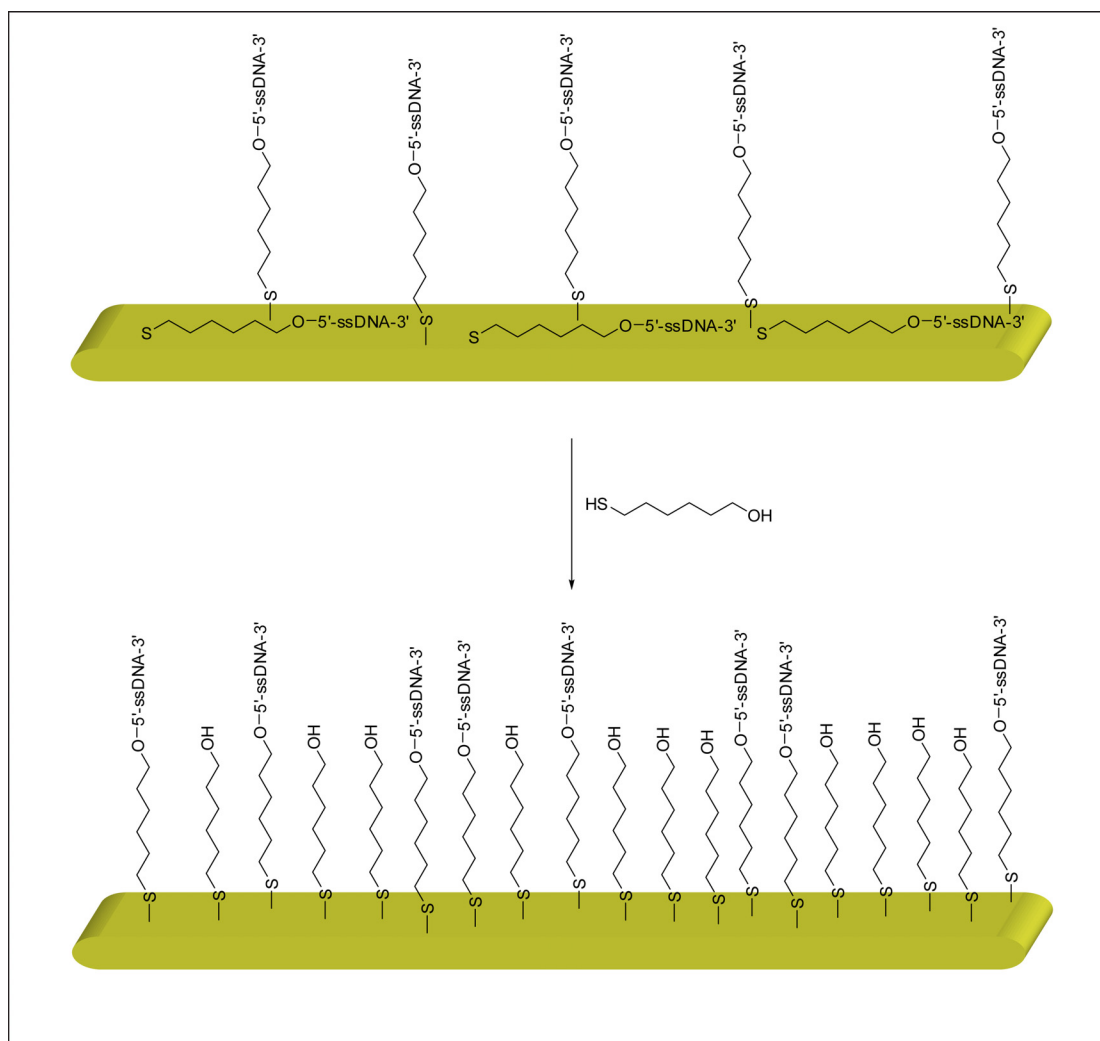


Figure 28. Schematic of ssDNA-alkanethiols adsorbed to gold before and after treatment with MCH.

Analysis of pattern transfer is an important aspect of our experimental design, and fluorophore-functionalized ssDNAs chemically adsorbed to glass substrates provide a useful probe for exploring the extent of enzymatic hydrolysis, with surfaces showing a decrease in fluorescence in areas of conformal contact with the enzyme-functionalized stamp (Figure 29). Amino-

terminated ssDNA covalently binds commercially available isothiocyanate (ITC) functionalized glass slides and was used for confocal microscopy work.

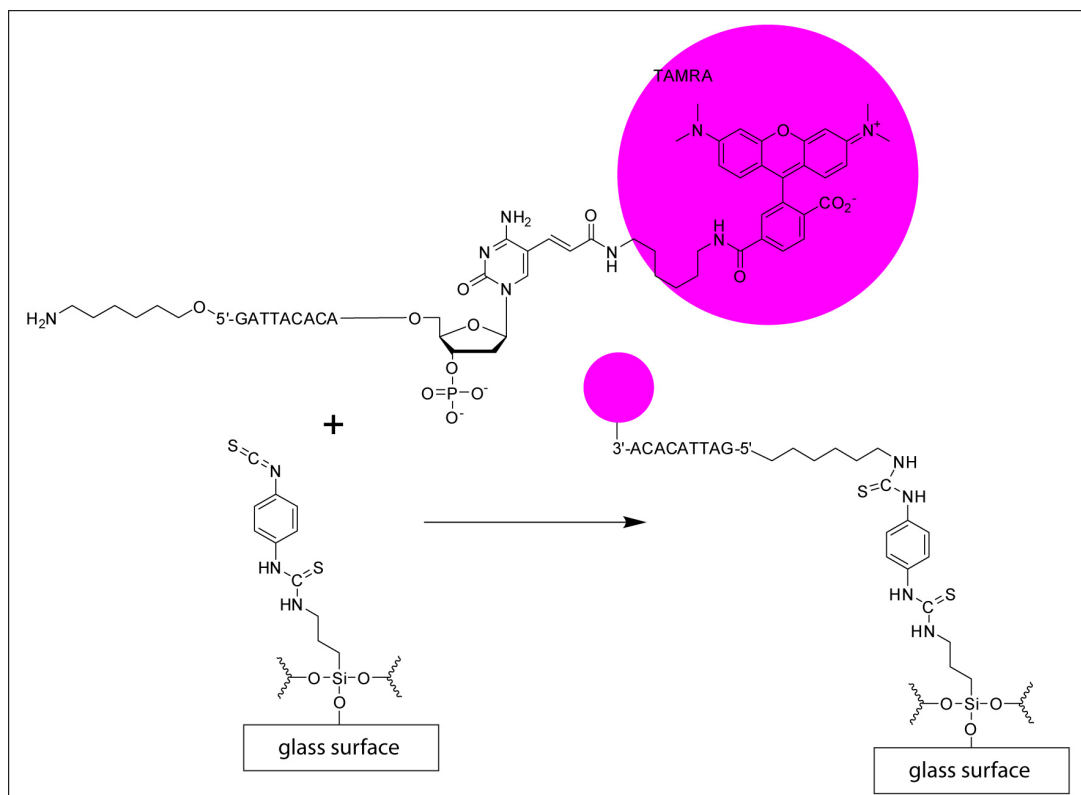


Figure 29. Reaction between 3'-TAMRA-ssDNA-NH₂-5' ssDNA with ITC-functionalized glass slides.

The substrate sequence 5'-GATTACAGATTACA-3' was purchased from Integrated DNA Technologies with a 5'-mercaptohexyl modification for SAM formation on gold surfaces and with a 5'-aminohexyl modification and 3'-cyTAMRA fluorophore for immobilization on ITC-functionalized atomically flat glass surfaces for confocal microscopy.

2.2.3 ExoI activity assays

The gene for wild type ExoI was obtained by PCR amplification from *E. coli* DH5 genomic DNA, digested with *NdeI* and *XhoI*, and ligated into a similarly prepared pET22b overexpression vector (a generous gift from Dr. B. W. Matthews, University of Oregon). The resulting construct was transformed into BL21 DE3 cells via heat shock. ExoI protein was expressed and purified via Ni²⁺ column following standard IMAC protocols.^{156, 164} The enzyme was concentrated to ~ 70 μ M (~3.8 mg/mL) and diluted to 0.1 μ M for stamp incubation.

2.2.3.1 MALDI-TOF mass spectrometry for ExoI-ssDNA solution-based assay¹³⁷

MALDI-TOF mass spectrometry has been used previously to analyze alkanethiolates¹⁶⁵ and ssDNA,¹⁶⁶ and this technique was used to confirm ExoI activity against ssDNA. Control samples (without enzyme) showed an ion for substrate at 2748.0 amu (calc'd MH⁺ 2747.1 amu). Incubation of 10 μ M enzyme with 1 mM ssDNA completely removed this peak. The most prevalent peak in enzyme-treated samples was 926.9 (calc'd MH⁺ 926.8), corresponding to a six base-ablation. This experiment successfully demonstrated ExoI activity in reaction buffer (66 mM glycine, 12 mM MgCl₂, pH 9.50), indicating gold-immobilized ssDNA could be used as a substrate for biocatalytic- μ CP.

2.2.3.2 Fluorescence microscopy of glass-immobilized 3'-TAMRA ssDNA after incubation with ExoI in solution

Surfaces of untreated glass (background), immobilized 3'-cyTAMRA-modified 5'-GATTACACA-3' DNA and enzyme-treated 3'cyTAMRA-ssDNA was prepared to determine the suitability of fluorescence microscopy as a tool for evaluating enzyme activity (TAMRA max: $\lambda_{\text{abs}} = 559 \text{ nm}$ and $\lambda_{\text{emm}} = 583 \text{ nm}$). A substrate displaying all three surfaces was created, excited at ~530-560 nm and imaged at ~580-640 nm using a fluorescence microscope. Edges at the interfaces are clearly visible (Figure 30), however the section containing enzyme-treated 3'cyTAMRA-ssDNA shows significantly more fluorescence than untreated glass. This observation indicates background fluorescence either from ssDNA on the surface or incomplete ablation of the 3'cyTAMRA-fluorophore, or both. In addition, ambient light could have penetrated into the apparatus enclosing the fluorescence microscope, causing background fluorescence from the treated section. Despite this limitation, it was clear that a decrease in fluorescence was produced by incubation with ExoI, and we moved on to a more quantitative analysis of ablation.

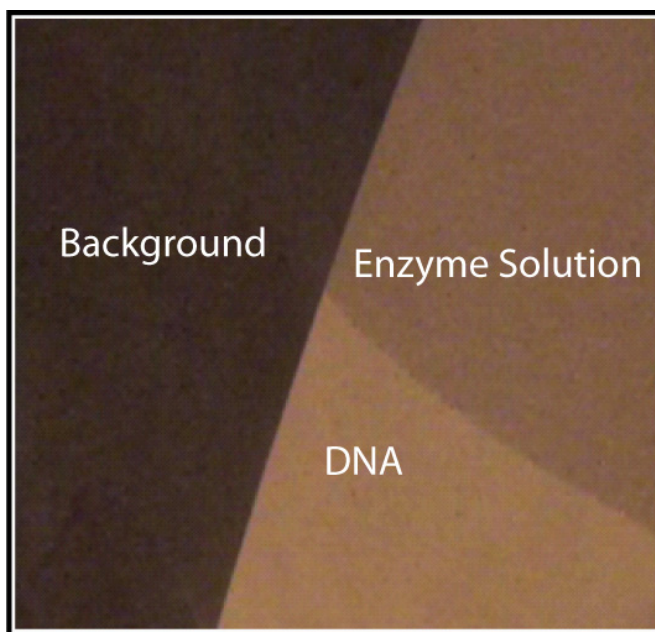


Figure 30. Fluorescent microscopy of isothiocyanate-functionalized glass surface ($\lambda_{\text{excited}} = 530\text{-}560\text{ nm}$ and $\lambda_{\text{emm}} = 580\text{-}640\text{ nm}$).

2.2.3.3 AFM of ssDNA SAMs on gold

To explore enzymatic digestion on gold substrates, 5'-thiolated oligonucleotides were adsorbed to a gold surface using previously established protocols.⁹¹ Lines were drawn on the surface with a fine-tip permanent marker, and enzyme solution (1 μM) in reaction buffer was aliquoted between the two lines. Due to the hydrophobicity of the ink, the drop remained between the two lines and was the surface incubated with enzyme for 2 hours at room temperature. Figure 31 shows juxtaposed AFM lateral force images displaying a significant, detectable pattern at the drop edge through three imposed AFM images. The image shows an obvious friction difference between the exposed

and unexposed areas, demonstrating that enzymatic digestion is detectable via AFM.

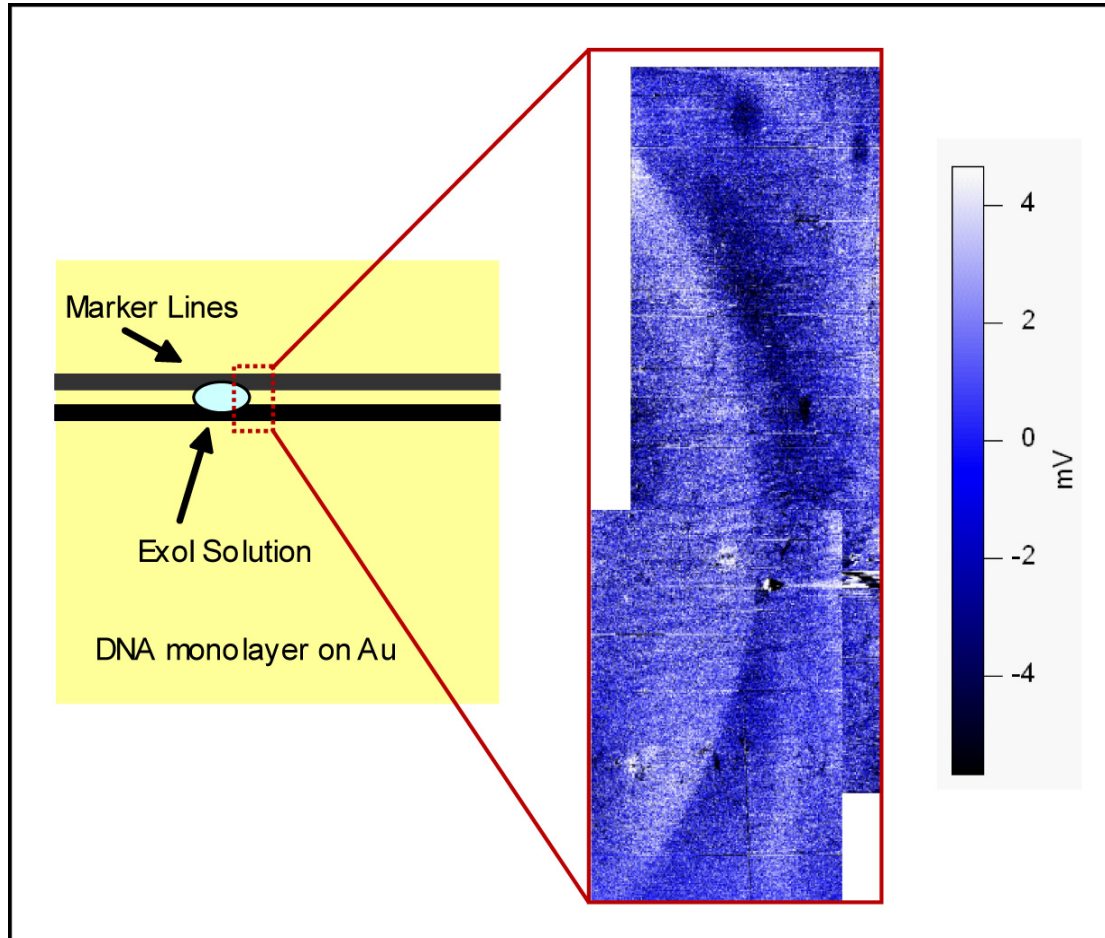


Figure 31. Three juxtaposed AFM lateral force images taken of a surface that had been incubated with a drop of ExoI enzyme solution. ExoI enzyme in reaction buffer was deposited on the ssDNA-functionalized surface, creating a meniscus line of enzymatic digestion.

2.2.4 Stamp activation and stamping protocols

Following bulk polymerization of acrylamide with NTA-acrylamido-lysine as described in *Section 2.2.1.3*, stamps immediately underwent a series of

incubations for specific immobilization of enzyme (Figure 32). All manipulations were conducted at 4 °C to maximize the binding of ExoI enzyme to the NTA group on the stamp. Stamps were first placed in sterile-filtered 50 mM NiSO₄ solution until a homogeneous light green color developed (15-20 minutes). A series of rinses and incubations followed: binding buffer (500 mM NaCl, 20 mM Tris-HCl, 5 mM imidazole, pH 7.9), 0.1 μM ExoI in binding buffer for 5 minutes, binding buffer, wash buffer (500 mM NaCl, 60 mM imidazole, 20 mM Tris-HCl, pH 7.9), 0.05% SDS rinse and sonication for 1 minute to remove nonspecifically adsorbed enzyme, two rinses with wash buffer, and reaction buffer (66 mM glycine, 12 mM MgCl₂, pH 9.50) to activate the enzyme. Stamps were then placed on filter paper soaked with reaction buffer.

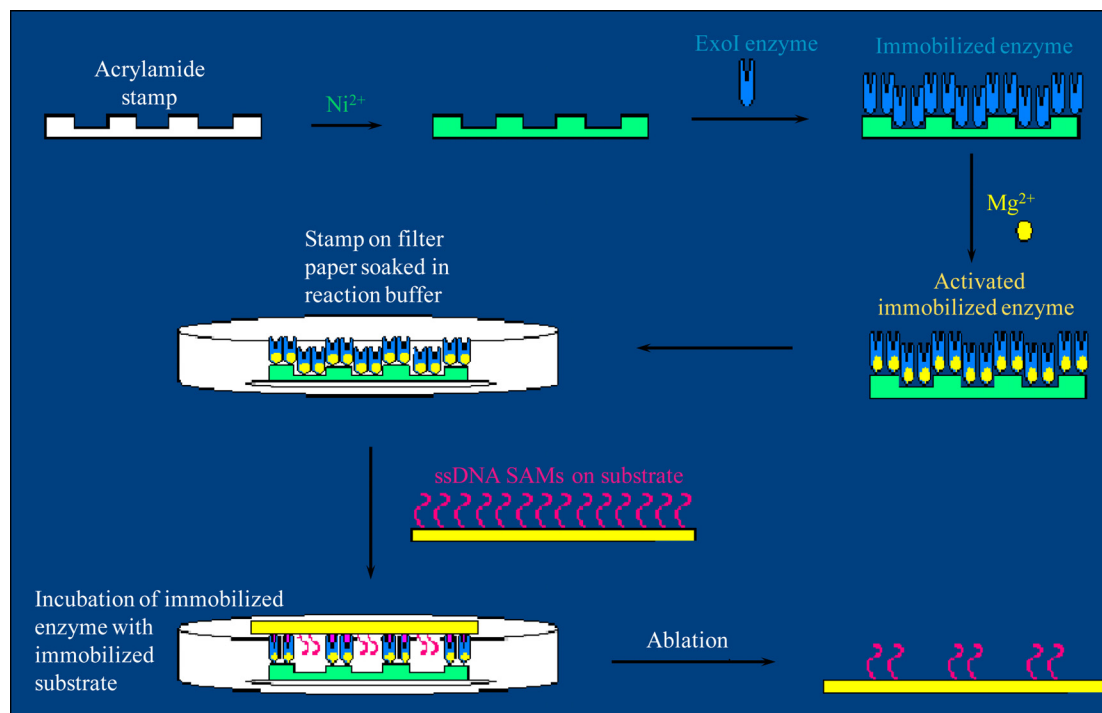


Figure 32. Protocol for the activation of NTA-acrylamide stamp and biocatalytic- μ CP stamping on substrate-immobilized ssDNA.

Stamp surfaces were dried under a stream of N_2 and gold or glass substrates functionalized with ssDNA were placed on top of the stamp. Gentle pressure was applied to ensure conformal contact, and the substrate/stamp was incubated for 1-12 hours at $4^\circ C$. Attainment of proper pressure was complicated in the case of gold substrates as these substrates were opaque and air bubbles between stamp and substrate could not be visualized. Transparent glass slides facilitated stamping as pressure was increased until conformal contact was achieved. After incubation with the stamp, the substrate was removed from the stamp and immediately rinsed with water and dried under N_2 . Substrates were

kept sealed with parafilm in closed containers until imaged by AFM and/or confocal fluorescence microscopy.

2.2.5 AFM imaging of biocatalytic- μ CP on ssDNA-functionalized gold substrates

Dry samples were imaged via contact-mode AFM. The first trial of biocatalytic- μ CP was performed for 12 hours to maximize ablation. Further MALDI-TOF experiments demonstrated that one hour of incubation was sufficient to observe enzymatic cleavage, but using both immobilized enzyme and immobilized substrate might affect enzyme activity.

The spacing between patterned features is approximately 35 μ m (center-to-center distance), which corresponds well to the spacing of the original stamp features (35 μ m center-to-center distance). However, digested patterns showed shapes distinctly different from the features of the original stamp. Rather, AFM height images showed enzymatic cleavage in oblong shapes instead of the original rounded-square features (Figure 33). Imaging several portions of the substrate with gold-coated SiN₃ AFM tips suggested all distorted images were oriented toward the center of the stamp. Apparently, despite keeping the stamping environment cool (4 °C) and enclosed, the stamp moist with reaction-buffer soaked filter paper, and minimizing vibrations or movement, radial stamp

shrinkage during the course of a 12 hour-stamping period produced oblong patterns as features were dragged across the surface. In fact, all stamping times longer than 4 hours showed similar defects caused by radial stamp shrinkage. The estimated height difference between DNA inside and outside of a feature is $1 - 2 \text{ \AA}$, which roughly corresponds to the removal of a single nucleotide from the 3'-terminus of exposed DNA. This level of DNA ablation produced patterns that were near the limit of sensitivity for AFM imaging. In confocal fluorescence imaging, the 3' nucleotide displayed the only reporting moiety and removal of a single base provided a vast improvement in the observed signal. Stamping with stamps not exposed to enzyme showed no detectable pattern or height difference.

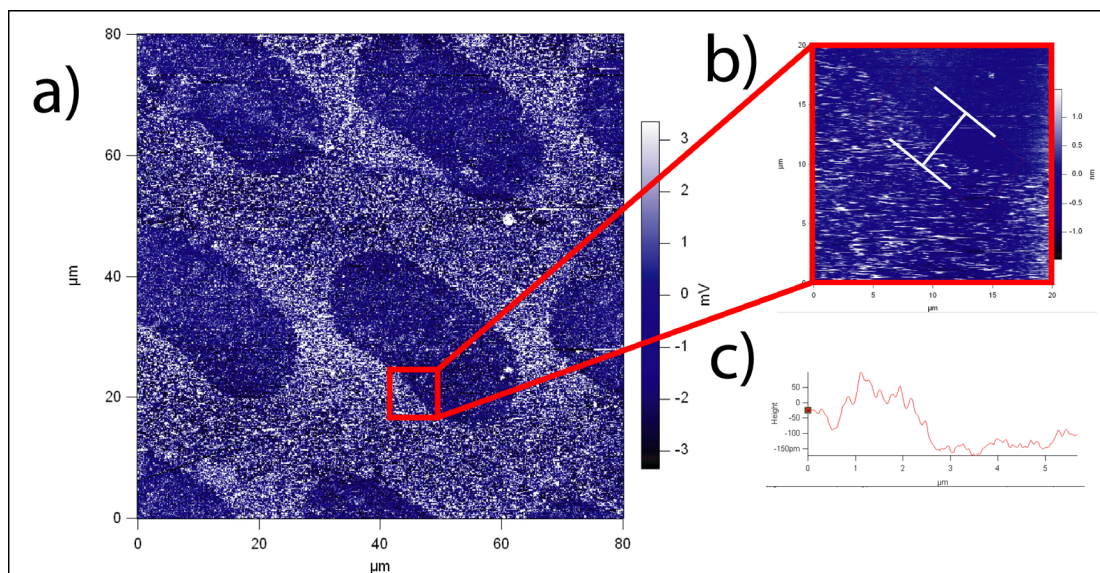


Figure 33. Biocatalytic- μ CP “writing.” a) AFM height image of ssDNA-gold surface exposed to ExoI-immobilized stamps for 12 hours at 4 °C. b) AFM height image of feature edge and c) corresponding 1D height profile of edge at white line.

Acrylamide-based hydrogels have been studied extensively, and their volume-phase transitions in the presence or absence of water and other solvents, temperature, and other environmental and chemical factors are well known.¹⁶⁷⁻¹⁶⁹ During removal of water from an acrylamide gel, shrinkage over time is directly proportional to the square of the gel radius,¹⁶⁷ and therefore explains the defects observed in Figure 33.

Finally, after evaluating the effect of enzyme-immobilized stamping over 1-3 hours, a 1-hour stamping time at 4 °C provided lateral AFM images of stamped features without defects from stamp shrinking (Figure 34). To demonstrate uniformity of pattern across the feature, statistical analysis (over

20,000 points) of the noise inside features (85 μV) and outside of patterned features (89 μV) was performed. Therefore, the mean of the noise (87 μV) is 20-fold greater than the difference in the noise mean (4 μV). The signal-to-noise ratio of the entire feature is roughly 7-fold (630 to 87 μV). Together, these observations suggest that surface roughness is equivalent inside and outside ablated pattern.¹³⁷

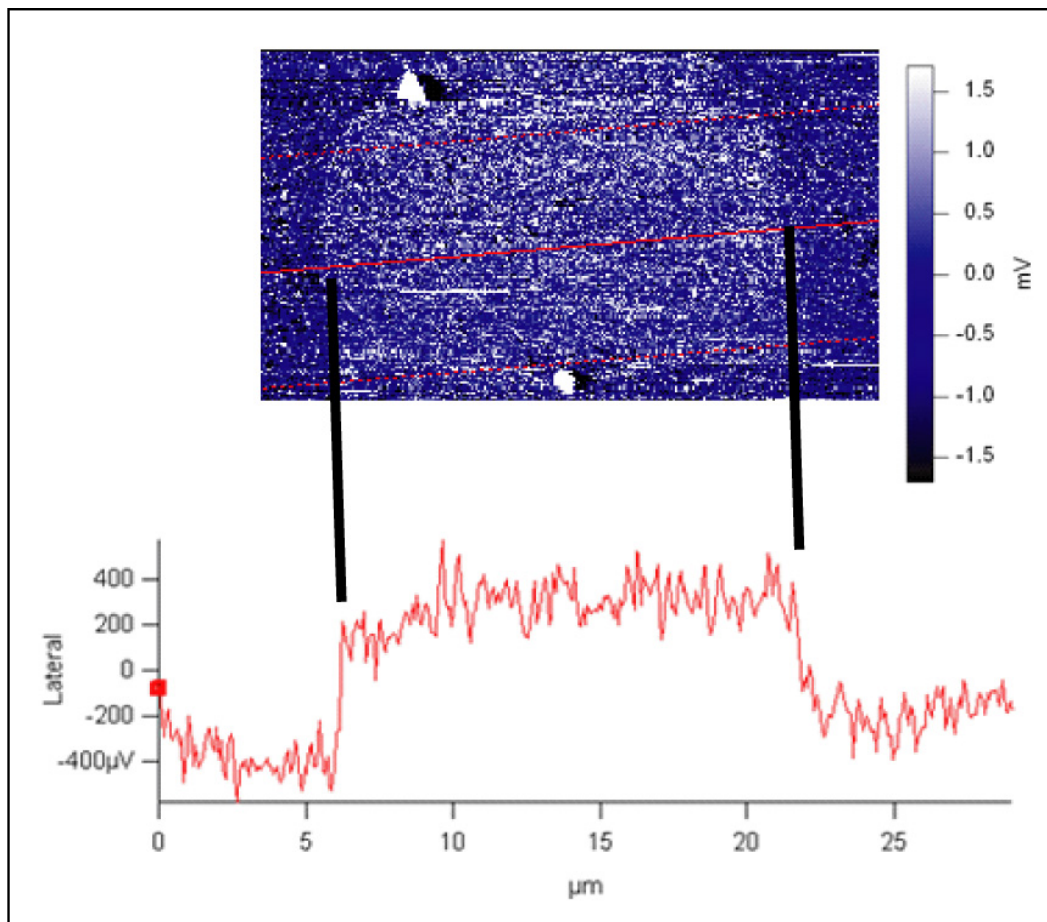


Figure 34. AFM lateral force image and trace of a 15- μm feature replicated from an acylamide hydrogel stamp via biocatalytic- μCP .

2.2.6 Confocal fluorescent microscopy of biocatalytic- μ CP on ssDNA-functionalized ITC-glass substrates

Activated, exonuclease-charged stamps were incubated with 5'-aminoethyl-5'-GATTACAGATTACA-3' DNA containing a 3'-cyTAMRA fluorophore on atomically flat glass slides at 4°C for 1-3 hours using our standard protocol (*Experimental Section*). Surfaces were analyzed by fluorescence microscopy ($\lambda_{\text{excited}} = 530\text{-}560$ nm and $\lambda_{\text{emm}} = 580\text{-}640$ nm) and areas that had been in conformal contact with the enzyme-immobilized stamp showed dark areas consistent with ablation of ssDNA 3'-cyTAMRA fluorophore (data not shown).

Although the fluorescence images showed obvious differences between ablated features and unablated 3'-cyTAMRA-ssDNA, determining edge resolution and quantifying fluorescence inside and outside of features was beyond the capabilities of the fluorescence microscope. Instead, surfaces were analyzed by confocal fluorescence microscopy using a HeNe laser ($\lambda_{\text{abs}} = 543$ nm and $\lambda_{\text{emm}} = 560\text{-}615$ nm). The surface features and spacing matched those of the stamp (± 500 nm). The 12-bit images shown in Figure 35 were obtained at 1024 x 1024 resolution. A clear decrease in fluorescence in the stamped areas confirms the enzyme-charged stamp both came into conformal contact with the cognate surface and removed at least the terminal base bearing the 3'-cyTAMRA

fluorophore. The lighter areas show unmodified fluorophore-functionalized DNA.

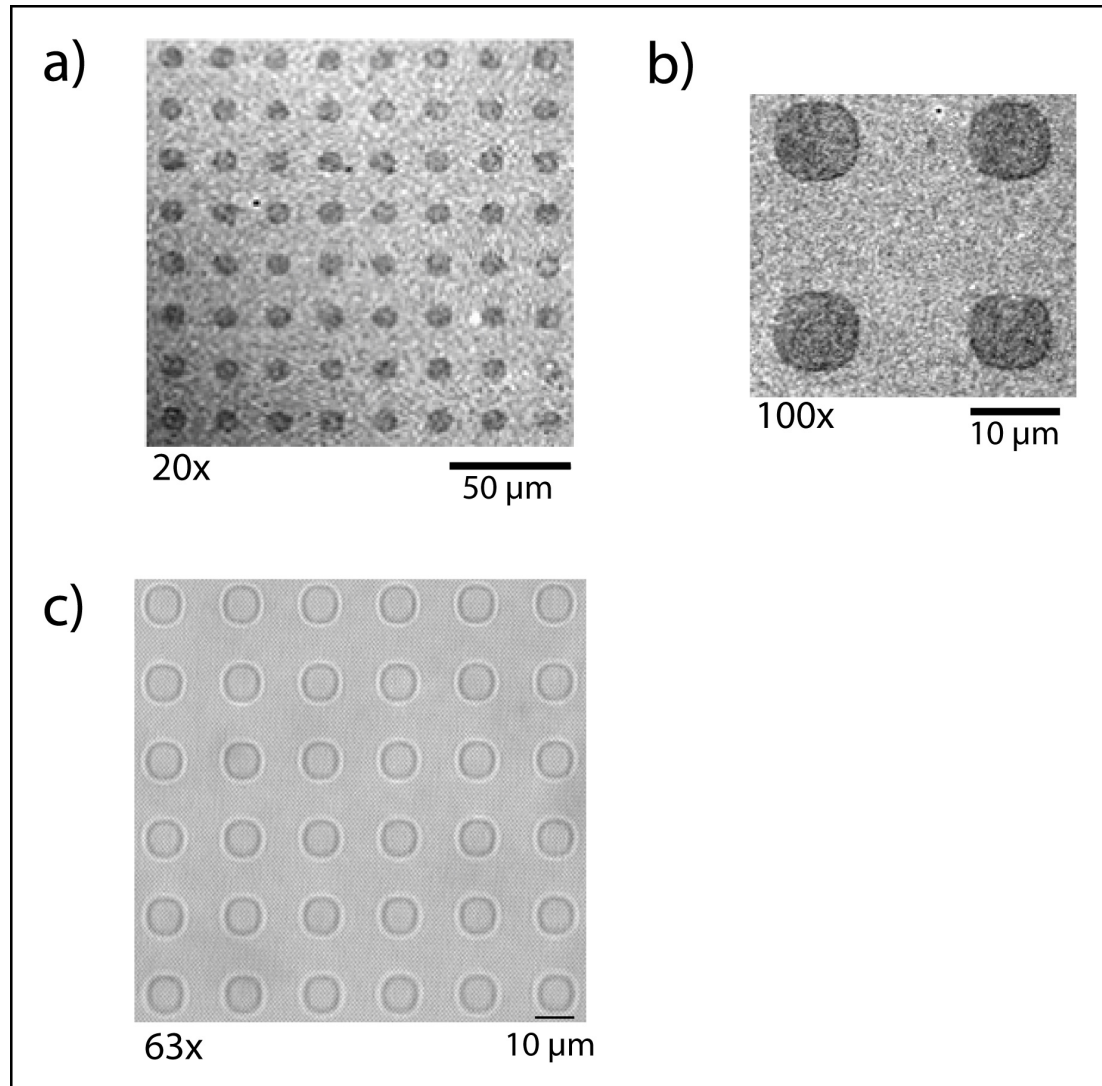


Figure 35. a) and b) Confocal fluorescence microscopy images of biocatalytic- μ CP on immobilized 3'-cyTAMRA-ssDNA. c) Optical micrograph of the stamp used for a and b in contact with glass.

2.2.7 Using confocal fluorescent microscopy of to determine extent of ablation caused by biocatalytic- μ CP

We next turned to the determination of ablation produced by stamp-immobilized ExoI enzyme. The extent of ablation was measured by comparing fluorescence intensity inside and the outside of the patterned features (Figure 36). This difference was related to a calibration plot, prepared by exposing ITC glass slides to ssDNA solutions containing 0%, 20% 40%, 60%, 80%, and 100% 5'-amine, 3'-TAMRA-ssDNA (with the remaining material as unlabeled 5'-amine-ssDNA). An identical experiment using a flat stamp in lieu of a patterned stamp containing immobilized enzyme was used to digest substrates in the same manner at 4 °C for 1-3 hours to ensure both patterned and flat stamps showed the same amount of ablation. Experimental results correspond to a $69.2 \pm 16.9\%$ decrease in intensity for the patterned stamp and a $63.8 \pm 15.5\%$ decrease for the flat stamp, indicating approximately 70% removal of the terminal 3'-cyTAMRA group.¹³⁷ No patterns were observed after stamping without incubating stamps in enzyme or without incubating stamps with Ni^{+2} .

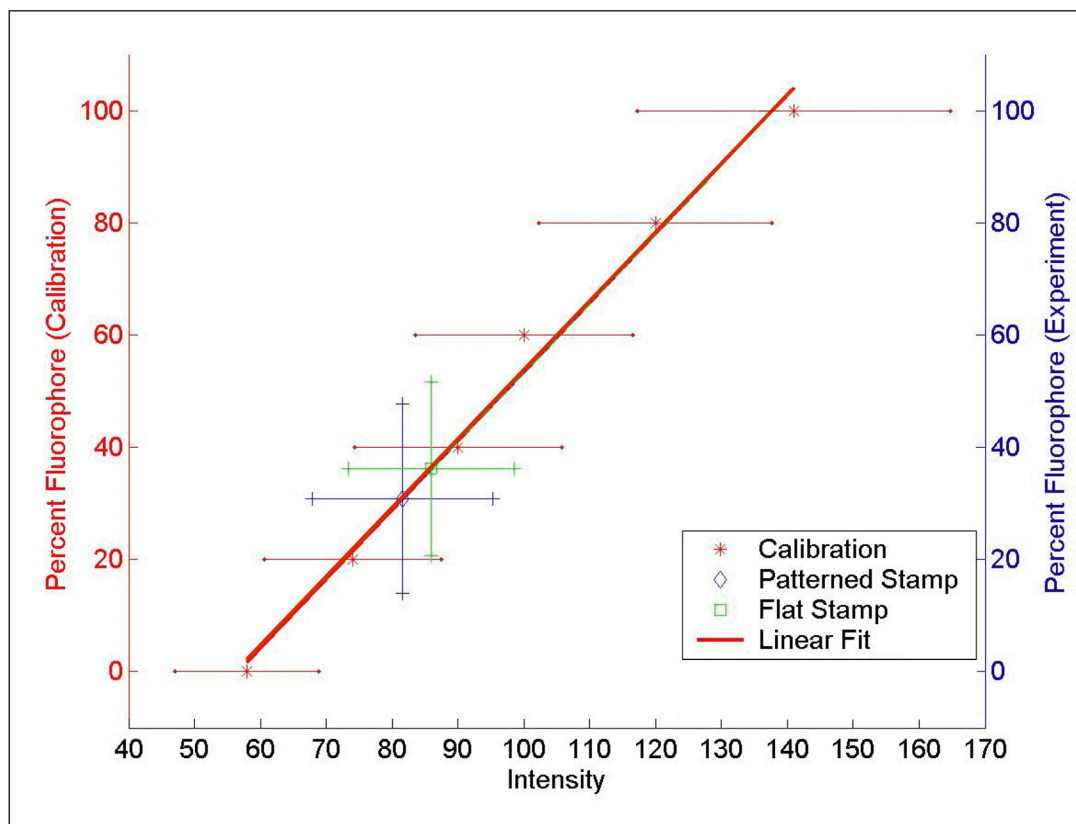


Figure 36. Confocal fluorescence microscopy shows a linear trend between percent immobilized 3'-cyTAMRA-ssDNA and fluorescence intensity.

Experimental results correspond to ~70% removal of the 3'-cyTAMRA fluorophore.¹³⁷

A number of effects might rationalize less than complete removal of the terminal fluorophore, as several parameters were explored: (1) cleaved fluorophore physisorbed on the surface, (2) incomplete reaction between immobilized substrate and immobilized enzyme, (3) measurement errors, (4) loss of ExoI enzyme activity during stamping time.

To investigate the possibility of cleaved TAMRA fluorophore remaining physisorbed on the surface after enzymatic stamping in biocatalytic- μ CP, ITC

surfaces were functionalized with TAMRA-functionalized ssDNA, incubated with (flat) stamp-immobilized enzyme, exposed to solutions containing sodium dodecyl sulfate (SDS) for an hour to remove any physisorbed ssDNA, and analyzed via confocal fluorescence microscopy. SDS is a commonly-used detergent in molecular biology used to separate cellular debris from DNA in DNA extraction protocols.¹⁷⁰ SDS is also used in DNA microarray buffers to minimize non-specific interaction with surfaces before and after DNA hybridization.¹⁷¹ A non-native DNA base, such as the hydrophobic TAMRA fluorophore, should be removed by SDS if it is only physisorbed to the surface, while intact ssDNA covalently immobilized on the surface should remain unaffected. As shown in Table 1, exposure to SDS did not significantly decrease the intensity on Samples 1-3; however, it did decrease the error (rms deviation) in every instance.

Table 1. Intensity values of cleaved fluorophore-functionalized ssDNA on ITC surfaces before and after exposure to detergent (SDS).

	<u>Intensity Before SDS Wash</u>	<u>Intensity After SDS Wash</u>
Sample 1: 10% SDS	83.4 ± 12.8	81.2 ± 5.4
Sample 2: 1% SDS	97.5 ± 11.9	91.3 ± 8.6
Sample 3: 0.5% SDS	79.0 ± 3.4	80.8 ± 2.6

Incomplete reaction between immobilized substrate and immobilized enzyme could also account for the only ~70% ablation of the 3'-cyTAMRA fluorophore. Glass surfaces were prepared as described previously, incubated with flat stamps charged with immobilized enzyme and incubated for 60, 100, and 120 minutes (Table 2). Due to the error in these results, there is little change in intensity between 60 minutes and 120 minutes. When compared to the observed intensities for patterned and flat stamps in Figure 36, the error between the two stamps is approximately ± 7 intensity units. Therefore, we hypothesize immobilized enzymatic digestion for the ExoI-ssDNA model system is complete after 60 minutes.

Table 2. (Flat) Stamp-immobilized ExoI activity assay on glass substrate.

<u>Time (minutes)</u>	<u>Measured confocal fluorescence intensity signal</u>
60	89.8 \pm 2.9
100	84.6 \pm 4.6
120	83.2 \pm 1.5

A third possibility for incomplete removal of the terminal fluorophore could be due to measurement error. After measuring the intensity of 20 different areas of one substrate digested with stamp-immobilized enzyme, intensity before stamping was 130 ± 4.54 and 87.8 ± 4.07 after stamping. Thus, the intensity error

throughout one substrate (intrasample error) was estimated to be ± 4 intensity units. To measure the sample intensity error between different surfaces (intersample error), five identical substrates were analyzed both before and after stamping with immobilized enzyme. Intersample intensity for the five substrates before stamping was 121.8 ± 11.6 and 85.8 ± 12.1 after stamping. Thus, the intersample intensity error was estimated at ± 12 . The experimental errors of ± 4 and ± 12 for intra- and intersample intensity, respectively, correspond well to the total sample error, which was approximately ± 16 , as shown in Figure 36.

A final question raised was whether discontinuation of ablation was due to loss of enzyme activity. To explore this issue, a flat, enzyme-activated stamp was incubated for 60 minutes with a TAMRA-ssDNA-functionalized glass surface and then removed, incubated again in reaction buffer, dried slightly, and placed on another TAMRA-ssDNA-functionalized glass surface for 60 minutes. The intensity obtained with confocal fluorescence microscopy after digestion of the first substrate was 96.7 ± 9.87 , and the intensity after digestion of the second substrate was 108 ± 10.7 . There was no significant difference between the intensities of the digested substrates; therefore, we concluded ExoI enzyme remains functional after 60 minutes and ablation of the substrate must be limited

by physical constraints of the immobilized enzyme-immobilized substrate system.

These physical constraints could arise from either surface. The manner in which enzyme is bound on the stamp is immobilized may result in incomplete digestion of the ssDNA-terminated surface. The density of NTA groups on the surface of the stamp could be increased by increasing NTA-acrylamido lysine to the stamping material to increase the amount of enzyme immobilized. More likely is that ssDNA substrate is not well-ordered. Some of the ssDNA could be laying flat on the surface, inaccessible to the enzyme but still emitting fluorescence intensity. Background fluorescence of plain ssDNA should not play a role as it was accounted for during construction of the calibration plot in Figure 36.

2.2.8 Using MALDI-TOF spectroscopy to determine the extent of ablation caused by biocatalytic- μ CP

In addition to determining horizontal ablation efficiency of our technique through confocal fluorescence microscopy, we also considered the vertical extent of ablation, i.e. the number of bases cleaved of ablation using MALDI-TOF spectroscopy. Aside from the height images provided by AFM (Figure 33), a more quantitative method for determining ablation was sought. Mrksich and co-

workers have shown that gold-immobilized thiol- and disulfide-functionalized oligoethyleneglycols displaying either a short peptide or carbohydrate can be detected via MALDI-TOF MS.^{165, 172-173} ssDNA oligomers have also been visualized from surfaces using MALDI-TOF MS.¹⁶⁶

Both ssDNA-gold and glass surfaces were incubated with 6-aza-2-thiothymine (ATT) as a matrix. No significant peaks were observed from gold surfaces before incubation with stamps, but glass surfaces showed a clear mass peak at 3885.90 g/mol for 3'-TAMRA-ssDNA (Figure 37). To simulate confocal microscopy experiments, ssDNA-functionalized glass surfaces were made and incubated with enzyme-immobilized flat stamps. Unfortunately, no significant mass peaks could be identified after stamping with an enzyme-functionalized stamp using MALDI-TOF MS as shown in Figure 37. It appears the enzyme has completely ablated the 3'-TAMRA-ssDNA mass peak and produced a range of products in the process (TIC > 3200 for both). This range of peaks could be from multiply-charged DNA products, MALDI-induced fragmentation, and/or subsequent binding of the resulting product(s) on the surface to various cations surfaces to which they had been exposed. Due to the nature of biocatalytic- μ CP, the stamp is exposed to many ions when undergoing incubations in various buffered solutions for enzyme immobilization and activation. Studies have

shown that upon exposure to H^+ , Na^+ , and K^+ ions, a variety of ionic species of the type $[(\text{analyte}^-) (H^+)_x(Na^+)_y(K^+)_z]^-$ are formed resulting in poor resolution of mass peaks and m/z assignments difficult.¹⁷⁴⁻¹⁷⁶ Fragmentation of the ssDNA oligonucleotide could have also occurred either separately or in conjunction with ion adduction.¹⁷⁷ In unrelated MALDI-based DNA experiments containing no terminal TAMRA group, a similar broad peak of ions was also observed but without exposure to enzyme, indicating MALDI-induced fragmentation (or multiply-charged DNA species).

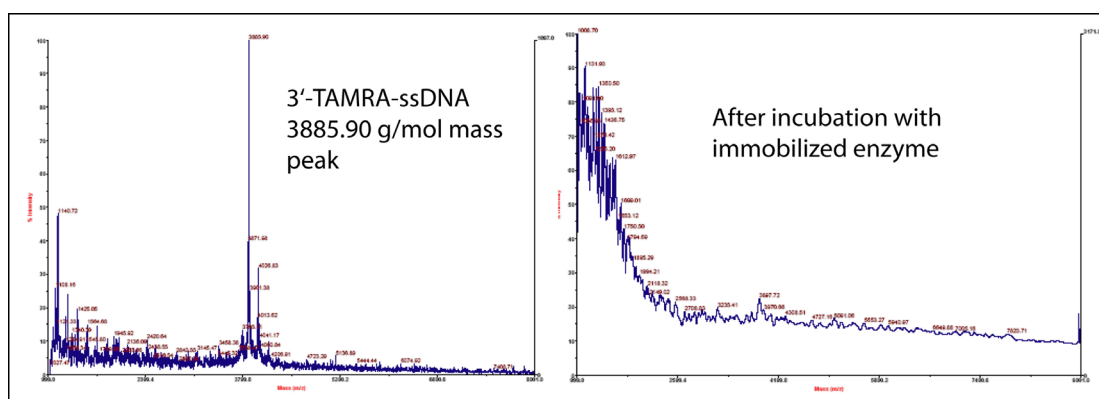


Figure 37. MALDI-TOF spectroscopy of 3'-TAMRA-ssDNA-hexylamine-5' immobilized on glass slides before (left) and after (right) exposure to biocatalytic- μ CP with flat stamps (with ATT matrix).

Resolution problems are not uncommon when analyzing ssDNA by mass spectrometry due to the tendency of the highly charged DNA backbone to form ionic bonds with sodium and potassium cations.^{176, 178} Although ATT is the most commonly-utilized matrix for analysis of ssDNA in the literature,¹⁷⁸ the use of

tetraamine spermine as a matrix additive instead of ammonium salts has been shown by Asara and Allison to significantly reduce cation adduction and improve detection limits, even after digestion with a DNA exonuclease.¹⁷⁶ Utilization of this protocol¹⁷⁶ with ssDNA-functionalized gold and glass surfaces failed to produce observable mass peaks in MALDI-TOF MS even for unablated samples.

2.2.9 Conclusions from biocatalytic- μ CP using ExoI-ssDNA as a model system

The results presented here demonstrate the feasibility of transferring pattern from a stamp bearing reversibly-immobilized catalyst to a surface bearing immobilized cognate substrate via a specific biochemical reaction. Conceivably, a variety of His₆-tagged enzymes could sequentially be applied to the stamp, providing a way to pattern surfaces with a series of biochemical reactions using a single stamp. To remove His₆-tagged enzyme from Ni⁺² columns using standard IMAC procedures, imidazole is used to competitively remove the enzyme from the Ni⁺²-chelated NTA group. Metal-chelating reagents such as ethylenediaminetetraacetic acid (EDTA) also could be used to chelate the Ni⁺², thus removing the enzyme from the NTA group.^{164, 179} Both of these

methods should be compatible with the immobilization strategy utilized in biocatalytic- μ CP.

Biocatalytic- μ CP as a patterning technique is not limited to ablative patterning – His₆-tagged enzymes for phosphorylation, oxidation, reduction, and other enzyme-catalyzed reactions could be used to transfer pattern in a variety of ways. This proof-of-concept system also opens the door to catalytic- μ CP, in which immobilized chemical moieties such as acids and bases are polymerized into a stamp and used to pattern cognate substrates.

In conclusion, we have demonstrated the feasibility of biocatalytic- μ CP using the model system ExoI-ssDNA on both gold and glass surfaces. (1) Copolymerization of an acrylamido-NTA monomer produces a stamp suitable for reversible non-covalent binding of enzyme catalyst. (2) The stamp bearing reversibly immobilized enzyme was successfully used to transfer pattern to a surface bearing cognate substrate, resulting in ~ 70% horizontal ablation in the areas of conformal contact. This represents a greater than two-fold improvement over previous catalytic- μ CP efforts.⁸¹ (3) “Inkless” catalytic- μ CP should improve resolution, by removing the diffusive process during pattern transfer. However, edge resolution was limited by the elastomechanical properties of the bulk acrylamide stamp and could not provide the same

resolution as stamping materials for previously demonstrated inkless catalytic- μ CP with more robust elastomechanical properties.⁸¹ As a whole, biocatalytic- μ CP shows promise as a technique for the transfer of nanoscale features through diffusionless pattern transfer.

2.3 Resolution of biocatalytic- μ CP dependence on tether length

In order to improve the resolution of inkless catalytic- μ CP methods, alternative stamping materials that circumvent stamp collapse and feature deformation associated with mechanically weak hydrogels (such as acrylamide) were considered. Of particular interest, polyurethane-based (PU) acrylates have shown great promise as rigid, elastomeric stamping materials capable of making conformal contact while maintaining mechanical integrity during stamping.^{109, 120, 180} PU stamps have been used in a traditional form of μ CP in which alkanethiols were stamped on gold¹⁰⁹ as well as in unconventional methods such as catalytic- μ CP on SAMs used in our laboratory.^{120, 139} Both applications resulted in pattern transfer of sub-300 nm features and demonstrated polyurethane-based acrylates are readily co-polymerized with other acrylates through a UV-light induced, radical reaction. Therefore, the PU-based acrylate could potentially be co-

polymerized with acrylamido-NTA lysine **3** or similar acrylates for subsequent immobilization of His₆-tagged enzyme via Ni⁺² chelation to the NTA group.¹³⁷

At some point, the resolution of biocatalytic- μ CP becomes dependent on the length of the tether between the polymerization terminus (acrylamide moiety) and the protein-immobilization terminus (NTA moiety). Varying the length of the tether should then vary the resolution accordingly. To explore the effect of linker length on resolution, a longer bifunctional molecule was synthesized using tetraethylene glycol (TEG) to increase the overall tether length by roughly 1.8 nm over that of NTA-acrylamido lysine **3**.

The increased distance between the polymerization terminus (acrylamide functionality) and the protein-immobilization terminus (NTA functionality) provides additional degrees of freedom at chain termini and may improve enzyme activity.

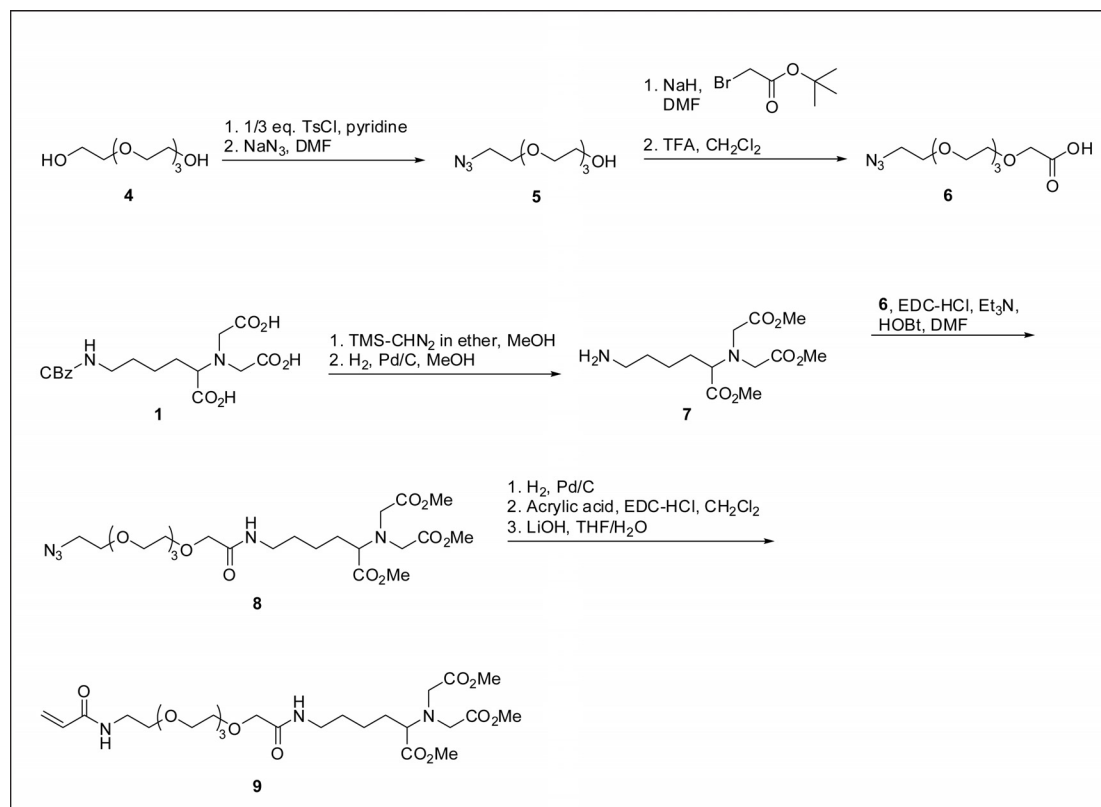


Figure 38. Synthesis of acrylamido-TEG-NTA lysine 11.

Acrylamido-tetraethyleneglycol NTA lysine **9** (acrylamido-TEG-NTA-Lys) was prepared from *N*^ε-benzyloxycarbonyl-L-lysine **1** and tetraethyleneglycol **4** in ten steps (Figure 38). Tetraethyleneglycol **4** was activated with 1/3 equivalent of tosyl chloride to produce sufficient monotosylate (over the ditosylate) for displacement with azide to produce azido-alcohol **5**. Addition of tert-butyl bromoacetate was then used to increase the chain length, providing a protected acid functionality that was deprotected via acid-catalyzed ester hydrolysis. NTA-lysine derivative **1** was synthesized according to the procedure of Schacher

and co-workers,¹⁵² protected as the triester, and *N*-deprotected via hydrogenolysis to yield amine **7**. Compounds **6** and **7** were then coupled via EDC-promoted amidation to form **8**. Catalytic reduction of the azide functionality, acylation with acrylic acid, and standard ester deprotection provided the desired acrylamido-TEG-lysine **9**.

Unfortunately, **9** proved insoluble in several PU-based acrylates, most likely due to the acidic NTA moiety. However, our efforts with chemical catalytic- μ CP using immobilized acids and bases showed more promise than biocatalytic- μ CP efforts and are generally applicable to patterning on a multitude of surfaces at a higher resolution and shorter time.^{120, 139} Thus, we continued forward with catalytic- μ CP (Chapter 4).

3. Expansion of biocatalytic- μ CP to other enzyme-substrate systems

3.1 Overview

Our initial embodiment of biocatalytic microcontact printing serves as a proof-of-concept demonstration of the use of immobilized biocatalysts to achieve pattern transfer of an elastomeric stamp. The practical utility of the specific system, however, is greatly limited by both the stamping material and the specific enzyme-substrate pair.¹³⁷ To improve the resolution and broad applicability of this technique, more robust stamping materials and new enzyme-substrate systems were explored.

The resolution of our initial demonstration was limited by the poor mechanical integrity of the acrylamide stamping materials. PDMS – the stamping material of choice for soft lithography – is of no value for biocatalytic lithography because of the hydrophobic nature of the material and an inability to functionalize the polymer with enzyme immobilization sites. Accordingly, we investigated new polymer materials. Of particular interest in this regard, polyurethane-based (PU) acrylates have recently shown great promise as rigid, elastomeric stamping materials capable of making conformal contact while preserving mechanical integrity during stamping.^{109, 120, 180} PU stamps have been

used to stamp patterns of alkanethiols on gold¹⁰⁹ as well as in catalytic- μ CP on SAMs used in our laboratory.^{120, 139} Both applications resulted in pattern transfer of sub-300 nm features. Polyurethane-based acrylates are also readily co-polymerized with other acrylates through a UV-light induced, radical reaction facilitating incorporation of both hydrophilic moieties and enzyme immobilization sites. For example, PU acrylate can easily react via Michael addition with a nucleophile to functionalize a stamp for catalytic activity, as demonstrated in recent catalytic- μ CP methods.^{120, 139} A PU-based acrylate could potentially be co-polymerized with acrylamido-NTA lysines **3** or **9** or reacted via Michael addition with their amine precursors. Both approaches would allow for subsequent immobilization of His₆-tagged enzyme via Ni⁺² chelation to the NTA group.¹³⁷ Because of these advantages, PU-based acrylate was considered as a material for stamp fabrication while examining other enzyme-substrate systems for high-resolution biocatalytic- μ CP.

To improve the versatility and broader applicability of biocatalytic- μ CP, new enzyme-substrate systems were explored. We focused our efforts on substrates that would facilitate further functionalization of SAMs after stamping, such as carboxylic acids and amines. Bifunctional SAMs consist of three regions: (1) a terminal headgroup allowing SAM assembly, (2) a terminal functional

group facing solution and capable of enzyme modification, and (3) a backbone connecting the two functionalities consisting a carbon and/or oligoethyleneglycol chain for use as a protective and ordering layer (Figure 39).¹⁸¹ For SAM formation, gold has historically proven an attractive substrate due to ease of preparation, ability to form a highly stable and covalent bond with sulfur resulting in ordered monolayer formation, chemical inertness, and resistance to oxidation.¹⁸¹ SAMs formed from alkanethiolates with various terminal functional groups have been studied extensively.^{21, 60-61, 63-64, 82, 160, 182} In addition, due to previous success and ease using ssDNA alkanethiols on gold, we decided to again use a gold-alkanethiolate system for the expansion of biocatalytic- μ CP to other enzyme-substrate systems.

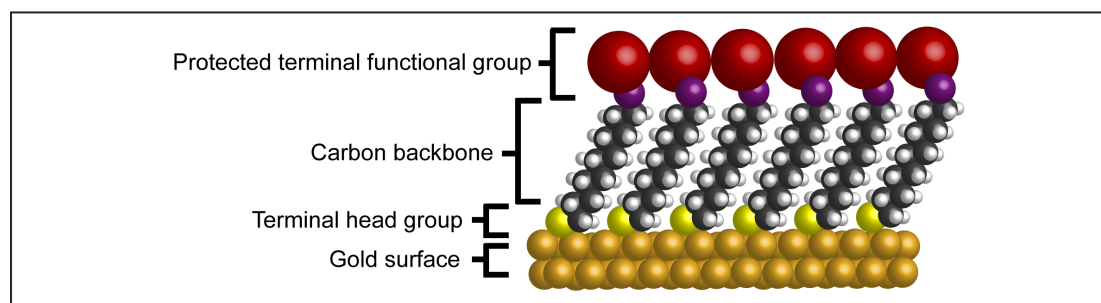


Figure 39. The three regions of bifunctional SAMs on gold.

With both the terminal head group and backbone selected, we focused our attention on finding a functional group that could be easily patterned using biocatalytic- μ CP. In synthetic organic chemistry, protecting groups are used to

mask the reactivity of a particular group. The functional group is able to react with another chemical moiety only after the protecting group is removed. The catalytic ablation of protecting groups has been applied to inkless catalytic- μ CP in patterning Fmoc-protected thiols with a basic stamp,¹³⁹ and TBS- and Boc-protected thiols with an acidic stamp.^{81, 120} This system might be applicable to biocatalytic- μ CP as well.

3.2 Carboxyesterases and lipases for use in biocatalytic- μ CP

Hydrolases are enzymes that catalyze the hydrolysis of a chemical bond and are the most frequently-used enzymes in organic synthesis, due to their broad substrate specificity, lack of cofactor requirement, and stability.¹⁸³ Among hydrolases, the lipases and carboxyesterases are especially useful enzymes that catalyze hydrolysis of ester bonds to their corresponding acids and alcohols at interfacial surfaces formed between water and water-insoluble lipid substrates.¹⁸⁴ Their ability to hydrolyze substrates at interfaces was especially appropriate for use in biocatalytic- μ CP. Synthetic precursors of ester substrates for lipases and carboxyesterases with varying functional groups are commercially available and easily converted into SAM substrates. Lipases and carboxyesterases are also active without cofactors and catalyze ester hydrolysis under mild conditions.¹⁸³

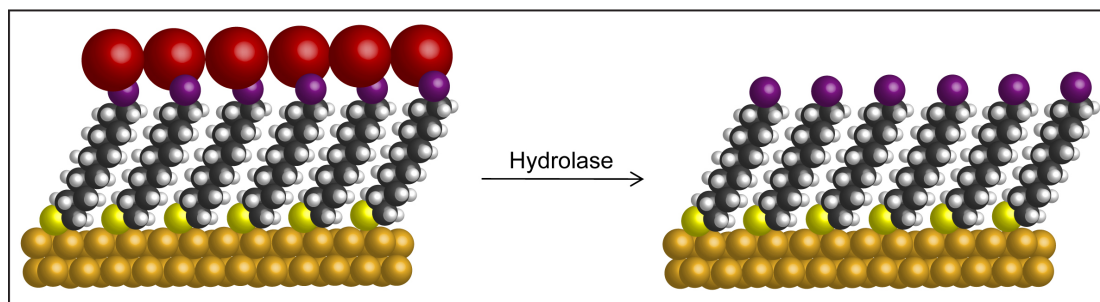


Figure 40. Reaction of a hydrolase with protected alkanethiols.

With an enzyme-substrate system in mind and a functional immobilization strategy for both enzyme and substrate, lipases and carboxyesterases were explored with the following properties: (1) The enzyme must be active in monomeric form to eliminate any issues associated with oligomerization at the stamp. (2) For facile expression and purification, expression of the enzyme in *E.coli* or yeast with a His₆-tag was required. (3) Finally, the enzyme must be functional without additional cofactors. Enzymes satisfying these criteria included acetyl esterase (AES), the carboxyesterase BioH, and *R.oryzae* lipase (ROL).

3.2.1 Acetyl esterase (AES)

Acetyl esterase (AES) is an esterase from *E.coli* and a member of the hormone-sensitive lipase family. In addition to cleaving acetates, AES has been shown to cleave phenyl esters with acyl chain lengths of C₂ to C₆ (Figure 41: n = 0 – 4).¹⁸⁵⁻¹⁸⁶ We received the AES gene in a pQE-lacIq vector, which contains an

engineered N-terminal hexahistidine-tag, from Dr. Kinga Gerber at the University of Konstanz. Transformation into BL-21 cells and subsequent protein expression, followed by purification on Ni²⁺ column provided ~ 0.1 mg of protein per liter of growth.

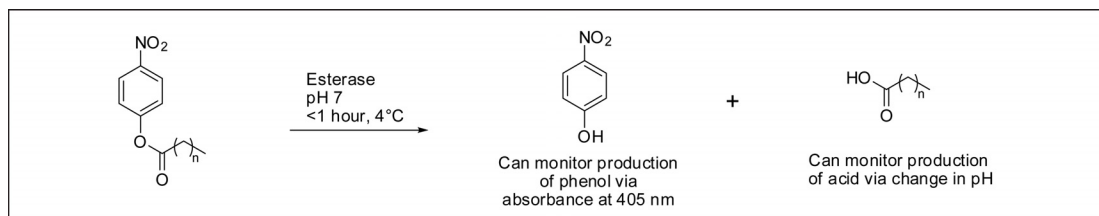


Figure 41. Methods to monitor activity of esterases with pNPEs.

Kinetic parameters for AES hydrolysis were evaluated using p-nitrophenyl esters (pNPEs) of fatty acids to explore the substrate specificity with respect to acyl chain length.¹⁸⁶ Para-nitrophenyl acetate (pNPA) (specific activity = 34.2 U/mg)¹⁸⁶ was used as a standard to test enzyme activity after expression and purification as well as immediately before substrate specificity experiments (Figure 41, n = 0).

AES activity can be measured by UV-VIS at 405 nm or via change in pH. Reactions monitored via pH were conducted at 4 °C to minimize the uncatalyzed hydrolysis of pNPA, and in 1/8X binding buffer without imidazole (62.5 mM NaCl, 2.5 mM Tris-HCl buffer, pH 7.0) since this buffer is used in stamping experiments. Reactions contained 10 μM enzyme and 1 mM substrate. Figure 42

shows the decrease in pH observed for enzyme-catalyzed reactions ($\Delta\text{pH} \sim 1.5$ over 30 minutes) compared to the controls containing no enzyme ($\Delta\text{pH} \sim 0.2$ over 30 minutes), showing that the enzyme is active against pNPA. The small change in pH for the controls is a result of the uncatalyzed hydrolysis of pNPA and has been observed by others.¹⁸⁷

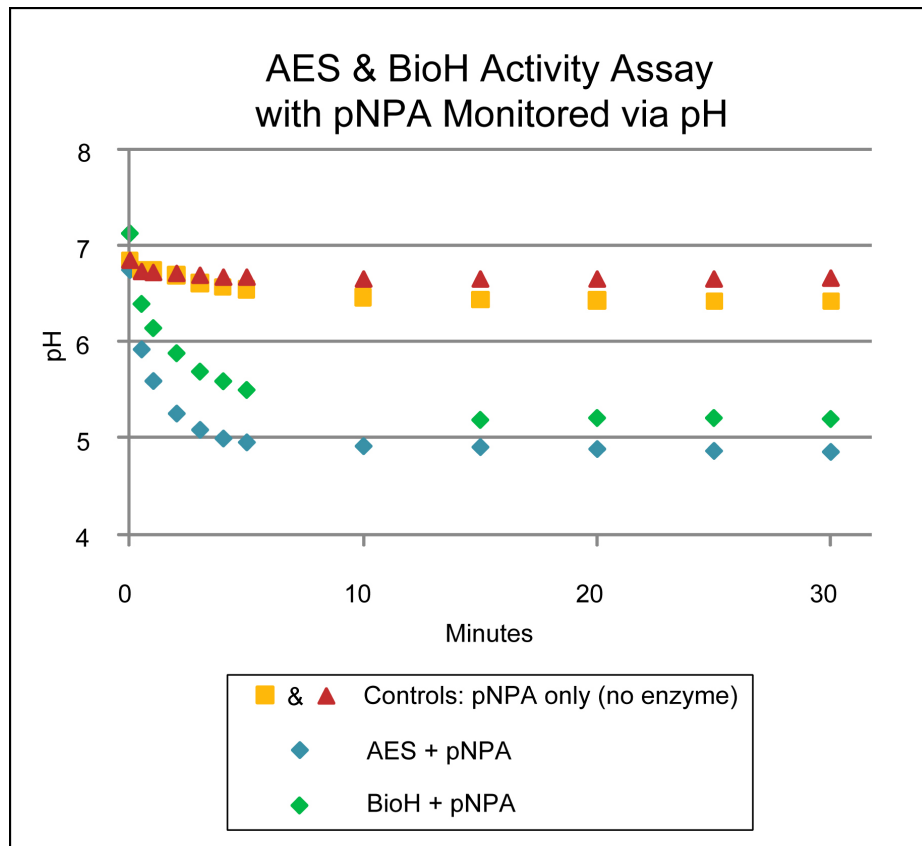


Figure 42. Testing AES and BioH activities with pNPA monitored via a change in pH over time.

3.2.2 BioH esterase (BioH)

BioH is a monomeric carboxylesterase isolated from *E.coli* that displays broad substrate specificity against many types of esters including acyl esters of

phenol with acyl chain lengths ranging from C₂ to C₁₂ (Figure 41, n = 0 – 10).¹⁸⁸

BioH includes the canonical Ser-His-Asp catalytic triad found in many lipases.¹⁸⁸

Genomic DNA was isolated from *E.coli* DH5 α cells, and BioH was amplified using standard PCR with forward and reverse primers 5'-TATAGGATCCATGAATAACATCTGGTG-3' and 5'-TATAAAGCTTCACCCTCTG CTTCAAC-3', respectively, cut with BamH1 and HindIII, and ligated into a pET-22b vector containing a C-terminal His₆-tag. Sequencing confirmed successful ligation of the BioH gene into the pET-22b vector. Transformation into BL-21 cells and subsequent overexpression of protein, followed by purification on Ni⁺² column, provided ~ 0.1 mg of protein per liter of growth.

Studies examining the kinetic parameters for BioH-catalyzed hydrolysis also used pNPEs of fatty acids to explore substrate specificity in relation to acyl chain length.¹⁸⁸ pNPA (specific activity = 22.5 U/mg)¹⁸⁸ was used as a standard to determine enzyme activity after expression and purification and immediately before hydrolysis experiments (Figure 41, n = 0). To determine the activity of BioH, the same protocol and concentrations used to determine the activity of AES were used. Figure 42 shows a significant decrease in pH for enzyme-catalyzed hydrolysis (Δ pH ~ 1.9 over 30 minutes) compared to the

controls containing no enzyme ($\Delta\text{pH} \sim 0.2$ over 30 minutes), showing that the enzyme is active against pNPA.

3.2.3 *R.oryzae* lipase (ROL)

Recently, a lipase from the fungus *Rhizopus oryzae* (*R. oryzae*) was expressed cytoplasmically in active form in Origami(DE3) *E. coli* cells.¹⁸⁹ *R. oryzae* lipase (ROL) shows good activity against short acyl chain esters of phenol and has been expressed with both C- and N-terminal His₆-tags, although only the C-terminal His₆-tag form maintained activity.¹⁸⁹ The ROL gene was provided by Drs. Uwe T. Bornscheuer and Michael Haas in a pET-11d vector containing a C-terminal His₆-tag sequence. Transformation into Origami(DE3) cells and subsequent overexpression of the protein, followed by purification on Ni²⁺ column provided ~ 2.4 mg of protein per liter of growth.

The specific activity of ROL has been determined using p-nitrophenyl butyrate (pNPB) as a substrate (specific activity = 47.3 U/mg),¹⁸⁹ and we used pNPB to determine enzyme activity after expression and purification, and immediately before hydrolysis experiments (Figure 41, n = 2). The same protocol used to determine the activity of AES and BioH was used except pNPB was used in place of pNPA. Figure 43 shows a significant decrease in pH for enzyme-catalyzed hydrolysis ($\Delta\text{pH} \sim 2.5$ over 30 minutes) compared to controls containing

no enzyme ($\Delta\text{pH} \sim 0.2$ over 30 minutes), showing that the enzyme is active against pNPB.

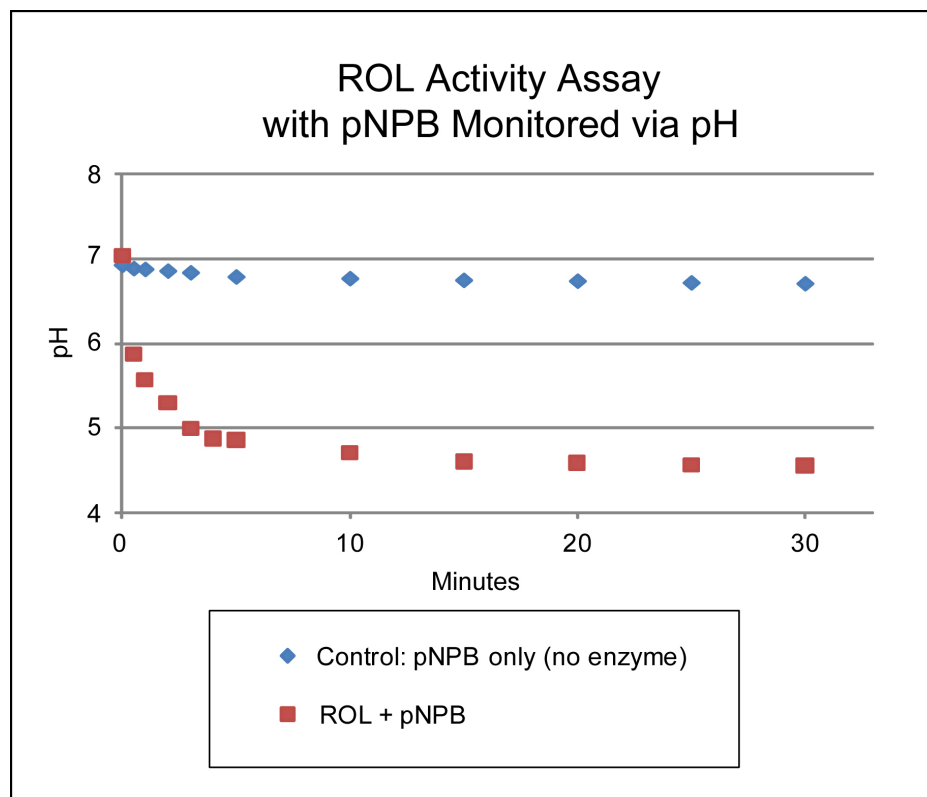


Figure 43. Testing ROL activity with pNPB monitored via a change in pH over time.

Having successfully demonstrated expression, purification by His₆-tag, and catalytic activity of three esterases, AES, BioH, and ROL with their known pNPE substrates, we turned to ester synthesis.

3.3 Selection of functional ester protecting group for carboxyesterase-benzoic ester model system

Substrates for biocatalytic- μ CP must provide both an attractive ester for carboxyesterases activity while simultaneously providing a functionality for SAM formation on gold. Alkanethiols and disulfides both form ordered SAMs on gold, as previously described.^{21, 26, 190} Commercially-available alkanethiols and alkanedisulfides of varying chain lengths functionalized with carboxylic acids can be readily transformed into esters using standard synthetic methods.

Two main criteria in ester selection must be considered. First, AES, BioH, and ROL must be active against the ester substrate. Because each of our selected enzymes has demonstrated an ability to hydrolyze phenyl esters of varying acyl chain length, aryl esters were explored as surface substrates.^{185, 188-189} Second, a means of quantitating ester hydrolysis must be incorporated. X-ray photoelectron spectroscopy (XPS) is a quantitative spectroscopic method for measuring the elemental composition and connectivity of atoms on a surface. XPS can also be used to determine the empirical chemical formula of surface immobilized compounds.¹⁹¹ Fluorine displays a high atomic sensitivity factor (ASF) in XPS (1.00) relative to carbon (0.278),¹⁹¹ which would make up the majority of atoms on the surface. In addition, the strong electron-withdrawing

capability of fluorine should increase the susceptibility of ester substrates to hydrolysis.

To determine if substitution of a single fluorine for the $-\text{NO}_2$ group would affect catalytic ester hydrolysis, commercially-available, p-fluorophenyl acetate (pFPA) was tested as a substrate for AES and BioH enzymes. The same protocol used to determine the activity of AES and BioH with pNPA was used to determine the activity of AES and BioH against pFPA. Figure 44 shows a significant decrease in pH for enzyme-catalyzed hydrolysis ($\Delta\text{pH} \sim 2.5$ for AES and ~ 1.5 for BioH over 30 minutes) compared to controls containing no enzyme ($\Delta\text{pH} \sim 0.2$ over 30 minutes). This experiment shows that both enzymes are active against pFPA, and substitution of fluorine for the $-\text{NO}_2$ group results in catalytic hydrolysis.

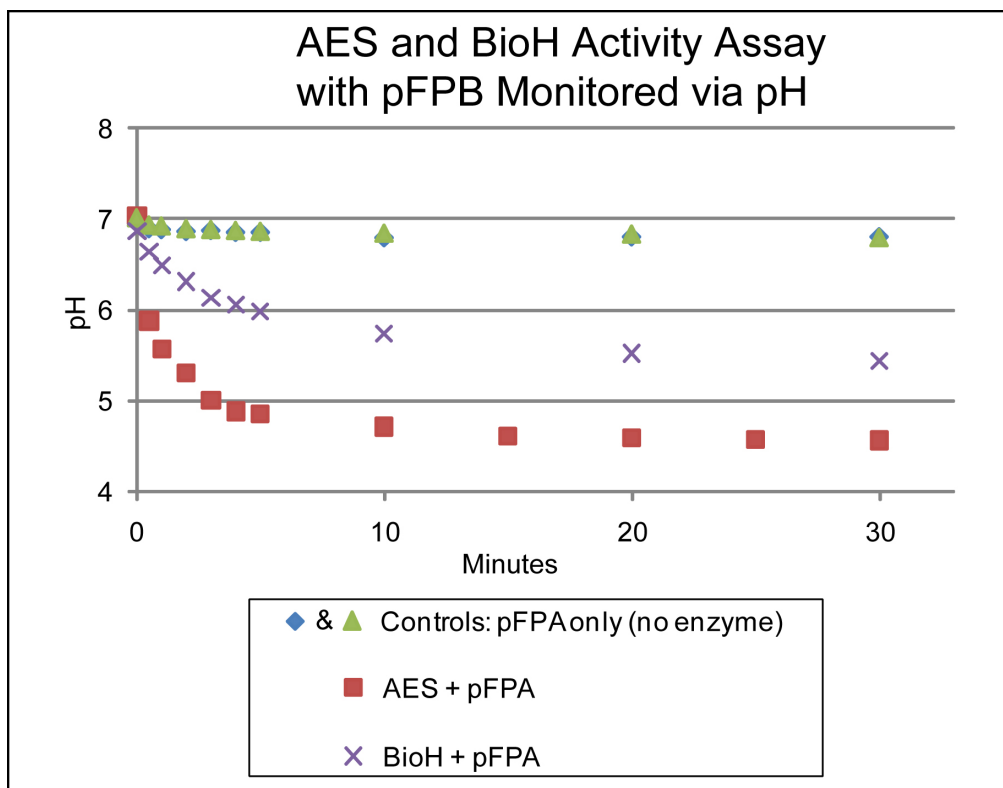


Figure 44. Testing AES and BioH activity with pFPA monitored via a change in pH over time.

3.4 Synthesis of para-fluorinated alkanethiol and disulfide benzyl esters and subsequent surface characterization

p-Fluorinated alkanethiol and disulfide benzyl esters of varying chain lengths were synthesized and tested as substrates for the various carboxyesterases. Because disulfides and the corresponding thiols both form ordered SAMs on gold,¹⁹²⁻¹⁹³ the disulfide forms of the esters were initially used for activity assays both in solution as well as on surfaces. Benzyl esters were used due to commercial availability of desired compounds and facile synthesis.

Mercaptoundecanoate **14** was synthesized from 11-mercaptoundecanoic acid **10** in three steps (Figure 45). Oxidation of thiol **10** to disulfide **11** with I₂ and methanol proceeded with concomitant formation of methyl esters of **11**. To avoid esterification, thiol oxidation was achieved with a 3% aqueous solution of H₂O₂. Disulfide **11** was esterified with either 4-fluorobenzyl bromide or 4-(trifluoromethyl)benzyl bromide, providing esters **12** and **13**, respectively. Disulfide **13** was reduced with dithiothreitol (DTT), providing free thiol **14**. Esters **12**, **13**, and **14** were used for surface experiments and/or in solution-based activity assays.

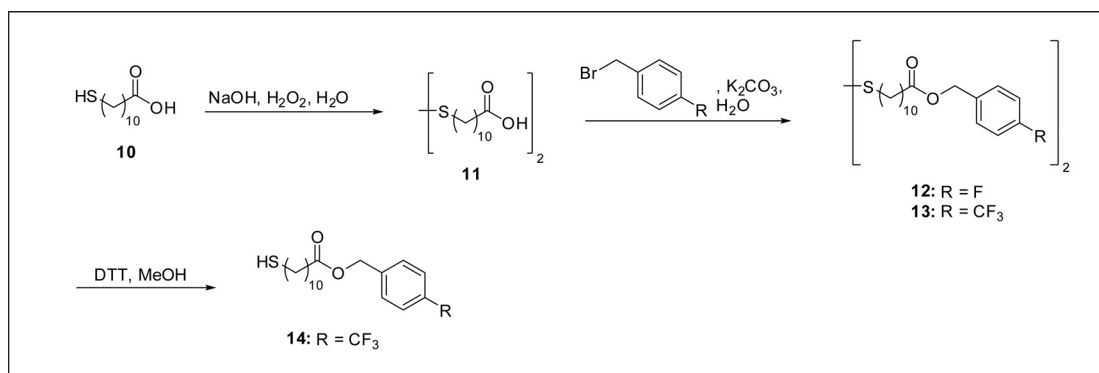


Figure 45. Synthesis of long p-fluorinated benzyl esters 12, 13, and 14 from 11-mercaptoundecanoic acid 10.

Mercaptobutyrate **18** was synthesized from 4,4'-dithiobutyric acid **15** in two steps (Figure 46). Disulfide **15** was benzylated with either 4-fluorobenzyl bromide or 4-(trifluoromethyl)benzyl bromide resulting in dibenzyl esters **16** or **17**, respectively. Disulfide **17** was reduced with dithiothreitol (DTT), providing

monolayers in comparison, thus leading to a higher F1s/Au4p signal ratio for the longer-chain alkanedisulfide **12**.^{21, 30, 82, 193}

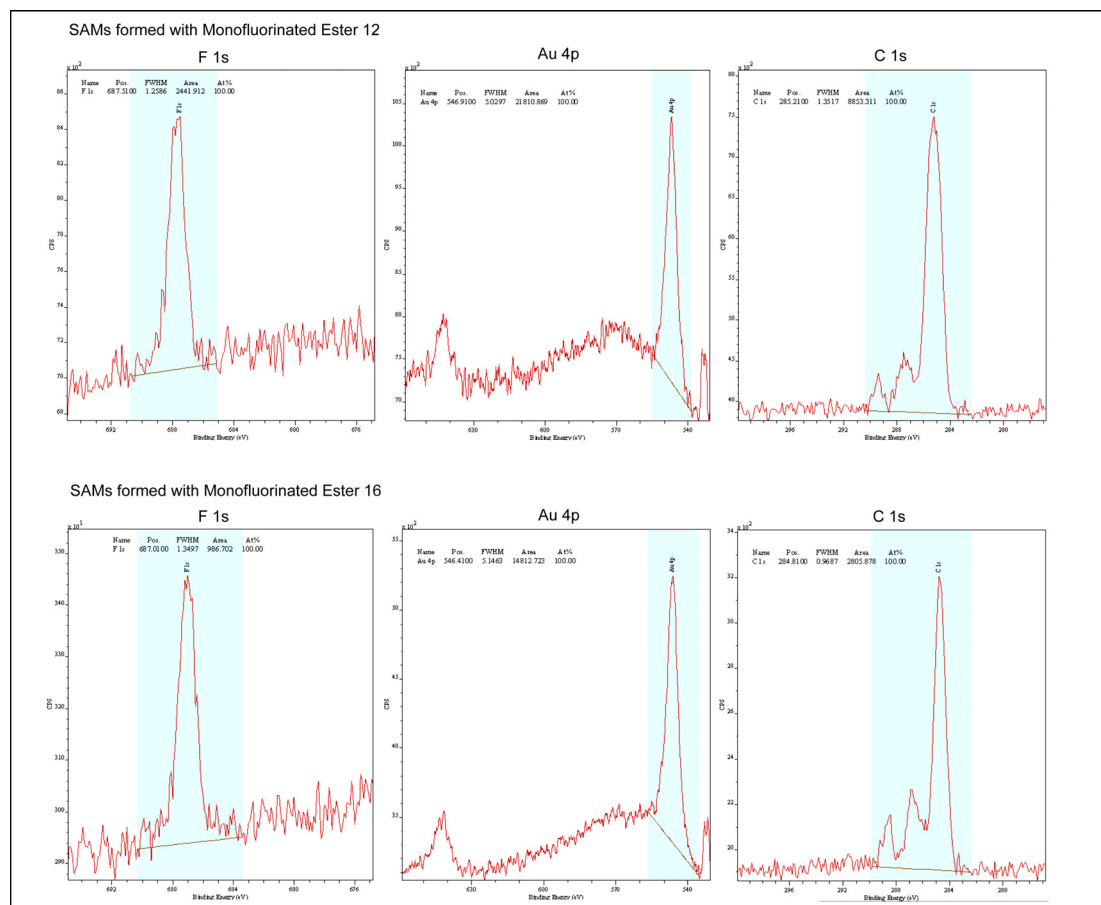


Figure 47. High-resolution XPS spectra of F1s, Au4p, and C1s peaks for SAMs formed on gold using para-fluorinated benzyl esters **12 and **16**.**

Contact angle measurements were also recorded for both surfaces (Table3). Static contact angles, $\sim 69.1^\circ$ and 64.2° respectively, were within the range previously reported previously for monofluorinated aromatic groups ($\sim 70^\circ$).¹⁹⁴ From these data, we determined that SAMs of fluorine-terminated esters were formed on gold surfaces from 1 mM solutions of both **12** and **16**.

Table 3. XPS signal ratios of F1s and C1s relative to gold and corresponding contact angles for SAMs formed from 12 and 16.

Sample:	F1s/Au4p	C1s/Au4p	Contact Angle
Plain Au	--	0.59	52.0°
SAMs of 12	0.37	4.17	69.1°
SAMs of 16	0.26	1.74	64.2°

3.5 Activity assays in solution with synthetic benzyl ester disulfide substrate 16

To determine which, if any, of the expressed carboxyesterases accepted synthetic substrates **12** or **16** in solution, activity assays monitored via change in pH were conducted. As observed for the hydrolysis of pNPE and pFPA substrates in solution, the hydrolysis of benzyl esters **12** and **16** should result in the formation of acid, detectable by monitoring the reaction pH. Substrate **12** was insoluble in ethanol/water mixtures, and solution-phase assays were completed only for substrate **16**. The activities of all enzymes were checked immediately before testing with substrate **16** in solution using the protocol for described in *Section 3.2.1* with either pNPA for AES and BioH and pNPB for ROL. The same protocol and concentrations (10 μ M enzyme and 1 mM substrate) were also used for synthetic substrate **16**.

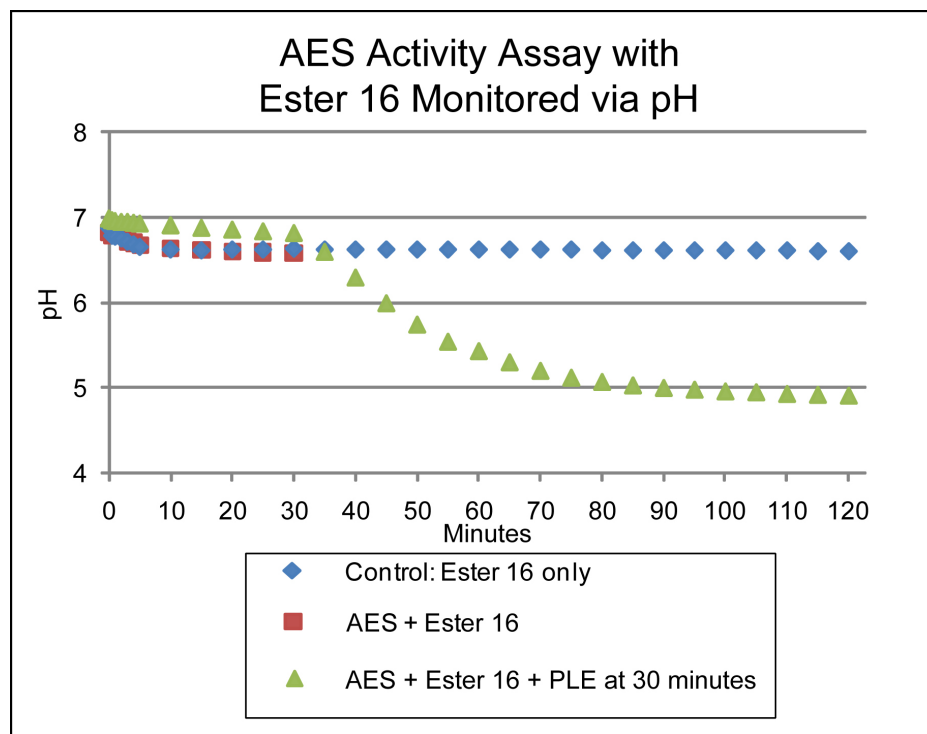


Figure 48. Testing AES activity with ester 16 monitored via a change in pH over time.

Figure 48 demonstrates AES showed no activity with ester **16**. To rule out uncatalyzed degradation of substrate **16**, pig liver esterase (PLE), a promiscuous esterase, was added to the reaction (green triangles) after 30 minutes. The decrease in pH observed after the addition of PLE demonstrates ester **16** was intact.

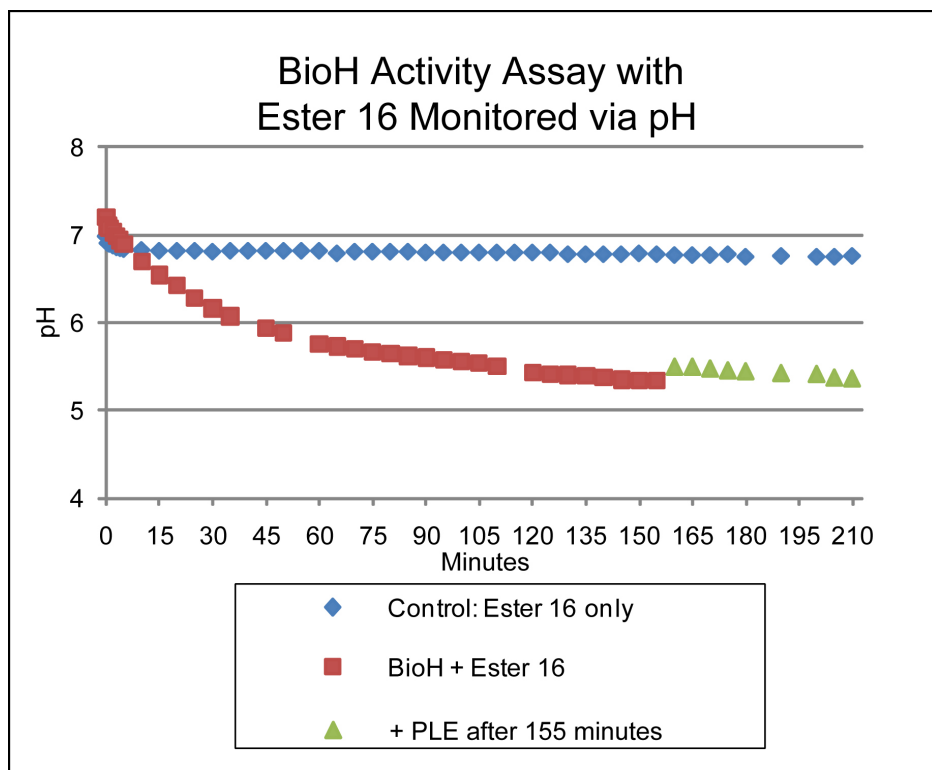


Figure 49. Testing BioH activity with ester 16 monitored via a change in pH over time.

Figure 49 demonstrates BioH shows activity against ester **16**, and a significant decrease in pH was observed relative to the control. To determine if hydrolysis of **16** was complete, PLE was added to the reaction (green triangles) after 155 minutes (~12 U/mg). No significant additional change in pH was observed after the addition of PLE, demonstrating ester **16** was completely hydrolyzed by BioH to the corresponding acid.

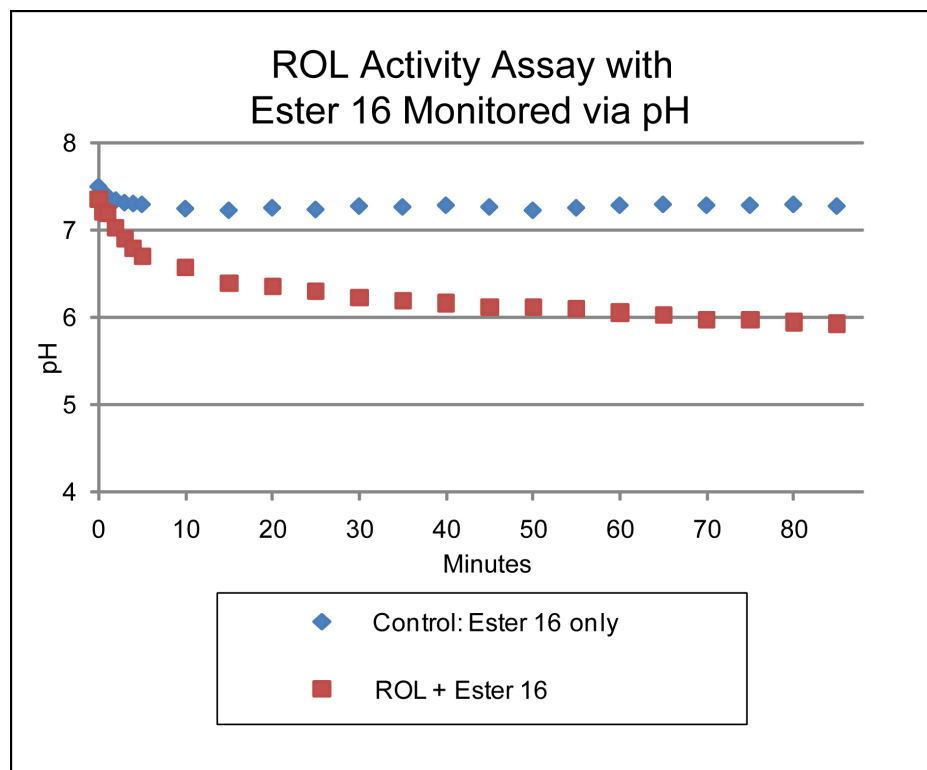


Figure 50. Testing ROL activity with ester 16 monitored via a change in pH over time.

Figure 50 demonstrates ROL shows activity against ester 16, and a significant decrease in pH was observed relative to the control (~14 U/mg). In conclusion, BioH and ROL show significant catalytic activity toward ester 16 in solution whereas AES showed no activity.

3.6 Activity assays of immobilized synthetic benzyl ester disulfide substrates **12** and **16** on gold

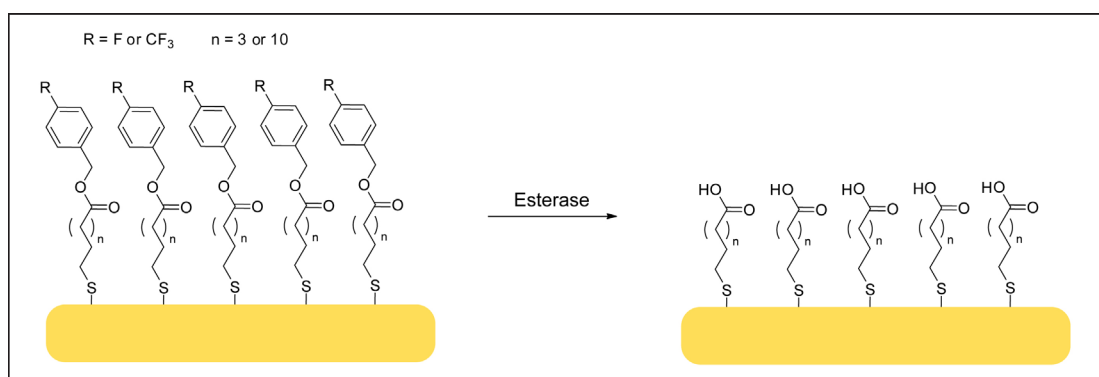


Figure 51. Desired reaction between esterase and fluorinated benzyl ester-terminated SAMs on gold.

We next sought to determine if BioH and ROL were active against immobilized substrates **12** and **16**. Gold substrates were incubated with 1 mM solutions of each substrate for 2 hours at room temperature in accordance with standard SAM formation procedures.⁸² Surfaces were washed with ethanol, dried with filtered nitrogen, and stored in sealed containers until further use. For hydrolysis experiments, substrates were then incubated in 25 μ M enzyme solutions for 3-4 hours to ensure enzymes had adequate time to react with the substrates and at 4 $^{\circ}$ C to minimize nonspecific degradation of the substrate. (25 μ M enzyme corresponds to 12.8 U for BioH and 40.6 U for ROL.) Surfaces were washed with water and ethanol, dried with filtered nitrogen, and stored in sealed containers. Table 4 shows normalized F1s/Au4p and C1s/Au4p signal

ratios for each of the two substrates before and after incubation with BioH and ROL enzyme. Hydrolysis of the fluorinated benzyl ester should produce a decrease in the F1s/Au4p and C1s/Au4p signal ratios, in addition to a decrease in contact angle.

Table 4. XPS signal ratios and corresponding contact angles for SAMs formed from 12 and 16 before and after incubation with BioH or ROL enzymes.

Sample:	F1s/Au4p	C1s/Au4p	Contact Angle
Plain Au	--	0.59	52.0°
1. SAMs of 12	0.37	4.17	69.1°
2. SAMs of 12 with BioH	0.33	4.18	68.2
3. SAMs of 12 with ROL	0.29	4.18	68.1°
4. SAMs of 16	0.26	1.74	64.2°
5. SAMs of 16 with BioH	0.26	2.95	58.9°
6. SAMs of 16 with ROL	0.26	3.10	61.9°

Table 4 shows that exposure of SAMs of **12** on gold to BioH or ROL produces a decrease in the F1s/Au4p ratio. No change in the contact angle was also observed, and the C1s/Au4p signal ratio remained constant relative to controls. On the basis of these data, we concluded that benzyl ester hydrolysis had not occurred. It is unclear why a decrease in the F1s/Au4p ratio was observed. Physisorption of adventitious material might decrease the F1s/Au4p

ratio, but should also produce an increase in the C1s/Au4p ratio, which was not observed. Desorption of SAMs would result in a decrease of both F1s/Au4p and C1s/Au4p signals. Nucleophilic aromatic substitution should not occur at neutral pH in a buffered solution in the absence of strong nucleophiles.

After exposure of SAMs of **16** to BioH or ROL (Table 4), no decrease in the F1s/Au4p ratio was observed. A decrease in the contact angle was also observed relative to SAMs not exposed to enzyme indicating physisorption of carbon-based, hydrophilic adventitious material. However, the C1s/Au4p ratio doubled after exposure to BioH or ROL, supporting the notion of physisorption sufficient to increase the C1s/Au4p ratio, but insufficient to affect the F1s/Au4p ratio. As mentioned previously, monolayers formed from short alkanethiolates are less-ordered than longer alkanethiols and disulfides due to a decreased amount of van der Waals interactions between molecules on the surface in comparison to longer-chain alkanethiolates.¹⁹² This effect could result in an increase in adventitious adsorption of carbon on SAMs from the shorter disulfide.

In conclusion, either no change was observed in the C1s/Au4p signal ratio or no change was observed in the F1s/Au4p signal ratio, confirming no hydrolytic activity against benzyl ester-terminated SAMs.

3.7 Formation of mixed SAMs using benzyl ester thiols 14 or 18 with butanethiol

To further investigate the basis for the lack of activity against SAM substrates, the quality of the SAMs from **12** or **16** was considered. If ester functional groups are too densely packed on the surface, enzymatic substrate recognition might be impossible. Mixed SAMs have been used to avoid dense packing of bulky groups as well as to form more ordered monolayers.^{161, 195} Because SAMs formed from **16** should be shorter than those formed from **12**, the use of mixed SAMs might also increase the order of monolayers of **16**. The use of a short molecule as a diluent to form mixed SAMs may produce more stable monolayers.^{161, 196}

Thiols are more effective diluents for mixed SAMs than are the corresponding disulfides, which tend to aggregate in islands on the surface.^{21, 26, 182, 190} However, reduction in mole fraction of **12** and **16** will also result in lower F1s/Au4p ratios by at least 50% (~ 0.15 signal ratio for F1s/Au4p) for a 1:1 dilution and by 90% for a 1:9 dilution with a “blank” thiol. These values are lower than desired since noise in spectral data after incubation with enzymes may complicate quantification.

Trifluorinated substrates were synthesized for the preparation of mixed monolayers with F1s/Au4p signals similar to those of homogeneous SAMs from

12 or **16** (Figure 51, R = CF₃). An increase in the number of fluorines on the benzyl ester should increase the F1s/Au4p signal. SAMs of disulfides **13** or **17** displayed F1s/Au4p signal ratios of 1.10 and 0.89, respectively (Figure 52). The F1s/Au4p ratio was triple that of the monofluorinated species, as expected, while the noise remained at the same level as SAMs formed from the monofluorinated species (Figure 47). Disulfides **14** and **18** were reduced to the corresponding thiols for use in dilution experiments at 1:9 and 1:1 with butanethiol (BT) as diluent. BT was chosen as a diluent because it was the shortest alkanethiol that could be used for the dilution of **18** without potentially blocking enzymatic access to benzyl ester functional groups. BT also provides a sufficient F1s/Au4p signal ratio for both **14** and **18** at a 1:1 dilution (0.97 and 0.56 respectively) and at 1:9 dilution (0.26 and 0.10) respectively (Table 5).

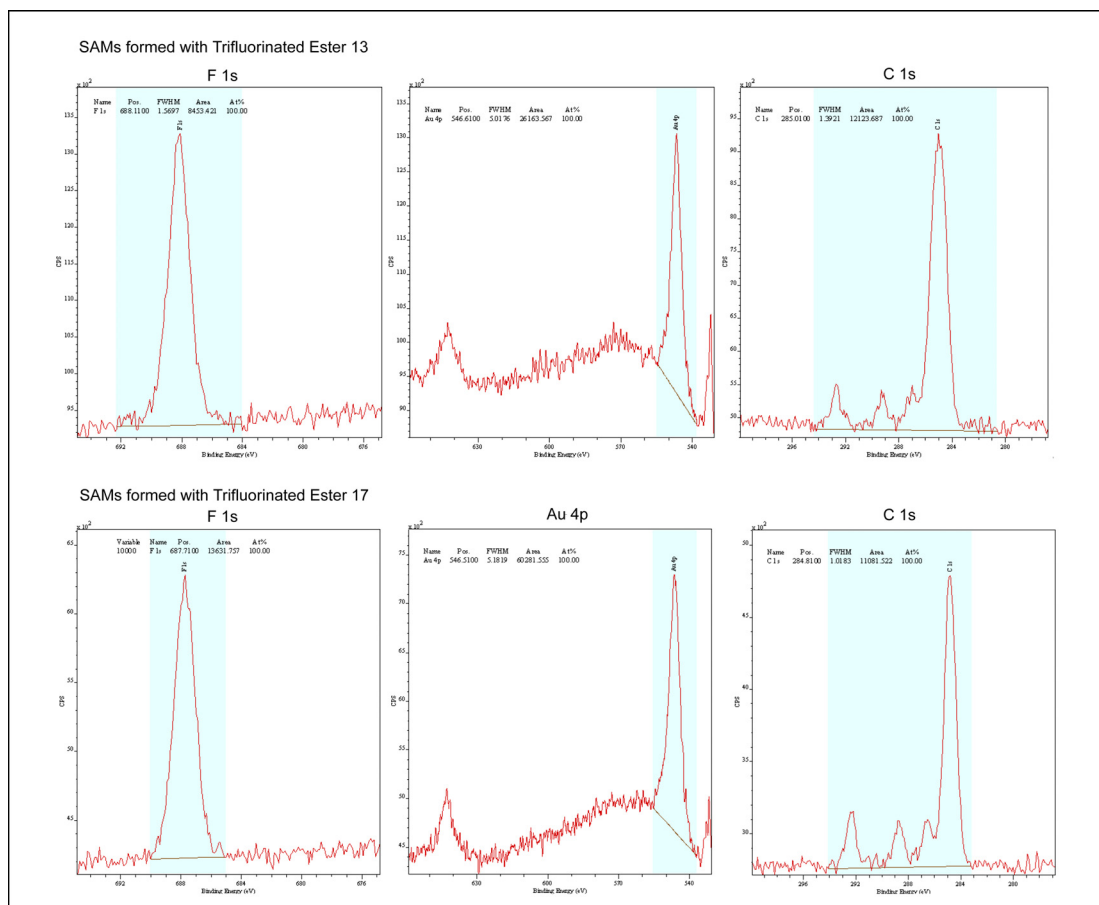


Figure 52. High-resolution XPS spectra of F1s, Au4p, and C1s peaks for SAMs formed on gold using trifluorinated benzyl esters 13 and 17.

After achieving a useful F1s/Au4p signal, we turned to enzyme activity experiments both in solution and on substrate-immobilized gold surfaces.

3.8 Activity assays in solutions with synthetic benzyl ester thiols 14 and 18

Immediately before testing with substrates **14** and **18** in solution, the activities of all enzymes were checked using the protocol described in *Section 3.2.1*. The same protocol and concentrations (10 μ M enzyme and 1 mM

substrate) were also used for testing synthetic substrates **14** and **18** with enzymes.

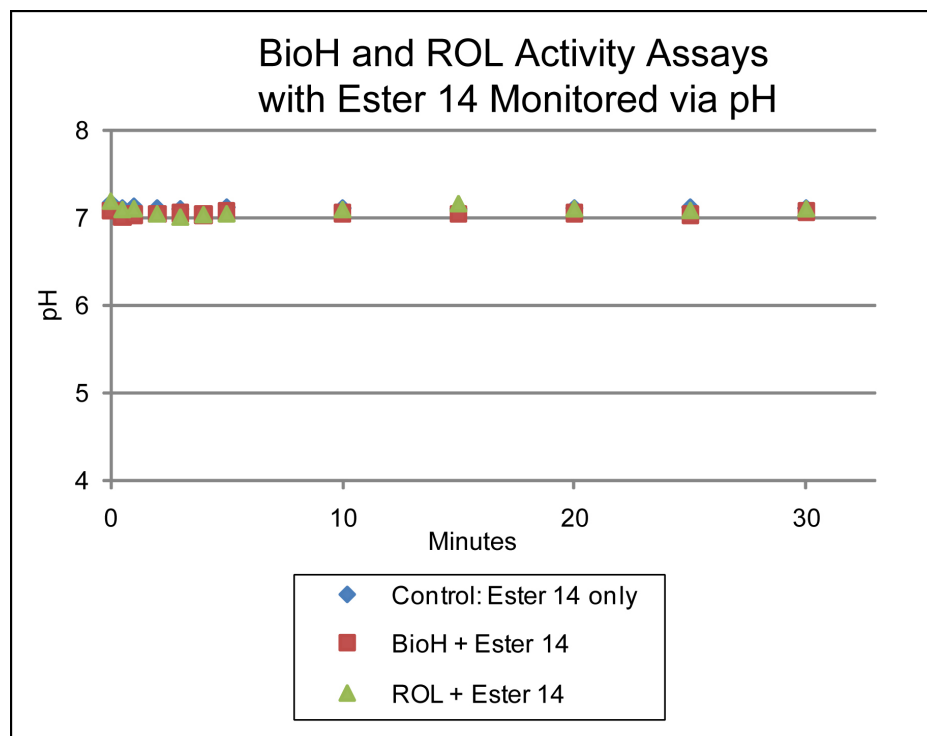


Figure 53. Testing BioH and ROL activity with ester 14 monitored via a change in pH over time.

Figure 53 demonstrates that neither BioH nor ROL exhibits any significant activity with ester **14** over time. Although BioH exhibited activity toward the monofluorinated ester alkanedisulfide **12**, the inability for BioH to catalyze the hydrolysis for the trifluorinated ester alkanethiol **14** may arise due to a difference in sulfur oxidation state, molecule size and/or shape difference, and/or the effect of the protonation state of thiol **14**. It is unclear which or what combination of these factors could have affected hydrolysis. This behavior was not shown in

previous assays with the monofluorinated form (ester **12**) because the sulfur was protected as the disulfide.

For ROL, it is also unclear why the enzyme exhibited activity toward the monofluorinated ester alkanedisulfide **12**, but not the trifluorinated ester alkanethiol **14**. ROL accepts 2,3-dimercaptopropan-1-ol tributyl ester as a substrate, resulting in the production of 2,3-dimercaptopropan-1-ol;¹⁹⁷ therefore, a thiol should not affect its activity. In addition, ROL also turns over acyl substrates with varying chain lengths from 4 to 16 carbons.¹⁹⁷ The crystal structure for the His₆-tagged form of ROL has not been solved, making speculation regarding substrate binding in the active site difficult. Perhaps the combination of a long-chain ester alkanedisulfide, as opposed to a shorter ester alkanethiol, inactivates ROL due to either oxidation state of the sulfur or substrate size and shape differences.

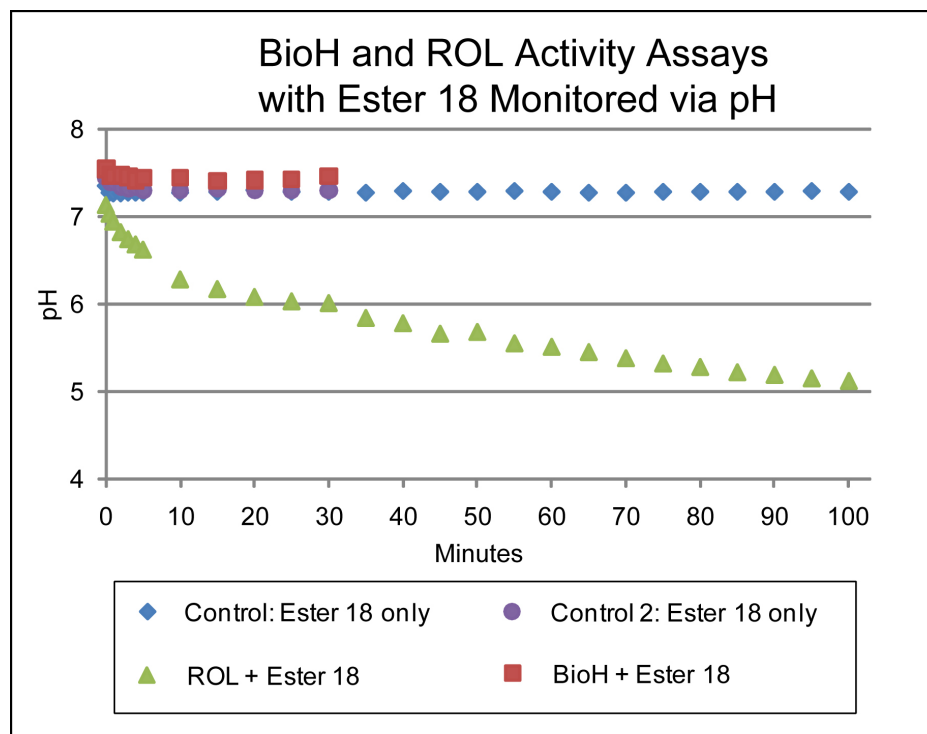


Figure 54. Testing BioH and ROL activity with ester 18 monitored via a change in pH over time.

Figure 54 demonstrates that BioH does not exhibit any significant activity with ester 18 (~ 12 U/mg). Again, this lack of activity could be due to binding of reasons discussed in the previous paragraph. ROL, however, does show significant activity relative to the control with ester 18. This observation indicates chain length may play a role in benzyl ester hydrolysis, since ROL accepts 18, but not 14. ROL also demonstrates activity toward disulfide 16, confirming the suggestion that a shorter acyl chain substrate is particularly active in ROL hydrolysis.

3.9 Activity assays on surfaces with synthetic benzyl ester thiols 14 and 18

Gold substrates exposed to both 1:9 or 1:1 solutions of **14** or **18** with BT were incubated with 25 μ M enzyme for 3-4 hours at 4 °C. Surfaces were washed with water and ethanol, dried with a stream of nitrogen, and placed in dust-free scintillation vials until analyzed. Tables 5 and 6 show the resulting XPS integrated F1s/Au4p and C1s/Au4p signal ratios. A significant decrease in both of these signal ratios would indicate benzyl ester hydrolysis.

Table 5. XPS data for Mixed SAMs of 14 and BT Before and After Incubation with enzymes BioH and ROL.

Sample:	F1s/Au4p	C1s/Au4p	Contact Angle
1. SAMs of 14	1.21	5.34	67.5°
2. 1:1 SAMs of 14:BT	0.97	4.74	69.0°
2B. 1:1 SAMs of 14:BT w/BioH	0.96	4.81	60.7°
2R. 1:1 SAMs of 14:BT w/ROL	0.86	4.85	61.0°
3. 1:9 SAMs of 18:BT	0.26	1.57	61.4°
3B. 1:9 SAMs of 14:BT w/BioH	0.27	2.21	46.0°
3R. 1:9 SAMs of 14:BT w/ROL	0.25	2.01	49.5°

Both Tables 5 and 6 show that no decrease in the F1s/Au4p signal ratio was observed, suggesting no hydrolysis occurred. In most spectra, the F1s/Au4p signal ratio fluctuates slightly from controls while the C1s/Au4p signal ratio increases, indicating adsorption of adventitious carbon. The decreases in surface angle in conjunction with an increase in the C1s/Au4p signal ratio indicate adsorption of hydrophilic species.

Table 6. XPS data for 1:1 Mixed SAMs of 18 and BT Before and After Incubation with Enzymes BioH and ROL.

Sample:	F1s/Au4p	C1s/Au4p	Contact Angle
1. SAMs of 18	0.93	2.50	72.1°
2. 1:1 SAMs of 18:BT	0.56	1.94	68.4°
2B. 1:1 SAMs of 18:BT w/BioH	0.58	3.05	49.5°
2R. 1:1 SAMs of 18:BT w/ROL	0.52	2.46	53.3°
3. 1:9 SAMs of 18:BT	0.10	1.11	52.2°
3B. 1:9 SAMs of 18:BT w/BioH	0.09	1.83	45.1°
3R. 1:9 SAMs of 18:BT w/ROL	0.11	1.98	47.4°

The failure of this system in biocatalytic- μ CP may be the result of esterases that could not bind immobilized substrate due to the orientation of the substrate on the surface. Monolayers of shorter chain length (substrates **16-18**)

may be too disordered to react with enzymes in solution even though activity was demonstrated in solution-phase assays. Adsorption of adventitious material could also block access to substrate. Using polyethyleneglycol-based alkanethiols could decrease biofouling of enzyme or other non-specifically adsorbed material.¹⁹⁸

4. Catalytic microcontact printing

4.1 Overview

μ CP-based methodologies are used extensively as an alternative to patterning techniques based on optical or electron diffraction to pattern a wide variety of inorganic surfaces. The resolution of μ CP is limited by three main factors: ink diffusion,^{28, 75, 84} stamp deformation,¹⁰¹⁻¹⁰² and the properties of substrate surfaces being patterned.¹²⁰ In order to improve the resolution attainable with μ CP, each of these parameters must be systematically optimized to provide a system capable of nanometer resolution and beyond. Current methods for traditional μ CP (PDMS stamping alkanethiols on gold) replicate patterns with high fidelity to roughly 300 nm.^{97, 100} The smallest features fabricated through unconventional μ CP methods using an inked stamp have edge resolutions of \sim 50 nm using a dendrimeric ink on silicon.¹²⁴

Our proof-of principle demonstration of biocatalytic- μ CP (Chapter 2) replaces the ink of traditional μ CP with an immobilized biochemical or chemical catalyst that transfers pattern to an appropriately-functionalized surface through a highly specific chemical reaction. A μ CP approach using an immobilized catalyst eliminates resolution degradation associated with ink diffusion.¹³⁷ Since our first report of biocatalytic- μ CP, further demonstrations of inkless catalytic-

μ CP using acid and base catalysts in our laboratory have resulted in sub-50 nm resolution of 200 nm features, using a piperidine-functionalized stamp with an Fmoc-terminated amine surface on gold as well as sulfonic acid-functionalized stamps for the deprotection of Boc- and TBS-protected SAMs on both gold and silicon.^{120-121, 139}

The nature of the stamping material also affects the resolution of μ CP. Historically, PDMS has been used as the elastomeric material of choice to stamp alkanethiols, siloxanes, and biological materials such as DNA and proteins. On the other hand, PDMS has several properties that significantly limit its utility for μ CP, especially catalytic variants of μ CP. PDMS can only support features having an aspect ratio (h/l) of 0.2 – 2.¹⁷ As a result, features <250 nm are difficult to pattern due to feature deformations such as stamp sagging or collapse of relief structures (Figure 13). Stamps with higher elastic moduli such as those made with hard-PDMS/PDMS, block-copolymers, or polyurethane (PU) show great promise for patterning features with aspect ratios beyond those accessible by PDMS.^{109, 199-200} In particular, a UV-curable, PU-based acrylate has been used to pattern 250-nm features using alkanethiols on gold.¹⁰⁹ This acrylate has adjustable mechanical properties that depend upon the mole fraction of high- or low- molecular weight acrylate added to the pre-polymeric solution, resulting in

the formation a stamp with a tensile modulus higher than that of h-PDMS.¹⁰⁹ PU can be prepared with acrylate copolymers, providing a convenient Michael acceptor for stamp functionalization. Shestopalov and co-workers demonstrated the utility of acrylate-modified PU stamps in the fabrication of piperidine and sulfonic acid stamps for ablative, catalytic patterning of base- or acid-labile surfaces, resulting in sub-50 nm edge resolution (Figure 55).^{120-121, 139}

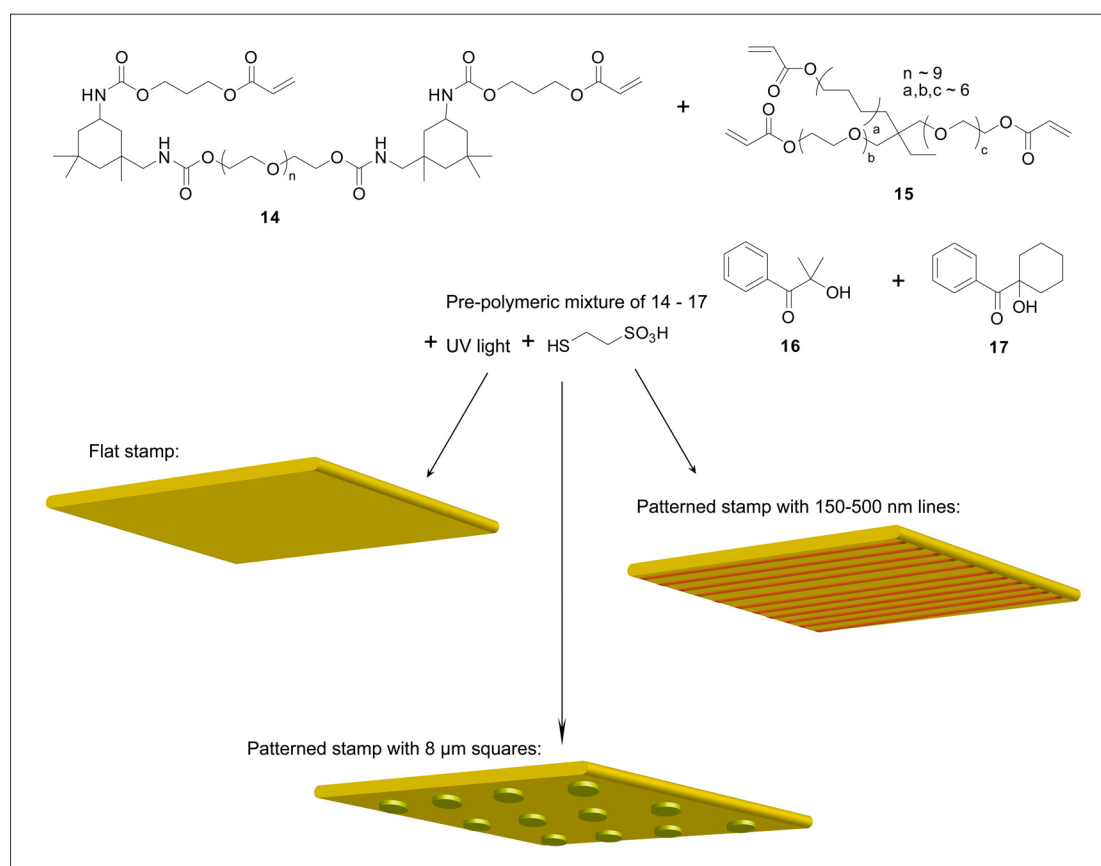


Figure 55. Preparation of polyurethane acrylate stamps co-polymerized with 2-mercaptoethanesulfonic acid.

In traditional μ CP, pattern transfer relies on the rapid reaction of a specific diffusible liquid ink and a cognate ink-reactive substrate. Most methods for μ CP can pattern only specific metal and metal oxide surfaces,^{25, 28-30} such as gold, and cannot easily be applied to technologically-relevant surfaces, such as silicon.²⁸ Using catalytic- μ CP, a variety of substrates covered by pre-formed monolayers can be manipulated by a catalyst; in this instance, pattern formation is not limited by the formation of monolayers on the underlying substrate material. In addition, the resolution of traditional μ CP is limited by the material properties of gold due to its grain size of 30-50 nm.¹¹⁶ Printing on atomically flat surfaces such as H-terminated silicon or mica would obviate limitations induced by grain size.¹¹⁹⁻¹²¹

Catalytic- μ CP methods with <100 nm resolution have been demonstrated on H-terminated silicon by Mizuno and Buriak¹³⁴⁻¹³⁵ and in our own laboratory on both gold and H-terminated silicon.^{120, 139} Mizuno and Buriak utilized a hydrosilylation reaction catalyzed by a h-PDMS/PDMS stamp containing 20 nm Pd or Pt nanoparticles (NPs) and inked with alkenes/alkynes to pattern silicon surfaces. Although replication of the NP features was achieved, the applicability of the approach is clearly limited. The shape and size of these stamp features is produced by self-assembly of block co-polymers that attract Pd or Pt NPs on

silicon. Stamps are formed by surrounding the NPs with h-PDMS pre-polymer and subsequent curing. Once the stamp is released, the NPs remain on the surface of the stamp for use in catalytic printing. However, due to the nature of the self-assembly process for NPs, features such as squares, lines, circles, and text cannot be patterned simultaneously. In previous studies, only circles and lines have been patterned. Furthermore, the reaction between the ink and the surface occurs in the absence of metal catalyst, promoted by both heat and UV light. Most importantly, areas not functionalized by hydrosilylation are susceptible to oxidation, resulting in degradation of electronic properties in those areas.

The inkless variants of catalytic- μ CP developed in our lab produced 200 nm features with \sim 50 nm edge resolution by utilizing catalyst immobilized on an elastomeric PU stamp to chemically pattern a surface of terminally-protected SAMs.^{120-121, 139} Stamp feature sizes were limited only by EBL-fabricated Si/PMMA or Si/SiO₂ master.¹²⁰⁻¹²¹ Finally, catalytic- μ CP significantly increases the range of patternable surfaces by manipulating surfaces already functionalized with SAMs. To build on our success in acid-catalyzed μ CP and to extend its applicability to other surfaces, we sought to develop a universal bi-layer approach to μ CP. In this approach, a protective underlayer would be functionalized with a labile, patternable surface. Additionally, we sought to

understand the relationship between stamp acidity and pattern transfer. Below we report our work in both regards.

4.2 Universal bi-layered patterning technique

To extend the applicability of catalytic- μ CP to a wider variety of substrates, a bi-layered patterning technique was designed as a universal approach that 1) displays a labile functional group for catalytic-stamp patterning, and 2) forms highly-ordered monolayers, which, in turn, protect the underlying metal or semiconductor surface from oxidation as an insulating layer (Figure 56). Such a system would be particularly useful for patterning organic thin-film transistors and photovoltaic devices⁵⁵⁻⁵⁹ as well as providing a universal system for patterning chemically- or biologically-relevant molecules.⁴⁶⁻⁴⁷

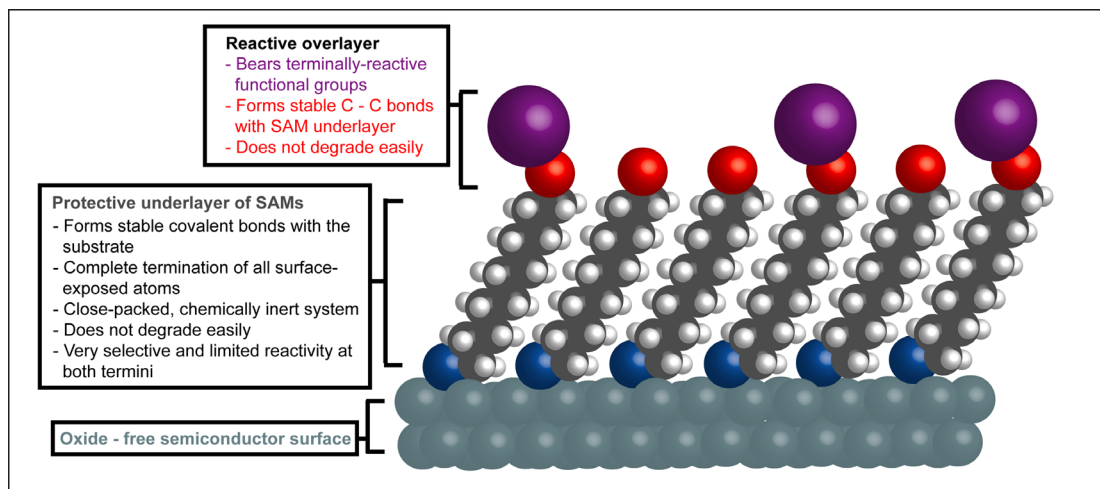


Figure 56. Structure and characteristics of the bi-layered system for SAMs.

4.2.1 Substrate properties and components

Monolayers previously used in catalytic- μ CP methods provided sufficient surface coverage of terminal functional groups to facilitate observation of pattern transfer.^{81, 120-121, 134-135, 137, 139} On the other hand, monolayers formed from species bearing bulky terminal functional groups are not well-ordered due to steric constraints.^{27, 30, 82 120} Because of the tendency of many semiconductor materials to oxidize, a highly ordered monolayer is required to shield surfaces from water and oxygen. Recent studies¹¹⁷⁻¹¹⁸ have shown that silicon surfaces passivated through a two-step chlorination/Grignard alkylation are robust against oxidation and degradation of the attached monolayers, and remain chemically inert in ambient environment for 60+ days.¹¹⁷ In particular, 1-propenylmagnesium bromide has been used to protect underlying silicon for long periods, achieving nearly 100% surface coverage in the two-step protocol. Propenyl functionalization also provides a reactive alkene for further functionalization. Of particular utility in this regard are carbene insertion reactions, conveniently achieved by photolysis of diazirine precursors. We^{121, 142} and others¹¹⁷ have carried out such functionalization using *N*-hydroxysuccinimide-functionalized (NHS) diazirines to create a reactive overlayer. NHS esters have been used for over 30 years as an amine-reactive species for coupling purposes in organic

synthesis and in protein and DNA functionalization.²⁰¹ Thus, any molecule bearing a primary (basic) amine could be coupled to this NHS-functionalized surface through a highly-stable amide bond.⁸² NHS-esters are also easily hydrolyzed to the corresponding acid, deactivating the surface toward further NHS-mediated coupling reactions. Thus, a sulfonic acid-modified PU stamp should act as an efficient acid catalyst with which to pattern NHS-functionalized bi-layered substrate without oxidation or degradation of the underlying silicon.

Using the protocol of Puniredd and co-workers,¹¹⁷ passivated silicon monolayers were prepared to protect silicon from oxidation and to provide a site for subsequent functionalization. H-functionalized silicon surfaces were passivated and reacted with NHS-diazirine using a three-step chlorination-alkylation-carbene addition pathway (Figure 57). A silicon <111> surface (**S1**) was incubated in Nanostrip solution to remove organic contaminants from the surface. After rinsing thoroughly with water, silicon was reacted with 5% aqueous HF solution to produce an oxide-free, H-functionalized silicon surface (**S2**). Subsequent chlorination was performed by heating the substrate to 110 °C in a saturated solution of PCl₅ in the presence of 0.5 w% benzoyl peroxide in chlorobenzene for 1 hour. Substrate (**S3**) was rinsed with chlorobenzene, dried in a stream of argon, and immediately placed in a high-pressure reaction vessel

containing a 0.5 M THF solution of 1-propenylmagnesium bromide. The Grignard reaction was performed overnight (16-22 hours) at 130 °C, forming surface (S4). Previous results using XPS¹⁴² demonstrate protection of the silicon surface from oxidation. The formation of a highly ordered monolayer was confirmed via the observation of very small contact angle hysteresis (~2°), and low surface roughness via lateral force AFM data ($R_a = 0.287$ nm, $R_{rms} = 0.366$ nm, Z range = 3.34 nm). In addition, literature results suggest this protocol should provide essentially 100% coverage of the silicon surface with C-Si bonds.¹¹⁷

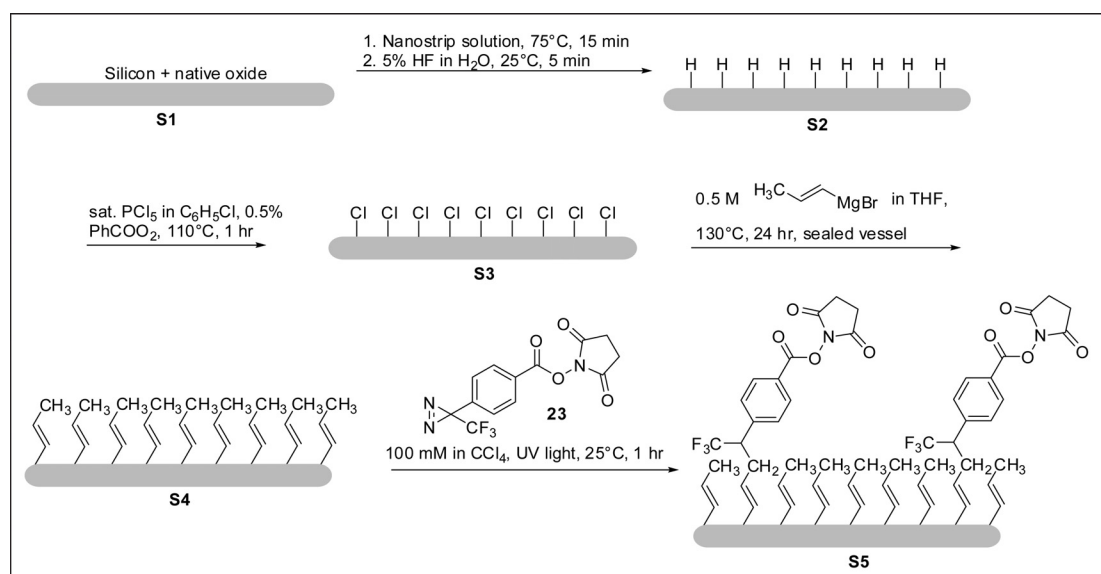


Figure 57. Functionalization of bi-layered SAMs on silicon surfaces.

To form a reactive secondary overlayer atop the passivated surface, substrate (S4) was reacted with a 0.1 M solution of NHS-diazirine **23** in CCl₄ under UV light at 25 °C for 1 hour. (Diazirine **23** was synthesized by A.

Shestopalov and C. Morris.^{138, 142}) Substrate (S5) was washed with ethanol and CH₂Cl₂, dried in a stream of argon, and stored in a sealed vial purged with argon to inhibit NHS hydrolysis. Previous studies¹⁴² using XPS, lateral AFM analysis, and contact angle hysteresis show this protocol both forms a reactive overlayer while preserving the protective SAM underlayer and silicon surface. Here, XPS analysis¹⁴² showed the presence of fluorine following diazirine treatment, but no detectable silicon oxide. These results confirm selective reaction between diazirine and propenyl-functionalized silicon surface without concomitant oxidation of the underlying silicon or degradation of protective monolayer. AFM lateral force experiments¹⁴² again confirmed a surface of low roughness ($R_a = 0.256$ nm, $R_{rms} = 0.320$ nm, Z range = 2.42 nm). However, contact angle hysteresis of 22° was observed,¹⁴² suggesting a loosely-packed reactive overlayer. Although a somewhat disordered overlayer is not surprising, given the bulky succinimide moiety, additional disorder may be induced by NHS-hydrolysis during contact angle measurements.^{142, 202}

Together, our results confirm the formation of a bi-layered silicon surface consisting of a (1) protective propenyl-functionalized SAM which shields the underlying silicon from oxidation and degradation and (2) a highly-reactive

overlayer which can be further used for the immobilization of any organic or biological molecule displaying a reactive (primary) amine.

4.2.2 Stamping materials

4.2.2.1 Masters for catalytic-PU stamps

Two different masters were used for preparing stamps with which to pattern our bi-layered, NHS-functionalized silicon surfaces. For the fabrication of stamps bearing micro-features, a Si/SiO₂ master bearing 8 μm squares was fabricated using photolithography and reactive ion etching (A. Shestopalov).¹⁴² For the fabrication of stamps bearing sub-micron features, electron beam lithography (EBL) was used to pattern poly(methyl methacrylate) (PMMA) on silicon producing a pattern of lines bearing widths ranging between 150-500 nm. Briefly, a positive photo resist (950 PMMA C2 resist, MicroChem Corp, 134 nm) was spin-cast on a 2.5 cm x 2.5 cm piece of silicon, pre-baked at 180 °C for 140 seconds, and then patterned by EBL using a current of 50 pA, a voltage of 50 kV, and a dosage dwell time of 1.75 μs. The patterned photoresist was developed in a 1:3 mixture of methyl isobutyl ketone (MIBK) to isopropyl alcohol (IPA), washed with IPA and water, dried with a stream of nitrogen, and stored in sealed containers until use.

4.2.2.2 Catalytic- μ CP stamp fabrication

To pattern NHS-terminated, bi-layered substrates, elastomeric PU-based stamps were used in the bi-layered patterning system.^{109, 120, 139, 142} PU is a highly useful stamp material for catalytic- μ CP because monomer can be polymerized in the presence of other acrylates and Michael donors, resulting in a reactive, reusable, and elastomeric catalytic stamp. PU stamps also provide a highly accurate replica mold of master features while supporting and patterning sub-micron features without stamp collapse.^{120, 139, 203}

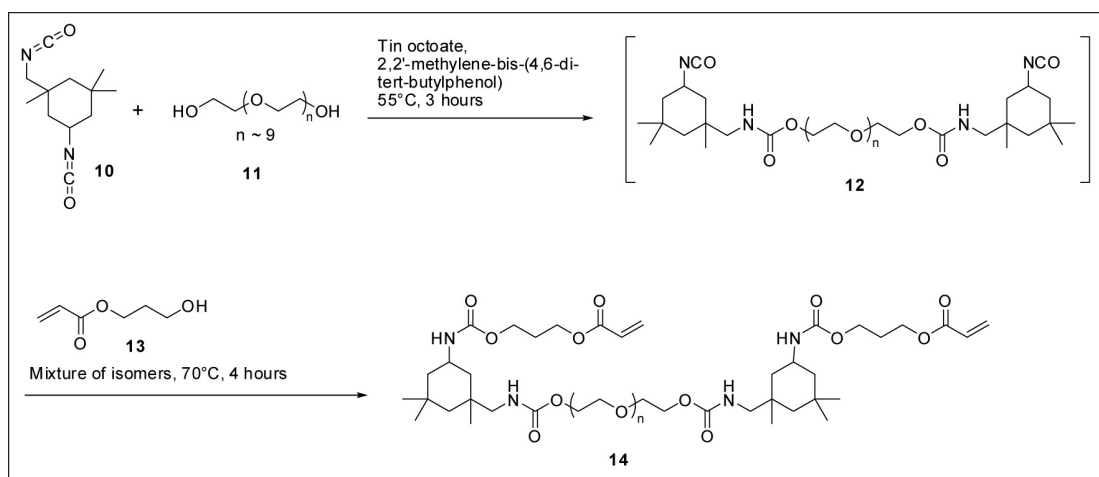


Figure 58. Preparation of PU monomer 14 from isophorone diisocyanate 10 and polyethylene glycol 11 (avg mw: 400 g/mol).¹⁰⁹

PU monomer 14 was prepared from isophorone diisocyanate 10 (Figure 58). Polyethylene glycol (0.5 eq., avg mw: 400g/mol) 11 was slowly added to a 55 °C solution of tin octanoate, 2,2'-methylene-bis(4,6-di-*tert*-butylphenol), and 10 and stirred for 3 hours to form intermediate 12. The temperature of the reaction

was then raised to 70 °C and hydroxypropyl acrylate **13** was added slowly to this solution. The reaction was stirred at 70 °C for 4 hours and shielded from light to suppress polymerization.¹⁰⁹ Polymerization of the pre-polymer mixture occurred at temperatures above 75 °C.

To decrease viscosity and lower the glass transition temperature of the resulting stamps, trimethylolpropane ethoxylate triacrylate **15** (avg mw: 912 g/mol) was added, diluting **14** by 30%. Photoinitiators **16** and **17** (1.5% wt% each) were then added, and the solution was stored at 4 °C until needed for stamp fabrication.

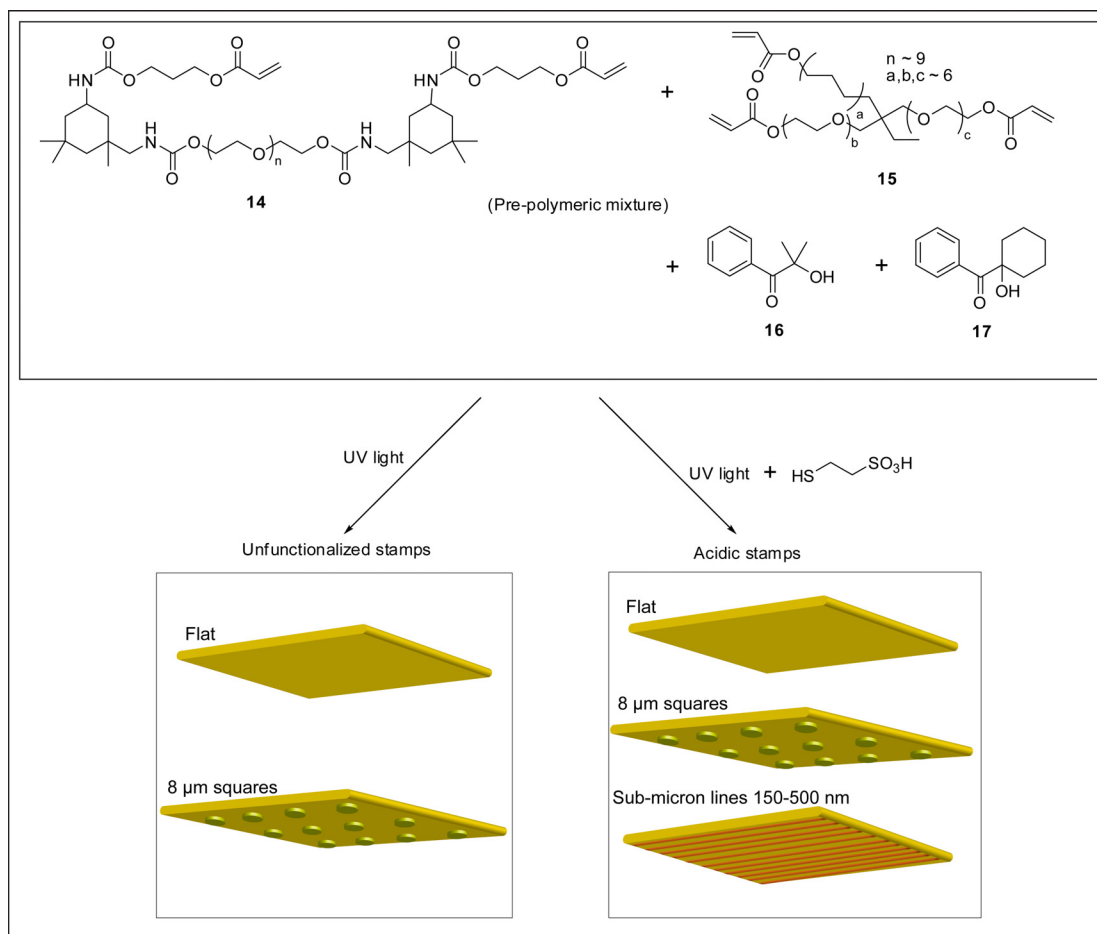


Figure 59. PU prepolymer mixture and fabrication of PU stamps.^{109, 120}

For polymerization of catalytically inactive PU stamps, the PU mixture was warmed to room temperature. For polymerization of acidic stamps, 8 v/v% 2-mercapto-ethanesulfonic acid was added to the room temperature PU mixture, resulting in covalent immobilization of the sulfonic acid via Michael addition. For the fabrication of both catalytically active and inactive stamps, the respective PU mixtures were heated to 50 °C under vacuum for ten minutes to remove bubbles, cooled to room temperature, and deposited on a silicon master

(patterned stamps) or plain silicon substrate (flat stamps), and polymerized between the master and a glass slide under UV light for 2 hours at room temperature. Stamps were peeled away from the silicon surfaces and cut to size.

Stamps bearing $8\ \mu\text{m}$ squares and flat stamps were cut to $\sim 1\ \text{cm}^2$ to maximize contact on $\sim 1\ \text{cm}^2$ substrate surfaces for analysis via SEM or XPS. Stamps bearing sub-micron features were cut to $\sim 0.3\ \text{cm} \times 1\ \text{cm}$ in order to stamp multiple times on a single $\sim 1\ \text{cm}^2$ substrate because the area bearing pattern ($\sim 1\ \text{mm}^2$) was small in comparison to stamps bearing micro-features. Their rectangular shape provided a region of the stamp bearing no pattern as a “handle” for moving the stamp without touching the sub-micron features. Stamps were washed with water and ethanol after each use, dried in a stream of argon, and placed in covered containers until needed for stamping experiments.

Stampings bearing both microfeatures and nanofeatures showed very high fidelity to their corresponding masters, as shown by SEM in Figures 60¹⁴² and 61.

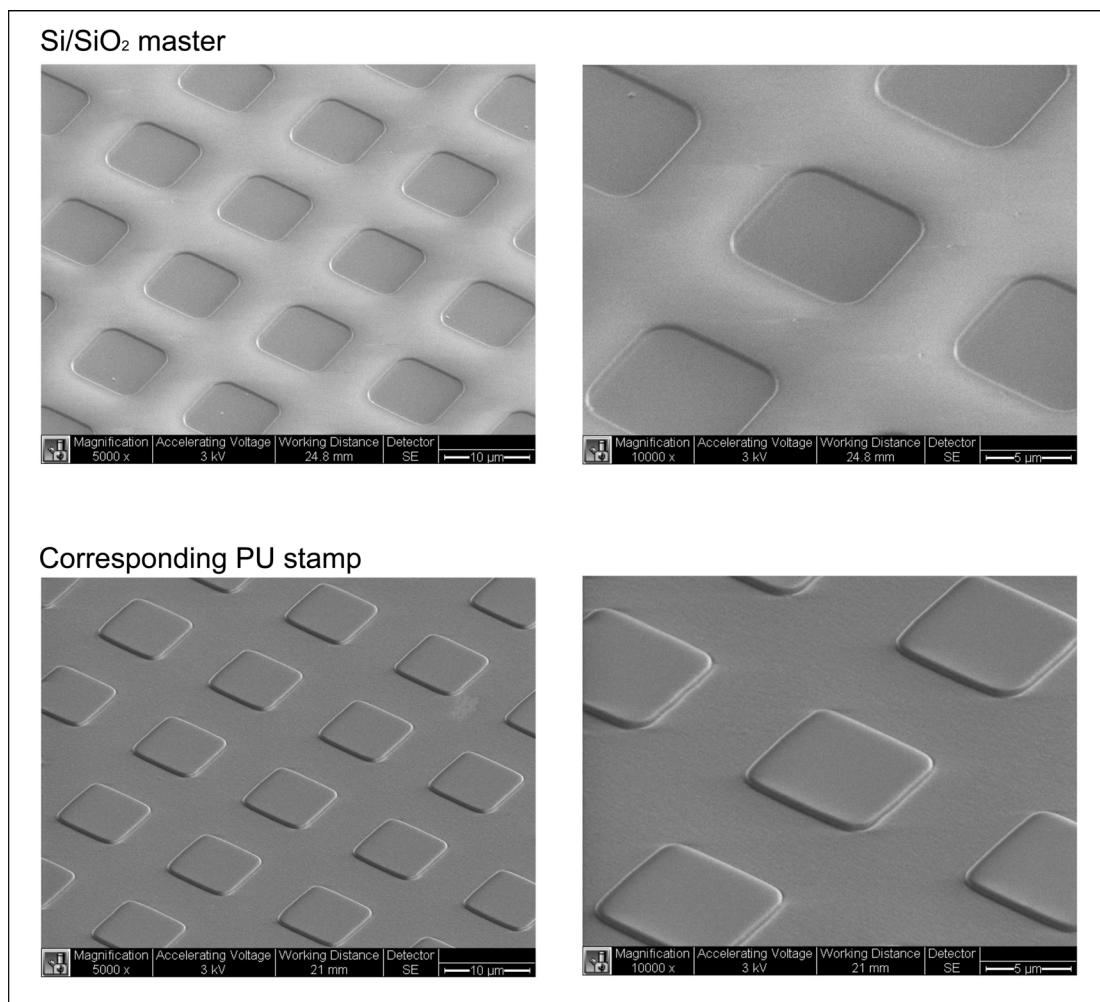


Figure 60. SEM images of Si/SiO₂ masters bearing 8 μm squares and corresponding patterned sulfonic acid-functionalized stamp.¹⁴²

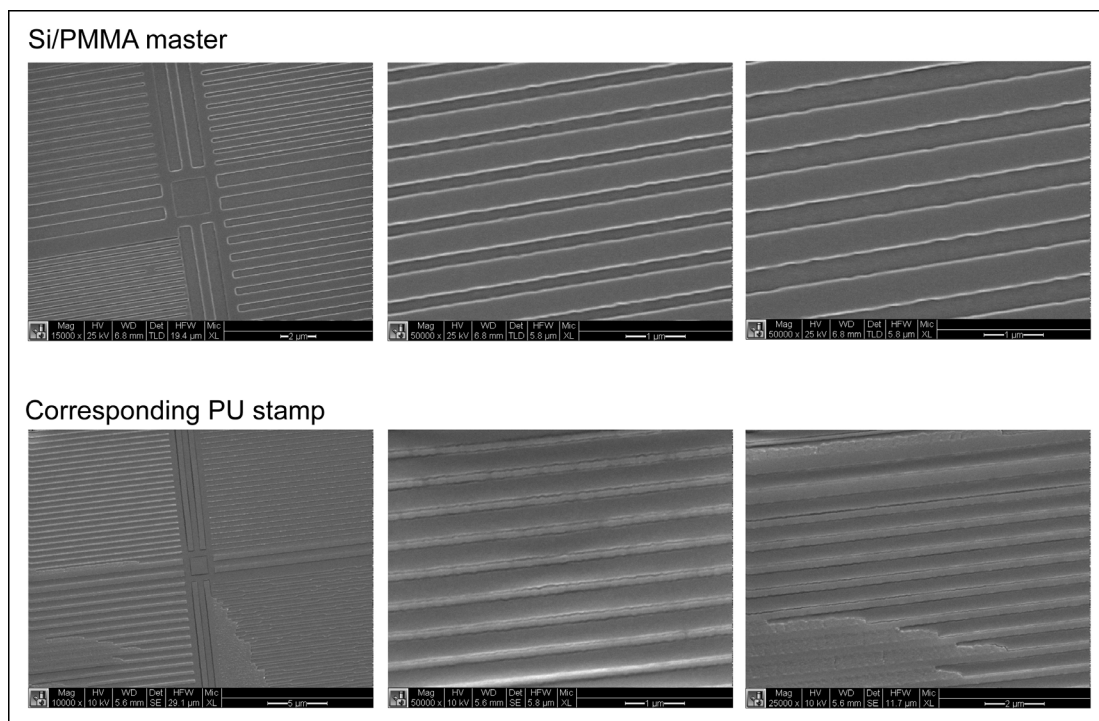


Figure 61. SEM images of Si/SiO₂ masters bearing lines of varying widths (150 – 500 nm) and corresponding patterned sulfonic acid-functionalized stamp.

Although catalytically active PU stamps corresponded well to their masters (Figure 61), slight defects were occasionally observed in patterned lines. An origin of this behavior is revealed by imaging the Si/PMMA master before (Figure 61) and after (Figure 62) stamp formation. When stamps are removed from masters, PMMA is sometimes removed from the master surface; reuse of damaged masters results in PU stamp conforming to damaged areas. Figure 62 shows an overview of a master and corresponding stamp showing identical patterns of feature defects. Higher magnification images show the roughness of the master is visible in the stamp.

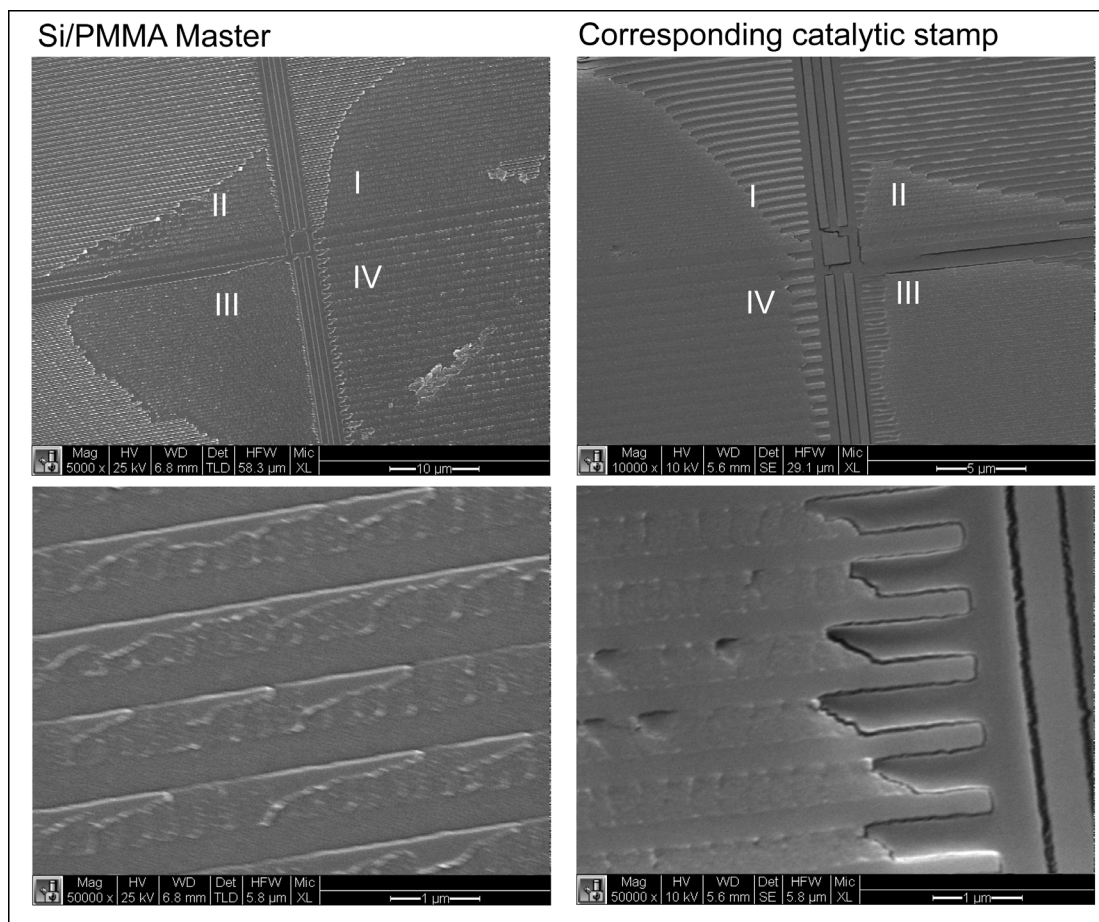


Figure 62. Master and catalytic stamp defects due to removal of PMMA from master.

No releasing compound was added to the stamp mixture providing a possible explanation for the damage to masters as stamps are polymerized and removed. Previous work by Shestopalov and co-workers did not utilize releasing compound with Si/PMMA masters bearing 620 nm features spaced 380 nm apart, and corresponding stamps were obtained without defects.¹³⁹ Stamps bearing lines ranging from 150 nm to 500 nm were spaced by a distance larger than their width (i.e. 1X – 2X) for EBL patterning purposes. The increased

contact area between PMMA master and PU pre-polymer may result in ablation of the features from the master. This behavior is especially apparent on the 320 nm features spaced 420 nm apart (Figure 62: quadrant IV).

Yoo et al.¹⁰⁹ used Rad 2200N (TEGO Chemie Service, Germany) as a releasing agent to decrease the surface energy of the stamp and facilitate removal of stamps without damage to the master; releasing agent here might reduce the interaction between PU and PMMA and prevent damage to the master. Damage was not observed with 8 μm squares presumably because a mechanically more robust Si/SiO₂ master was used.

4.2.3 Patterning NHS-functionalized SAMs using catalytic- μCP at the microscale

Previous work with sulfonic acid-modified PU stamps and Boc-protected SAMs showed essentially complete deprotection to primary amine after only 5 minutes of stamp-substrate contact.¹²⁰ An identical protocol was followed here to determine the reaction time required for removal of NHS ester; again near 100% deprotection was observed in 5 minutes.¹⁴² Featureless catalytic and inactive stamps were reacted with NHS-terminated monolayers at room temperature for 5 - 30 minutes. Conformal contact was visible through the transparent stamp. Following reaction, the substrates were rinsed with ethanol, dried in a stream of

filtered argon, and analyzed by XPS. As is evident from Figure 63, treatment with the sulfonic acid stamp resulted in a decrease of carbon concentrations in by approximately the same proportion to the HCl-treated sample, whereas inactive stamps did not change SAM compositions. The sulfonic acid stamp achieved the same level of hydrolysis as a 1 M HCl solution within just 5 minutes of stamp-substrate contact, indicating exceptionally high NHS-hydrolysis efficiency. The fluorine concentration in all analyzed samples remained constant and did not change from the value showed by initial NHS-modified substrates. This observation suggests transformations induced by the sulfonic acid stamp and the HCl solution were specific to the NHS groups and did not affect other components of the bi-layered system.

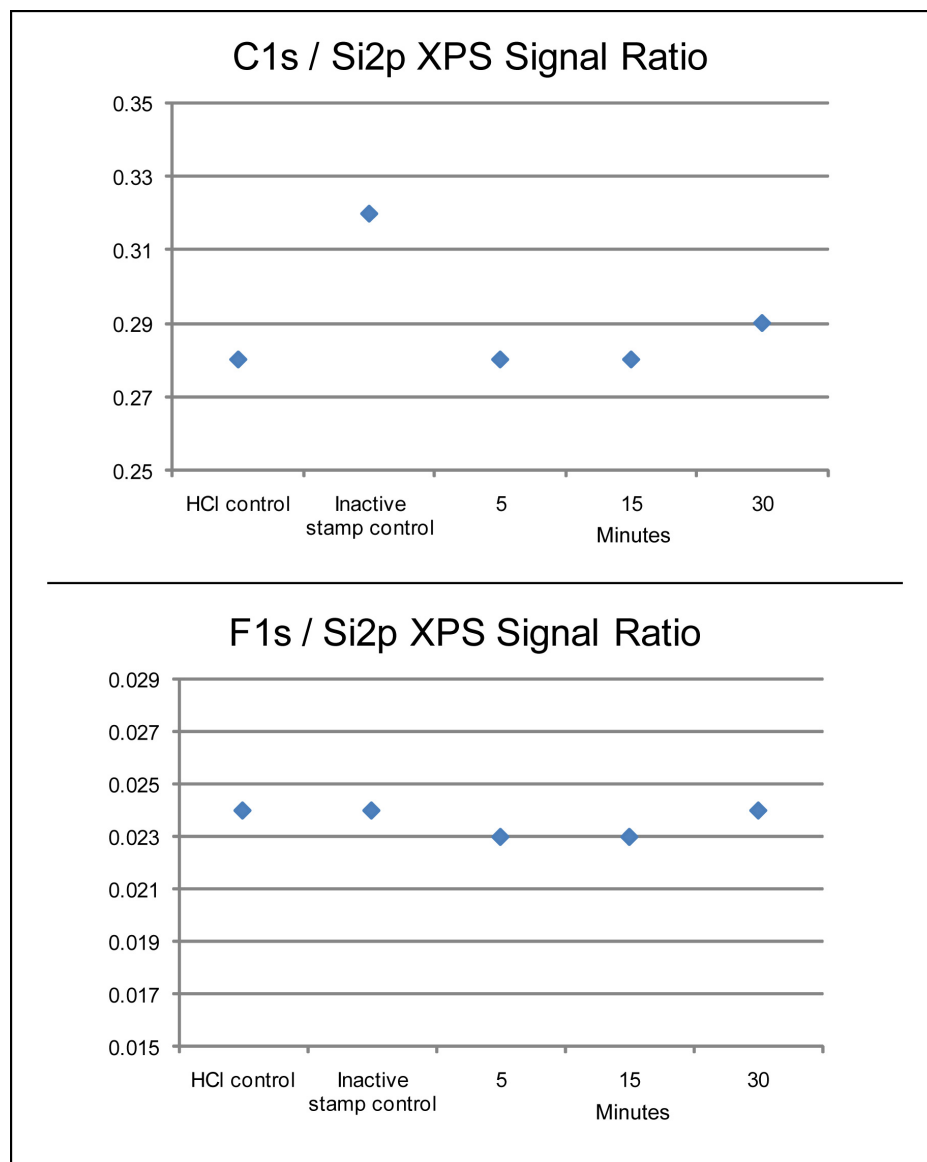


Figure 63. XPS analysis of the NHS-hydrolysis efficiency with featureless catalytic stamps.

Sulfonic acid-modified PU stamps and inactive control stamps (no acid) bearing 8- μm square features were used to determine the efficiency of pattern transfer on NHS-functionalized, oxide-free silicon surfaces. During stamping for 5 minutes with catalytically-active patterned stamp, the NHS-ester is hydrolyzed

to the corresponding acid in the areas of conformal contact between stamp and substrate resulting in patterned, bifunctional surfaces bearing both NHS and carboxylic acid functionalities (Figure 64). Inactive control stamps were also stamped for 5 minutes, but no hydrolysis was observed after conformal contact with NHS-functionalized surfaces. After stamping, substrates were washed with ethanol, dried in a stream of argon, and placed in dust-free vials purged with argon until analyzed via SEM. Stamps were thoroughly washed with water and ethanol, dried with a stream of argon, and placed in closed containers until used for further stamping experiments.

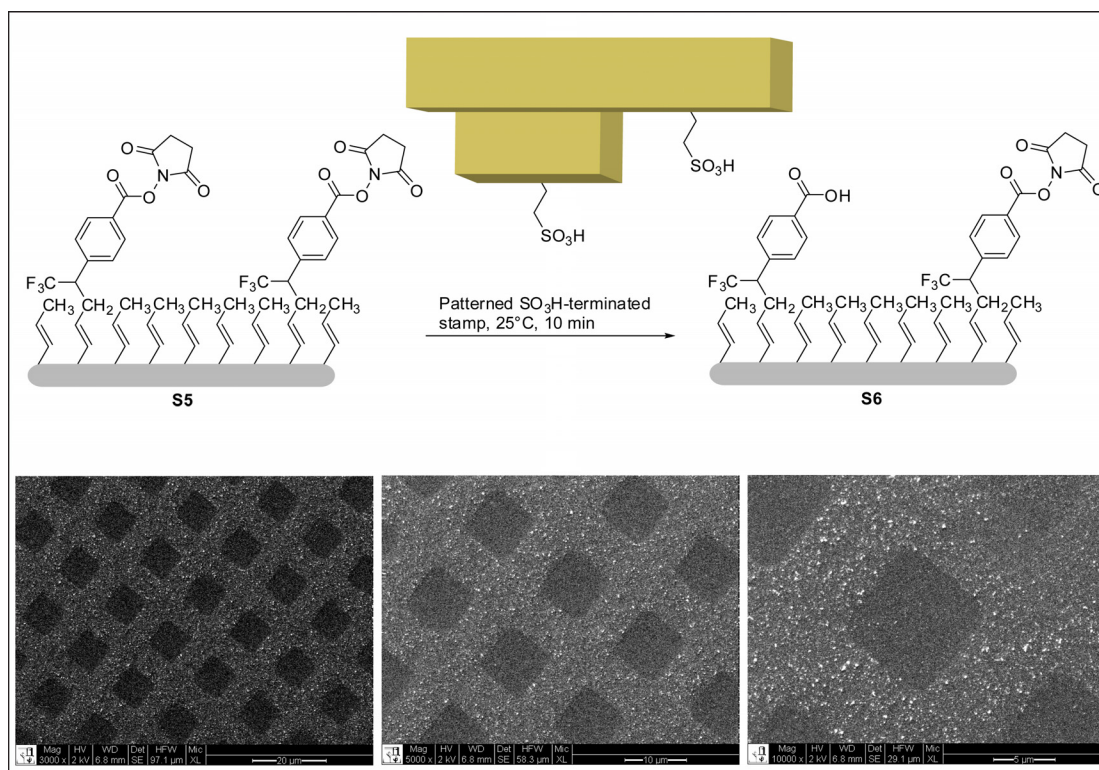


Figure 64. SEM images of the patterned NHS-functionalized SAMs after reacting with catalytic stamp bearing 8 μm squares.

Figure 64 demonstrates the efficiency and reproducibility of patterning surfaces with catalytic-μCP using a sulfonic acid-functionalized stamp. Patterns were reproduced uniformly with identical features over the entire stamped surface, even after using the same stamp multiple times on different NHS-functionalized surfaces during the course of over a week. The shape and size of the square features were identical to those of the stamp and master. NHS-functionalized surfaces were patterned without deformation of the catalytic

stamp, producing a chemical change on NHS-terminated surface observable by XPS and pattern observable by SEM.

4.2.4 Patterning NHS-functionalized SAMs using catalytic- μ CP sub-microscale

Sub-micron features were also replicated on NHS-functionalized SAMs using the previously described approach, demonstrating catalytic- μ CP with sulfonic acid-functionalized PU stamps on NHS-functionalized substrates obviates the diffusive limitations of traditional μ CP methods. Catalytic stamps bearing 500 nm, 320 nm, and 150 nm features were reacted with NHS-functionalized substrates, resulting in accurate pattern transfer onto the NHS-functionalized surface – a result not possible using conventional μ CP methods in which ink spreading is responsible for at least 50 nm enlargements of the feature edges.⁷⁵ Figure 65 demonstrates the efficiency of the developed technique for producing patterns across the entire substrate surface and generating sub-micron features identical to those on the PU stamp. Notably, the same acidic stamp bearing sub-micron features can be used multiple times without losing catalytic efficiency or reduction of accuracy and efficiency in pattern transfer.

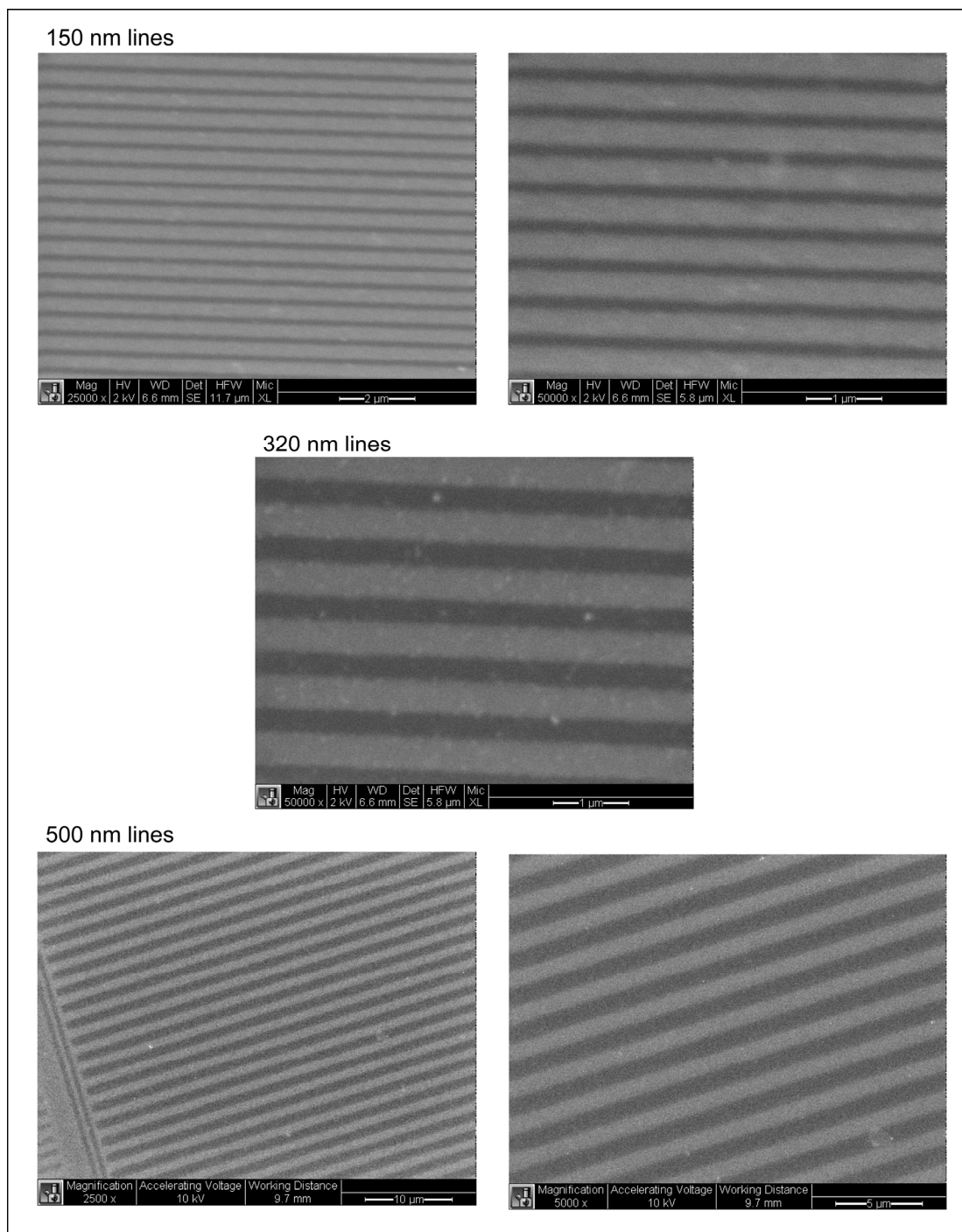


Figure 65. SEM images of the patterned NHS-modified SAMs on silicon after reacting with patterned catalytic stamp bearing lines with 150, 320, and 500 nm widths.

4.2.5 Conclusions from universal bi-layered patterning technique using catalytic- μ CP

In conclusion, we have developed a general patterning protocol for oxide-free silicon SAMs that simultaneously protects the underlying silicon from degradation and oxidation while providing a reactive overlayer for the facile functionalization of the SAM with organic and biological molecules. Subsequent reaction of these surfaces with an acidic catalytic stamp results in hydrolysis of the NHS ester in areas of conformal contact both at the micron and sub-micron scales. By successfully and accurately replicating uniform 150-nm features on oxide-free silicon with reusable catalytic stamps, our technique approaches resolution of current photolithographic techniques without relying on controlled environments or expensive equipment and reagents. This technique could be expanded beyond patterning oxide-free silicon to patterning diamond and semiconducting materials for technological development in fields such as biological and chemical sensing and organic electronics.²⁰⁴⁻²⁰⁹

4.3 The relationship between the hydrolyzing efficiency and pKa of the catalytic PU stamps

Our laboratory has demonstrated that sulfonic acid-modified PU stamps rapidly (within 5 minutes) deprotect Boc-modified SAMs on both gold and silicon¹²⁰⁻¹²¹ and hydrolyze NHS-modified SAMs to the corresponding carboxylic

acid on silicon.¹⁴² An important factor contributing to the efficiency of hydrolysis is stamp pKa. Previously, we have utilized sulfonic acid stamps used in catalytic- μ CP experiments. We sought to explore the effect of the pKa of stamp-immobilized acids on rate of NHS hydrolysis.

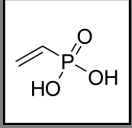
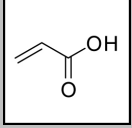
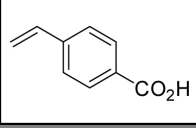
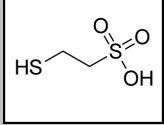
The rate of stamp-catalyzed reaction can be monitored via XPS: the integration of C1s/Si2p peaks reflects the density of NHS groups at the surface. Upon hydrolysis of the NHS ester, a decrease in the C1s peak (normalized to Si2p) corresponding to the removal of this functional group is observed. No significant change in the F1s/Si2p peak is observed throughout the course of the reaction.¹⁴² These data not only provide information about the rate of hydrolysis, but also indicate the specific removal of the NHS group without damage to the underlying monolayer, which bears a CF₃ moiety (Figure 62).

To determine the limiting C1s/Si2p signal ratios, the limiting substrates were examined. 1) Before reaction occurs, we assume maximal NHS coverage of the surface permitted by the bi-patterning technique, which corresponds to a maximum C1s/Si2p value. 2) Complete hydrolysis of this surface with 1 M HCl for 30 minutes provides a lower limit corresponding to a minimum C1s/Si2p value. Previous experiments¹⁴² have shown no significant difference between the C1s/Si2p value associated with NHS-functionalized surfaces incubated with 1 M

HCl solution for 30 minutes and those associated with catalytic- μ CP with flat sulfonic acid-modified stamps ranging from 5 – 30 minutes.

The same stamp fabrication protocol used to form sulfonic acid-functionalized stamps (*Section 4.2.2.2*) was followed, but mercaptoethanesulfonic acid was replaced by an equimolar amount of other acids of varying pKa (Table 7). Acids for catalytic stamping experiments were chosen based upon three main criteria: (1) The pKa range of the acid when polymerized in the stamp should be between that of sulfonic acid (pKa \sim -0.6), the standard model of efficient catalysis demonstrated for catalytic- μ CP, and the pKa where base-catalyzed hydrolysis could occur (pKa \sim 8). (2) The acid must bear a chemical moiety capable of reacting with the PU polymeric mix through a Michael addition or radical polymerization induced by UV light. (3) The inability of the conjugate base to act as a nucleophile in this pKa range, which could lead to covalent bond formation through NHS-displacement instead of the desired acid-catalyzed hydrolysis of the NHS ester to the corresponding acid.

Table 7. Acids co-polymerized with PU pre-polymeric mixture for catalytic- μ CP.

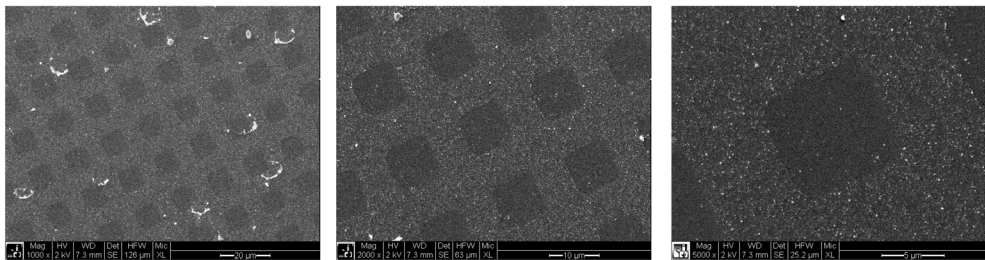
<u>Acid</u>	<u>Estimated pKa (in stamp)</u>
2-Propene-1-phosphonic acid 	2.5, 7.7 ²¹⁰
Acrylic acid 	4.8 ²¹¹
4-Vinylbenzoic acid 	4.2 ²¹²
2-Mercapto-ethanesulfonic acid 	-0.6 ²¹³

To determine if PU stamps bearing acids of varying pKa would hydrolyze NHS-modified surfaces for catalytic- μ CP, substituted PU stamps bearing 8- μ m features were fabricated with each acid. Stamps bearing no acid were also fabricated as controls. All stamps were used as described previously in stamping protocols except stamps bearing phosphonic acid. To manipulate the protonation state of phosphonic acid-functionalized stamps, stamps were incubated either at pH 1 or pH 5, washed with ethanol, dried thoroughly in a

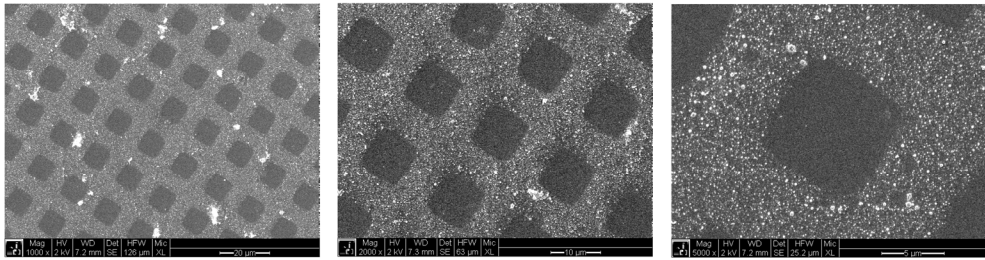
stream of argon, and allowed to dry overnight before stamping experiments to ensure catalytic transfer of features.

NHS-modified surfaces were fabricated according to previously described protocols,¹¹⁷ and stamping on these substrates was conducted for 3-5 hours to ensure pattern transfer. Figure 66 shows pattern transfer for each acid, indicating qualitative success using all four acids. No pattern transfer was observed with unfunctionalized stamps bearing relief features. It is of note that phosphonic acid-modified stamps produce a very light pattern after being incubated in pH 5 water whereas those incubated at pH 1 produced a highly defined pattern. This observation suggests pattern transfer occurs with both mono- and diprotic acids.

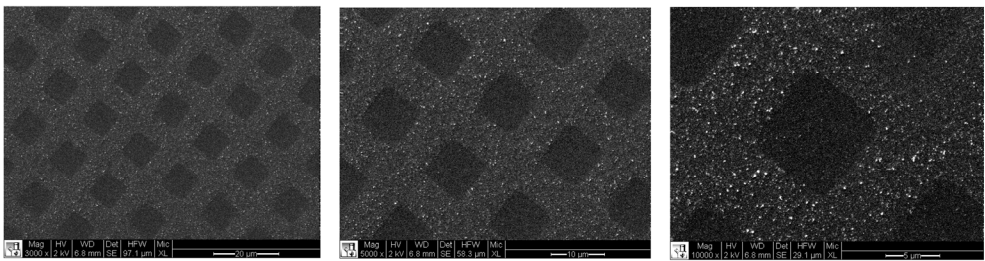
Phosphonic acid stamp (pH 5) for 5 hours, pKa ~7.7



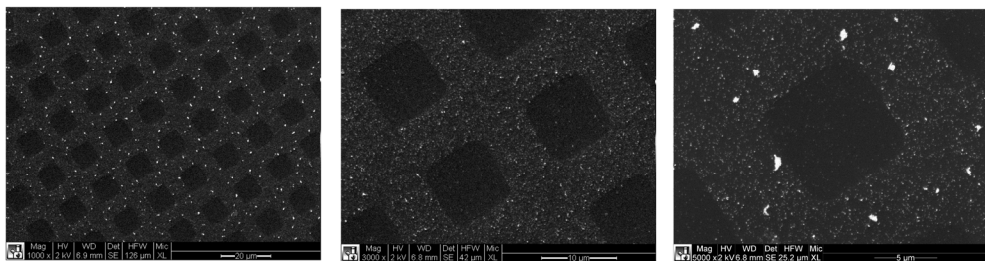
Phosphonic acid stamp (pH 1) for 3 hours, pKa ~2.5



Acrylic acid stamp for 3 hours, pKa ~ 4.8



Benzoic acid stamp for 3 hours, pKa ~ 4.2



Sulfonic acid stamp for 5 minutes, pKa ~ -0.6

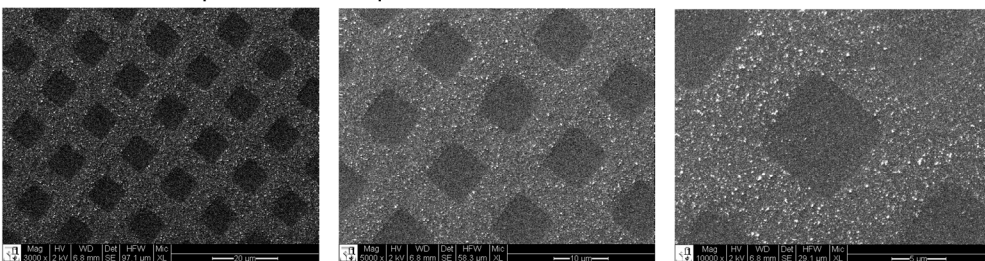


Figure 66. SEM images of surfaces patterned with different acidic stamps.

Quantitative measurements of NHS hydrolysis were performed using XPS to monitor the change in the C1s/Si2p signal ratio over time. For each experiment, four NHS-functionalized surfaces were treated with acid-functionalized, flat stamps for 5, 30, 60, and 120 minutes each. Two control samples for each set of surfaces were run simultaneously – an NHS-functionalized surface without further modification, providing a maximum C1s/Si2p value; and an NHS-functionalized surface that had been incubated in 1 M aqueous HCl, providing a minimum C1s/Si2p value.

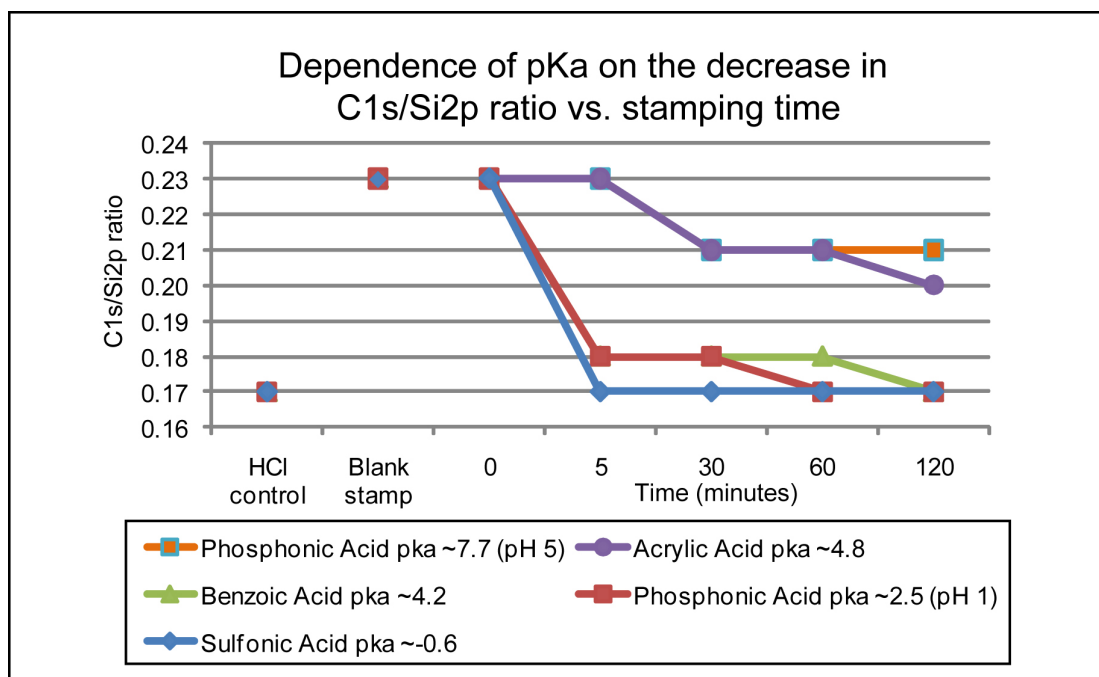


Figure 67. Dependence of pKa on the decrease in C1s/Si2p ratio vs. stamping time for catalytic hydrolysis of the NHS ester on surfaces.

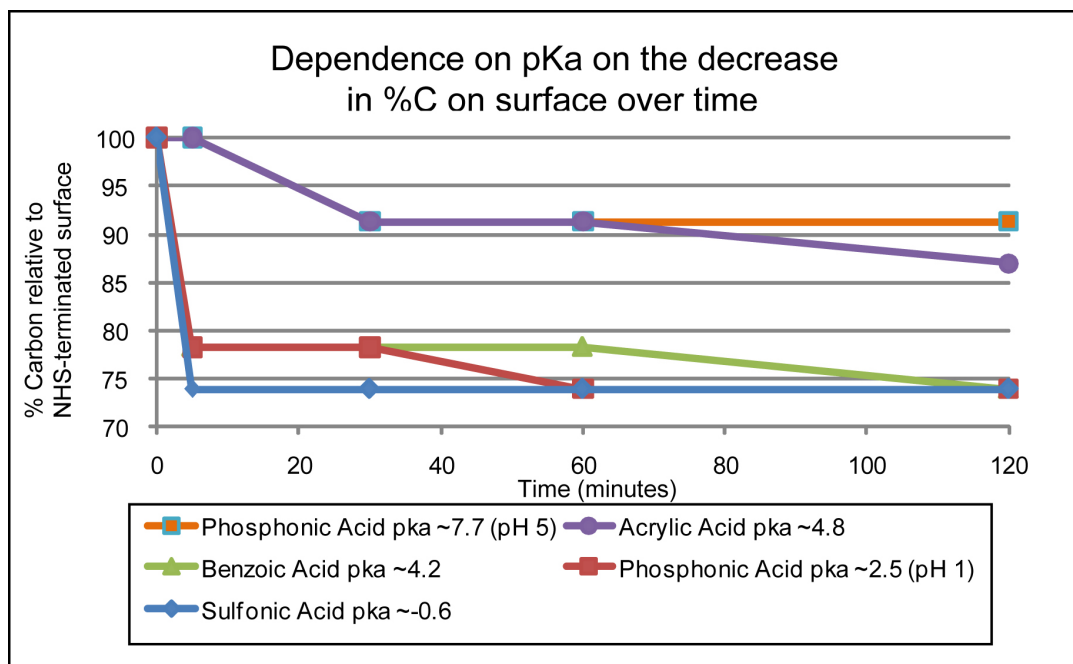


Figure 68. Dependence on pKa on the decrease in %C on NHS-functionalized surface over time during stamping with acidic stamps.

Figures 67 and 68 demonstrate that the rate of NHS ester hydrolysis is a function of stamp pKa. Not surprisingly, acids with higher pKa values (acrylic acid, phosphonic acid at pH 5) show a much slower rate of hydrolysis than do those with lower pKas (benzoic acid, phosphonic acid at pH 1, sulfonic acid). Figure 67 shows control values for maximum and minimum C1s/Si2p signal ratios. Figure 68 shows the decrease in carbon ratio on the surface before, during, and after stamping referenced to NHS-functionalized surfaces. Complete hydrolysis of the NHS group should produce a reduction in carbon on the surface of approximately 25% (4 carbons on NHS / 16 total carbons). This behavior is observed in Figure 68 for all three acids with pKa values below 4.5,

indicating complete hydrolysis with those stamps within the observed reaction time. This value also corresponds to NHS-functionalized surfaces exposed to 1 M HCl, again indicating complete hydrolysis of the NHS ester in the control experiment.

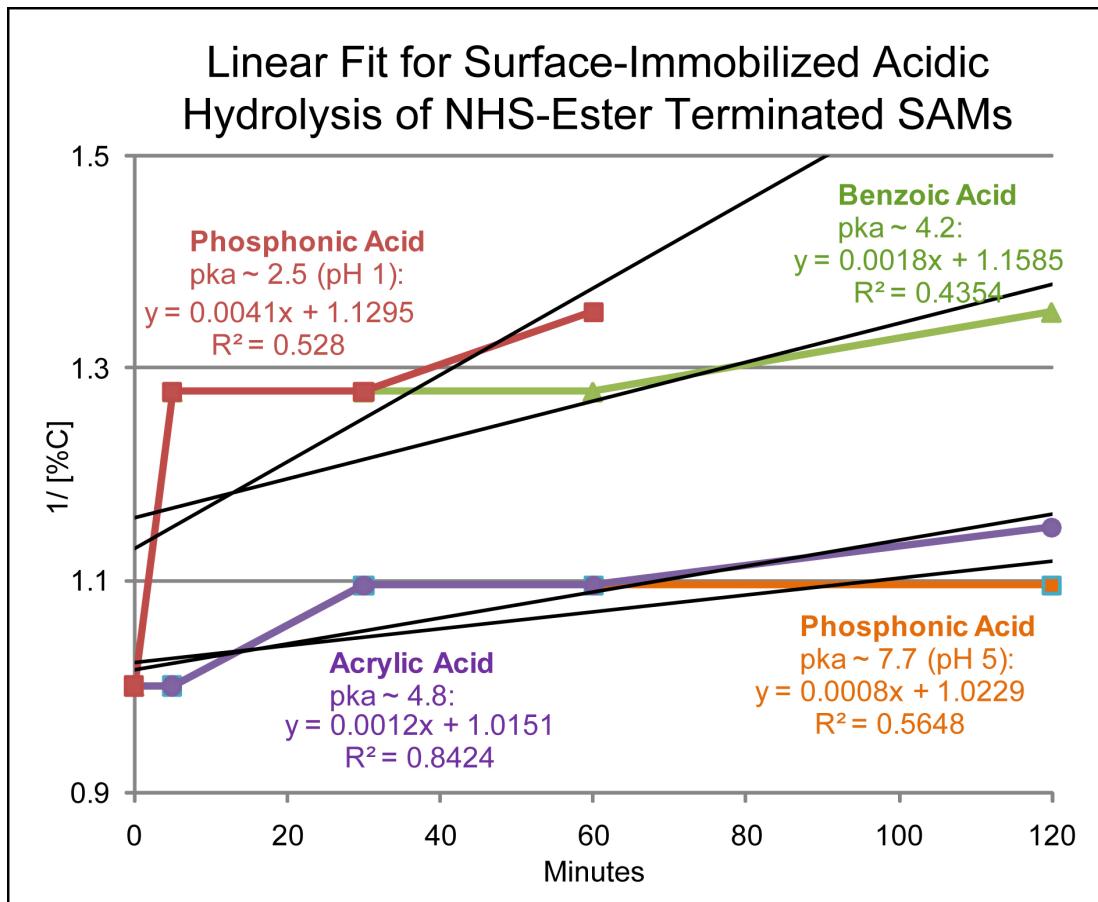


Figure 69. Linear fit of second-order kinetics for surface-immobilized acidic hydrolysis of NHS-ester terminated SAMs.

As plotted in Figure 69, the reaction rate increased upon increased immobilized acid strength, as expected. After fitting data using the terminal start and end points of acid-catalyzed reactions except sulfonic acid to zero, first,

and second order kinetics, the best R^2 fit values (≥ 0.44) yielded evidence of a second-order reaction ($1/[\%C]$) over the other orders (≥ 0.39 for 0th order and ≥ 0.41 for 1st order). However, these R^2 values are too low to determine quantitative parameters of this reaction such as rate constants.

Qualitatively, the four stamping reactions using acids with a $pK_a > 0$ show biphasic kinetics – a fast initial hydrolysis followed by a slower hydrolysis phase. (Reaction using sulfonic acid stamps is too fast to observe a biphasic behavior mechanism.) This initial rapid catalysis most likely corresponds to the hydrolysis from the concentration of acid catalyst whereas the second phase corresponds to the number of positions on the surface the flexible linker will permit the acid to access. Because pK_a is indicative of acid strength and decreases as the concentration of protons increases, it is logical the first step is fast upon initial contact between the two surfaces. Once the initial rapid hydrolysis occurs, the reaction is dependent on the flexibility of the linker that connects stamp to the catalytic acid groups. With increase in time, there is an increase in the probability of the linker accessing more positions on the surface, therefore allowing the acid to hydrolyze esters within a greater radius. This step is much slower.

As weak acids and thus comparatively poor proton donors in this experiment, both phosphonic acid at pH 5 and acrylic acid show catalytic behavior indicative of being almost entirely dependent on the flexibility of the linker. The stronger acids, benzoic acid and phosphonic acid at pH 1, both show biphasic behavior. Finally, sulfonic acid, the strongest acid used, shows such a rapid hydrolysis, both phases cannot be distinguished.

In conclusion, a strong correlation between increasing acid strength of a surface-immobilized acid and decreasing reaction time with immobilized cognate substrate when in conformal contact has been demonstrated for catalytic- μ CP with acid-functionalized PU stamps.

5. Experimental section

5.1 Biocatalytic- μ CP on SAMs of ssDNA

5.1.1 General procedures for biocatalytic- μ CP

All reagents and solvents were purchased from either Sigma-Aldrich or VWR and used as supplied. Water used in aqueous solutions was purified by the Millipore system with a minimum resistivity of 18 M Ω . All solutions, both aqueous and organic, were sterile-filtered through a 0.22 μ m filter and stored in closed containers, except during use.

Thin-layer chromatography was performed on glass-backed Merc Silica Gel 60 F₂₅₄ plates using a 20% solution of phosphomolybdic acid (PMA) in isopropanol or CAM stain²¹⁴ for visualization. Column chromatography was performed using Silicycle Silica-P Flash Silica Gel.

¹H and ¹³C NMR spectra were recorded on a Varian 300 MHz Mercury spectrometer. ElectroSpray Ionization (ESI-MS) mass spectra were collected using Agilent Technologies 1100 LCMSD Trap. Matrix-Assisted Laser Desorption Ionization Time of Flight (MALDI-TOF) mass spectrograms were collected using Voyager DE-Pro. For AFM height and lateral force images, standard V-shaped Si₃N cantilevers (Veeco Metrology) with a force constant of 0.06 nN/nm were used at a force setpoint of ~1 nN (Asylum MFP-3D). Ultra-

violet-visible spectra were collected in 1 cm path length quartz cuvettes using a Hewlet-Packard 1100 spectrophotometer. Infrared spectra were collected using a Nicolet Avatar-360 FT-IR. Combustion analysis was conducted by Atlantic Microlabs.

Si/PMMA masters containing 10 or 15 μm features and donated from the Clark laboratory at Duke University. These masters were stored covered and immediately cleaned before and after use with water, and dried with N_2 . Gold substrates ($\sim 1 \text{ cm}^2$) were manufactured using by coating silicon wafers with a 70Å chromium adhesion layer followed by a 230Å layer of gold using an electron-beam metal evaporator (CHA industries). Fresh stamps were fabricated prior to each experiment.

5.1.2 Synthesis of NTA-acrylate 3 for use in acrylamide-based stamps for biocatalytic- μCP

***N* ^{α} ,*N* ^{α} -Bis(carboxymethyl)-L-lysine (1).**

N ^{α} ,*N* ^{α} -Bis(carboxymethyl)-L-lysine **1** was synthesized from *N*'-benzyloxycarbonyl-L-lysine according to the protocol of Ho and co-workers.¹⁵⁴ *N*'-Benzyloxycarbonyl-L-lysine (6.45g, 23.0 mmol) was dissolved in 2 M NaOH (35 mL), cooled to 0 °C, and added dropwise to a stirring solution of bromoacetic acid (9.59g, 69.0 mmol) in 2 M NaOH (35 mL), also cooled to 0 °C. The reaction

was stirred at 0 °C for 2 hours and then allowed to equilibrate to room temperature overnight. The following day, the solution was heated for 2 hours at 50 °C. 1 M HCl (70 mL) was added to the solution. After cooling to 0 °C to maximize precipitation, the product was filtered and purified by dissolving in 1 M NaOH (100 mL) and reprecipitating with an equivalent amount of 1 M HCl. The final white solid **1** was dried by lyophilization (88%). ¹H NMR (DMSO) δ 7.4-7.3 (m, 5H), 7.2 (t, *J* = 5.2, 1H), 5.0 (s, 2H), 3.6 (m, 4H), 3.4 (t, *J* = 7.5, 1H), 3.0 (m, 2H), 1.6-1.3 (m, 6H); ¹³C NMR (DMSO) δ 172.8, 172.0, 155.3, 136.6, 127.6, 127.0, 64.4, 63.7, 52.6, 28.4, 22.3.

***N*^α,*N*^α-bis(carboxymethyl), *N*^ε-benzyloxycarbonyl-lysine tris(2-trimethylsilylethyl) ester.**¹³⁷

A 1.0 L flask was charged with 10.8 g of **1**, 19.0 g EDC, 23.0 mL 2-trimethylsilylethanol, 5.0 g DMAP and 200 mL DMF. The reaction was stirred for 56 hours, and after completion, the suspension clarified. The solution was dissolved in 1.0 L Et₂O and extracted three times with both 1 M NH₄Cl and then with 1 M aqueous HCl. The ether layer was dried over MgSO₄, filtered and concentrated under reduced pressure. The mixture was then chromatographed over silica gel using a gradient from hexane to 9:1 hexane/ ethyl acetate resulting in a clear, colorless oil (11.0 g). ¹H NMR (300 MHz, CDCl₃) δ 7.34 (m, 5H), 5.08

(s, 2H), 4.90 (bt, 1H), 4.16 (m, 6H), 3.60 (s, 4H), 3.39 (t, 1H, $J = 7.5$ Hz), 3.18 (m, 2H), 1.76 – 1.36 (bm, 7H), 0.97 (m, 6H), 0.036 (s, 9H), 0.022 (s, 18H); ^{13}C NMR (75 MHz, CD_3Cl) δ 172.9, 171.5, 152.0, 128.5, 128.0, 103.8, 100.2, 66.5, 64.7, 62.8, 52.9, 40.8, 30.0, 28.2, 23.0, 17.5, 17.3, -1.5; IR (cm^{-1}) 3357, 2954, 2896, 1731, 1249, 1176, 1037, 8645, 694; MS 696.37(calc.), 697.5 (found MH^+).

N $^{\alpha}$,N $^{\alpha}$ -bis(carboxymethyl)-lysine tris(2-trimethylsilylethyl)ester (2).

In accordance to the procedure of Ho and co-workers,¹⁵⁴ a 1.0 L flask, under a funnel of nitrogen, was charged with 10.95 g N^{ϵ} -benzyloxycarbonyl, N^{α} -bis(carboxymethyl)-lysine tris(2-trimethylsilylethyl) ester, 300 mL methanol (Omnisolve, EMD), and ~500 mg 10% dry palladium on carbon. The stirring suspension was degassed for 5 minutes under house vacuum and repressurized using a balloon of H_2 . This cycle was repeated twice and the reaction was left to stir under H_2 gas for 1.5 hours. The reaction was diluted with 600 mL dichloromethane and filtered through a pad of silica. The filtrate was again filtered over celite and concentrated under reduced pressure. Some remnants of carbon black and silica were typically evident in the otherwise clear oil (7.15 g), but the amine was used without further purification. ^1H NMR (300 MHz, CDCl_3) δ 4.12(m, 6H), 3.57 (s, 4H), 3.36 (t, 1H, $J = 7.2$ Hz), 2.64 (t, 2H, $J = 6.9$ Hz), 1.74 – 1.22

(m, 10H), 0.94 (m, 6H), 0.01(s, 9H), 0.09 (s, 18H); ^{13}C NMR (75 MHz, CD_3Cl) δ 173.0, 171.5, 64.9, 62.7, 62.6, 60.0, 52.8, 41.9, 41.9, 33.2, 30.3, 23.2, 22.1, 17.5, 17.3, -1.6.

***N* $^{\alpha}$,*N* $^{\alpha}$ -bis(carboxymethyl), *N* $^{\epsilon}$ -acrylamido-lysine tris(2-trimethylsilylethyl)ester.¹³⁷**

A 2.0 L flask was charged with 7.15 g *N* $^{\alpha}$ -bis(carboxymethyl)-lysine tris(2-trimethylsilylethyl)ester **2**, 700 mL dichloromethane (Omnisolve, EMD), 1.1 mL acrylic acid and 2.9 g EDC. The reaction was left to stir for 3 hours and then was concentrated under reduced pressure. The resulting yellow oil was triturated under pentane and then concentrated at reduced pressure. The resulting yellow oil was chromatographed on silica gel using a gradient of dichloromethane to 3% methanol in dichloromethane to give a clear, colorless oil (4.95 g). ^1H NMR (300 MHz, CDCl_3) δ 7.90 (bt, 1H), 6.18(m, 2H), 5.56(dd, 1H, $J = 2.4, 9.9$ Hz), 4.13(m, 6H), 3.54 (s, 4H), 3.45 (m, 4H), 1.71 – 1.20 (m, 6H), 0.967 (m, 6H), 0.07 (s, 9H), 0.04(s, 18H); ^{13}C NMR (75 MHz, CD_3Cl) δ 173.1, 171.6, 165.7, 131.1, 125.7, 164.2, 62.9, 62.7, 53.4, 53.07, 39.1, 29.4, 27.91, 27.9, 22.6, 17.5, 17.3, -1.6; MS (ESI) 616.34 (calc.) 617.5 (found MH^+).

N^ε-acrylamido, N^α-bis(carboxymethyl)-lysine (3).¹³⁷

A 1.0 L flask was charged with 4.95 g N^ε-acrylamido, N^α-bis(carboxymethyl)-lysine tris(2-trimethylsilylethyl)ester and 25 mL of fresh trifluoroacetic acid. The reaction was left to stir at room temperature for 4 hours and concentrated at reduced pressure. Residual trifluoroacetic acid was removed by redissolving in 100 mL methanol three times and concentrating at reduced pressure. The resulting white foam was chromatographed on C₁₈-bonded silica by eluting with water and fractions were analyzed by UV-visible spectrometry. Fractions containing the desired compound were lyophilized to provide the desired acrylamide as a white amorphous powder (1.7 g). R_f <0.01 (SiO₂, 10% methanol in dichloromethane) visualized by fluorescence quenching and charring with PMA; melting point analysis: the white powder slowly decomposed over 45 – 50 °C, then foamed (perhaps as a polymer) and eventually achieved the molten state between 100 – 105 °C; ¹H NMR (300 MHz, D₂O, positions reported relative to HOD, 4.7ppm) δ6.08 (m, 2H), 5.61 (dt, 1H, J = 2.1, 9.6 Hz), 4.09 (s, 4H), 4.03 (m, 1H), 3.16 (t, 2H, J = 6.3 Hz), 1.89 – 1.78 (m, 2H), 1.51 – 1.39 (m, 4H); ¹³C NMR (75 MHz, D₂O) δ170.9, 169.4, 168.5, 130.1, 127.1, 54.2, 38.8, 27.9, 22.9; MS (ESI) 315.307 (calc.) 315.1 (found); Anal. Calcd for

$C_{13}H_{20}N_2O_7 \cdot F_3CCO_2H \cdot H_2O$: C, 40.18; H, 5.17; N, 6.25; O, 35.69. Found: C, 41.85; H, 5.37; N, 6.60; O, 37.07.

5.1.3 ExoI expression and purification.¹⁵⁶

Dr. B. W. Matthews (University of Oregon) generously provided the gene encoding ExoI with a C-terminal His-tag in a pET22b overexpression vector. The vector containing ExoI was transformed into BL-21 DE3 cells via heat-shock. Single colonies from this transformation were grown to an OD_{600} of 0.9 – 1.0, induced overnight at 25°C with 125 mg/L isopropyl thiogalactopyranoside (IPTG), concentrated by centrifugation, and resuspended in 500 mM NaCl, 20 mM Tris-HCl, 5 mM imidazole, pH 7.9 (binding buffer). The cell solution was physically lysed at high pressure. The lysate was centrifuged, and the supernatant was applied to a column of charged Ni-IDA agarose resin (Novagen®). Standard buffers were used for Ni²⁺-column purification and elution with the exception of wash buffer, in which half the normal concentration was used (250 mM NaCl, 30 mM imidazole, 10 mM Tris-HCl, pH 7.9). Purified ExoI was dialyzed into 500 mM NaCl, 20 mM Tris-HCl, pH 7.9 (binding buffer without imidazole). This construct yielded approximately 5 mg protein per liter of cell growth.

5.1.4 ssDNA immobilization on surfaces.

5.1.4.1 ssDNA SAMs on gold surfaces.⁹¹

An electron-beam metal evaporator (CHA Industries) was used to manufacture gold substrates (~1 cm²). Silicon disks were coated with a 70 Å chromium adhesion layer preceded by a 230 Å gold layer. Lyophilized ssDNA-alkanethiol oligonucleotide with 5'-mercaptohexyl modification of the sequence 5'-GATTACAGATTACA-3' was purchased from IDT DNA Technologies. The ssDNA was suspended in 10 mM Tris-Cl buffer, pH 8.5 (Quiagen EB Buffer) for storage and purified before each use using a NAP-10 column. Purification was performed according to the manufacturer's instructions. ssDNA SAMs were formed on freshly-evaporated gold substrates using previously published protocol.⁹¹ To maximize vertically-standing ssDNA-alkanethiols, freshly purified/sterile-filtered 1 μM ssDNA-alkanethiol oligonucleotides in 800 mM KH₂PO₄ solution were exposed to clean gold surfaces for 2 hours at room temperature followed by a 1-hour incubation with aqueous 1 mM mercaptohexanol (MCH). The substrates were rinsed with water and ethanol and dried using a stream of N₂ and placed in dust-free petry dishes for no more than 2 hours before stamping.

5.1.4.2 ssDNA immobilization on glass surfaces.

Isothiocyanate-functionalized (ITC) glass slides (SAL-0.1) were purchased from Genorama®. All oligonucleotides were purchased from IDT DNA Technologies with 5'-aminoethyl, 3'-TAMRA modification of the sequence 5'-GATTACAGATTACA-3'. Oligonucleotides were stored in sterile-filtered phosphate buffer solution (PBS), pH = 7.00. For immobilization experiments, a 100 µL aliquot of 0.1 µM ssDNA in PBS was delivered to the surface of ITC substrate and incubated for 1 hour at room temperature. The solution was then removed and rinsed via aspiration. The substrates were dried using a stream of N₂. The substrates were dried using a stream of N₂ and placed in dust-free petry dishes for no more than 2 hours before stamping.

5.1.5 MALDI-TOF mass spectrometry activity assay for ssDNA-ExoI in solution.

Lyophilized ssDNA oligonucleotide with 3'-TAMRA modification of the sequence 5'-GATTACACA-3' was purchased from IDT. Confirmation of ExoI activity was assayed in solution by mixing a 1 µM solution of enzyme in reaction buffer (66 mM glycine, 12 mM MgCl₂, pH 9.50) with 10 µM solution of ssDNA oligonucleotide 5'-GATTACACA-3' with 3'-TAMRA and 5'-amino modifications and incubating for 1 hour. The solution was then lyophilized and analyzed using MALDI-MS. The mass peak for the oligonucleotide (3715.8 g/mol) was

clearly visible for the control experiment (no enzyme) and was not detected for the sample containing active enzyme.

5.1.6 Stamp fabrication, activation, and biocatalytic- μ CP stamping protocols.¹³⁷

Silicon-PMMA masters containing patterns of 15- μ m squares and 10- μ m squares were stored in closed containers when not in use. Immediately before use, the masters were cleaned with ethanol and water, and dried under N₂. Stamp formation and μ CP were completed in a laminar-flow hood to minimize exposure to dust. New stamps were fabricated before each new stamping experiment. Acrylamido-NTA lysine **3** (25 mg) was dissolved in 300 μ L of commercially-available 40% w/v acrylamide/bisacrylamide (19:1) aqueous solution and 200 μ L of 1.5 M tris, pH 8.8. This was proceeded by the addition of polymerization radical-forming reagents: 10 μ L of 20% ammonium persulfate (APS) and 0.4 μ L of tetramethylethylenediamine (TEMED). The solution was briefly agitated and 185 μ L was deposited onto a polyethylene platform. The silicon-PMMA master attached to another polyethylene platform was brought in contact with the solution and was suspended above the platform by 1.5-mm spacers as shown in Figure 26. All solutions were cooled to and all incubations were carried out at \sim 4 °C. Following polymerization (10-15 minutes), stamps

were immediately placed in sterile-filtered 50 mM NiSO₄ solution until homogeneously-colored light green (15-20 minutes). A series of rinses and incubations followed: 500 mM NaCl, 20 mM Tris-HCl, 5 mM imidazole, pH 7.9 (500 mM NaCl, 20 mM Tris-HCl, 5 mM imidazole, pH 7.9), 0.1 μM ExoI in binding buffer for ~5 minutes, binding buffer, wash buffer, 0.05% SDS sonication rinse for ~1 minute to remove nonspecifically adsorbed enzyme, two rinses with wash buffer, and reaction buffer. Stamps were then placed on filter paper soaked with reaction buffer. The tips of the stamp were dried slightly by N₂, and gold or glass substrates were placed on top of the stamp. Gentle pressure was applied to create conformal contact, and the substrate/stamp was incubated for 1-12 hours at ~4 °C. The substrate was then gently removed from the stamp and placed immediately in room temperature 50 mM EDTA (volumetric standard) to chelate any remaining Mg⁺², rinsed with Milli-Q, and dried under N₂. Substrates were kept in sealed containers with until imaging with AFM or CFM.

5.1.7 AFM tips and MHA-modified AFM tips.

Standard V-shaped Si₃N cantilevers (Veeco Metrology) with a force constant of 0.06 nN/nm were used at a force setpoint of ~1 nN (Asylum MFP-3D) in AFM imaging experiments. The same type of cantilevers was modified for chemical AFM imaging by coating sequentially with a 70 Å chromium adhesion

layer proceeded by a 230 Å gold layer. For mercaptohexadecanoic acid-functionalized (MHA) tips, gold-coated cantilevers were submerged for 5 minutes at room temperature in a 1 mM mercaptohexadecanoic acid (MHA) in ethanol solution and then dried using a stream of N₂.

5.1.8 Preparation of glass-immobilized ssDNA for MALDI-TOF spectroscopy.

ssDNA-functionalized slides were made using the procedure described in *Section 5.1.4.2*. 6-Aza-3-thiothymine (ATT) and ammonium citrate were purchased from Sigma. A 20 mg/mL solution of ATT in acetonitrile and a 40 mM solution of ammonium citrate in H₂O were combined 1:1 to make a 10 mg/mL ATT, 20 mM ammonium citrate, 1:1 acetonitrile:H₂O solution to be used as a matrix for MALDI-TOF MS. 1- μ L aliquots of this solution were deposited on ssDNA-functionalized glass slides and exposed to an accelerating voltage of 25000V, delay time of 1500 nsec, laser intensity of 2123, and a low mass gate of 500Da.

5.2 Synthesis of acrylamide-TEG-NTA-lys 9.

11-[(Toluenesulfonyl)oxy]-3,6,9-trioxaundecanol.²¹⁵

p-Toluenesulfonyl chloride (7.362g, 38.6 mmol) was added to a solution of tetraethyleneglycol 4 (20 mL, 115.8 mmol) in dry pyridine (6.23 mL, 77.2 mmol).

The reaction was stirred at 0 °C for 2 hours before solution was warmed to room temperature. After stirring for 1 hour at room temperature, the reaction mixture was exposed to 250 mL of 1.4 M HCl and extracted with 3 X 100 mL of dichloromethane. The organic layer was evaporated and the remaining residue was purified by gradient chromatography (EtOAc, 15:1 EtOAc:ACN, 10:1 EtOAc:ACN) giving 7.71g (57%) of a colorless oil. TLC (15:1 EtOAc:ACN) R_f 0.3; ^1H NMR (CDCl_3) δ 7.80 (d, J = 8.1, 2H), 7.35 (d, J = 8.1, 2H), 4.20 (t, J = 5.0, 2H), 3.70-3.60 (m, 14H), 2.50 (broad s, 1H), 2.45 (s, 3H); ^{13}C NMR (CDCl_3) δ 144.9, 133.1, 129.9, 128.1, 72.6, 70.8, 70.6, 70.4, 69.4, 68.8, 61.8, 21.7.

11-Azido-3,6,9-trioxaundecanol (5).²¹⁵

Sodium azide (2.16g, 33.2 mmol) was added to a solution of 11-[(toluenesulfonyl)oxy]-3,6,9-trioxaundecanol (7.71g, 22.13 mmol) in dry DMF (50 mL). The mixture was heated at 110 °C for 12-16 hours (overnight) and then allowed to equilibrate to room temperature. The reaction mixture was coevaporated with toluene (300 mL), tritrated with ether, and filtered, giving 5.02g (69%) of **5** as a gold-colored oil. (Note: This is an approximate yield obtained from NMR data – not all DMF was removed before quantitation because the next step also required DMF as a solvent.) TLC (EtOAc) R_f 0.6; ^1H

NMR (CDCl₃) δ 3.74-3.67 (m, 12H), 3.60 (t, J = 4.5, 2H), 3.40 (t, J = 5.1, 2H), 3.10 (broad s, 1H); ¹³C NMR (CDCl₃) δ 72.5, 70.7-70.0, 61.7, 50.7.

***tert*-Butyl 14-azido-3,6,9,12-tetraoxatetradecanoate.**²¹⁵

Alcohol **5** (~2.60g, 11.86 mmol) was dissolved in dry DMF (60 mL) and cooled to 0 °C. Under nitrogen gas, NaH (569 mg, 23.72 mmol) powder (95%) was added to the reaction mixture. After the formation of H₂ gas had ended, a solution of *tert*-butyl bromoacetate (2.63 mL, 17.79 mmol) in DMF (10 mL) was added quickly under N₂ atmosphere. The mixture was stirred at 0 °C for 2 hours, then allowed to equilibrate to room temperature, and stirred for 12-14 hours (overnight). Then the reaction was diluted with EtOAc (300 mL) and was extracted with 3 x 150 mL water, dried over MgSO₄, and concentrated in vacuo. The residue was then purified by flash chromatography (9:1 EtOAc:Hex) to yield 1.91 g (48%) of a golden oil. TLC (EtOAc) R_f 0.7; ¹H NMR (CDCl₃) δ 4.02 (s, 2H), 3.68-3.67 (m, 14H), 3.41-3.37 (t, J = 5.3, 2H), 1.48 (s, 9H); ¹³C NMR (CDCl₃) δ 169.7, 81.6, 70.9-70.4, 70.1, 69.1, 50.2, 28.2.

14-Azido-3,6,9,12-tetraoxatetradecanoic acid (6).²¹⁶

TFA (40 mL) was added to a solution of *tert*-butyl 14-azido-3,6,9,12-tetraoxatetradecanoate (1.91g, 5.73 mmol) in CH₂Cl₂ (40 mL) and stirred for 5 hours at room temperature. After concentrating in vacuo, the reaction was suspended in 60 mL of toluene and concentrated in again. This cycle was repeated five times to remove all TFA, finally yielding 1.45g (95%) of **6** as a brownish-gold oil. TLC (9:1 DCM:MeOH) *R_f* <0.1; ¹H NMR (CDCl₃) δ 9.23 (broads, 1H), 4.18 (s, 2H), 3.77-3.62 (m, 14H), 3.42-3.39 (t, *J* = 5.1, 2H); ¹³C NMR (CDCl₃) δ 173.3, 71.4, 70.8-70.6, 70.4, 70.1, 68.8, 50.8.

6-Benzylcarbonylamino-2-(bis-methoxycarbonylmethyl-amino)-hexanoic acid methyl ester.²¹⁷

A solution of 2.0 M TMS-diazomethane in diethyl ether (3.0 mL) was added to a solution of **1** (260 mg, 0.656 mmol) in dry MeOH (30 mL) under an N₂ atmosphere. The TMS-diazomethane was added until the solution remained a slight yellow color for at least 30 minutes, indicating an excess of TMS-diazomethane. The reaction was stirred for 30 minutes at room temperature, concentrated in vacuo, and purified by gradient chromatography (EtOAc, 15:1 EtOAc:ACN, 10:1 EtoAc:ACN) giving 267 mg (97%) of a colorless oil. TLC (10:1

EtoAc:Hexane) R_f 0.6; ^1H NMR (CDCl_3) δ 7.36-7.27 (m, 5H), 5.09 (s, 2H), 4.95 (broad s, 1H), 3.72-3.63 (m, 13H), 3.44-3.39 (t, $J = 3.7$, 1H), 3.20-3.16 (m, 2H), 1.73-1.46 (m, 6H); ^{13}C NMR (CDCl_3) δ 173.2, 171.9, 156.7, 136.8, 128.5, 128.1, 66.6, 64.6, 52.5, 51.7, 51.5, 40.8, 30.0, 29.3, 23.0.

6-Amino-2-(bis-methoxycarbonylmethyl-amino)-hexanoic acid methyl ester (7).¹⁵⁴

6-Benzylocarbonylamino-2-(bis-methoxycarbonylmethyl-amino)-hexanoic acid methyl ester (267 mg, 0.609 mmol) was dissolved in a minimal amount of MeOH. Palladium (10% wt) on activated carbon (2.7 mg) was then added under N_2 atmosphere. The reaction was exposed to H_2 and then vacuum three times in order to remove residual air. After 10 minutes, the exposure to H_2 and vacuum was again repeated. The reaction was left to stir overnight at room temperature. The solution was then filtered, concentrated in vacuo, and dried overnight to yield 78 mg (42%) of 7 as a colorless oil. ^1H NMR (D_2O) δ 3.80-3.64 (m, 13H), 3.57-3.52 (t, $J = 7.5$, 1H), 3.02-2.97 (t, $J = 7.5$, 2H), 1.75-1.30 (m, 6H); ^{13}C NMR (D_2O) δ 175.8, 174.8, 65.3, 53.5, 53.0, 52.8, 40.0, 29.6, 27.2, 23.0.

6-(2-[2-(2-[2-(2-Azido-ethoxy)-ethoxy]-ethoxy)-ethoxy]-acetylamino)-2-(bis-methoxycarbonylmethyl-amino)-hexanoic acid methyl ester (8).²¹⁸

Compounds **6** (153 mg, 0.552 mmol) and **7** (168 mg, 0.552 mmol) were dissolved together in DMF (2 mL). Triethylamine (77 μ L, 0.552 mmol), *N*-(3-dimethylaminopropyl)-*N'*-ethylcarbodiimide hydrochloride (EDC-HCl) (106 mg, 0.552 mmol), and 1-hydroxybenzotriazole HOBt) were added to solution while stirring at 0 °C. After all reagents were added, the reaction was stirred at room temperature for 5 hours. The solution was concentrated in vacuo, dissolved in 50 mL EtOAc, and washed three times with 10% K₂CO₃. The organic layer was then dried with MgSO₄, filtered, and concentrated in vacuo yielding 100 mg (32%) of **8** as a yellow-colored oil. ¹H NMR (CDCl₃) δ 6.96 (t, *J* = 5.1, 1H), 3.91 (s, 2H), 3.68-3.51 (m, 27H), 3.37-3.30 (m, 3H), 3.24-3.17 (q, *J* = 6.6, 2H), 1.66-1.30 (m, 6H); ¹³C NMR (CDCl₃) δ 173.1, 171.8, 169.9, 70.8-70.1, 64.7, 52.4, 51.7, 51.5, 50.7, 38.7, 30.1, 29.3, 23.3; IR (cm⁻¹) 3353, 2951, 2870, 2108, 1736, 1670, 1540, 1437, 1346, 1281, 1205, 1147, 1012, 947, 852, 732, 669, 560.

6-(2-[2-(2-[2-(2-Amino-ethoxy)-ethoxy]-ethoxy)-ethoxy]-acetylamino)-2-(bis-methoxycarbonylmethyl-amino)-hexanoic acid methyl ester.¹⁵⁴

Compound **8** (500 mg, 0.887 mmol) was dissolved in 45 mL MeOH. Palladium (10% wt) on activated carbon (50 mg) was added under N₂ atmosphere. The reaction was exposed to H₂(g) and then vacuum three times in order to remove residual air. After 10 minutes, the exposure to H₂ and vacuum was again repeated three more times. The reaction was left to stir overnight at room temperature. The solution was then filtered and concentrated in vacuo to yield 470 mg (98%) of a yellow-colored oil. ¹H NMR (CDCl₃) δ 7.10 (broad t, *J* = 4.5, 1H), 3.98 (s, 2H), 3.72-3.62 (m, 27H), 3.53-3.49 (t, *J* = 5.4, 2H), 3.44-3.39 (t, *J* = 7.5, 1H), 3.30-3.24 (q, *J* = 6.6, 2H), 2.88-2.84 (t, *J* = 5.4, 2H), 2.42-2.22 (broad s, 2H), 1.75-1.45 (m, 6H); ¹³C NMR (CDCl₃) δ 173.0, 171.8, 169.9, 73.3, 70.9-70.3, 64.7, 52.4, 51.7, 51.4, 41.7, 38.6, 30.1, 29.3, 23.3.

6-(2-[2-(2-[2-(2-Acryloylamino-ethoxy)-ethoxy]-ethoxy)-ethoxy]-acetylamino)-2-(bis-methoxycarbonylmethyl-amino)-hexanoic acid methyl ester.¹³⁷

6-(2-[2-(2-[2-(2-Amino-ethoxy)-ethoxy]-ethoxy)-ethoxy]-acetylamino)-2-(bis-methoxycarbonylmethyl-amino)-hexanoic acid methyl ester (440 mg, 0.818 mmol), acrylic acid (70.8 μL, 1.03 mmol), and EDC-Cl (392 mg, 2.04 mmol) were

dissolved in 49 mL CH₂Cl₂ (in that order) and stirred overnight at room temperature. The reaction was concentrated in vacuo and purified by column chromatography (6:1 CH₂Cl₂:MeOH) giving 59 mg (12%) of a yellow-colored oil. TLC (6:1 CH₂Cl₂:MeOH) R_f 0.7; ¹H NMR (CDCl₃) δ 7.00 (broad m, 1H), 6.69 (broad m, 1H), 6.32-6.11 (m, 2H), 5.63-5.59 (m, 1H), 3.98 (s, 2H), 3.72-3.24 (m, 32H), 1.75-1.43 (m, 6H); ¹³C NMR (CDCl₃) δ 173.2, 171.9, 170.0, 165.8, 131.2, 126.3, 71.0-70.0, 64.8, 52.6-51.6, 39.4, 38.8, 30.2-29.4, 23.4.

6-(2-[2-(2-[2-(2-Acryloylamino-ethoxy)-ethoxy]-ethoxy)-ethoxy]-acetylamino)-2-(bis-carboxymethyl-amino)-hexanoic acid (9).

6-(2-[2-(2-[2-(2-Acryloylamino-ethoxy)-ethoxy]-ethoxy)-ethoxy]-acetylamino)-2-(bis-methoxycarbonylmethyl-amino)-hexanoic acid methyl ester (59 mg, 0.0997 mmol) was dissolved in 300 μL THF and 100 μL H₂O. While stirring at room temperature, 658 μL (0.658 mmol) of 1 M LiOH was added to the solution. The reaction was stirred overnight at room temperature (standard procedure for deprotection of the methyl ester). The solution was then transferred to a flask containing prepared AmberLite IR-120 ion-exchange resin. The solution was stirred in the resin for 10 minutes, filtered, concentrated in vacuo, and lyophilized overnight giving 40 mg (73%) of **9** as a white solid. ¹H

NMR (D₂O) δ 6.32-6.15 (m, 2H), 5.78-5.74 (m, 1H), 4.13-3.99 (m, 6H), 3.81-3.66 (m, 11H), 3.49-3.45 (t, $J = 5.3$, 1H), 3.29-3.3.25 (broad m, $J = 5.7$, 2H), 1.96-1.59 (m, 6H);
¹³C NMR (D₂O) δ 174.4, 172.5, 172.0, 170.4, 168.7, 130.0, 127.5, 70.5-69.7, 68.9, 67.8, 67.4, 54.7, 39.2, 38.5, 28.2, 26.9, 23.3.

5.3 Expansion of enzyme-substrate system for biocatalytic- μ CP: Carboxyesterase/lipase and aromatic ester-functionalized SAMs.

5.3.1 Carboxyesterase and lipase DNA isolation and transformation, and protein transformation, expression, and purification.

5.3.1.1 PCR amplification of the BioH gene from genomic DNA.

Genomic DNA isolation.

The protocol for genomic DNA isolation was provided by Amanda Jane Lind (McCafferty Lab, Duke University Department of Chemistry).

Dr. Dewey McCafferty generously donated a 100- μ L aliquot of DH5 α cells for the isolation of genomic DNA. This aliquot was resuspended in 500 μ L of cell lysis buffer (25 mM Tris, 25 mM EDTA, 10 mg/mL lysozyme, pH 8.09) and incubated for 2 hours with shaking at 37 °C. A 125- μ L aliquot of 10% SDS solution was added to the growth, and the solution was incubated for 20 minutes at 65 °C using a heat block. After adding 216 μ L of 5 M potassium acetate solution was added to the tube, a white precipitate formed. The tube was then inverted gently to mix and incubated on ice for 30 minutes. This solution was

then centrifuged at 13000 RPM for 10 minutes. The supernatant (~600 μ L) was decanted into a clean tube and the remaining fluffy white pellet was discarded. One volume of isopropanol (600 μ L) was added to this supernatant to precipitate genomic DNA. The tube was then inverted gently to prevent shearing of the DNA. Small transparent strands of DNA were observed, and the sample was incubated at room temperature for 10 minutes.

To harvest DNA, the sample was centrifuged at 13000 RPM for 20 minutes. The supernatant was then aspirated, and the remaining pellet washed with 500 μ L 75% EtOH and centrifugation at 13000 RPM for 10 minutes. The supernatant was aspirated, and the remaining pellet was again washed with 500 μ L 75% EtOH and centrifugation at 13000 RPM for another 10 minutes. (The tube orientation was rotated only 90° between washes so that the EtOH gently “rolled over” DNA, washing it without shearing.) The supernatant was aspirated and the DNA was allowed to air dry (cap open) for 10 minutes. The pellet was then resuspended in 50 μ L TE buffer (10 mM Tris, 1 mM EDTA, pH 8.0) with 1 μ L of RNase solution (100 mg/mL of deoxyribonucleaseI from bovine pancreas) and incubated at 65 °C for 15 minutes to redissolve DNA.

PCR amplification of BioH from genomic DNA.

BioH was amplified successfully using standard PCR and the forward primer, 5'-TATAGGATCCATGAATAACATCTGGTG-3', which contained the BamH1 cut site and had a calculated T_m of 54.6 °C. The reverse primer was a 26-mer, 5'-TATAAAGCTTCACCCTCTG CTTCAAC-3', which contained the HindIII cut site and had a calculated T_m of 56.0 °C.

The following were added to a 500- μ L eppendorf tube: 79.0 μ L ddH₂O, 10 μ L of 10X Pfu Buffer, 2 μ L of 10 mM dNTPs solution, 2 μ L of 20 μ M forward primer, 2 μ L of 20 μ M reverse primer, 4 μ L of genomic DNA, and 1 μ L of Pfu polymerase. This 100 μ L reaction mixture was added in aliquots of 50 μ L to two separate PCR tubes. The PCR program was set up to complete 50 cycles of the following temperatures and times: 98 °C for 5 minutes, 98 °C for 45 seconds, 49 °C for 45 seconds, 72 °C for 1 minute, and 72 °C for 7 minutes. The reaction was kept at 4 °C once completed.

Both samples were run on a 1% agarose gel containing 0.01% EtBr at 130V for 33 minutes. Each sample (50 μ L DNA solution, 5 μ L dye) showed a band between 500 bp and 1000 bp, indicating the correct fragment (786 bp) had been isolated. This band was excised and the QIAquick® Gel Extraction Protocol was followed to purify and isolate DNA. To ensure we had successfully isolated

BioH DNA, another 1% agarose gel was completed with each sample (2 μ L DNA solution, 2 μ L dye) and corresponding bands were observed.

BamH1 and HindIII restriction enzymatic digests of BioH and pET22b vector DNAs.

BamH1 and HindIII enzymatic digests must be performed sequentially. To each reaction tube (one tube for the BioH DNA and the other tube for the pET22b vector DNA), 48 μ L of PCR product (the respective DNAs), 6.5 μ L of 10X BamH1 buffer, 6.5 μ L of 10X BSA, 2 μ L of BamH1 restriction enzyme, and 2 μ L H₂O were added to make 65 μ L of reaction solution in each tube. These reactions were incubated for 3 hours at 37 °C (for the digestion reaction) and then 20 minutes at 80 °C (to denature the BamH1 endonuclease). A 1% agarose gel was performed on the sample immediately after completion of the digestion. (A 6.5 μ L aliquot of dye was used for each 65 μ L reaction for loading.) One band was present on the gel after the BamH1 digestion of BioH DNA between 500 bp and 1000 bp. Three bands were present on the gel after the BamH1 digestion of pET22b. The gel could have been overloaded and that could be the reason three bands were observed (instead of two). However, to be safe, the middle band that corresponded to the desired molecular weight (5462bp) was excised. Both the BioH and pET22b bands were excised and subjected to DNA isolation and purification by using the QIAquick® Gel Extraction Protocol.

The HindIII enzymatic digestion was performed by adding the following to each reaction tube (one tube for the BamH1-digested BioH DNA and the other tube for the BamH1-digested pET22b vector DNA): 48 μL of PCR product (the respective DNAs), 6.5 μL of 10X HindIII buffer, 6.5 μL of 10X BSA, 2 μL of HindIII restriction enzyme, and 2 μL H₂O to make 65 μL of reaction solution in each tube. A 1% agarose gel containing 0.01% ethidium bromide was performed on the sample immediately after completion of the digestion. (A 6.5- μL aliquot of dye was used for each 65 μL reaction for loading.) Bands corresponding to each of the DNAs were visualized and excised from the gel. DNA was isolated and purified using the QIAquick® Gel Extraction Protocol.

Ligation of BioH DNA into pET22b vector.

The following reactants were added to a 500- μL eppendorf tube to make 25 μL of reaction solution: 6 μL BioH linear insert, 9 μL pET22b linear vector, 2.5 μL T4 ligase buffer, 2.5 μL of 10 mM ATP solution (10X), 1 μL T4 DNA ligase, and 4 μL H₂O. The reaction tube was placed on ice and allowed to react overnight. An attempt to visualize the DNA by electrophoresis using a 1% agarose gel was performed; however, it was postulated the concentration of DNA (2 μL DNA and 2 μL dye) was too low in order to observe DNA. The

transformation was performed in spite of the fact DNA was not visualized on the agarose gel.

For the isolation of BioH-pET22b plasmid DNA, nine 15-mL Falcon tubes contained 2 mL of LB/carbenicillin solution (100 mg of carbenicillin per liter). A pipette tip with no colony on it was added to the control tube, and pipette tips with colonies on them were added to each of two experimental tubes. Cells were grown at 37 °C overnight with shaking and then harvested by centrifugation at 9000 RPM in a table-top microcentrifuge for 3 minutes at room temperature. No growth was observed in the control sample.

The QIAprep® Spin Miniprep Kit was used to lyse the cells and isolate plasmid DNA. The BioH gene contains an NcoI restriction endonuclease cut site within it while the pET22b vector does not. To ensure the gene was present in the vector, 10- μ L aliquots of DNA from each colony, 1 μ L of NcoI enzyme, 2 μ L of Buffer 3, and 7 μ L H₂O were incubated together at 37 °C for 1 hour.

After an hour had elapsed, plasmid DNA from all nine colonies was immediately visualized on a 1% agarose gel containing 0.01% ethidium bromide. A 1- μ L aliquot of DNA (from colonies 4 and 9) in addition to 0.5 μ L T7 primer and 11 μ L H₂O was submitted for DNA sequencing because these showed

evidence of cleavage. The remainder of BioH-pET22b plasmid DNA was stored in the -20 °C freezer for later use.

Sequences were analyzed via BLAST and Clustal X for homology to the published literature sequence. Colony 4 yielded 97% homology and 9 yielded 99% homology; thus, plasmid DNA from 9 was used to overexpress BioH in BL-21 cells from this point onward.

5.3.1.2 DNA transformation methods for all vectors containing carboxyesterase or lipase into XL-10, BL-21, and/or Origami(DE3) cells.

For vectors containing DNA sequences for AES, BioH, or ROL proteins, the protocol for all transformations was adapted from Hanahan, et al.²¹⁹ For the purpose of DNA amplification, all DNA vectors were transformed into XL-10 cells. For the purpose of protein overexpression, AES^{185, 220} and BioH^{188, 221} vectors were transformed into BL-21 cells, but the ROL vector was transformed into Origami(DE3) cells.¹⁸⁹ SOB-Mg growth medium (50 mL) was made using the following ingredients: 1g bacto-tryptone, 0.25g bacto-yeast extract, 10 mM NaCl, and 2.5 mM KCl. SOB-Mg was then autoclaved for 1 hour and sterile-filtered. To make SOC broth, 0.5 mL 2 M MgCl₂ and MgSO₄ solution and 0.5 mL 2 M glucose solution were added to the SOB-Mg solution. For transformation, SOC

broth was heated to 42 °C. XL-10 (~150 µL) and BL-21 (~150 µL) cells were thawed on ice for 15 minutes.

β-Mercaptoethanol solution (4 µL) was added to each of the experimental (100 µL) and control (~50 µL) samples for XL-10 transformations only. The samples were vortexed gently and then incubated on ice for 10 minutes, vortexing gently every 2 minutes. One aliquot (2 µL) of the donated DNA vector in TE buffer or from a previously performed transformation/purification was added to 100 µL of XL-10, BL-21, or Origami(DE3) cells. One aliquot of Buffer EB (2 µL) was added to the control sample (~50 µL) of cells. These samples were first vortexed gently to mix and incubated on ice for 30 minutes. The samples were then heat-pulsed in a 42 °C water bath for 30 seconds and immediately incubated on ice for 2 minutes. Each sample was added to 900 µL of preheated SOC broth in 15-mL Falcon culture tubes and incubated at 37 °C for 45-60 minutes with shaking. A 50- to 200-µL aliquot of each sample was plated on LB/ampicilin agar plates (100 mg/L amp) except when working with the ROL vector in Origami(DE3) cells, which was plated on LB/amp/tet/kan agar plates (100 mg/L amp, 10 mg/L tet, 30 mg/L kan). All plates were inverted and allowed to grow overnight at 37 °C. No colonies observed on the control plates, but a

moderate lawn of colonies was observed on the experimental plate for each of the three vectors.

For the isolation of plasmid DNA, three 15-mL Falcon tubes contained 2 mL of LB/carbenicillin solution (100 mg of carbenicillin per liter). A pipette tip unexposed to bacteria was added to the control tube, and a pipette tip containing with a colony of bacteria was added to each of two experimental tubes. Cells were grown at 37 °C overnight with shaking and then harvested by centrifugation at 9000 RPM in a table-top microcentrifuge for 3 minutes at room temperature. The QIAprep® Spin Miniprep Kit was used to lyse the cells and isolate plasmid DNA. After elution of DNA, plasmid DNA was visualized on a 1% agarose gel containing 0.01% ethidium bromide. Plasmid DNA was then stored in the -20 °C freezer for later use.

5.3.1.3 AES protein overexpression and purification.

Notes: The AES gene was a generous gift from Dr. Kinga Gerber. The gene was ligated into a pQE31-lacIq vector (ampicillin-resistant) and cloned between BamHI and Sall sites. "ROL plasmid" refers to this ligated version of ROL gene and vector.

For overnight growth of cells, one colony from the BL-21 experimental plate on LB/amp was added to 50 mL of LB solution containing 50 µL of a 100 mg/mL carbenicillin solution. This growth was incubated overnight at 37 °C

with shaking. In the morning, 10 mL of this growth was added to a flask containing 1L of LB/carbenicillin media (100 mg carb per 1 liter of LB) and grown to an optical density ($\lambda = 600$ nm) of ~ 1.0 . The 1L growth was then induced overnight with 101 mg of IPTG at 25 °C with shaking. This procedure was adapted from Gerber and co-workers.¹⁸⁵

Cells were harvested via centrifugation at 5000 RPM, pelleted after centrifugation at 4000 RPM, and lysed via sonication. The lysate was centrifuged at 16000 RPM (X2), and the supernatant was applied to a column of charged Ni-IDA agarose resin (Novagen®). Standard buffers were used for Ni²⁺-column purification and elution with the exception of wash buffer, in which half the normal concentration was used (250 mM NaCl, 30 mM imidazole, 10 mM Tris-HCl, pH 7.9). Purified protein was dialyzed into binding buffer without imidazole (500 mM NaCl, 20 mM Tris-HCl, pH 7.9). In addition, purified protein could be dialyzed into $\frac{1}{8}$ X binding buffer as well.

The concentration of overexpressed protein was determined in Edelhoch buffer (70 μ L protein solution in 630 μ L buffer) via absorbance at 280 nm subtracting background at 320 nm. Protein concentration was then calculated using the Beer-Lambert Law: $A = \epsilon lc$, where A represents the absorbance of

protein at 280 nm, ϵ represents the molar absorptivity (54570 M⁻¹cm⁻¹ for AES), and c represents the concentration of enzyme.

5.3.1.4 BioH protein overexpression and purification.

For overnight growth of cells, one colony from the BL-21 experimental plate was added to 50 mL of LB media containing 50 μ L of a 50 mg/mL carbenicillin solution. This growth was incubated overnight at 37 °C with shaking. In the morning, 10 mL of this growth was added to a flask containing 1L of LB/carbenicillin media (50 mg per 1 liter of LB) and grown to an optical density of 0.6. The 1 L growth was then induced overnight with 51 mg of IPTG at 25 °C with shaking. This procedure was adapted from previous literature.^{188, 222} Cells were harvested via centrifugation at 5000RPM, pelleted after centrifugation at 4000RPM, and lysed via sonication.

The lysate was centrifuged at 16000RPM (X2), and the supernatant was applied to a column of charged Ni-IDA agarose resin (Novagen®). Standard buffers were used for Ni²⁺-column purification and elution with the exception of wash buffer, in which half the normal concentration was used (250 mM NaCl, 30 mM imidazole, 10 mM Tris-HCl, pH 7.9). Purified protein was dialyzed into binding buffer without imidazole (500 mM NaCl, 20 mM Tris-HCl, pH 7.9). The protein precipitated out of solution when dialyzed into 1/8X binding buffer.

Concentration of protein was determined in Edelhoch buffer (70 μ L protein solution in 630 μ L buffer) via absorbance at 280 nm subtracting background at 320 nm. Protein concentration was then calculated using the Beer-Lambert Law: $A = \epsilon lc$, where A represents the absorbance of protein at 280 nm, ϵ represents the molar absorptivity (48533 $M^{-1}cm^{-1}$ for BioH), and c represents the concentration of enzyme.

5.3.1.5 ROL protein overexpression and purification.

Notes: The ROL gene was a generous gift from Drs. Uwe T. Bornscheuer and Michael Haas in a pET-11d vector (ampicilin-resistant) containing a C-terminal His₆-tag. "ROL plasmid" refers to this ligated version of ROL gene and vector.

For overnight growth of cells, one colony from the experimental plate was added to 50 mL of LB solution containing amp/tet/kan antibiotic solution (100 mg/L amp, 10 mg/L tet, 30 mg/L kan). This growth was incubated overnight at 37 °C with shaking. In the morning, 15 mL of this growth was added to a flask containing 1.5 L of LB/amp/tet/kan media and grown to an optical density ($\lambda = 600$ nm) of ~0.5, which took ~9-10 hours at 23 °C with shaking. The 1.5 L growth was then induced overnight with 39 mg of IPTG at 23 °C with shaking. This procedure was adapted from DiLorenzo and co-workers.¹⁸⁹ Cells were harvested via centrifugation at 5000 RPM, pelleted after centrifugation at 5000 RPM, and

lysed via sonication (4X: 30% amplitude, 1 minute, 10 seconds pulse on, 5 seconds pulse off). The lysate was centrifuged at 16000RPM (X2), and the supernatant was applied to a column of charged Ni-IDA agarose resin (Novagen®). Standard buffers were used for Ni²⁺-column purification and elution with the exception of wash buffer, in which half the normal concentration was used (250 mM NaCl, 30 mM imidazole, 10 mM Tris-HCl, pH 7.9). Purified protein was dialyzed into binding buffer without imidazole (500 mM NaCl, 20 mM Tris-HCl, pH 7.0). The protein precipitated out of solution when dialyzed into 1/8X binding buffer.

Concentration of protein was determined in Edelhoch buffer (70 μ L protein solution in 630 μ L buffer) via absorbance at 280 nm subtracting background at 320 nm. Protein concentration was then calculated using the Beer-Lambert Law: $A = \epsilon lc$, where A represents the absorbance of protein at 280 nm, ϵ represents the molar absorptivity (43110 M⁻¹cm⁻¹ for ROL), and c represents the concentration of enzyme.

5.3.2 Synthesis of fluorinated benzylic esters for use with esterases and lipases for biocatalytic- μ CP.

Synthesis of 11-(10-Carboxy-decyldisulfanyl)-undecanoic acid (11) from 11-mercaptoundecanoic acid (10).²²³

Sodium hydroxide (500 mg, 12.5 mmol) was added to a solution of **10** (200 mg, 0.92 mmol) in H₂O (100 mL). A 3% hydrogen peroxide solution (2 mL) was then added to a well-stirred resulting mixture. After being stirred for 30 minutes, concentrated HCl (2 mL) was added, and the reaction was extracted with EtOAc (2X55 mL). The organic layers were dried over MgSO₄ and concentrated in vacuo, yielding 218 mg (55%) of **11** as a white solid. ¹H NMR (DMSO) δ 11.94 (broad s, 2H), 2.70-2.66 (t, $J = 5.4$, 4H), 2.20-2.16 (t, $J = 5.4$, 4H), 1.64-1.57 (m, $J = 5.4$, 4H), 1.49-1.46 (t, $J = 5.1$, 4H), 1.35-1.20 (m, 24H); ¹³C NMR (DMSO) δ 175.1, 38.6, 34.3, 29.5, 29.4, 29.2, 28.4, 25.1; IR (cm⁻¹) 3671, 2979, 2912, 1693, 1405, 1231, 1060, 893; MS-ESI 434.25 (calc.), 457.24 (found MNa⁺), 473.79 (found MK⁺), 433.0 (found M⁻).

Synthesis of 11-[10-(4-Fluoro-benzyloxycarbonyl)-decyldisulfanyl]-undecanoic acid 4-fluoromethyl-benzyl ester (12) from 11-(10-Carboxy-decyldisulfanyl)-undecanoic acid (11).²²⁴

Compound **11** (100 mg, 0.230 mmol) was added to a solution of K₂CO₃ (79 mg, 0.5751 mmol) and p-fluorobenzyl bromide (71 μ L, 0.5751 mmol) in DMF (3 mL). The reaction was stirred at room temperature for 36 hours and

concentrated in vacuo to yield 98 mg (65%) of **12** as a white solid. TLC (EtOAc) R_f 0.7; ^1H NMR (CDCl_3) δ 7.35-7.31 (t, $J = 7.2$, 4H), 7.07-7.01 (t, $J = 8.7$, 4H), 5.07 (s, 4H), 2.70-2.65 (t, $J = 7.5$, 4H), 2.36-2.31 (t, $J = 7.8$, 4H), 1.69-1.60 (m, 8H), 1.37-1.26 (m, 24H); ^{13}C NMR (CDCl_3) δ 173.8, 132.5, 130.4, 130.3, 115.8, 115.5, 65.5, 39.4, 34.5, 29.6, 29.4, 29.3, 28.7, 25.1; ^{19}F NMR (CDCl_3) δ -114.2; MS-ESI 650.33 (calc.), 673.3 (found MNa^+), 689.2 (found MK^+).

Synthesis of 11-[10-(4-Trifluoromethyl-benzyloxycarbonyl)-decyldisulfanyl]-undecanoic acid 4-trifluoromethyl-benzyl ester (13) from 11-(10-Carboxydecyldisulfanyl)-undecanoic acid (11). ²²⁴

Compound **11** (400 mg, 0.920 mmol) was added to 40 mL of DMF. After dissolution, K_2CO_3 (382 mg, 2.761 mmol) was added. The mixture was stirred for 10 minutes and then 4-(trifluoromethyl)benzyl bromide (427 μL , 2.761 mmol) was also added. The reaction was stirred at room temperature for 48 hours and concentrated in vacuo and purified via flash column chromatography to yield 387 mg (60%) of **13** as a white solid. TLC (1:20 EtOAc:Hex) R_f 0.1; ^1H NMR (CDCl_3) δ 7.64-7.61 (d, $J = 8.1$, 4H), 7.48-7.45 (m, 4H), 5.16 (s, 4H), 2.70-2.65 (t, $J = 7.5$, 4H), 2.40-2.35 (t, $J = 7.5$, 4H), 1.69-1.64 (m, 8H), 1.39-1.23 (m, 24H); ^{13}C NMR (CDCl_3) δ 173.7, 140.4, 128.3, 125.7, 65.2, 39.3, 34.4, 29.6-29.3, 28.7, 25.1; MS-ESI 750.32 (calc.), 773.2 (found MNa^+), 789.2 (found MK^+), 750.3 (found M^-).

Synthesis of 4-(trifluoromethyl)benzyl 11-mercaptoundecanoate (14) from 11-[10-(4-trifluoromethyl-benzyloxycarbonyl)-decylsulfanyl]-undecanoic acid 4-trifluoromethyl-benzyl ester (13).

Dithiothreitol (904 mg, 5.86 mmol) was added to a solution of compound **13** (880 mg, 1.172 mmol) in 5 mL of methanol at 40 °C. The reaction was stirred overnight (17 hours). The reaction was concentrated in vacuo and purified via flash column chromatography to yield 196 mg (30%) of **14** as a colorless oil. TLC (1:1 CH₂Cl₂:hexanes) *R_f* 0.4; ¹H NMR (CDCl₃) δ 7.64-7.61 (d, *J* = 8.1, 2H), 7.48-7.45 (d, 2H), 5.16 (s, 2H), 2.56-2.48 (dd, *J* = 7.5, 2H), 2.40-2.35 (t, *J* = 7.5, 2H), 1.65-1.58 (m, 4H), 1.35-1.27 (m, 12H); ¹³C NMR (CDCl₃) δ 173.4, 140.1, 128.1, 125.5, 65.0, 34.2, 34.0, 29.4-29.0, 28.3, 24.9, 24.6; MS-ESI 376.48 (calc.), 399.3 (found MNa⁺).

Synthesis of bis(4-fluorobenzyl) 4,4'-disulfanediyldipropoate (16) from 4,4'-dithiobutyric acid (15).²²⁴

Compound **15** (113 mg, 0.4742 mmol) was added to a solution of K₂CO₃ (164 mg, 1.185 mmol) and p-fluorobenzyl bromide (139 μL, 1.185 mmol) in DMF (4 mL). The reaction was stirred at room temperature for 24 hours and concentrated in vacuo and purified via flash column chromatography to yield 140 mg (65%) of **16** as a clear oil. TLC (10:1 Hex:EtOAc) *R_f* 0.4; ¹H NMR (CDCl₃) δ 7.35-7.30 (t, *J* = 3.6, 4H), 7.08-7.01 (t, *J* = 8.7, 4H), 5.08 (s, 4H), 2.71-2.66 (t, *J* = 6.9, 4H), 2.49-2.45 (t, *J* = 7.2, 4H), 2.07-1.87 (m, 4H); ¹³C NMR (CDCl₃) δ 172.9, 164.5,

161.2, 130.5, 115.8, 65.8, 37.9, 32.8, 24.3; MS-ESI 454.11 (calc.), 454.11 (found MH⁺), 477.1 (found MNa⁺), 493.0 (found MK⁺).

Synthesis of bis(4-trifluoromethylbenzyl) 4,4'-disulfanedioldipropionate (17) from 4,4'-dithiobutyric acid (15). ²²⁴

Compound 15 (412 mg, 1.729 mmol) was added to 40 mL of DMF. After dissolution, K₂CO₃ (718 mg, 5.186 mmol) was added to the mixture and let stir for 10 minutes before adding p-trifluoromethylbenzyl bromide (802 μL, 5.186 mmol). The reaction was stirred for 48 hours at room temperature and then concentrated in vacuo and purified via flash column chromatography yielding 410 mg (43%) of **17** as a clear oil. TLC (1:1 EtOAc:Hex) R_f 0.4; ¹H NMR (CDCl₃) δ 7.63-7.61 (d, J = 8.1, 4H), 7.47-7.45 (d, J = 8.1, 4H), 5.17 (s, 4H), 2.73-2.69 (t, J = 7.2, 4H), 2.54-2.50 (t, J = 7.2, 4H), 2.10-2.00 (m, J = 7.2, 4H); ¹³C NMR (CDCl₃) δ 172.7, 140.1, 128.3, 125.7, 65.5, 37.8, 32.6, 24.3; MS-ESI 554.57 (calc.), 577.2 (found MNa⁺), 552.8 (found M).

Synthesis of 4-(trifluoromethyl)benzyl 4-mercaptobutanoate (18) from 11-[10-(4-trifluoromethyl-benzyloxycarbonyl)-decylsulfanyl]-undecanoic acid 4-trifluoromethyl-benzyl ester (13).

Dithiothreitol (1.391g, 9.02 mmol) was added to a solution of compound **13** (1.00g, 1.80 mmol) in 50 mL of methanol at 40 °C. The reaction was stirred overnight (17 hours). The reaction was concentrated in vacuo and purified via

flash column chromatography to yield 195 mg (39%) of **14** as a colorless oil. TLC (7:3 CH₂Cl₂:hexanes) *R_f* 0.3; ¹H NMR (CDCl₃) δ 7.64-7.62(d, *J* = 8.1, 2H), 7.48-7.46 (d, *J* = 8.1, 2H), 5.17 (s, 2H), 2.62-2.52 (m, 4H), 2.00-1.93 (m, 2H), 1.33 (t, *J* = 7.2, 1H); ¹³C NMR (CDCl₃) δ 172.6, 139.8, 128.1, 125.5, 65.3, 32.5, 28.8, 23.9.

Synthesis of 11,11'-Disulfanediylbis(undecan-1-ol) from 11-mercapto-1-undecanol **19.**²²⁵

A solution of 11-mercapto-1-undecanol **19** (0.544g, 2.662 mmol) in methanol (8 mL) was titrated by 1 M I₂/MeOH solution until the solution turned light yellow and stayed that color for more than 15 minutes. The reaction was then quenched with NaHSO₃ and put in an ice bath (0 °C) to aid in precipitation of **20**. The reaction was filtered to remove MeOH; the remaining solid was resuspended in EtOH with some heating. Solid that did not dissolve was filtered out and the remaining solution was left to crystallize overnight 4 °C. Lyophilization provided 495 mg (46%) of **20** as a white solid. TLC (3:7 EtOAc:hexanes) *R_f* <0.1; ¹H NMR (CDCl₃) δ 3.72-3.66 (dd, *J* = 7.2, 4H), 3.62-3.59 (t, *J* = 6.6, 4H), 2.68-2.64 (t, *J* = 7.4, 4H), 1.78 (broad s, 2H), 1.68-1.61 (dt, *J* = 7.2, 4H), 1.57-1.50 (dt, *J* = 6.8, 4H), 1.37-1.18 (m, 24H); ¹³C NMR (CDCl₃) δ 61.3, 38.8, 32.8, 30.5, 28.2-26.9; MS-ESI 406.73 (calc.), 407.3 (found MH⁺), 429.3 (found MNa⁺).

Synthesis of disulfanediylbis(undecane-11,1-diyl) bis(2-(4-(trifluoromethyl)phenyl)acetate) 21 from 11,11'-disulfanediylbis(undecan-1-ol) 20.

In order, DMAP (241 mg, 1.976 mmol), 4-(trifluoromethyl)phenylacetic acid (403 mg, 1.976 mmol), and EDC-HCl (474 mg, 2.471 mmol) were added to a solution of disulfide **20** in dry CH₂Cl₂ and stirred for 20 hours at room temperature. When the reaction had ceased, it was diluted with 100 mL anhydrous ether and washed with 1 M NaHCO₃, water, and brine each one time. The organic layer was separated and dried with MgSO₄ overnight. The MgSO₄ was filtered out and the remaining solution was concentrated in vacuo and purified via flash column chromatography to yield 305 mg (20%) of **14** as a colorless oil. TLC (1:8 EtOAc:hexanes) *R_f* 0.5; ¹H NMR (CDCl₃) δ 7.47-7.45 (d, *J* = 7.6, 4H), 7.30-7.28 (d, *J* = 7.6, 4H), 4.07-3.97 (m, 4H), 3.56 (s, 4H), 1.59-1.51 (m, 4H), 1.28-1.10 (m, 32H); ¹³C NMR (CDCl₃) δ 170.9, 138.3, 129.8, 129.6, 129.3, 125.7-125.5, 122.9, 65.4, 61.2, 41.2, 39.2, 29.6, 29.3, 28.6, 25.9, 14.2; MS-ESI 778.99 (calc.), 801.5 (found MNa⁺), 817.3 (found MK⁺).

Synthesis of 11-mercaptoundecyl 2-(4-(trifluoromethyl)phenyl)acetate 22 from disulfanediylbis(undecane-11,1-diyl) bis(2-(4-(trifluoromethyl)phenyl)acetate) 21.

Dithiothreitol (822 mg, 5.327 mmol) was added to a solution of compound **22** (1.00g, 1.80 mmol) in 90 mL of methanol at 40 °C. The reaction was stirred

overnight (18 hours). The reaction was concentrated in vacuo and purified via flash column chromatography to yield 87 mg (22%) of **22** as a colorless oil. TLC (1:1 CH₂Cl₂:hexanes) *R_f* 0.3; ¹H NMR (CDCl₃) δ 7.59-7.57(d, *J* = 8.0, 2H), 7.41-7.39 (d, *J* = 8.0, 2H), 4.11-4.07 (t, *J* = 6.8, 2H) 3.67 (s, 2H), 2.54-2.49 (dd, *J* = 7.2, 2H), 1.64-1.56 (m, 5H), 1.39-1.20 (m, 14H); ¹³C NMR (CDCl₃) δ 170.1, 139.2, 129.6, 129.3, 129.1, 125.8-125.6, 123.1, 66.4, 62.2, 40.8, 38.9, 29.3, 29.1, 27.9, 25.8, 14.1.

5.3.3 Activity assays of fluorinated benzylic esters in solution and as gold SAMs with esterases and lipases.

For each experiment, the enzyme used was less than 1 day old after dialysis and concentration. The pH meter used in all experiments was calibrated before each timed reaction. For all enzymatic reactions monitored in solution via pH change, the total reaction volume was 2.00 mL (microcentrifuge tube). The described conditions are those that were the most successful in obtaining data for all substrates.

All reactions were run in binding buffer without imidazole added (BB-i). However, 1XBB-i was too concentrated for monitoring pH. A more dilute concentration of BB-i, 1/8X BB-i (pH 7.0 unless otherwise noted to be pH 5.5-9.0), was therefore used in experiments to obtain pH data unless otherwise noted.

Substrates used in experiments were pNPA, pFPA, pNPB, **12, 13, 14, 16, 17, and 18**. For each experimental trial involving these substrates, a stock solution of 100 mM in ethanol was diluted to a final substrate concentration of 1 mM in the reaction (aqueous). In short, 0.020 mL of 100 mM substrate was used in all pH-monitored reactions for AES, BioH, and ROL.

AES, BioH, and ROL enzymes were also dialyzed into 1X BB-i, pH 7.0. Enzyme concentration was determined via the Beer-Lambert law. Enzyme was then diluted for the solution-phase reaction to produce a final concentration of 10 μ M and 25 μ M for surface reactions.

To obtain pH data, a reaction time of "0 Minutes" corresponded to the pH of the enzyme diluted into $\frac{1}{8}$ X BB-i. After the addition of substrate which commenced the reaction, the microcentrifuge tube was inverted 3-5 times and placed back under the pH meter. Timepoints were then taken at 0, 0.5, 1, 2, 3, 4, 5, and 10 minutes and then every 5 minutes thereafter for at least 15 minutes. Inversion of the reaction occurred after every timepoint to ensure the solution was mixed. The pH change recorded was the difference between the pH at 0 minutes and the pH at the end of the reaction. Once the pH values remained the same for several readings, it was assumed the reaction had gone to completion.

Gold substrates were incubated with a 0.22-um filtered 1 mM solution of disulfide or thiol for approximately 2 hours at room temperature. Substrates were then removed from this solution and immediately washed with water and ethanol, and dried with N₂ or argon. Two tweezers were used to minimize the effects of the environment and wet samples were not placed on lens paper until fully dry. Surfaces were stored in dust-free glass scintillation vials sealed with parafilm until analysis via XPS. Each scan was completed 5-7 times to minimize the signal-to-noise ratio.

For reaction with enzyme solutions, ester-functionalized surfaces were incubated in 25 μM solutions of BioH or ROL in filtered 1/8X BB-I for 3-4 hours at 4 °C. Surfaces were then sonicated for 10-15 minutes in filtered 1% SDS solution, rinsed with water and ethanol, and dried with filtered air. Surfaces were stored in dust-free glass scintillation vials sealed with parafilm until analyzed.

5.4 Catalytic microcontact printing.

5.4.1. General methods for catalytic-μCP.

All reagents and solvents were purchased from Sigma-Aldrich or TCI America and used as supplied unless otherwise noted. XPS spectra were recorded on a Kratos Axis Ultra XPS spectrometer using the mono-Al X-ray

source. Si/SiO₂ masters containing 8.5 μm features were fabricated by Alexander Shestopalov and graciously donated to this project.

SEM images were recorded on an FEI XL30 SEM-FEG microscope detecting secondary electrons at a 6 cm working distance. For SEM imaging purposes, PU stamps were coated with a 10-12 nm layer of gold using an electron-beam metal evaporator (CHA Industries) (SEM accelerating voltage 10-20 kV with a size 3 spot size). Silicon/PMMA masters and silicon surfaces containing SAMs were imaged without modification after washing (accelerating voltage 25 kV for masters and 2 kV for SAMs with a size 3 spot size).

5.4.2. Silicon-PMMA master fabrication for small features ≤500 nm.

The Si/PMMA master containing a pattern of 146.24 μm lines with varying widths of 130-500 nm was prepared using electron-beam lithography (EBL). 950 PMMA C2 (Microchem) was spin-cast on a clean silicon chip (2 cm x 2 cm) at 500 RPM for 5 seconds and 3000 RPM for 40 seconds. The resulting substrate was baked at 180 °C for 140 seconds to produce a Si-PMMA chip with a 135-nm layer of polymerized PMMA. Once cool, the substrate was patterned using EBL with the Elionix EBeam Lithography System equipped with WecaS CAD for pattern generation (resolution down to 10 nm) with the following conditions:

Field size: 300 μm

Number of dots: 60,000

Beam Current: 50 pA

Dose value: 250 $\mu\text{C}/\text{cm}^2$

Dosage dwell time: 1.75 ms

Accelerating voltage: 50 kV

After e-beam exposure, the patterned photoresist substrate was developed in a 1:3 mixture of methyl isobutyl ketone (MIBK) to isopropyl alcohol (IPA) for 140 seconds. Development was then quenched by incubating in IPA for 20 seconds followed by washing with filtered deionized water for 20 seconds. The resulting substrate was dried under N_2 and subsequently used as a mask for the formation of PU-based stamps.

5.4.2 Materials for polyurethane acrylate (PU) stamps.

5.4.2.1 Synthesis of PU pre-polymer.²²⁶

A solution of isophorone diisocyanate **10** (41.89 mL, 200 mmol), tin octoate (0.064 mL), and 2,2'-methylene-bis(4,6-di-*tert*-butylphenol) (0.09 g) was heated to 50 °C and held between this temperature and 55 °C. Polyethyleneglycol **11** (avg. mw = 400 g/mol, 35.46 mL, 100 mmol) was slowly added dropwise at 50 °C to this solution and stirred in the dark following addition of **11** for 3 hours at 55 °C resulting in the formation of intermediate **12**.

The reaction temperature was then increased to 70 °C and hydroxypropyl acrylate **13** (mixture of isomers, 25.55 mL, 205 mmol) was added dropwise, carefully maintaining the temperature between 70 – 75 °C. The final reaction mixture was stirred for 4 hours at 70 – 75 °C to produce diacrylate **14**. This acrylate was then diluted by 30% with trimethylolpropane ethoxylate triacrylate **15** (avg. mw = 912 g/mol) in order to reduce viscosity. Photoinitiators 2-hydroxy-2-methyl-propiofenone **16** (97%) and 1-hydroxycyclohexylphenylketone **17** (99%) were thoroughly mixed into this solution. Solutions of the pre-polymeric mixture were stored in the dark at 4 °C until used for stamp polymerization.

5.4.2.2 Fabrication for acid-immobilized stamps from PU pre-polymer.

When creating acidic stamps, each stamp was fabricated using 0.6091 mmol per mL PU (1.2182 mmoles for 2 mL of PU prepolymer). Acids used in stamps were: 2-mercapto-ethanesulfonic acid (200 mg sodium-2-mercaptoethene sulfonate - see below for acidification conditions), 4-vinylbenzoic acid (180 mg), 2-propene-1-phosphonic acid (132 mg, 93 µL), and acrylic acid (88 mg, 84 µL).

For sulfonic acid stamps, 200 mg sodium-2-mercaptoethene sulfonate was added to 5 mL of dioxane:HCl and stirred for 10-15 minutes at room temperature to acidify the compound forming 2-mercapto-ethansulfonic acid. The solution was filtered through a glass filter, a PTFE filter, and concentrated

under reduced pressure. PU (2 mL) was added immediately and directly to this container once sufficiently concentrated. The solution was heated slightly and degassed under vacuum before polymerization into stamps.

Stamps containing micron- and nanofeatures were fabricated by polymerizing the desired PU/acid mixture between the corresponding Si/PMMA or Si/SiO₂ master and a parafilm-covered glass slide. In lieu of a master, flat stamps were polymerized using clean, flat silicon surfaces. Stamps were allowed to polymerize under UV light for 2-3 hours, removed and placed on the benchtop under ambient light for 16-20 hours, and removed from stamps using gentle heat and force. Stamps were cut so that patterns could easily be transferred or, in the case of flat stamps, ~ 1 cm x 1 cm. Stamps were washed thoroughly with filtered water and ethanol, dried with argon, and kept covered until use. The shape and size of the stamp features were identical to those on the corresponding masters and remained unaffected by storage for several weeks.

5.4.3 Formation of NHS-functionalized SAMs on silicon <111> surfaces.

Silicon <111> surfaces were scored and cut with minimal handling. Surfaces were incubated in Nanostrip solution (Cyantek: 90% SO₄H₂, 5% SO₅H₂, 5% H₂O, <1% H₂O₂) for 10-15 minutes at 75 °C before washing with water and incubating in a 5% aqueous HF solution for 5 minutes. H-Si surfaces were dried

with argon and placed directly into scintillation vials containing a filtered solution of saturated PCl_5 in chlorobenzene with a small amount of benzoyl peroxide (0.1% m/v), flushed with argon, and placed in a heat block at 110-115 °C for 1 hour. The chlorinated surfaces were then removed from vials, rinsed with chlorobenzene, dried with argon, and placed in solutions of 1-propylmagnesium bromide in THF (0.5 M). Vials containing the Grignard were tightly sealed and incubated in a heat block at 130-135 °C for 16-22 hours. Propylene-functionalized surfaces were removed from the Grignard solutions after cooling to ~ 90 °C, washed thoroughly with EtOH 2X, CH_2Cl_2 1X, and EtOH 1X before blowing dry with argon. Surfaces were dried additionally on a hot plate at 75 °C for 5 minutes and cooled to room temperature (5 minutes). Surfaces were covered with ~75 μL of a 0.1 M solution of 2,5-dioxopyrrolidin-1-yl 4-(3-(trifluoromethyl)-3H-diazirin-3-yl)phenyl ester in CCl_4 , synthesized either by Dr. Alexander Shestopalov or Carleen Morris, and reacted with UV light for 1 hour at room temperature. NHS-functionalized surfaces were then washed with CH_2Cl_2 2X and EtOH 1X, dried with a stream of argon, and used within one hour of fabrication.

5.4.4 Stamping protocol.

Once stamps and surfaces were both fabricated using the protocols described previously, stamps were placed on top of surfaces, pressed into conformal contact gently, and incubated for 3 minutes to 2 hours, as indicated in the text. Stamped substrates were washed with EtOH, dried with filtered argon, and placed in dust-free scintillation vials until same-day analysis by SEM or XPS. Stamps were rinsed with H₂O and EtOH thoroughly, dried with filtered argon, and kept covered at room temperature until needed again.

References

1. Jean-Marie Chauvet, E. B. D., Christian Hillaire, *Dawn of Art: The Chauvet Cave*. 1 ed.; Harry N. Abrams, Inc.: London, 1996; p 135.
2. Gaur, A., *A History of Writing*. 1st ed.; Charles Scribner's Sons: New York, 1985; p 224.
3. Noone, J.; McNair, D.; Grimes, Z.; Marchand, R.; Tucei, R.; Young, R.; Ducote, D., How the Bible was Written. In *To Tell You the Whole Truth About the Catholic Church and the Holy Bible*, St. Charles Borromeo Catholic Church: Picayune, MS, 2002.
4. Fischer, S. R., *A History of Writing*. 1st ed.; Reaktion Books Ltd: London, 2001.
5. Intaglio Printing. In *Encyclopaedia Britannica*, Encyclopaedia Britannica Online: Chicago, 2010; p 1.
6. Weber, W., *A History of Lithography*. 2nd ed.; McGraw-Hill Book Company: London, 1966; p 259.
7. Twyman, M., *The British Library Guide to Printing*. 1st ed.; University of Toronto Press: London, 1998; p 88.
8. Senefelder, A., *A Complete Course of Lithography*. 2nd ed.; Da Capo Press: New York, 1968; p 342.
9. Madou, M. J., *Fundamentals of Microfabrication: The Science of Miniaturization*. 2nd ed.; CRC Press LLC: Boca Raton, 2002; p 723.
10. Chris73 Wikipedia: Lithography negative stone and positive paper. (18 March 2010),

11. Pixel:-) Wikipedia: Integrated Circuit. (18 March 2010),
12. Hutcheson, G. D., The Economic Implications of Moore's Law. In *Into the Nano Era: Moore's Law Beyond Planar Silicon CMOS*, 1st ed.; Huff, H. R., Ed. Springer-Verlag: Berlin, 2009; pp 11-38.
13. Markoff, J., I.B.M. Researchers Find a Way To Keep Moore's Law on Pace. *The New York Times* February 20, 2006, p 4.
14. Barbulovic-Nad, I.; Lucente, M.; Sun, Y.; Zhang, M. J.; Wheeler, A. R.; Bussmann, M., Bio-microarray fabrication techniques - A review. *Crit Rev Biotechnol* **2006**, 26, (4), 237-259.
15. Morgan, T. P., IBM, AMD Expect 45-Nanometer Chips in Mid-2008. *IT Jungle* 12/12/2006, 2006, p 1.
16. Gates, B. D.; Xu, Q. B.; Stewart, M.; Ryan, D.; Willson, C. G.; Whitesides, G. M., New approaches to nanofabrication: Molding, printing, and other techniques. *Chem Rev* **2005**, 105, (4), 1171-1196.
17. Xia, Y. N.; Whitesides, G. M., Soft lithography. *Annual Review of Materials Science* **1998**, 28, 153-184.
18. Geissler, M.; Xia, Y. N., Patterning: Principles and some new developments. *Adv Mater* **2004**, 16, (15), 1249-1269.
19. Gooding, J. J.; Mearns, F.; Yang, W. R.; Liu, J. Q., Self-assembled monolayers into the 21(st) century: Recent advances and applications. *Electroanalysis* **2003**, 15, (2), 81-96.
20. Huck, W. T. S., Self-assembly meets nanofabrication: Recent developments in microcontact printing and dip-pen nanolithography. *Angew Chem Int Edit* **2007**, 46, (16), 2754-2757.

21. Kumar, A.; Biebuyck, H. A.; Whitesides, G. M., Patterning Self-Assembled Monolayers - Applications in Materials Science. *Langmuir* **1994**, 10, (5), 1498-1511.
22. Michel, B.; Bernard, A.; Bietsch, A.; Delamarche, E.; Geissler, M.; Juncker, D.; Kind, H.; Renault, H.; Rothuizen, H.; Schmid, H.; Schmidt-Winkel, P.; Stutz, R.; Wolf, H., Printing Meets Lithography: Soft Approaches to High Resolution Patterning. *Chimia* **2003**, 56, 527-542.
23. Quist, A. P.; Pavlovic, E.; Oscarsson, S., Recent advances in microcontact printing. *Analytical and Bioanalytical Chemistry* **2005**, 381, (3), 591-600.
24. Kumar, A.; Whitesides, G. M., Features of Gold Having Micrometer to Centimeter Dimensions Can Be Formed through a Combination of Stamping with an Elastomeric Stamp and an Alkanethiol Ink Followed by Chemical Etching. *Appl Phys Lett* **1993**, 63, (14), 2002-2004.
25. Xia, Y. N.; Whitesides, G. M., Soft lithography. *Angew Chem Int* **1998**, 37, (5), 551-575.
26. Kumar, A.; Whitesides, G. M., Patterning Self-Assembled Monolayers - Applications in Microelectronics and Biotechnology. *Abstr Pap Am Chem S* **1993**, 206, 172-COLL.
27. Li, X. M.; Huskens, J.; Reinhoudt, D. N., Reactive self-assembled monolayers on flat and nanoparticle surfaces, and their application in soft and scanning probe lithographic nanofabrication technologies. *Journal of Materials Chemistry* **2004**, 14, (20), 2954-2971.
28. Perl, A.; Reinhoudt, D. N.; Huskens, J., Microcontact Printing: Limitations and Achievements. *Adv Mater* **2009**, 21, (22), 2257-2268.
29. Gates, B. D., Nanofabrication with molds and stamps. *Materials Today* **2005**, 8, (2), 44-49.

30. Smith, R. K.; Lewis, P. A.; Weiss, P. S., Patterning self-assembled monolayers. *Progress in Surface Science* **2004**, 75, 1-68.
31. James, C. D.; Davis, R. C.; Kam, L.; Craighead, H. G.; Isaacson, M.; Turner, J. N.; Shain, W., Patterned protein layers on solid substrates by thin stamp microcontact printing. *Langmuir* **1998**, 14, (4), 741-744.
32. Coyer, S. R.; Garcia, A. J.; Delamarche, E., Facile preparation of complex protein architectures with sub-100-nm resolution on surfaces. *Angew Chem Int Edit* **2007**, 46, (36), 6837-6840.
33. Feng, C. L.; Vancso, G. J.; Schonherr, H., Fabrication of robust biomolecular patterns by reactive microcontact printing on N-hydroxysuccinimide ester-containing polymer films. *Adv Funct Mater* **2006**, 16, (10), 1306-1312.
34. Anderson, A. B.; Robertson, C. R., Absorption-Spectra Indicate Conformational Alteration of Myoglobin Adsorbed on Polydimethylsiloxane. *Biophys J* **1995**, 68, (5), 2091-2097.
35. Bernard, A.; Delamarche, E.; Schmid, H.; Michel, B.; Bosshard, H. R.; Biebuyck, H., Printing patterns of proteins. *Langmuir* **1998**, 14, (9), 2225-2229.
36. Biasco, A.; Pisignano, D.; Krebs, B.; Cingolani, R.; Rinaldi, R., Microcontact printing of metalloproteins. *Synthetic Met* **2005**, 153, (1-3), 21-24.
37. Biasco, A.; Pisignano, D.; Krebs, B.; Pompa, P. P.; Persano, L.; Cingolani, R.; Rinaldi, R., Conformation of microcontact-printed proteins by atomic force microscopy molecular sizing. *Langmuir* **2005**, 21, (11), 5154-5158.
38. Patel, N.; Bhandari, R.; Shakesheff, K. M.; Cannizzaro, S. M.; Davies, M. C.; Langer, R.; Roberts, C. J.; Tendler, S. J. B.; Williams, P. M., Printing patterns of biospecifically-adsorbed protein. *J Biomat Sci-Polym E* **2000**, 11, (3), 319-331.

39. Tan, J. L.; Tien, J.; Chen, C. S., Microcontact printing of proteins on mixed self-assembled monolayers. *Langmuir* **2002**, 18, (2), 519-523.
40. Yang, Z. P.; Chilkoti, A., Microstamping of a biological ligand onto an activated polymer surface. *Adv Mater* **2000**, 12, (6), 413-+.
41. Lange, S. A.; Benes, V.; Kern, D. P.; Horber, J. K. H.; Bernard, A., Microcontact printing of DNA molecules. *Anal Chem* **2004**, 76, (6), 1641-1647.
42. Thibault, C.; Le Berre, V.; Casimirius, S.; Trevisiol, E.; Francois, J.; Vieu, C., Direct microcontact printing of a oligonucleotides for biochip applications. *Journal of Nanobiotechnology* **2005**, 3.
43. Xu, H.; Ling, X. Y.; van Bennekom, J.; Duan, X.; Ludden, M. J. W.; Reinhoudt, D. N.; Wessling, M.; Lammertink, R. G. H.; Huskens, J., Microcontact Printing of Dendrimers, Proteins, and Nanoparticles by Porous Stamps. *J Am Chem Soc* **2009**, 131, (2), 797-803.
44. Xu, H. P.; Gomez-Casado, A.; Liu, Z. H.; Reinhoudt, D. N.; Lammertink, R. G. H.; Huskens, J., Porous Multilayer-Coated PDMS Stamps for Protein Printing. *Langmuir* **2009**, 25, (24), 13972-13977.
45. Godula, K.; Rabuka, D.; Nam, K. T.; Bertozzi, C. R., Synthesis and Microcontact Printing of Dual End-Functionalized Mucin-like Glycopolymers for Microarray Applications. *Angew Chem Int Edit* **2009**, 48, (27), 4973-4976.
46. Gross, G. W.; Rhoades, B. K.; Azzazy, H. M. E.; Wu, M. C., The Use of Neuronal Networks on Multielectrode Arrays as Biosensors. *Biosens Bioelectron* **1995**, 10, (6-7), 553-567.
47. Mrksich, M.; Whitesides, G. M., Patterning Self-Assembled Monolayers Using Microcontact Printing - a New Technology for Biosensors. *Trends Biotechnol* **1995**, 13, (6), 228-235.

48. Ruiz, A.; Ceriotti, L.; Buzanska, L.; Hasiwa, M.; Bretagnol, F.; Ceccone, G.; Gilliland, D.; Rauscher, H.; Coecke, S.; Colpo, P.; Rossi, F., Controlled micropatterning of biomolecules for cell culturing. *Microelectron Eng* **2007**, *84*, (5-8), 1733-1736.
49. Ruiz, S. A.; Chen, C. S., Microcontact printing: A tool to pattern. *Soft Matter* **2007**, *3*, (2), 168-177.
50. Mrksich, M., Using self-assembled monolayers to model the extracellular matrix. *Acta Biomater* **2009**, *5*, (3), 832-841.
51. Jung, D. R.; Kapur, R.; Adams, T.; Giuliano, K. A.; Mrksich, M.; Craighead, H. G.; Taylor, D. L., Topographical and physicochemical modification of material surface to enable patterning of living cells. *Crit Rev Biotechnol* **2001**, *21*, (2), 111-154.
52. They, M.; Pepin, A.; Dressaire, E.; Chen, Y.; Bornens, M., Cell distribution of stress fibres in response to the geometry of the adhesive environment. *Cell Motil Cytoskel* **2006**, *63*, (6), 341-355.
53. Xia, N.; Thodeti, C. K.; Hunt, T. P.; Xu, Q. B.; Ho, M.; Whitesides, G. M.; Westervelt, R.; Ingber, D. E., Directional control of cell motility through focal adhesion positioning and spatial control of Rac activation. *Faseb J* **2008**, *22*, (6), 1649-1659.
54. Gomez, N.; Lu, Y.; Chen, S. C.; Schmidt, C. E., Immobilized nerve growth factor and microtopography have distinct effects on polarization versus axon elongation in hippocampal cells in culture. *Biomaterials* **2007**, *28*, (2), 271-284.
55. Rogers, J. A.; Bao, Z.; Baldwin, K.; Dodabalapur, A.; Crone, B.; Raju, V. R.; Kuck, V.; Katz, H.; Amundson, K.; Ewing, J.; Drzaic, P., Paper-like electronic displays: Large-area rubber-stamped plastic sheets of electronics and microencapsulated electrophoretic inks. *P Natl Acad Sci USA* **2001**, *98*, (9), 4835-4840.

56. Li, D. W.; Guo, L. J., Organic thin film transistors and polymer light-emitting diodes patterned by polymer inking and stamping. *J Phys D Appl Phys* **2008**, *41*, (10), -.
57. Niggemann, M.; Zimmermann, B.; Haschke, J.; Glatthaar, M.; Gombert, A., Organic solar cell modules for specific applications - From energy autonomous systems to large area photovoltaics. *Thin Solid Films* **2008**, *516*, (20), 7181-7187.
58. Briseno, A. L.; Ling, M. M.; Roberts, M.; Moon, H.; Brehm, D.; Bao, Z. N., Patterning organic semiconductors for organic electronic applications. *Abstr Pap Am Chem S* **2005**, *229*, U1128-U1128.
59. Briseno, A. L.; Roberts, M.; Ling, M. M.; Moon, H.; Nemanick, E. J.; Bao, Z. N., Patterning organic semiconductors using "dry" poly(dimethylsiloxane) elastomeric stamps for thin film transistors. *J Am Chem Soc* **2006**, *128*, (12), 3880-3881.
60. Wilbur, J. L.; Kumar, A.; Kim, E.; Whitesides, G. M., Microfabrication by Microcontact Printing of Self-Assembled Monolayers. *Adv Mater* **1994**, *6*, (7-8), 600-604.
61. Wilbur, J. L.; Kumar, A.; Biebuyck, H. A.; Kim, E.; Whitesides, G. M., Microcontact printing of self-assembled monolayers: Applications in microfabrication. *Nanotechnology* **1996**, *7*, (4), 452-457.
62. Biebuyck, H. A.; Larsen, N. B.; Delamarche, E.; Michel, B., Lithography beyond light: Microcontact printing with monolayer resists. *Ibm J Res Dev* **1997**, *41*, (1-2), 159-170.
63. Kim, E.; Kumar, A.; Whitesides, G. M., Combining Patterned Self-Assembled Monolayers of Alkanethiolates on Gold with Anisotropic Etching of Silicon to Generate Controlled Surface Morphologies. *J Electrochem Soc* **1995**, *142*, (2), 628-633.

64. Kumar, A.; Abbott, N. L.; Kim, E.; Biebuyck, H. A.; Whitesides, G. M., Patterned Self-Assembled Monolayers and Mesoscale Phenomena. *Accounts Chem Res* **1995**, 28, (5), 219-226.
65. Geissler, M.; Wolf, H.; Stutz, R.; Delamarche, E.; Grummt, U. W.; Michel, B.; Bietsch, A., Fabrication of metal nanowires using microcontact printing. *Langmuir* **2003**, 19, (15), 6301-6311.
66. Love, J. C.; Wolfe, D. B.; Chabinyc, M. L.; Paul, K. E.; Whitesides, G. M., Self-assembled monolayers of alkanethiolates on palladium are good etch resists. *J Am Chem Soc* **2002**, 124, (8), 1576-1577.
67. Benor, A.; Hoppe, A.; Wagner, V.; Knipp, D., Microcontact printing and selective surface dewetting for large area electronic applications. *Thin Solid Films* **2007**, 515, (19), 7679-7682.
68. Benor, A.; Wagner, V.; Knipp, D., Microstructuring by microcontact printing and selective surface dewetting. *J Vac Sci Technol B* **2007**, 25, (4), 1321-1326.
69. Harriott, L. R. a. H., R., Nanolithography. In *Introduction to Nanoscale Science and Technology*, 1st ed.; Di Ventra, M. E., Stephane; Heflin, Jr., James R., Ed. Kluwer Academic Publications: Boston, 2004; pp 1-40.
70. Fujimaru, K. O., T.; Nagai, R.; Matsumura, H., Nanometer Pattern-Mask Fabricated by Conventional Photolithography. *Jpn. J. Appl. Phys.* **1997**, 36, 7786-7790.
71. McDonald, J. C.; Whitesides, G. M., Poly(dimethylsiloxane) as a material for fabricating microfluidic devices. *Accounts Chem Res* **2002**, 35, (7), 491-499.
72. Xia, Y. A.; Venkateswaran, N.; Qin, D.; Tien, J.; Whitesides, G. M., Use of electroless silver as the substrate in microcontact printing of alkanethiols and its application in microfabrication. *Langmuir* **1998**, 14, (2), 363-371.

73. Jongerius, M. J. Roller Micro-Contact Printer with Pressure Control. 2009.
74. Chaudhury, M. K.; Whitesides, G. M., Direct Measurement of Interfacial Interactions between Semispherical Lenses and Flat Sheets of Poly(Dimethylsiloxane) and Their Chemical Derivatives. *Langmuir* **1991**, 7, (5), 1013-1025.
75. Delamarche, E.; Schmid, H.; Bietsch, A.; Larsen, N. B.; Rothuizen, H.; Michel, B.; Biebuyck, H., Transport mechanisms of alkanethiols during microcontact printing on gold. *J Phys Chem B* **1998**, 102, (18), 3324-3334.
76. Delamarche, E.; Geissler, M.; Bernard, A.; Wolf, H.; Michel, B.; Hilborn, J.; Donzel, C., Hydrophilic poly (dimethylsiloxane) stamps for microcontact printing. *Adv Mater* **2001**, 13, (15), 1164-+.
77. Hu, S. W.; Ren, X. Q.; Bachman, M.; Sims, C. E.; Li, G. P.; Allbritton, N. L., Tailoring the surface properties of poly(dimethylsiloxane) microfluidic devices. *Langmuir* **2004**, 20, (13), 5569-5574.
78. Hu, S. W.; Ren, X. Q.; Bachman, M.; Sims, C. E.; Li, G. P.; Allbritton, N. L., Surface-directed, graft polymerization within microfluidic channels. *Anal Chem* **2004**, 76, (7), 1865-1870.
79. Ferguson, G. S.; Chaudhury, M. K.; Biebuyck, H. A.; Whitesides, G. M., Monolayers on Disordered Substrates - Self-Assembly of Alkyltrichlorosilanes on Surface-Modified Polyethylene and Poly(Dimethylsiloxane). *Macromolecules* **1993**, 26, (22), 5870-5875.
80. De Silva, M. N.; Desai, R.; Odde, D. J., Micro-patterning of animal cells on PDMS substrates in the presence of serum without use of adhesion inhibitors. *Biomed Microdevices* **2004**, 6, (3), 219-222.
81. Li, X. M.; Peter, M.; Huskens, J.; Reinhoudt, D. N., Catalytic microcontact printing without ink. *Nano Lett* **2003**, 3, (10), 1449-1453.

82. Love, J. C.; Estroff, L. A.; Kriebel, J. K.; Nuzzo, R. G.; Whitesides, G. M., Self-assembled monolayers of thiolates on metals as a form of nanotechnology. *Chem Rev* **2005**, 105, (4), 1103-1169.
83. Nuzzo, R. G.; Allara, D. L., Adsorption of Bifunctional Organic Disulfides on Gold Surfaces. *J Am Chem Soc* **1983**, 105, (13), 4481-4483.
84. Larsen, N. B.; Biebuyck, H.; Delamarche, E.; Michel, B., Order in microcontact printed self-assembled monolayers. *J Am Chem Soc* **1997**, 119, (13), 3017-3026.
85. Bain, C. D.; Biebuyck, H. A.; Whitesides, G. M., Comparison of Self-Assembled Monolayers on Gold - Coadsorption of Thiols and Disulfides. *Langmuir* **1989**, 5, (3), 723-727.
86. Wilhelm, T.; Wittstock, G., Generation of periodic enzyme patterns by soft lithography and activity imaging by scanning electrochemical microscopy. *Langmuir* **2002**, 18, (24), 9485-9493.
87. Xu, C.; Taylor, P.; Ersoz, M.; Fletcher, P. D. I.; Paunov, V. N., Microcontact printing of DNA-surfactant arrays on solid substrates. *Journal of Materials Chemistry* **2003**, 13, (12), 3044-3048.
88. Shestopalov, A. A.; Vogen, B. N.; Clark, R. L.; Toone, E. J., Catalytic patterning and functionalization of oxide-free silicon. **In preparation.**
89. Bernard, A.; Fitzli, D.; Sonderegger, P.; Delamarche, E.; Michel, B.; Bosshard, H. R.; Biebuyck, H., Affinity capture of proteins from solution and their dissociation by contact printing. *Nature Biotechnology* **2001**, 19, (9), 866-869.
90. Weibel, D. B.; Lee, A.; Mayer, M.; Brady, S. F.; Bruzewicz, D.; Yang, J.; DiLuzio, W. R.; Clardy, J.; Whitesides, G. M., Bacterial printing press that regenerates its ink: Contact-printing bacteria using hydrogel stamps. *Langmuir* **2005**, 21, (14), 6436-6442.

91. Herne, T. M.; Tarlov, M. J., Characterization of DNA probes immobilized on gold surfaces. *J Am Chem Soc* **1997**, 119, (38), 8916-8920.
92. Perl, A.; Peter, M.; Ravoo, B. J.; Reinhoudt, D. N.; Huskens, J., Heavyweight dendritic inks for positive microcontact printing. *Langmuir* **2006**, 22, (18), 7568-7573.
93. Trimbach, D. C.; Al-Hussein, M.; de Jeu, W. H.; Decre, M.; Broer, D. J.; Bastiaansen, C. W. M., Hydrophilic elastomers for microcontact printing of polar inks. *Langmuir* **2004**, 20, (11), 4738-4742.
94. Liebau, M.; Huskens, J.; Reinhoudt, D. N., Microcontact printing with heavyweight inks. *Adv Funct Mater* **2001**, 11, (2), 147-150.
95. Bass, R. B.; Lichtenberger, A. W., Microcontact printing with octadecanethiol. *Appl Surf Sci* **2004**, 226, (4), 335-340.
96. Saalmink, M.; van der Marel, C.; Stapert, H. R.; Burdinski, D., Positive microcontact printing with mercaptoalkyloligo(ethylene glycol)s. *Langmuir* **2006**, 22, (3), 1016-1026.
97. Libioulle, L.; Bietsch, A.; Schmid, H.; Michel, B.; Delamarche, E., Contact-inking stamps for microcontact printing of Alkanethiols on gold. *Langmuir* **1999**, 15, (2), 300-304.
98. Sharpe, R. B. A.; Burdinski, D.; Huskens, J.; Zandvliet, H. J. W.; Reinhoudt, D. N.; Poelsema, B., Spreading of 16-mercaptohexadecanoic acid in microcontact printing. *Langmuir* **2004**, 20, (20), 8646-8651.
99. Workman, R. K.; Manne, S., Molecular transfer and transport in noncovalent microcontact printing. *Langmuir* **2004**, 20, (3), 805-815.

100. Michel, B.; Bernard, A.; Bietsch, A.; Delamarche, E.; Geissler, M.; Juncker, D.; Kind, H.; Renault, J. P.; Rothuizen, H.; Schmid, H.; Schmidt-Winkel, P.; Stutz, R.; Wolf, H., Printing meets lithography: Soft approaches to high-resolution printing. *Ibm J Res Dev* **2001**, 45, (5), 697-719.
101. Delamarche, E.; Schmid, H.; Michel, B.; Biebuyck, H., Stability of molded polydimethylsiloxane microstructures. *Adv Mater* **1997**, 9, (9), 741-746.
102. Bietsch, A.; Michel, B., Conformal contact and pattern stability of stamps used for soft lithography. *J Appl Phys* **2000**, 88, (7), 4310-4318.
103. Hui, C. Y.; Jagota, A.; Lin, Y. Y.; Kramer, E. J., Constraints on microcontact printing imposed by stamp deformation. *Langmuir* **2002**, 18, (4), 1394-1407.
104. Sharp, K. G.; Blackman, G. S.; Glassmaker, N. J.; Jagota, A.; Hui, C. Y., Effect of stamp deformation on the quality of microcontact printing: Theory and experiment. *Langmuir* **2004**, 20, (15), 6430-6438.
105. Pagliara, S.; Persano, L.; Camposeo, A.; Cingolani, R.; Pisignano, D., Registration accuracy in multilevel soft lithography. *Nanotechnology* **2007**, 18, (17), -.
106. Wiggenius, J. A.; Hamed, M.; Inganäs, O., Limits to nanopatterning of fluids on surfaces in soft lithography. *Adv Funct Mater* **2008**, 18, (17), 2563-2571.
107. Xia, Y. N.; Whitesides, G. M., Soft lithography. *Angew Chem Int Edit* **1998**, 37, (5), 551-575.
108. Geissler, M.; Schmid, H.; Bietsch, A.; Michel, B.; Delamarche, E., Defect-tolerant and directional wet-etch systems for using monolayers as resists. *Langmuir* **2002**, 18, (6), 2374-2377.

109. Yoo, P. J.; Choi, S. J.; Kim, J. H.; Suh, D.; Baek, S. J.; Kim, T. W.; Lee, H. H., Unconventional patterning with a modulus-tunable mold: From imprinting to microcontact printing. *Chem Mater* **2004**, 16, (24), 5000-5005.
110. Gannon, G.; Larsson, J. A.; Greer, J. C.; Thompson, D., Quantification of Ink Diffusion in Microcontact Printing with Self-Assembled Monolayers. *Langmuir* **2009**, 25, (1), 242-247.
111. Schmid, H.; Michel, B., Siloxane polymers for high-resolution, high-accuracy soft lithography. *Macromolecules* **2000**, 33, (8), 3042-3049.
112. Xia, Y. N.; Whitesides, G. M., Extending microcontact printing as a microlithographic technique. *Langmuir* **1997**, 13, (7), 2059-2067.
113. Bohm, I.; Lampert, A.; Buck, M.; Eisert, F.; Grunze, M., A spectroscopic study of thiol layers prepared by contact printing. *Appl Surf Sci* **1999**, 141, (3-4), 237-243.
114. Graham, D. J.; Price, D. D.; Ratner, B. D., Solution assembled and microcontact printed monolayers of dodecanethiol on gold: A multivariate exploration of chemistry and contamination. *Langmuir* **2002**, 18, (5), 1518-1527.
115. Thibault, C.; Severac, C.; Mingotaud, A. F.; Vieu, C.; Mauzac, M., Poly(dimethylsiloxane) contamination in microcontact printing and its influence on patterning oligonucleotides. *Langmuir* **2007**, 23, (21), 10706-10714.
116. Okuda, S.; Kobiyama, M.; Inami, T.; Takamura, S., Thermal stability of nanocrystalline gold and copper prepared by gas deposition method. *Scripta Mater* **2001**, 44, (8-9), 2009-2012.
117. Puniredd, S. R.; Assad, O.; Haick, H., Highly stable organic monolayers for reacting silicon with further functionalities: The effect of the C-C bond nearest the silicon surface. *J Am Chem Soc* **2008**, 130, (41), 13727-13734.

118. Reddy, S.; Assad, P. O.; Haick, H., Highly stable organic modification of Si(111) surfaces: Towards reacting Si with further functionalities while preserving the desirable chemical properties of full Si-C atop site terminations. *J Am Chem Soc* **2008**, 130, (29), 9184-+.
119. Hamers, R. J., Formation and characterization of organic monolayers on semiconductor surfaces. *Annual Review of Analytical Chemistry* **2008**, 1, 707-736.
120. Shestopalov, A. A.; Clark, R. L.; Toone, E. J., Inkless Microcontact Printing on SAMs of Boc- and TBS-Protected Thiols. *Nano Lett* **2010**, 10, (1), 43-46.
121. Shestopalov, A. A.; Clark, R. L.; Toone, E. J., Catalytic Microcontact Printing on Chemically Functionalized H-Terminated Silicon. *Langmuir* **2010**, 26, (3), 1449-1451.
122. Liebau, M.; Janssen, H. M.; Inoue, K.; Shinkai, S.; Huskens, J.; Sijbesma, R. P.; Meijer, E. W.; Reinhoudt, D. N., Preparation of dendritic multisulfides and their assembly on air/water interfaces and gold surfaces. *Langmuir* **2002**, 18, (3), 674-682.
123. Delamarche, E.; Geissler, M.; Wolf, H.; Michel, B., Positive microcontact printing. *J Am Chem Soc* **2002**, 124, (15), 3834-3835.
124. Li, H. W.; Muir, B. V. O.; Fichet, G.; Huck, W. T. S., Nanocontact printing: A route to sub-50-nm-scale chemical and biological patterning. *Langmuir* **2003**, 19, (6), 1963-1965.
125. Li, H. W.; Kang, D. J.; Blamire, M. G.; Huck, W. T. S., High-resolution contact printing with dendrimers. *Nano Lett* **2002**, 2, (4), 347-349.
126. Helmuth, J. A.; Schmid, H.; Stutz, R.; Stemmer, A.; Wolf, H., High-speed microcontact printing. *J Am Chem Soc* **2006**, 128, (29), 9296-9297.

127. Dameron, A. A.; Hampton, J. R.; Smith, R. K.; Mullen, T. J.; Gillmor, S. D.; Weiss, P. S., Microdisplacement printing. *Nano Lett* **2005**, 5, (9), 1834-1837.
128. Dameron, A. A.; Hampton, J. R.; Gillmor, S. D.; Hohman, J. N.; Weiss, P. S., Enhanced molecular patterning via microdisplacement printing. *J Vac Sci Technol B* **2005**, 23, (6), 2929-2932.
129. Bessueille, F.; Pla-Roca, M.; Mills, C. A.; Martinez, E.; Samitier, J.; Errachid, A., Submerged microcontact printing (S mu CP): An unconventional printing technique of thiols using high aspect ratio, elastomeric stamps. *Langmuir* **2005**, 21, (26), 12060-12063.
130. Loo, Y. L.; Willett, R. L.; Baldwin, K. W.; Rogers, J. A., Interfacial chemistries for nanoscale transfer printing. *J Am Chem Soc* **2002**, 124, (26), 7654-7655.
131. Loo, Y. L.; Hsu, J. W. P.; Willett, R. L.; Baldwin, K. W.; West, K. W.; Rogers, J. A., High-resolution transfer printing on GaAs surfaces using alkane dithiol monolayers. *J Vac Sci Technol B* **2002**, 20, (6), 2853-2856.
132. Spruell, J. M.; Sheriff, B. A.; Rozkiewicz, D. I.; Dichtel, W. R.; Rohde, R. D.; Reinhoudt, D. N.; Stoddart, J. F.; Heath, J. R., Heterogeneous Catalysis through Microcontact Printing. *Angew Chem Int Edit* **2008**, 47, (51), 9927-9932.
133. Sullivan, T. P.; van Poll, M. L.; Dankers, P. Y. W.; Huck, W. T. S., Forced peptide synthesis in nanoscale confinement under elastomeric stamps. *Angew Chem Int Edit* **2004**, 43, (32), 4190-4193.
134. Mizuno, H.; Buriak, J. M., Nanoscale Patterning of Organic Monolayers by Catalytic Stamp Lithography: Scope and Limitations. *Acs Appl Mater Inter* **2009**, 1, (12), 2711-2720.
135. Mizuno, H.; Buriak, J. M., Catalytic Stamp Lithography for Sub-100 nm Patterning of Organic Monolayers. *J Am Chem Soc* **2008**, 130, (52), 17656-+.

136. Hsu, K. H.; Schultz, P. L.; Ferreira, P. M.; Fang, N. X., Electrochemical nanoimprinting with solid-state superionic stamps. *Nano Lett* **2007**, 7, (2), 446-451.
137. Snyder, P. W.; Johannes, M. S.; Vogen, B. N.; Clark, R. L.; Toone, E. J., Biocatalytic microcontact printing. *Journal of Organic Chemistry* **2007**, 72, (19), 7459-7461.
138. Shestopalov, A. A.; Vogen, B. N.; Morris, C. J.; Clark, R. L.; Toone, E. J., Universal soft-lithographic technique for patterning oxide-free silicon. *Science* **In submission**.
139. Shestopalov, A. A.; Clark, R. L.; Toone, E. J., Inkless microcontact printing on self-assembled monolayers of Fmoc-Protected aminothiols. *J Am Chem Soc* **2007**, 129, (45), 13818-13819.
140. Roca-Cusachs, P.; Rico, F.; Martinez, E.; Toset, J.; Farre, R.; Navajas, D., Stability of microfabricated high aspect ratio structures in poly(dimethylsiloxane). *Langmuir* **2005**, 21, (12), 5542-5548.
141. Loo, Y. L.; Willett, R. L.; Baldwin, K. W.; Rogers, J. A., Additive, nanoscale patterning of metal films with a stamp and a surface chemistry mediated transfer process: Applications in plastic electronics. *Appl Phys Lett* **2002**, 81, (3), 562-564.
142. Shestopalov, A. A. Chemical reactions and self-assembly in nano-confined environments: the development of new catalytic microcontact printing techniques and multicomponent inorganic Janus particles. Duke University, Durham, 2009.
143. Hyun, J.; Kim, J.; Craig, S. L.; Chilkoti, A., Enzymatic nanolithography of a self-assembled oligonucleotide monolayer on gold. *J Am Chem Soc* **2004**, 126, (15), 4770-4771.
144. Riemenschneider, L.; Blank, S.; Radmacher, M., Enzyme-assisted nanolithography. *Nano Lett* **2005**, 5, (9), 1643-1646.

145. Campbell, C. J.; Smoukov, S. K.; Bishop, K. J. M.; Grzybowski, B. A., Reactive surface micropatterning by wet stamping. *Langmuir* **2005**, *21*, (7), 2637-2640.
146. Sandbrook, J.; Russell, D. W., *Molecular Cloning: A Laboratory Manual*. 3rd ed.; Cold Spring Harbor Laboratory Press: Cold Spring Harbor, NY, 2001; Vol. 1.
147. Matsuda, S.; Kawasaki, H.; Moriguchi, T.; Gotoh, Y.; Nishida, E., Activation of Protein-Kinase Cascades by Osmotic Shock. *J Biol Chem* **1995**, *270*, (21), 12781-12786.
148. Schlaff, S., Acrylamide-Gel Recombination Assay for Glycoprotein Hormone Subunits. *Endocrinology* **1976**, *98*, (2), 527-533.
149. Vilorio-Cols, M. E.; Hatti-Kaul, R.; Mattiasson, B., Agarose-coated anion exchanger prevents cell-adsorbent interactions. *J Chromatogr A* **2004**, *1043*, (2), 195-200.
150. Seiffert, S.; Oppermann, W., Amine-functionalized polyacrylamide for labeling and crosslinking purposes. *Macromol Chem Physic* **2007**, *208*, (16), 1744-1752.
151. Seiffert, S.; Oppermann, W.; Saalwaechter, K., Hydrogel formation by photocrosslinking of dimethylmaleimide functionalized polyacrylamide. *Polymer* **2007**, *48*, (19), 5599-5611.
152. Hochuli, E.; Dobeli, H.; Schacher, A., New metal chelate adsorbent selective for proteins and peptides containing neighbouring histidine residues. *Journal of Chromatography* **1987**, *411*, 177-184.
153. Schmid, E. L.; Keller, T. A.; Dienes, Z.; Vogel, H., Reversible oriented surface immobilization of functional proteins on oxide surfaces. *Anal Chem* **1997**, *69*, (11), 1979-1985.

154. Ho, C. H.; Limberis, L.; Caldwell, K. D.; Stewart, R. J., A metal-chelating pluronic for immobilization of histidine-tagged proteins at interfaces: Immobilization of firefly luciferase on polystyrene beads. *Langmuir* **1998**, *14*, (14), 3889-3894.
155. Dwyer, M. A.; Huang, A. J.; Pan, C. Q.; Lazarus, R. A., Expression and characterization of a DNase I-Fc fusion enzyme. *J Biol Chem* **1999**, *274*, (14), 9738-9743.
156. Breyer, W. A.; Matthews, B. W., Structure of Escherichia coli exonuclease I suggests how processivity is achieved. *Nature Structural Biology* **2000**, *7*, (12), 1125-1128.
157. Wolf, E.; Brukner, I.; Suck, D., Mutational Analysis of Dnase-I DNA Interactions - Design, Expression and Characterization of a Dnase-I Loop Insertion Mutant with Altered Sequence Selectivity. *Protein Eng* **1995**, *8*, (3), 283-291.
158. Burdett, V.; Baitinger, C.; Viswanathan, M.; Lovett, S. T.; Modrich, P., In vivo requirement for RecJ, ExoVII, ExoI, and ExoX in methyl-directed mismatch repair. *P Natl Acad Sci USA* **2001**, *98*, (12), 6765-6770.
159. Brewer, S. H.; Anthireya, S. J.; Lappi, S. E.; Drapcho, D. L.; Franzen, S., Detection of DNA hybridization on gold surfaces by polarization modulation infrared reflection absorption spectroscopy. *Langmuir* **2002**, *18*, (11), 4460-4464.
160. Sakao, Y.; Ueno, N.; Nakamura, F.; Nakamura, F.; Ito, E.; Hayasi, J.; Hara, M., Formation of DNA self-assembled monolayer on a gold substrate. *Mol Cryst Liq Cryst* **2003**, *407*, 537-542.
161. Levicky, R.; Herne, T. M.; Tarlov, M. J.; Satija, S. K., Using self-assembly to control the structure of DNA monolayers on gold: A neutron reflectivity study. *J Am Chem Soc* **1998**, *120*, (38), 9787-9792.

162. Tarlov, M. J.; Herne, T. M.; Levicky, R.; Steel, A. B., Controlling the structure of DNA monolayers using self-assembly. *Abstr Pap Am Chem S* **1999**, 217, U661-U661.
163. Guo, Z.; Guilfoyle, R. A.; Thiel, A. J.; Wang, R. F.; Smith, L. M., Direct Fluorescence Analysis of Genetic Polymorphisms by Hybridization with Oligonucleotide Arrays on Glass Supports. *Nucleic Acids Res* **1994**, 22, (24), 5456-5465.
164. Block, H.; Maertens, B.; Spriestersbach, A.; Brinker, N.; Kubicek, J.; Fabis, R.; Labahn, J.; Schafer, F., Immobilized-Metal Affinity Chromatography (Imac): A Review. *Method Enzymol* **2009**, 466, 439-473.
165. Su, J.; Mrksich, M., Using mass spectrometry to characterize self-assembled monolayers presenting peptides, proteins, and carbohydrates. *Angew Chem Int Edit* **2002**, 41, (24), 4715-4718.
166. Wu, K. J.; Shaler, T. A.; Becker, C. H., Time-of-Flight Mass-Spectrometry of Underivatized Single-Stranded-DNA Oligomers by Matrix-Assisted Laser-Desorption. *Anal Chem* **1994**, 66, (10), 1637-1645.
167. Tanaka, T., Kinetics of Phase Transition in Polymer Gels. *Physica* **1986**, 140A, 261-268.
168. Caykara, T.; Dogmus, M., The effect of solvent composition on swelling and shrinking properties of poly(acrylamide-co-itaconic acid) hydrogels. *Eur Polym J* **2004**, 40, (11), 2605-2609.
169. Ji, S. C.; Ding, J. D., The wetting process of a dry polymeric hydrogel. *Polym J* **2002**, 34, (4), 267-270.
170. Miller, D. N.; Bryant, J. E.; Madsen, E. L.; Ghiorse, W. C., Evaluation and optimization of DNA extraction and purification procedures for soil and sediment samples. *Appl Environ Microb* **1999**, 65, (11), 4715-4724.

171. Shalon, D.; Smith, S. J.; Brown, P. O., A DNA microarray system for analyzing complex DNA samples using two-color fluorescent probe hybridization. *Genome Res* **1996**, 6, (7), 639-645.
172. Houseman, B. T.; Gawalt, E. S.; Mrksich, M., Maleimide-functionalized self-assembled monolayers for the preparation of peptide and carbohydrate biochips. *Langmuir* **2003**, 19, (5), 1522-1531.
173. Su, J.; Mrksich, M., Using MALDI-TOF mass spectrometry to characterize interfacial reactions on self-assembled monolayers. *Langmuir* **2003**, 19, (12), 4867-4870.
174. Nordhoff, E., Matrix-assisted laser desorption/ionization mass spectrometry as a new method for the characterization of nucleic acids. *Trac-Trend Anal Chem* **1996**, 15, (6), 240-250.
175. Nordhoff, E.; Kirpekar, F.; Roepstorff, P., Mass spectrometry of nucleic acids. *Mass Spectrom Rev* **1996**, 15, (2), 67-138.
176. Asara, J. M.; Allison, J., Enhanced detection of oligonucleotides in UV MALDI MS using the tetraamine spermine as a matrix additive. *Anal Chem* **1999**, 71, (14), 2866-2870.
177. Zhu, L.; Parr, G. R.; Fitzgerald, M. C.; Nelson, C. M.; Smith, L. M., Oligodeoxynucleotide Fragmentation in Maldi/Tof Mass-Spectrometry Using 355-Nm Radiation. *J Am Chem Soc* **1995**, 117, (22), 6048-6056.
178. Lecchi, P.; Le, H. M. T.; Pannell, L. K., 6-Aza-a-Thiothymine - a Matrix for Maldi Spectra of Oligonucleotides. *Nucleic Acids Res* **1995**, 23, (7), 1276-1277.
179. Renzi, F.; Panetta, G.; Vallone, B.; Brunori, M.; Arceci, M.; Bozzoni, I.; Laneve, P.; Caffarelli, E., Large-scale purification and crystallization of the endoribonuclease XendoU: troubleshooting with His-tagged proteins. *Acta Crystallogr F* **2006**, 62, 298-301.

180. Kim, Y. S.; Lee, H. H.; Hammond, P. T., High density nanostructure transfer in soft molding using polyurethane acrylate molds and polyelectrolyte multilayers. *Nanotechnology* **2003**, 14, (10), 1140-1144.
181. Vericat, C.; Vela, M. E.; Benitez, G. A.; Gago, J. A. M.; Torrelles, X.; Salvarezza, R. C., Surface characterization of sulfur and alkanethiol self-assembled monolayers on Au(111). *J Phys-Condens Mat* **2006**, 18, (48), R867-R900.
182. Vaidya, B.; Chen, J. H.; Porter, M. D.; Angelici, R. J., Effects of packing and orientation on the hydrolysis of ester monolayers on gold. *Langmuir* **2001**, 17, (21), 6569-6576.
183. Gotor-Fernández, V.; Vicente, G., Use of Lipases in Organic Synthesis. In *Industrial Enzymes: Structure, Function and Applications*, Polaina, J.; MacCabe, A. P., Eds. Springer: Dordrecht, The Netherlands, 2007; pp 301-315.
184. Brockman, H. L.; Momsen, W. E.; Tsujita, T., Lipid-Lipid Complexes - Properties and Effects on Lipase Binding to Surfaces. *J Am Oil Chem Soc* **1988**, 65, (6), 891-896.
185. Gerber, K.; Schiefner, A.; Seige, P.; Diederichs, K.; Boos, W.; Welte, W., Crystallization and preliminary X-ray analysis of Aes, an acetyl-esterase from *Escherichia coli*. *Acta Crystallographica Section D-Biological Crystallography* **2004**, 60, 531-533.
186. Kanaya, S.; Koyanagi, T.; Kanaya, E., An esterase from *Escherichia coli* with a sequence similarity to hormone-sensitive lipase. *Biochemical Journal* **1998**, 332, 75-80.
187. Kay, M. J.; McCabe, R. W.; Morton, L. H. G., Chemical and Physical Changes Occurring in Polyester Polyurethane during Biodegradation. *Int Biodeter Biodegr* **1993**, 31, (3), 209-225.

188. Sanishvili, R.; Yakunin, A. F.; Laskowski, R. A.; Skarina, T.; Evdokimova, E.; Doherty-Kirby, A.; Lajoie, G. A.; Thornton, J. M.; Arrowsmith, C. H.; Savchenko, A.; Joachimiak, A.; Edwards, A. M., Integrating structure, bioinformatics, and enzymology to discover function - BioH, a new carboxylesterase from *Escherichia coli*. *J Biol Chem* **2003**, 278, (28), 26039-26045.
189. Di Lorenzo, M.; Hidalgo, A.; Haas, M.; Bornscheuer, U. T., Heterologous production of functional forms of *Rhizopus oryzae* lipase in *Escherichia coli*. *Appl Environ Microb* **2005**, 71, (12), 8974-8977.
190. Whitesides, G. M.; Kumar, A.; Biebuyck, H. A.; Abbott, N. L.; Dimilla, P. A., Self-Assembled Monolayers and Their Uses. *Abstr Pap Am Chem S* **1994**, 207, 373-PHYS.
191. Wagner, C. D. R., W. M.; Davis, L. E.; Moulder, J.F., *Handbook of X-ray Photoelectron Spectroscopy*. 1st ed.; Perkin-Elmer Corporation: 1995.
192. Biebuyck, H. A.; Bian, C. D.; Whitesides, G. M., Comparison of Organic Monolayers on Polycrystalline Gold Spontaneously Assembled from Solutions Containing Dialkyl Disulfides or Alkenethiols. *Langmuir* **1994**, 10, (6), 1825-1831.
193. Strong, L.; Whitesides, G. M., Structures of Self-Assembled Monolayer Films of Organosulfur Compounds Adsorbed on Gold Single-Crystals - Electron-Diffraction Studies. *Langmuir* **1988**, 4, (3), 546-558.
194. Perry, S. S., Miniaturization Science for Space: Lubrication of Micro-Electro-Mechanical Systems (MEMS) for Space Environments. In United States Air Force: University of Houston, 2006; pp 1-11.
195. Kim, H.; Noh, J.; Hara, M.; Lee, H., Characterization of mixed self-assembled monolayers for immobilization of streptavidin using chemical force microscopy. *Ultramicroscopy* **2008**, 108, (10), 1140-1143.

196. Bain, C. D.; Evall, J.; Whitesides, G. M., Formation of Monolayers by the Coadsorption of Thiols on Gold - Variation in the Head Group, Tail Group, and Solvent. *J Am Chem Soc* **1989**, 111, (18), 7155-7164.
197. Takahashi, S.; Ueda, M.; Tanaka, A., Independent production of two molecular forms of a recombinant *Rhizopus oryzae* lipase by KEX2-engineered strains of *Saccharomyces cerevisiae*. *Appl Microbiol Biot* **1999**, 52, (4), 534-540.
198. Gong, P.; Grainger, D. W., Nonfouling Surfaces: A Review of Principles and Applications for Microarray Capture Assay Designs. In *Microarrays: Volume 1: Synthesis Methods*, Rampal, J. B., Ed. Beckman Coulter, Inc.: Brea, 2007; pp 59-92.
199. Odom, T. W.; Love, J. C.; Wolfe, D. B.; Paul, K. E.; Whitesides, G. M., Improved pattern transfer in soft lithography using composite stamps. *Langmuir* **2002**, 18, (13), 5314-5320.
200. Trimbach, D.; Feldman, K.; Spencer, N. D.; Broer, D. J.; Bastiaansen, C. W. M., Block copolymer thermoplastic elastomers for microcontact printing. *Langmuir* **2003**, 19, (26), 10957-10961.
201. Madler, S.; Bich, C.; Touboul, D.; Zenobi, R., Chemical cross-linking with NHS esters: a systematic study on amino acid reactivities. *J Mass Spectrom* **2009**, 44, (5), 694-706.
202. Wagner, P.; Hegner, M.; Kern, P.; Zaugg, F.; Semenza, G., Covalent immobilization of native biomolecules onto Au(111) via N-hydroxysuccinimide ester functionalized self-assembled monolayers for scanning probe microscopy. *Biophys J* **1996**, 70, (5), 2052-2066.
203. Movassagh, B.; Shaygan, P., Michael addition of thiols to alpha,beta-unsaturated carbonyl compounds under solvent-free conditions. *Arkivoc* **2006**, 130-137.

204. Hamers, R. J.; Butler, J. E.; Lasseter, T.; Nichols, B. M.; Russell, J. N.; Tse, K. Y.; Yang, W. S., Molecular and biomolecular monolayers on diamond as an interface to biology. *Diam Relat Mater* **2005**, 14, (3-7), 661-668.
205. Yang, W. S.; Butler, J. E.; Russell, J. N.; Hamers, R. J., Interfacial electrical properties of DNA-modified diamond thin films: Intrinsic response and hybridization-induced field effects. *Langmuir* **2004**, 20, (16), 6778-6787.
206. Yang, W. S.; Auciello, O.; Butler, J. E.; Cai, W.; Carlisle, J. A.; Gerbi, J.; Gruen, D. M.; Knickerbocker, T.; Lasseter, T. L.; Russell, J. N.; Smith, L. M.; Hamers, R. J., DNA-modified nanocrystalline diamond thin-films as stable, biologically active substrates (vol 1, pg 253, 2002). *Nat Mater* **2003**, 2, (1), 63-63.
207. Fritz, J.; Cooper, E. B.; Gaudet, S.; Sorger, P. K.; Manalis, S. R., Electronic detection of DNA by its intrinsic molecular charge. *P Natl Acad Sci USA* **2002**, 99, (22), 14142-14146.
208. Souteyrand, E.; Cloarec, J. P.; Martin, J. R.; Wilson, C.; Lawrence, I.; Mikkelsen, S.; Lawrence, M. F., Direct detection of the hybridization of synthetic homo-oligomer DNA sequences by field effect. *J Phys Chem B* **1997**, 101, (15), 2980-2985.
209. Souteyrand, E.; Martin, J. R.; Martelet, C., Direct-Detection of Biomolecules by Electrochemical Impedance Measurements. *Sensor Actuat B-Chem* **1994**, 20, (1), 63-69.
210. Freedman, L. D.; Doak, G. O., *Chem Rev* **1957**, 57, 479.
211. Dippy, J. F. J.; Hughes, S. R. C.; Rozanski, A., *J Am Chem Soc* **1959**.
212. Brown, H. C., *Determination of Organic Structures by Physical Methods*. New York, 1955.

213. Kolthoff, I. M., Treatise on Analytical Chemistry. In *Interscience Encyclopedia, Inc.*, New York, 1959.
214. Leonard, J.; Lygo, B.; Procter, G., *Advanced Practical Organic Chemistry*. Nelson Thornes Ltd: Cheltenham, 2001.
215. Svedhem, S.; Hollander, C. A.; Shi, J.; Konradsson, P.; Liedberg, B.; Svensson, S. C. T., Synthesis of a series of oligo(ethylene glycol)-terminated alkanethiol amides designed to address structure and stability of biosensing interfaces. *Journal of Organic Chemistry* **2001**, 66, (13), 4494-4503.
216. Roberts, C.; Chen, C. S.; Mrksich, M.; Martichonok, V.; Ingber, D. E.; Whitesides, G. M., Using mixed self-assembled monolayers presenting RGD and (EG)(3)OH groups to characterize long-term attachment of bovine capillary endothelial cells to surfaces. *J Am Chem Soc* **1998**, 120, (26), 6548-6555.
217. Hashimoto, N.; Aoyama, T.; Shioiri, T., New Methods and Reagents in Organic-Synthesis .14. A Simple Efficient Preparation of Methyl-Esters with Trimethylsilyldiazomethane (Tmschn₂) and Its Application to Gas-Chromatographic Analysis of Fatty-Acids. *Chemical & Pharmaceutical Bulletin* **1981**, 29, (5), 1475-1478.
218. Sehgal, D.; Vijay, I. K., A Method for the High-Efficiency of Water-Soluble Carbodiimide-Mediated Amidation. *Analytical Biochemistry* **1994**, 218, (1), 87-91.
219. Hanahan, D.; Jessee, J.; Bloom, F. R., Plasmid Transformation of Escherichia-Coli and Other Bacteria. *Methods in Enzymology* **1991**, 204, 63-113.
220. Peist, R.; Koch, A.; Bolek, P.; Sewitz, S.; Kolbus, T.; Boos, W., Characterization of the aes gene of Escherichia coli encoding an enzyme with esterase activity. *Journal of Bacteriology* **1997**, 179, (24), 7679-7686.

221. O'Regan, M.; Gloeckler, R.; Bernard, S.; Ledoux, C.; Ohsawa, I.; Lemoine, Y., Nucleotide-Sequence of the BioH Gene of Escherichia-Coli. *Nucleic Acids Res* **1989**, *17*, (19), 8004-8004.
222. Zhang, R. G.; Skarina, T.; Katz, J. E.; Beasley, S.; Khachatryan, A.; Vyas, S.; Arrowsmith, C. H.; Clarke, S.; Edwards, A.; Joachimiak, A.; Savchenko, A., Structure of Thermotoga maritima stationary phase survival protein SurE: A novel acid phosphatase. *Structure* **2001**, *9*, (11), 1095-1106.
223. Naka, K.; Itoh, H.; Chujo, Y., Self-assembly of gold nanoparticles utilizing a charge-transfer interaction between carbazolyl and dinitrophenyl units. *Bulletin of the Chemical Society of Japan* **2005**, *78*, (3), 501-505.
224. Greenfield, A. A.; Butera, J. A., Convenient synthesis and isolation of conformationally rigid glutamic acid analogues. *Synthetic Communications* **2004**, *34*, (21), 3939-3947.
225. Chen, S. F.; Zheng, J.; Li, L. Y.; Jiang, S. Y., Strong resistance of phosphorylcholine self-assembled monolayers to protein adsorption: Insights into nonfouling properties of zwitterionic materials. *J Am Chem Soc* **2005**, *127*, (41), 14473-14478.
226. Wolf, J.-P.; Schulthess, A.; Steinmann, B.; Hunziker, M. Tetraacrylate-containing polymerizable mixtures. 1994.

Biographical sketch

Briana Noelle Vogen

Born 03 February 1982 in Minneapolis, Minnesota, to Noel W. & Judith L. Vogen

EDUCATION

- *Duke University in Durham, NC*
Doctor of Philosophy Degree in Chemistry 04/2010
Advisor: Professor Eric J. Toone
- *Duke University in Durham, NC*
Certificate in Biological and Biologically Inspired Materials and Material Systems 04/2010
Program Director: Professor Robert L. Clark
- *Loras College in Dubuque, IA*
Bachelor of Science and Honors Degrees in Biochemistry 05/2004
Advisor: Professor David C. Speckhard

RESEARCH EXPERIENCE

- *Duke University in Durham, NC*
Graduate Student in Chemistry 2004 - 2010
Advisor: Professor Eric J. Toone
- *Duke University in Durham, NC*
Undergraduate Research Fellow in the Pratt School of Engineering 2003
Advisors: Professor Robert L. Clark and Dr. Daniel G. Cole

AWARDS & FELLOWSHIPS

- **NSF IGERT Fellowship** 2005 - 2008
Duke University, Durham, NC
- **American Chemical Society (ACS) Student Poster Award in the Division of Colloid and Surface Chemistry** 2008
233rd National Meeting, New Orleans, LA
- **Fellowship in the Program of Biological Chemistry** 2004 - 2005
Duke University, Durham, NC

PUBLICATIONS

- "Biocatalytic microcontact printing," Phillip W. Snyder, Matthew S. Johannes, **Briana N. Vogen**, Robert L. Clark, Eric J. Toone, *Journal of Organic Chemistry*, **2007**, 72 (19), 7459-7461.

MANUSCRIPTS IN PREPARATION

- "Universal soft-lithographic technique for patterning oxide-free silicon," Alexander A. Shestopalov, **Briana N. Vogen**, Carleen J. Morris, Robert L. Clark, Eric J. Toone, *Science*, **in submission**.
- "Catalytic Patterning and Functionalization of Highly Ordered SAMs on Passivated Silicon Using Inkless Microcontact Printing," Alexander A. Shestopalov, **Briana N. Vogen**, Robert L. Clark, Eric J. Toone, **in submission**.
- "Dependence of pKa on Stamping Time in Acidic Inkless Catalytic Microcontact Printing," **Briana N. Vogen**, Carleen J. Morris, Alexander A. Shestopalov, Robert L. Clark, Eric J. Toone, **in preparation**.

POSTERS & PRESENTATIONS

- **233rd National Meeting of the American Chemical Society (ACS) Poster** **2008**
New Orleans, LA
- **Annual IGERT Project Meeting Poster** **2007**
Arlington, VA
- **40th National Organic Chemistry Symposium Poster** **2007**
Duke University, Durham, NC
- **Invited research talks** **2005, 2007**
Loras College, Dubuque, IA

MEMBERSHIPS

- American Chemical Society
- Phi Lambda Upsilon

TEACHING EXPERIENCE

- **Teaching Assistant.** General Chemistry 31 Recitation and Laboratory, and General Chemistry 32 Recitation **2009 - 2010**
Duke University, Durham, NC